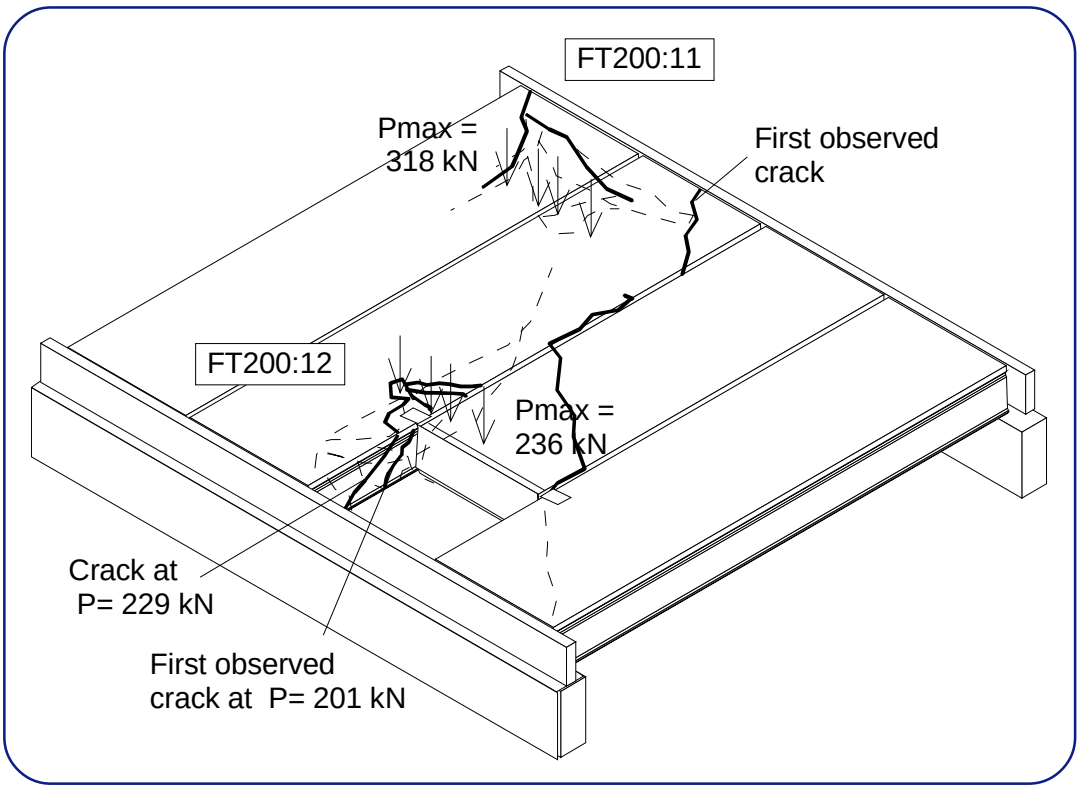

Matti Pajari

Shear–torsion tests on 200 mm hollow core floor

VTT TIEDOTTEITA – RESEARCH NOTES 2276

Shear-torsion tests on 200 mm hollow core floor

Matti Pajari
VTT Building and Transport

ISBN 951–38–6520–7 (URL: http://www.vtt.fi/inf/pdf/)
ISSN 1455–0865 (URL: http://www.vtt.fi/inf/pdf/)

JULKAISIJA – UTGIVARE – PUBLISHER

VTT, Vuorimiehentie 5, PL 2000, 02044 VTT
puh. vaihde (09) 4561, faksi (09) 456 4374

VTT, Bergsmansvägen 5, PB 2000, 02044 VTT
tel. växel (09) 4561, fax (09) 456 4374

VTT Technical Research Centre of Finland, Vuorimiehentie 5, P.O.Box 2000, FIN–02044 VTT, Finland
phone internat. + 358 9 4561, fax + 358 9 456 4374

VTT Rakennus- ja yhdyskuntatekniikka, Kemistintie 3, PL 1805, 02044 VTT
puh. vaihde 020 722 111, faksi 020 722 7007

VTT Bygg och transport, Kemistvägen 3, PB 1805, 02044 VTT
tel. växel 020 722 111, fax 020 722 7007

VTT Building and Transport, Kemistintie 3, P.O.Box 1805, FIN–02044 VTT, Finland
phone internat. +358 20 722 111, fax +358 20 722 7007

Technical editing Leena Ukskoski

Pajari, Matti. Shear-torsion tests on 200 mm hollow core floor. Espoo 2004. VTT Tiedotteita – Research Notes 2276. 55 p. + app. 116 p.

Keywords shear tests, torsion tests, hollow core slabs, floors, testing, test specimens, load testing, failure loads, load distribution, concrete, precast, prestressed, structure

Abstract

To clarify the interaction of shear and torsion in prestressed hollow core floors, ten service load tests and two failure tests on a 200 mm hollow core floor were carried out. The floor comprised four slab units. It was 4.8 m in width, 7.0 m in length and provided with an opening at one end. The ends of the slabs were simply supported. In each test the loading consisted of four closely spaced point loads on the same line which was perpendicular to the direction of the slab units.

The purpose of the tests was to provide experimental data for verification of computer models. For this reason, as many as 120 transducers were used to measure the loads, strains and displacements of the floor specimen.

The results were qualitatively as expected: nearly linear response not only in service load tests but also in failure tests until a high load level. The observed failure loads were considerably higher than what was observed in a similar load test on a single slab unit.

It was also observed that the trimmer beam next to the opening carried only a small share of the support reaction due to imposed load on the slab supported on the trimmer beam. The rest of the support reaction was carried by the grouted joints between slab units.

Preface

In 2002–2004, a European research project named HOLCOTORS was carried out. It aimed at providing numerical methods for analysis and simplified methods for design of prestressed hollow core floors subjected to shear and torsion. The calculation models were developed by Chalmers University of Technology, Sweden. The tests used for verification of the models were carried out and documented by VTT, Finland. The researchers in the involved research institutes were

Helen Broo	Chalmers
Björn Engström	Chalmers
Karin Lundgren	Chalmers
Matti Pajari	VTT
Mario Plos	Chalmers.

In addition to the researchers, the following representatives of the industrial partners participated in the work as members of the steering group and by participating in the workshops organised on the day before the steering group meetings:

Olli Korander	Consolis Technology, Finland, Chairman
Arnold van Acker	Belgium
Willem Bekker	Echo, Belgium
David Fernandez-Ordonez	Castelo, Spain
Ronald Klein-Holte	BVSH (VBI) The Netherlands
Gösta Lindström	Strängbetong, Sweden
Aad van Paassen	BVSH (VBI), The Netherlands
Nordy Robbens	Echo, Belgium
Bart Thijs	Echo, Belgium
Jan de Wit	IPHA (Dycore), The Netherlands
Javier Zubia	Castelo, Spain

Gösta Lindström also worked in close co-operation with the researchers, participated in extra workshops between the steering group meetings and made proposals for the future design practice.

The experimental part of the research project, a part of which is documented in this report, was financed by the Fifth Framework Programme of European Commission (Competitive and Sustainable Growth, Contract Nº G6RD-CT-2001-00641); International Prestressed Hollow Core Association, Bundesverband Spannbeton-Hohlplatten, Castelo, Consolis, Echo, Strängbetong, and VTT. The test specimens were provided by Parma Betonila, Finland.

Contents

E Measured strains and displacements in tests FT200:47–FT200:11

F Error in vertical displacements

G Measured tilting and sliding of supporting beams

1. Introduction

The tests documented in this report were planned to clarify the effect of shear and torsion on the deflection and resistance of a floor made of prestressed hollow core slab units. By placing the loads close to the support, bending failure modes were eliminated.

In all figures of this report, the measures are given in millimetres unless otherwise specified.

2. Test arrangements

Ten tests with service load were carried out. In these tests the floor was subjected to four equal point loads which were increased monotonously until a certain predefined limit load was achieved. After unloading the loads were moved to another position and the same procedure was repeated. All positions of the service point loads are shown in Fig. 1.a.

After the service load tests the floor was loaded to failure in two tests. The location of the loads is illustrated in Fig. 1.b. Some characteristics of the test specimens are given in Table 1. Different tests are identified by symbol FT200:x where x is the number of the test shown in Fig. 1.

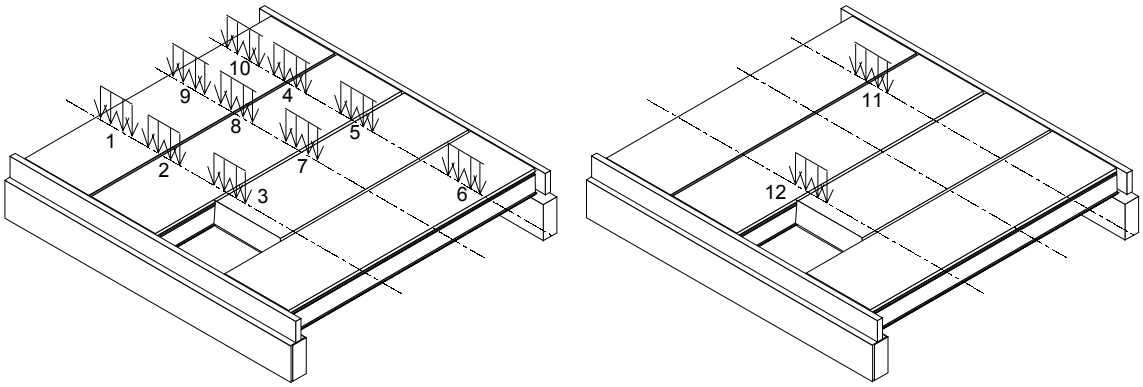

a) *b)*

Fig. 1. General view on loading arrangements. a) Location of point load in service load tests FT200:1–FT200:10. b) Location of point loads in failure tests FT200:11 and FT200:12.

Table 1. Characteristics of slab units in test FT200:1–FT200:12.

Thickness mm	Strands	Initial prestress MPa	Length mm	Cast (Extruded)
200	7 *d* 12.5 mm	900	7060 or 6020	10.10.2003

For comparison, a load test called ST200E2M with similar support conditions as in the present floor but with only one slab unit was carried out, see Fig. 2. This test has been reported elsewhere [3].

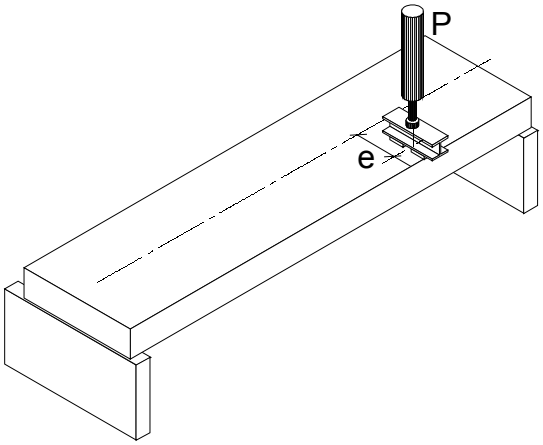

Fig. 2. Loading arrangements in test ST200E2M [3].

The slabs were cast by Parma Oy at Hyrylä factory. The material data provided by the manufacturer of the slab units are collected in Table 2.

Table 2. Data provided by the slab manufacturer.

Concrete	K60
Cement	CEM I 52,5 R
Cement kg/m^3	245
Water l/m^3	120
Maximum aggregate size # [mm]	13
Number of aggregates	3
Strands - strength/0.2% yield strength [MPa] - initial prestress [MPa]	 1860 / 1640 900

The nominal cross-section of the slab units is given in Fig. 3 and the measured geometry in Appendix C. The measurements show that the real voids were considerably smaller than either the nominal ones or the voids in the slabs used in previous tests [3]. The difference in the real cross-sections must be taken into account when comparing the results of the present and previous tests, see Chapter 6.

When assembling the test specimen, two supporting beams were placed on the floor of the laboratory without any smoothing material. The slab ends were placed on the beams (one end of slab 2 on a trimmer beam). The longitudinal joints were grouted on the 28th of October 2003. On the next day the joints were precracked by wedges, see Figs 4–7 in App. A. The crosswise tie beams on the supporting beams were cast on the 30th of October. The crack widths due to the precracking are shown in Fig. 4. They were measured optically, close to transducers 41–46 and 241–246, on the 11th of November 2003.

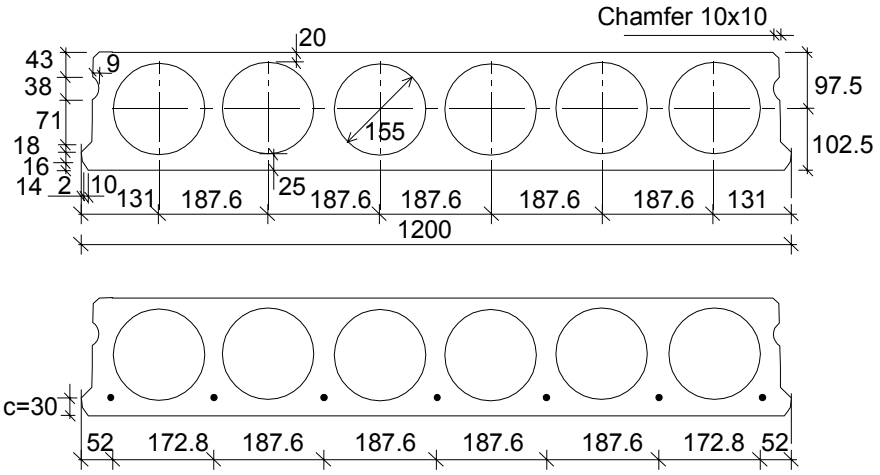

Fig. 3. Nominal cross-section and location of strands in slabs. c refers to concrete cover below the strand.

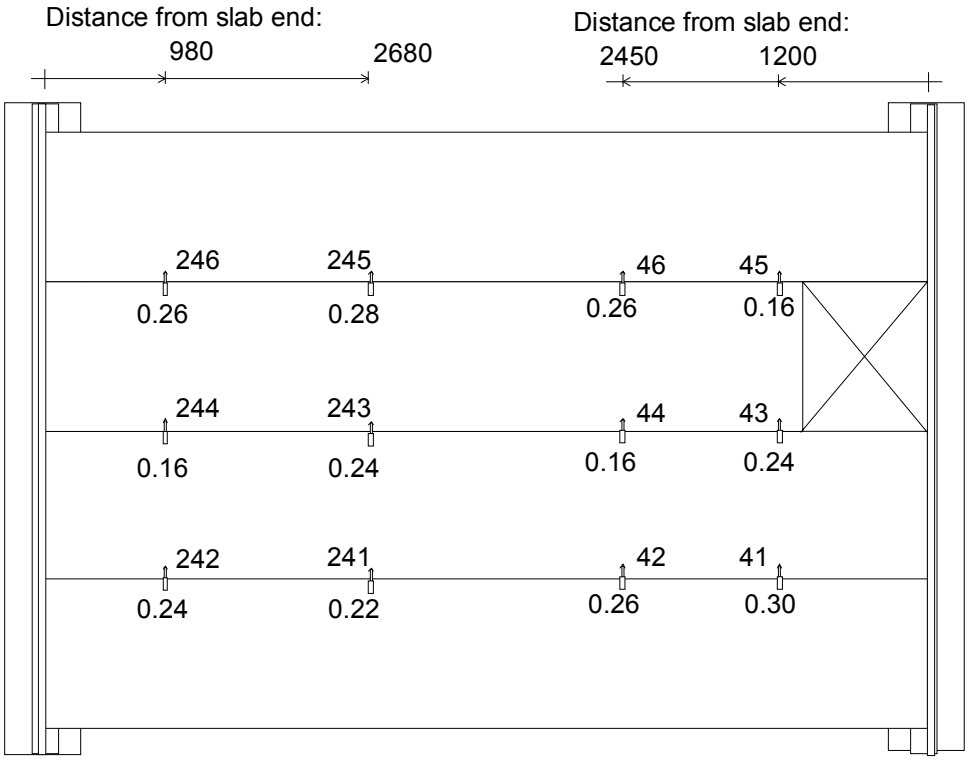

Fig. 4. Crack width due to precracking. For the location of transducers see Figs 16 and 18.

The design of the supporting beams and that of the trimmer beam are shown in Fig. 5 and Figs 6–8, respectively. The support conditions and test arrangements are presented in Figs 9–22.

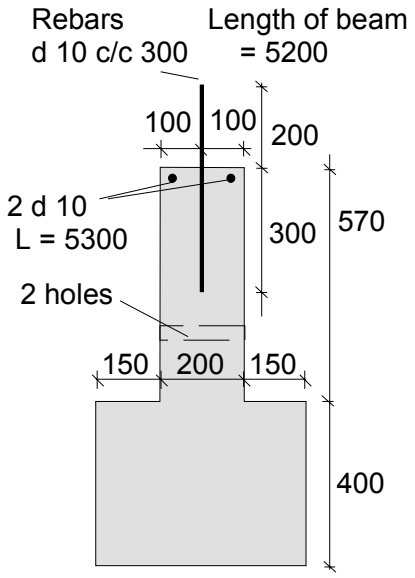

Fig. 5. Design of supporting beams. The grade of concrete was K30.

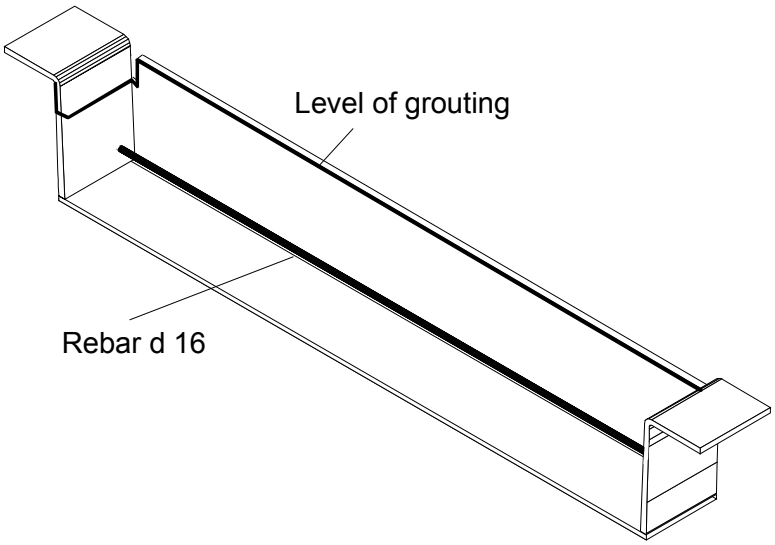

Fig. 6. Overview on trimmer beam POK200 made by Teräspeikko Oy, Lahti. The slots at the ends of the end plate were made by VTT. They do not belong to the design of POK200.

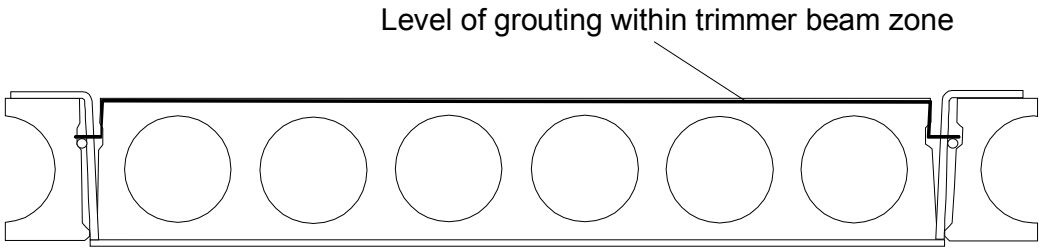

Fig. 7. Cross-section of slab place on trimmer beam. Note that, to facilitate undisturbed measuring of strains, the grouting level at the ends of the trimmer beam was lower than elsewhere.

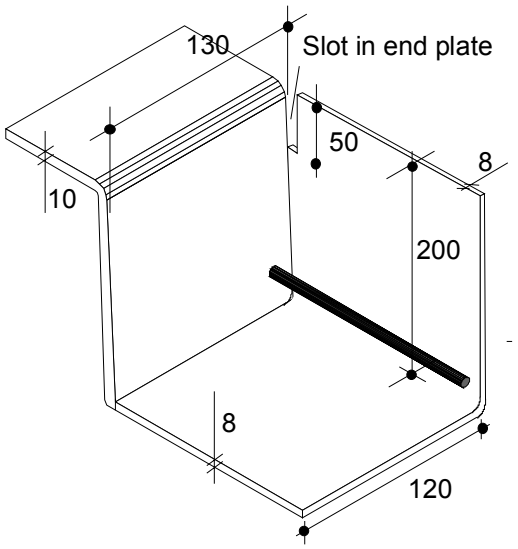

a)

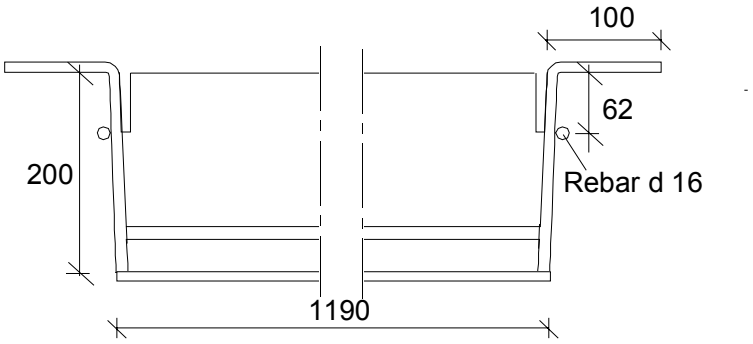

b)

Fig. 8. Design of trimmer beam. a) 3-dimensional illustration. b) Side view. Note the slots at the ends of the end plate. The steel plates were made of steel S355JO.

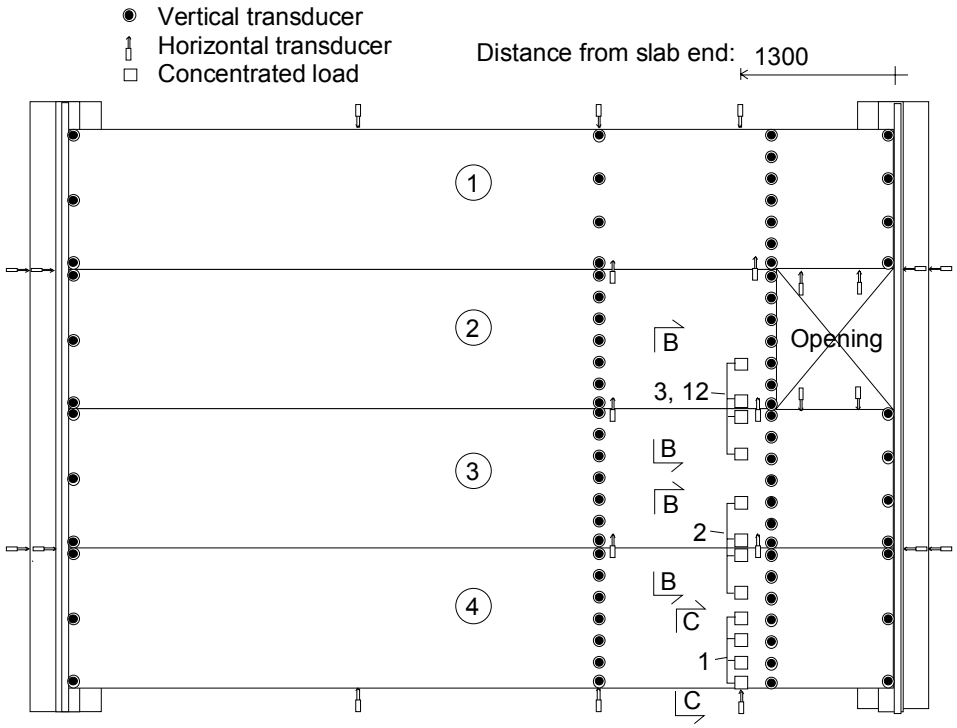

Fig. 9. Location of loads in tests FT200:1–FT200:3 and FT200:12. For transducers, see Figs 16–17. For sections A–A, B–B and C–C, see Fig. 13.

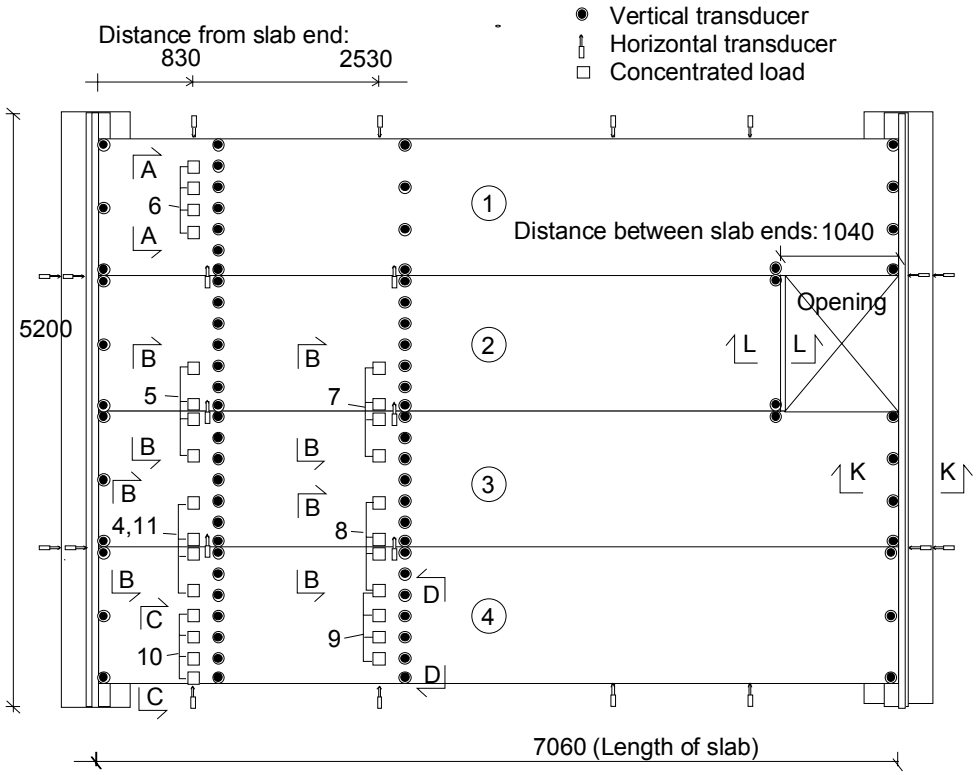

Fig. 10. Location of loads in tests FT200:4–FT200:11. For transducers, see Figs 18–19. For sections K–K and L–L, see Fig. 11.

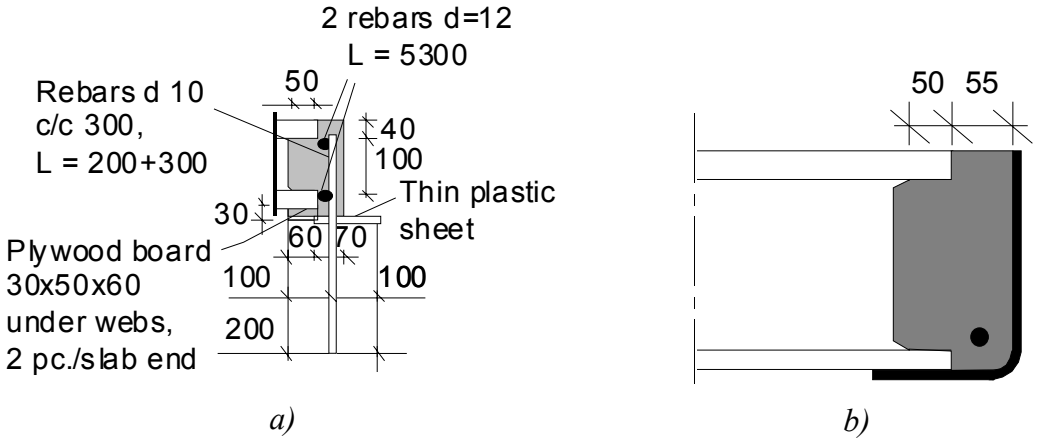

Fig. 11. Arrangements at supports of floor. a) Arrangements at supporting beam, section K–K in Fig. 10. b) Arrangements at trimmer beam, section L–L in Fig. 10.

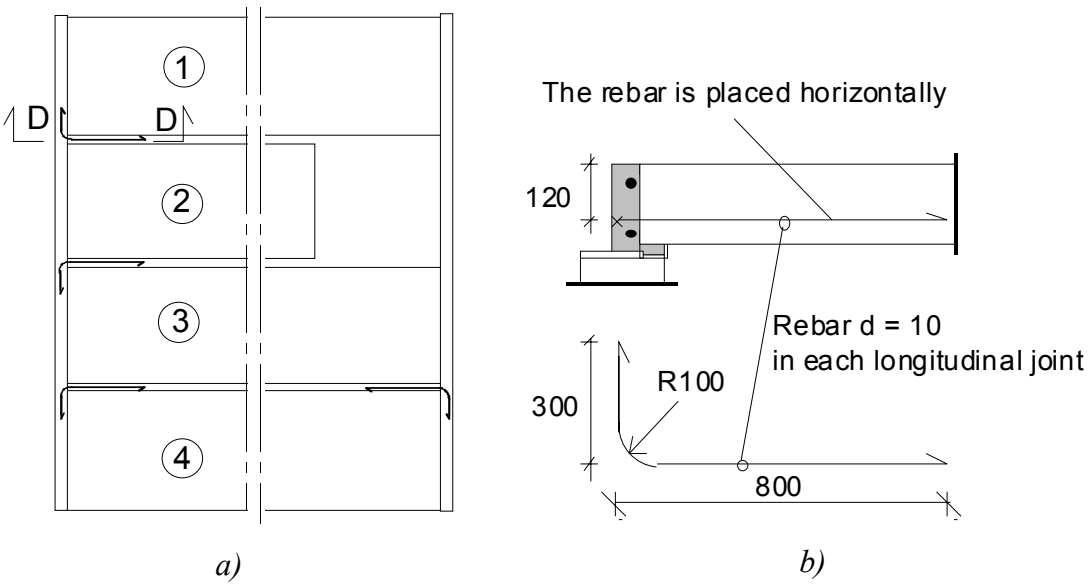

Fig. 12. Tie reinforcement in longitudinal joints of floor. a) Plan. b) Section D–D.

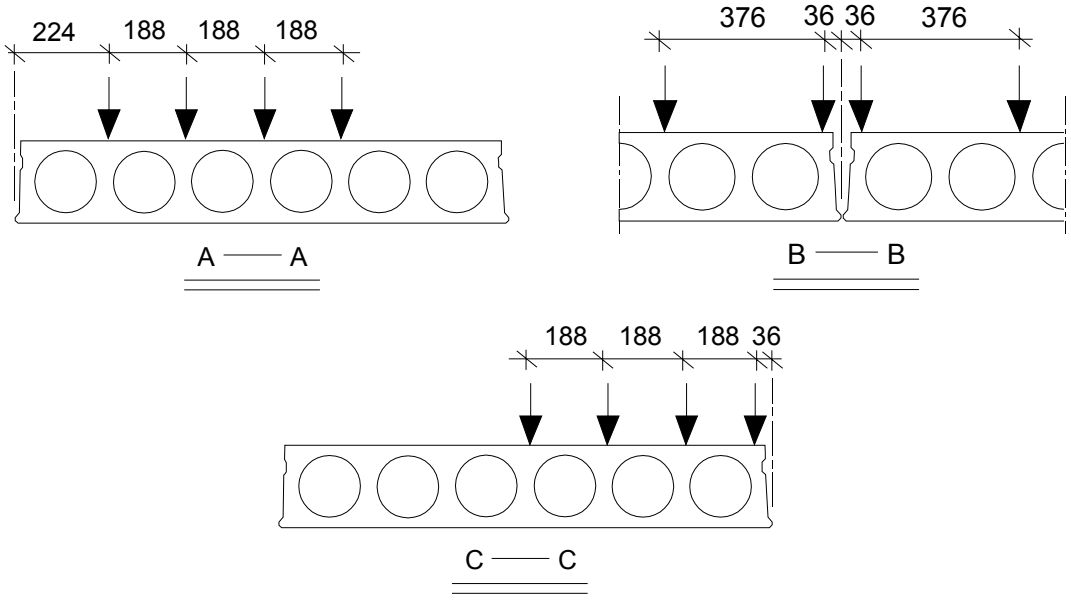

Fig. 13. Loads in different tests. Sections A–A, B–B and C–C, see Figs 9–10.

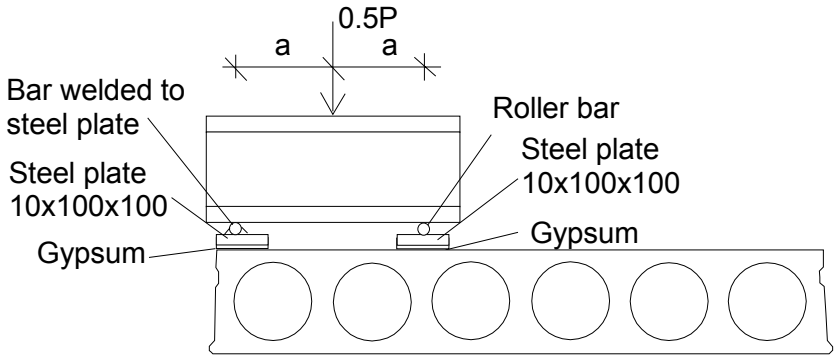

Fig. 14. Loading arrangements above outermost web (on the left) and above inner web (on the right).

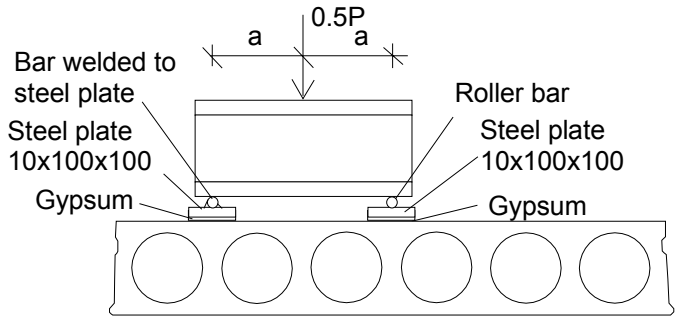

Fig. 15. Loading arrangements above two inner webs.

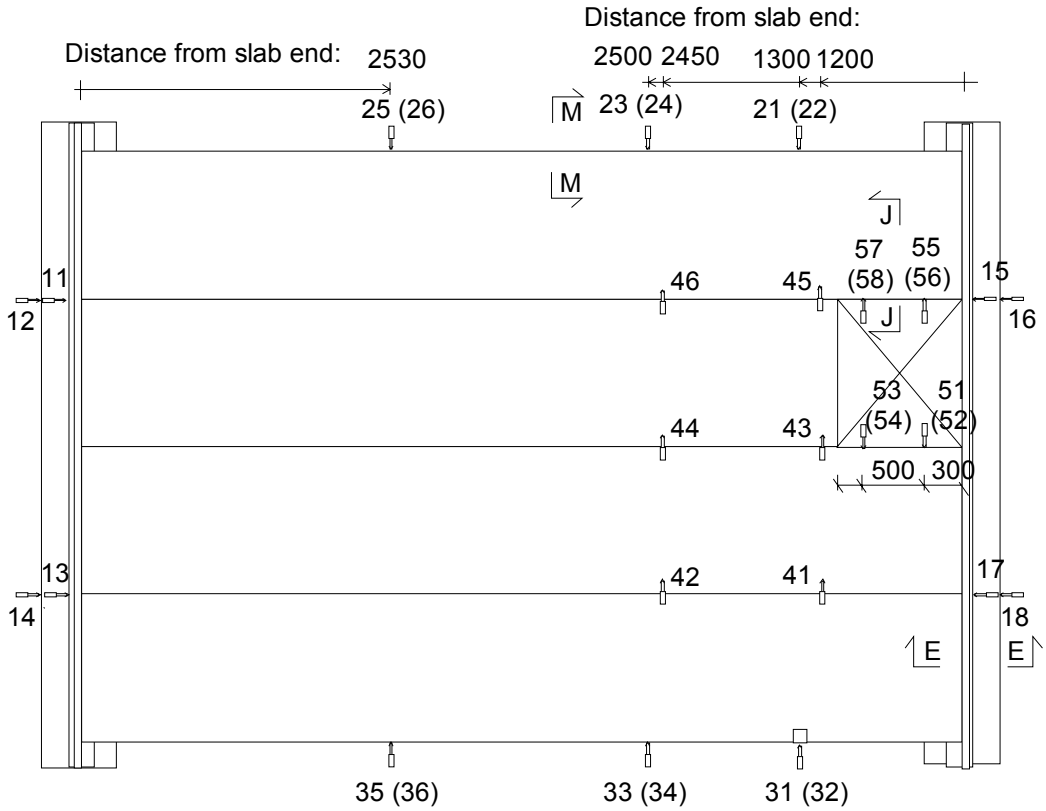

Fig. 16. Horizontal transducers 11–18, 21–26, 31–36 and 41–46 in stages I and IV. Numbers in parentheses refer to transducers at a lower level.

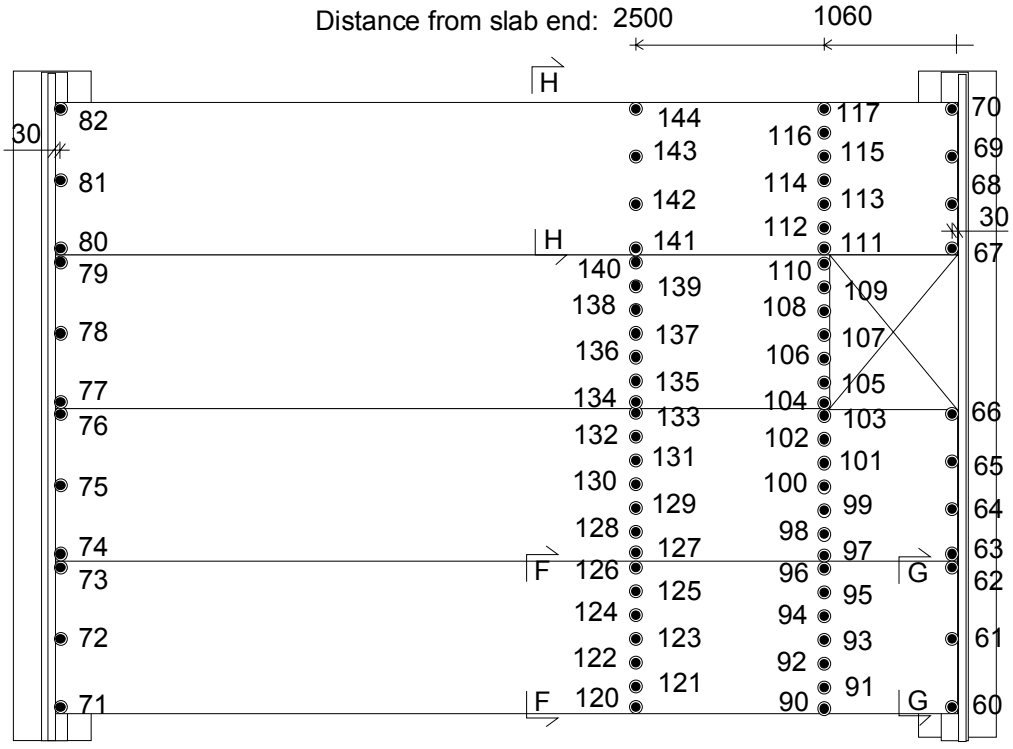

Fig. 17. Vertical transducers in stages I and IV.

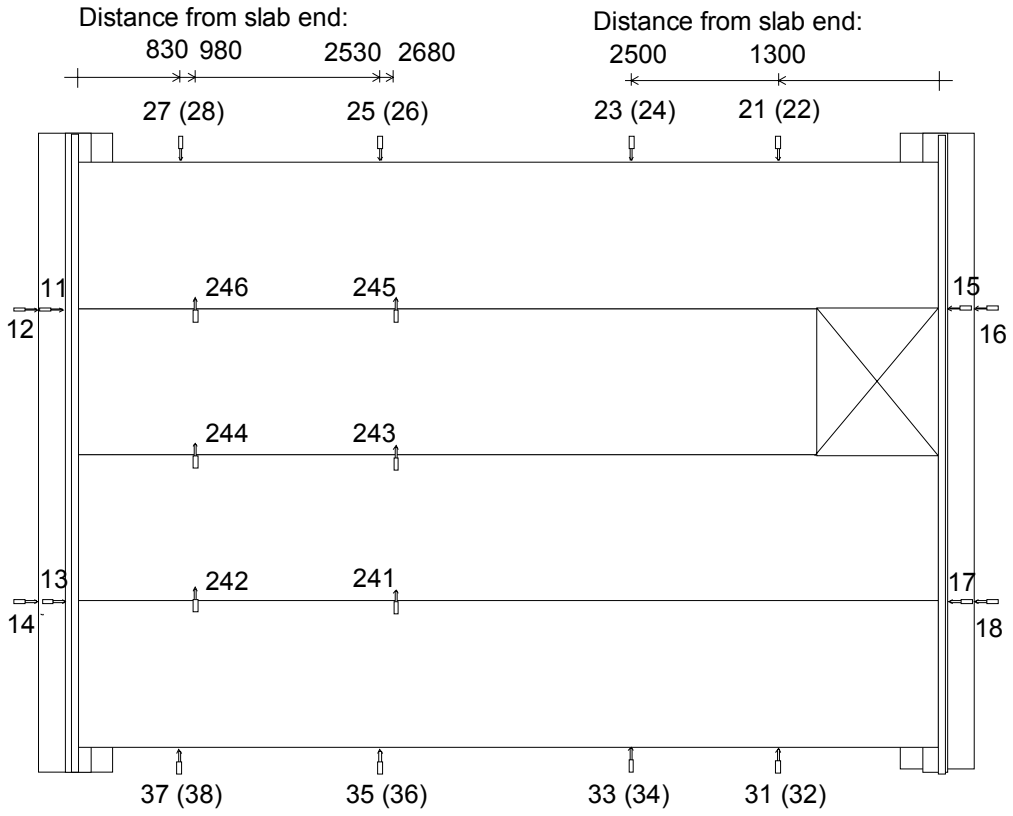

Fig. 18. Horizontal transducers 11–18, 21–28, 31–38 and 241–246 in stages II and III. Numbers in parentheses refer to transducers at a lower level.

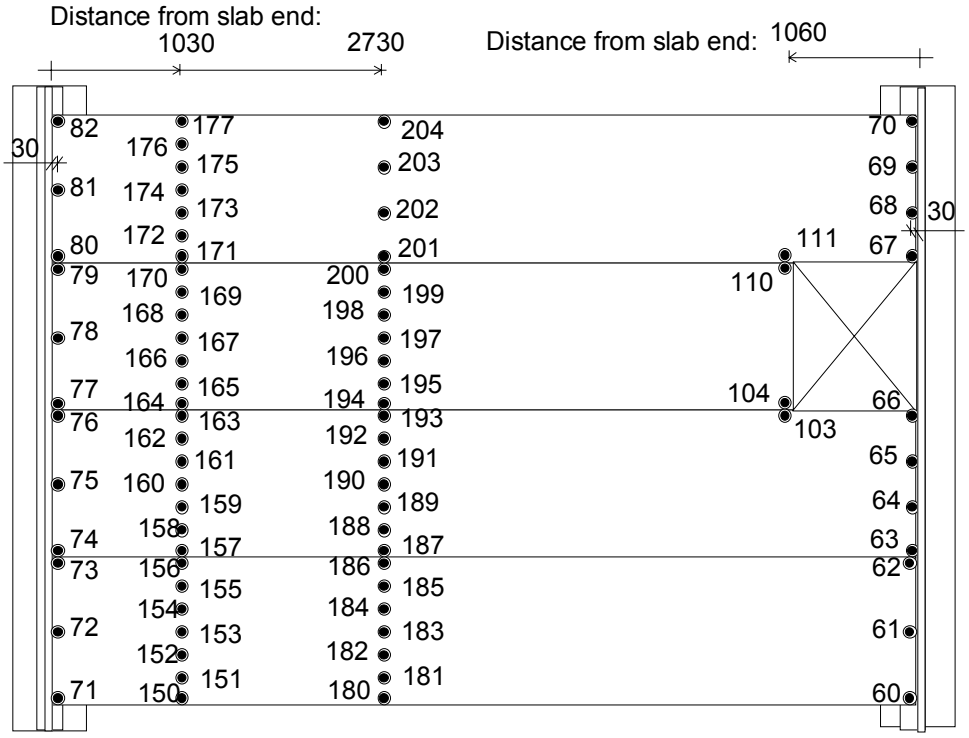

Fig. 19. Vertical transducers in stages II and III.

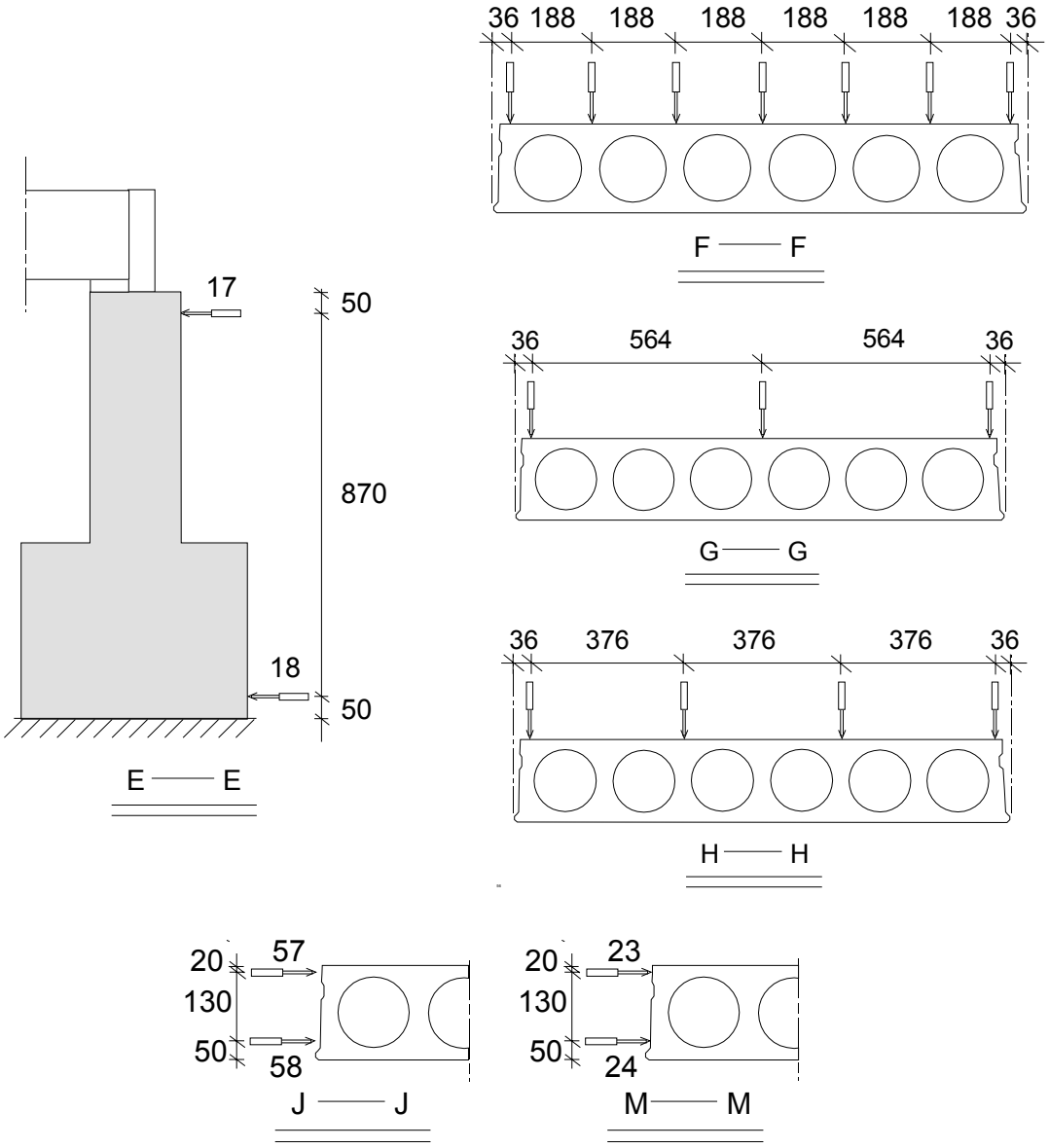

Fig. 20. Sections E–E, G–G, H–H, J–J and M–M, see Figs 16 and 17.

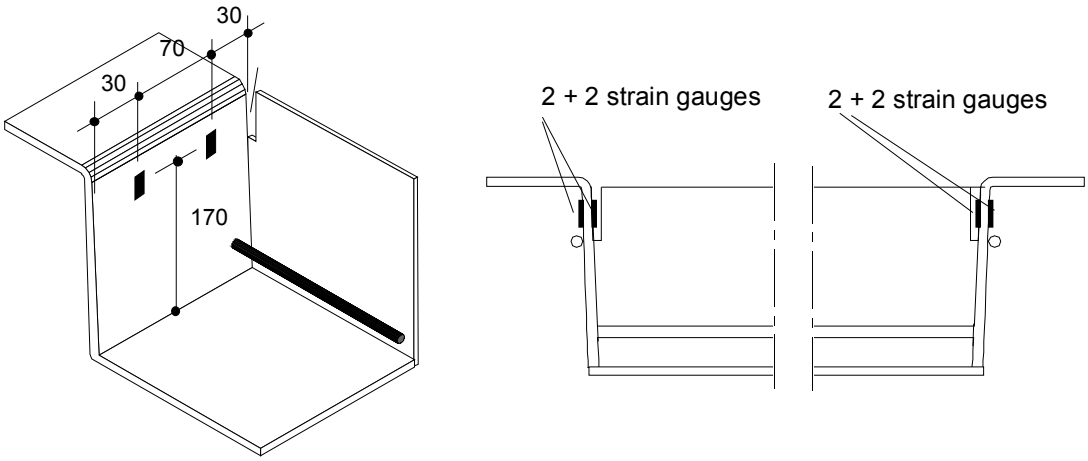

Fig. 21. Location of straing gauges 211–218 fixed to trimmer beam. See also Fig. 22.

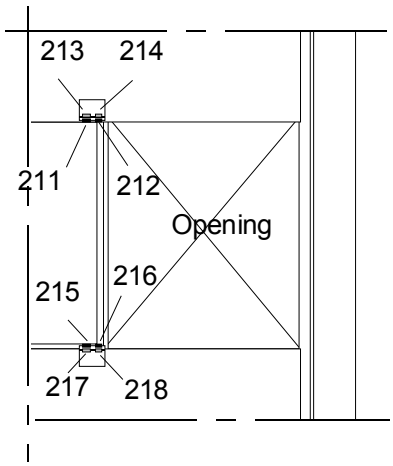

Fig. 22. Location of strain gauges 211–218. Plan view. See also Fig. 21.

3. Test on trimmer beam

Next to the opening, the end of slab 2 was placed on a trimmer beam, which in its turn was supported on the top of the two neighbouring slabs 1 and 3 as shown in Figs 1–3 and 7 in App. A. Before grouting the joints, the trimmer beam was loaded with the self weight of slab 2, with another slab and with additional weight of material placed on the slab end as shown in Fig. 23. The aim of these measurements was to facilitate interpretation of the strain measurements during the floor tests.

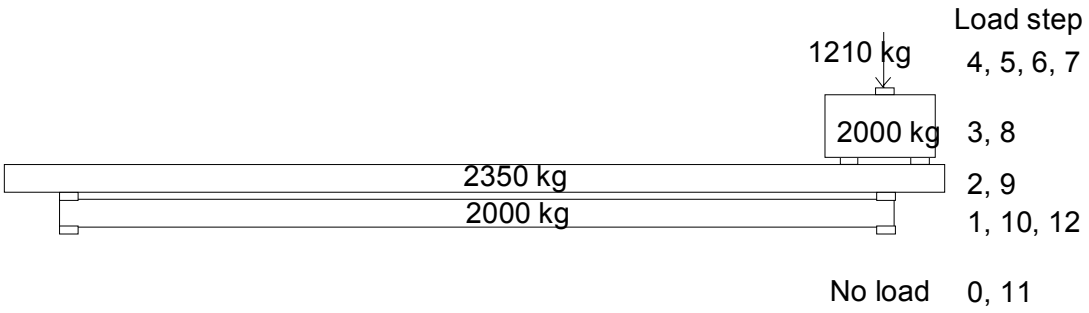

Fig. 23. Loading arrangements at load steps 0, 1, ... ,12. The trimmer beam supports the right end of the lower slab.

After load step 5, the protruding parts of edges of slabs 1 and 3 close to the trimmer beam, see Fig. 24, were removed by chiseling, and the operation was completed after load step 6. The aim was to eliminate contact between the end plates of the trimmer beam and the edges of slabs 1 and 3. This contact was non-existing before loading, but developed gradually, obviously due to the tapered shape of the trimmer beam and bending of the wings of the trimmer beam.

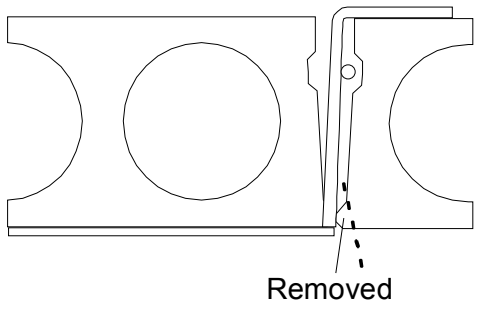

Fig. 24. Protruding part of slab edge removed after load step 4

Fig. 25 illustrates the idea behind the measurements. From the strains measured on the surface of the steel plate, the average strain is calculated as the mean of the measured strains. When the average strain is multiplied by the elasticity modulus of the steel and

cross-sectional area of the steel plate, an estimate for the normal force carried by the steel plate is obtained provided that the yield strain has not been exceeded anywhere.

The measured strains and loads as well as some additional data are given in App. C. The measured load-strain curves are shown in Fig. 26 and the average strain in Fig. 27.

During the chiseling the strains changed only slightly except the one measured by gauge 213. The behaviour of gauge 213 is difficult to explain unless there has been some error in the measuring devices. The sudden drop between load steps 5 and 6 not only in strain at 213 but also in average strain (Fig. 27) means that, thanks to the chiseling, the load carried by the trimmer beam considerably decreased which is unlogical.

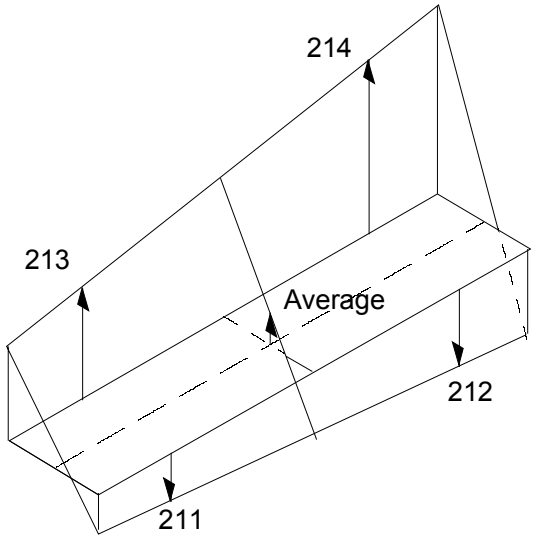

Fig. 25. Hypothetical distribution of vertical strain in end plate of trimmer beam. Horizontal cross-section. Strains measured by strain gauges 211–214 and the average strain illustrated by arrows.

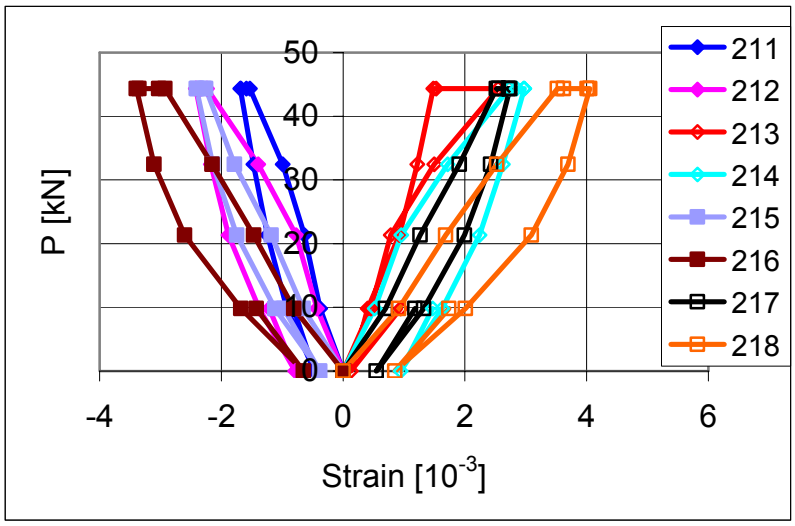

Fig. 26. Strain measured by strain gauges 211–218.

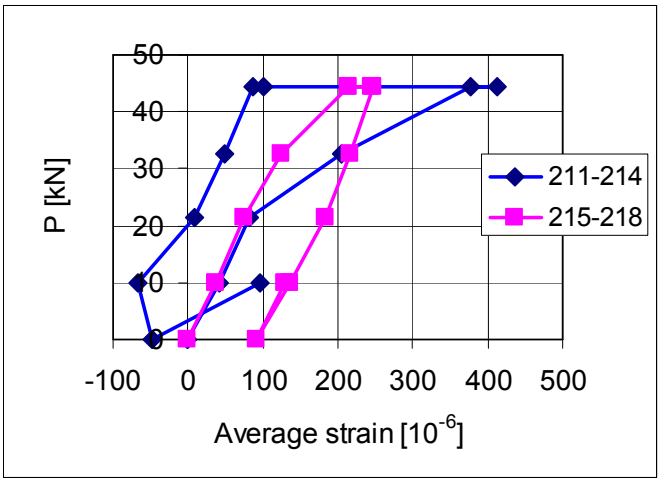

Fig. 27. Average strain.

The virtual stress curves calculated from $\sigma = (210\ \text{GPa}) \cdot \varepsilon$ are shown in Fig. 28. The measured stress exceeds the nominal yield strength 355 MPa after load step 2 ($P = 21.4$ kN). On the other hand, the strains seem to be nearly proportional to the load until the maximum load. The assumption of proportionality in the load-strain relationship seems to work relatively well even after yielding has started because

- a major part of the cross-section did not yield
- the errors in the tensile stresses, calculated ignoring the plastification, are partly counterweighted by errors of the same order in the compressed zone.

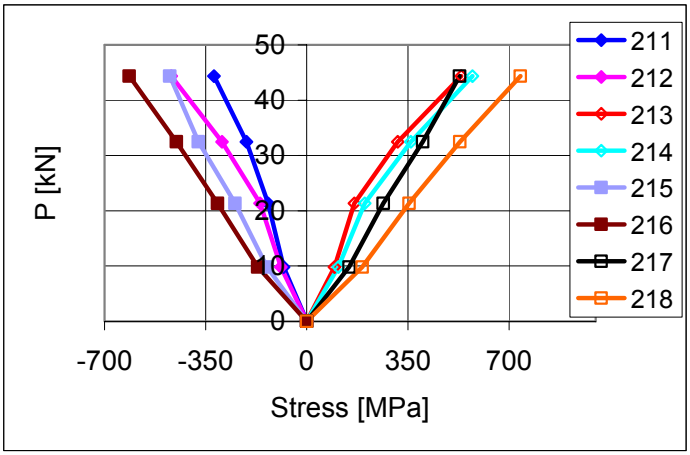

Fig. 28. Virtual stress, ascending part of the curves.

Fig. 29 illustrates the load carried by the trimmer beam versus vertical force F in the end plates calculated from the average strain. The sum of forces F should equal P but it equals $2P$. No good explanation to this discrepancy could be found. A damage in gauge 213 does not seem likely because in later tests this gauge behaved in a way very similar to that of the other gauges.

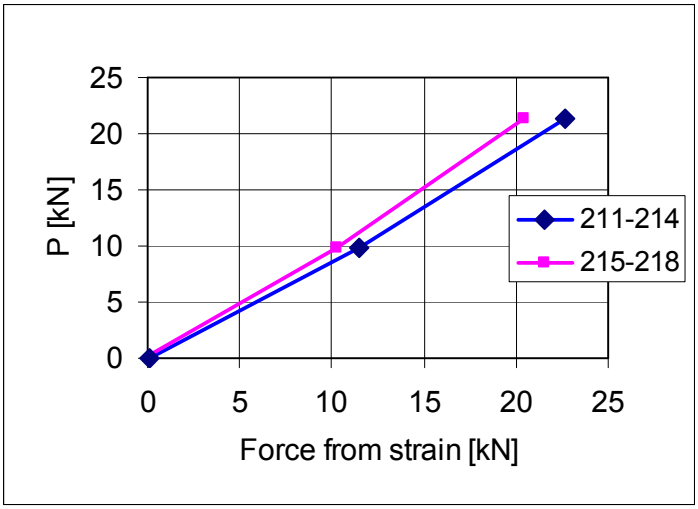

Fig. 29. Force in end plate of trimmer beam, calculated from stress distribution before yielding.

4. Results of floor tests

4.1 General on floor tests

The type and date of each test are given in Table 2. The tests were carried out in the order in which they are mentioned in Table 3.

Table 3. Type of load, weight of loading equipment P_{eq} and date of test.

Test	Type of load	P_{eq} kN	Nov 2003
FT200:1x, FT200:2x	*Service*	*0.70*	*11*
FT200:3x	*Service*	*0.79*	*12*
FT200:1	Service	0.79	12
FT200:2, FT200:3	Service	0.79	12
FT200:4, FT200:5	Service	0.83	13
FT200:6	Service	0.73	14
FT200:7, FT200:8	Service	0.83	14
FT200:9, FT200:10	Service	0.73	17
FT200:11	Failure	0.83	18
FT200:12	Failure	0.79	18

The tests were carried out by keeping the rate of elongation of the actuator at a predefined level. When necessary, this level was shifted. The rate of loading is given later in Figs 31–33.

The first three tests (FT200:1x–FT200:3x) were repeated with a slightly different loading arrangements. In the latter three tests (FT200:1–FT200:3) there was a swivel above the actuator, in the first three tests the swivel was missing, see Fig 30. The aim of the swivel with two lubricated spherical surfaces was to eliminate the possible eccentricity of the vertical load. Obviously the role of the swivel was unimportant in these tests because the results were both quantitatively and qualitatively very close to each other in both test series. Therefore, the results obtained without the swivel (i.e. tests FT200:1x–FT200:3x) are not documented and discussed in this report. The swivel was also applied in test FT200:12.

In tests FT200:4–FT200:11 a single actuator with three rotational degrees of freedom at its both ends was used and no extra arrangement to eliminate eccentricity was necessary.

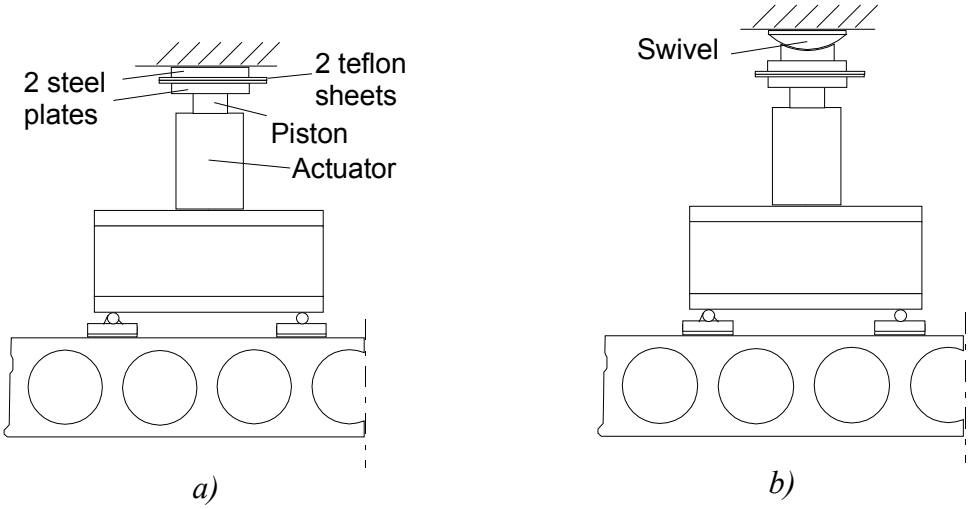

Fig. 30. Load arrangements above hydraulic actuator. a) Tests FT200:1x–FT200:3x. b) Tests FT200:1–FT200:3 and FT200:12.

4.2 Rate of loading

Before each test the measuring devices were zero-balanced. The load was increased monotonously up to a value which was estimated to be 50% or less of the failure load. Figs 31 and 33 illustrate the rate of loading.

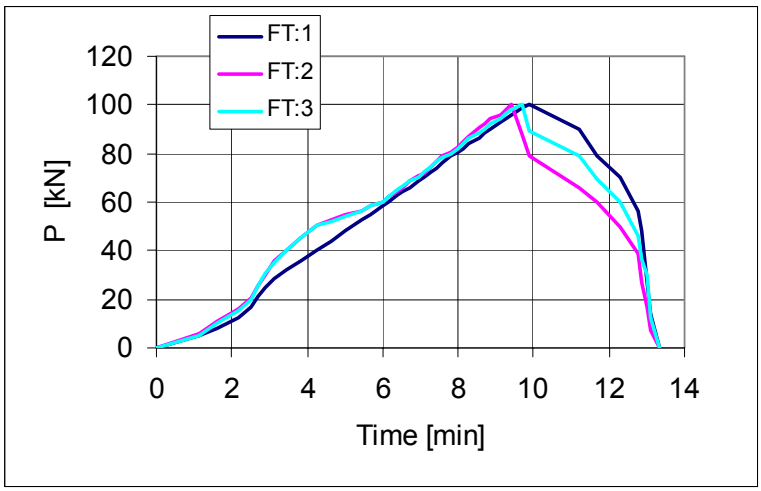

Fig. 31. FT200:1. Rate of loading in tests FT200:1–FT200:3.

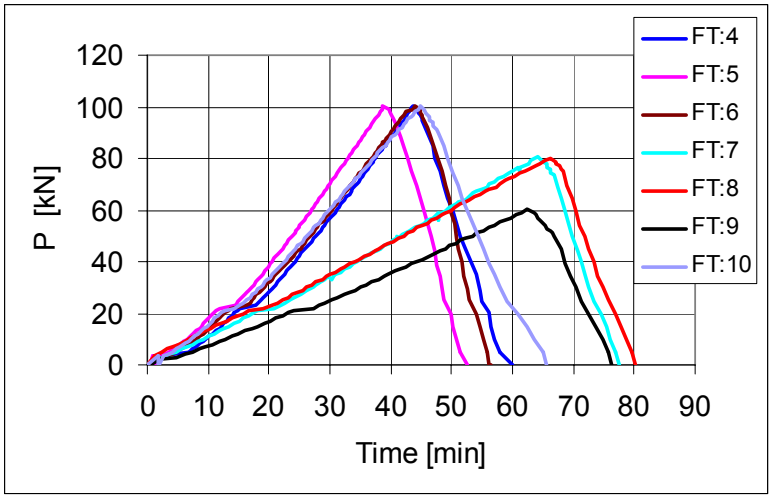

Fig. 32. Rate of loading in tests FT200:4–FT200:10.

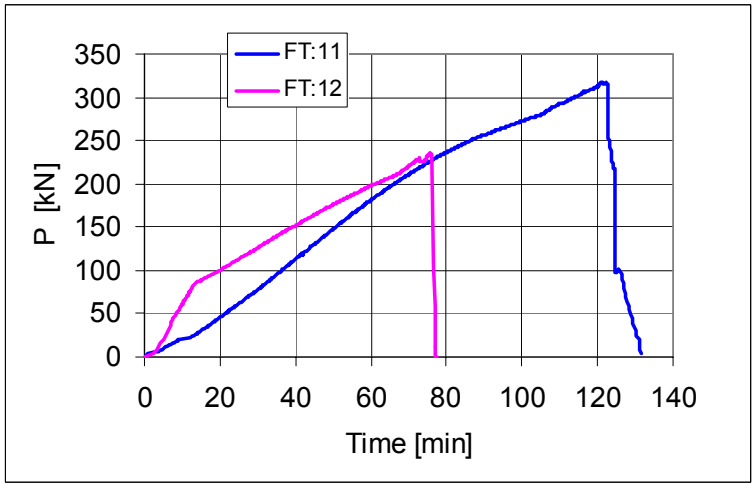

Fig. 33. Rate of loading in tests FT200:11–FT200:12.

4.3 Cracking pattern and failure load

4.3.1 Cracking pattern after service tests

Before the tests, the longitudinal joints between adjacent slabs were precracked on purpose and the tie beams were at least partly cracked along the slab ends, obviously due to the shrinkage of the concrete. After the tests the tie beams were cracked throughout along slab ends. No other additional cracks could be seen after the service tests.

4.3.2 Failure load and cracking pattern after failure tests

In test FT200:11 the cracking of the soffit obviously started far before cracks could be observed on the top surface. Visually these cracks could not be seen without going below the floor which was not done for safety reasons, but the softening of the load displacement curves and the sounds heard supported the presented conclusion. At actuator load P = 317.1 the floor failed.

In test FT200:12 an inclined shear crack appeared in the edge of slab 3 at actuator load P = 201 kN. When increasing the load, this crack grew in width, other cracks appeared close to the first one and on the top surface. At actuator load P = 235.5 kN the floor failed.

The failure loads are given in Table 4. The cracking patterns after failure are shown in Figs 34–35 and in App. A, Figs 17–44.

Table 4. Actuator load P_{act}, weight of loading equipment P_{eq} and total load on floor F_{obs}.

Test	P_{act} kN	P_{eq} kN	F_{obs} kN
FT200:11	317.1	0.8	317.9
FT200:12	235.5	0.8	236.3

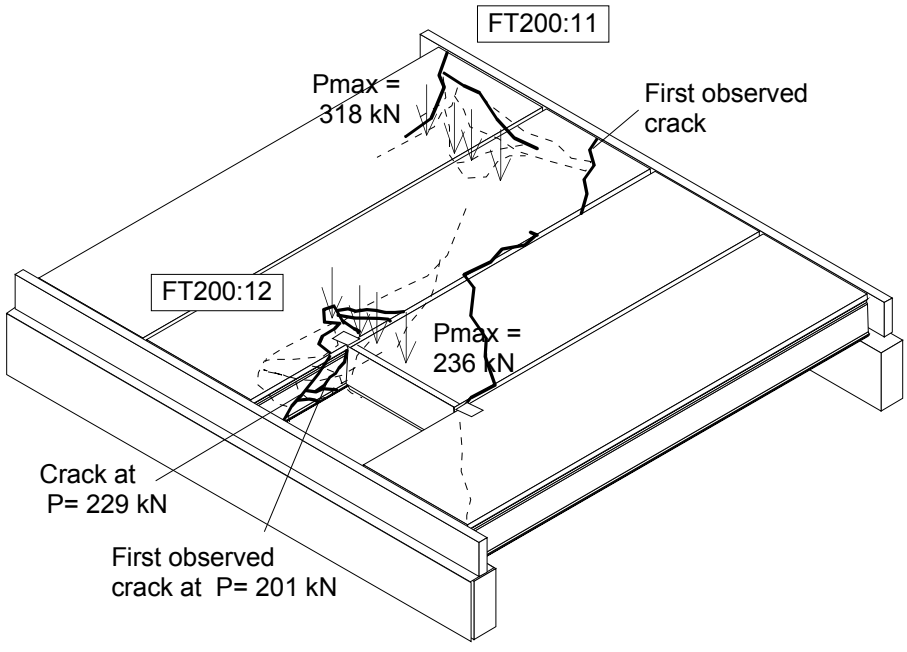

Fig. 34. Illustration of cracking after failure tests. The continuous lines correspond to cracks on the top surface of floor or at the edges of the opening, the dashed lines those on the soffit.

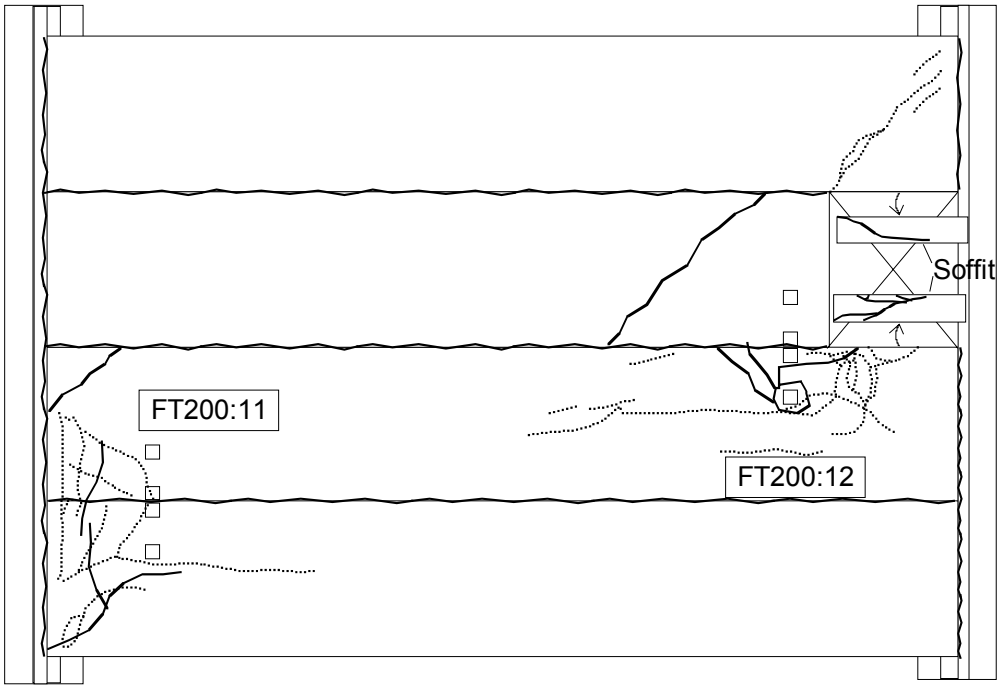

Fig. 35. Craks observed after tests FT200:11 and FT200:12. The continuous lines correspond to cracks on the top surface of floor or at the edges of the opening, the dotted lines those on the soffit.

4.4 General on measured results

The measured strains, crack widths and displacements are given graphically in Appendices D and E. Maximum and minimum values of other measured results are collected in Table 5 where the symbol Δ stresses the fact that the result tells the change of the measured property with respect to the start of the test, not the cumulative change with respect to the start of the whole test series.

Table 5. Maximum and minimum of measured results. Absolute value of differential horizontal displacement between upper and lower part of slab measured by transducers 21–38 ($\Delta u_{hor,edge}$), horizontal displacement of slab measured by transducers 51–58 ($\Delta u_{hor,opening}$), change in crack width (Δw_{crack}), settlement of supports ($\Delta \delta_{supp,max}$), maximum deflection ($\Delta \delta_{max}$) and strain in trimmer beam measured by transducers 211–218 ($\Delta \varepsilon_s$).

Test	$\Delta u_{hor,edge}$ mm	$\Delta u_{hor,opening}$ mm	Δw_{crack} mm	$\Delta \delta_{supp,max}$ mm	$\Delta \delta_{max}$ mm	$\Delta \varepsilon_s$ 10^{-6}
FT200:1	0.26	-0.04/0.015	-0.02/0.10		5.8	-40/60
FT200:2	0.16	-0.05/0.002	-0.10/0.12		4.3	-70/75
FT200:3	0.12	-0.18/0.02	-0.16/0.12		3.5	-200/200
FT200:4	0.15		-0.07/0.03	-0.07/0.10	2.4	-20/30
FT200:5	0.10		-0.07/0.02	-0.08/0.16	2.1	-40/45
FT200:6	0.25		-0.02/0.04	-0.09/0.20	3.2	-35/30
FT200:7	0.23		-0.14/0.05	-0.07/0.08	4.8	-100/120
FT200:8	0.31		-0.10/0.08	-0.07/0.11	5.2	-50/50
FT200:9	0.17		-0.01/0.06	-0.06/0.18	5.2	-35/45
FT200:10	0.14		-0.01/0.06	-0.05/0.20	3.5	-15/25
FT200:11[1)]	**0.70**		**-0.4/0.4**	**-0.25/0.07**	**13**	**-80/100**
FT200:12[2)]	**0.40**	**-0.5/0.2**	**-0.5/0.3**	**-0.5/0.3**	**12**	**-2000/2000**

1) Before yielding
2) Before start of failure (first unloading)

The measured results are discussed in more detail in the following few sections.

4.4.1 Deflection

Figs 36–71 illustrate the measured deflection of the floor along lines transverse to the slab direction. In service load tests the floor seemed to recover well after unloading. The recovering would have been more complete if the measurements with zero load had been continued after unloading.

It is likely that the failure in test FT200:11, taking place locally at a long distance from the load in test FT200:12, affected only slightly the results of the latter test.

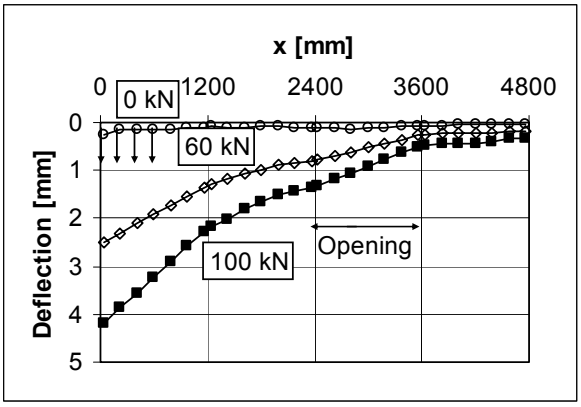

Fig. 36. FT200:1. Deflection measured by transducers 90–117 at 60, 100 and 0 kN.

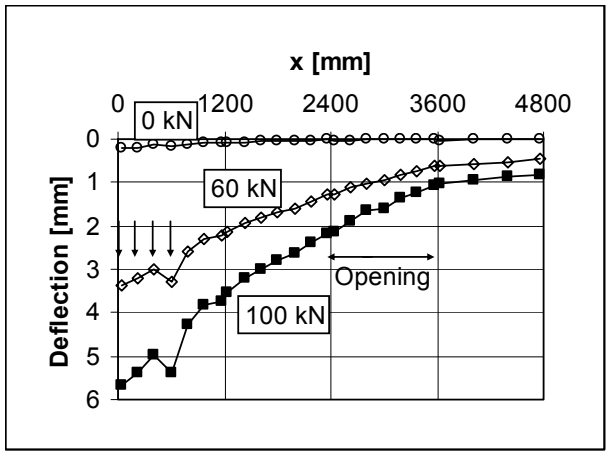

Fig. 37. FT200:1. Deflection measured by transducers 120–144 at 60, 100 and 0 kN.

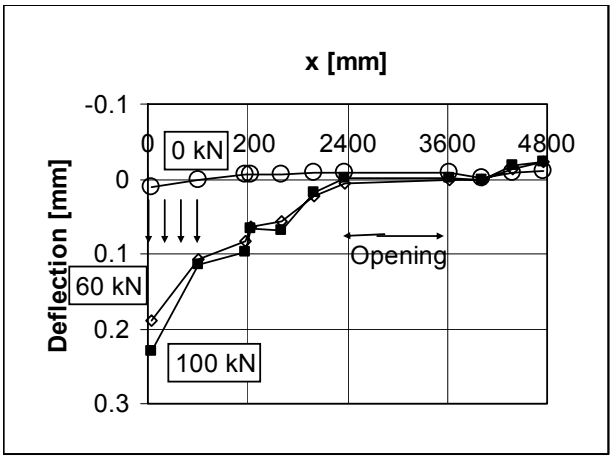

Fig. 38. FT200:1. Deflection measured by transducers 60–70 at 60, 100 and 0 kN.

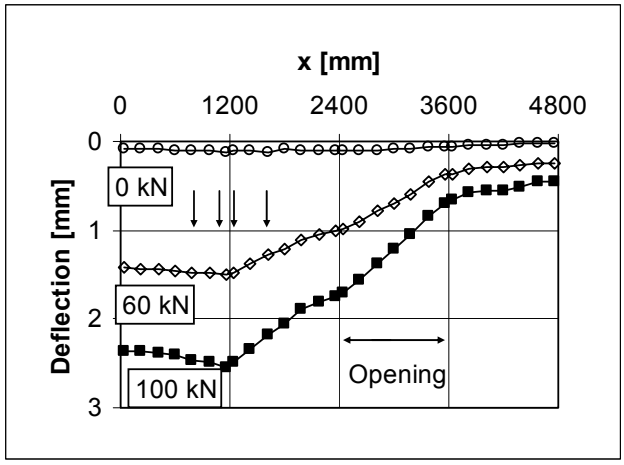

Fig. 39. FT200:2. Deflection measured by transducers 90–117 at 60, 100 and 0 kN.

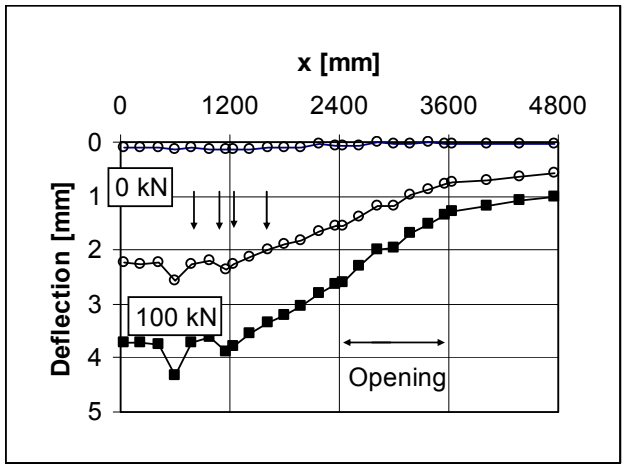

Fig. 40. FT200:2. Deflection measured by transducers 120–144 at 60, 100 and 0 kN.

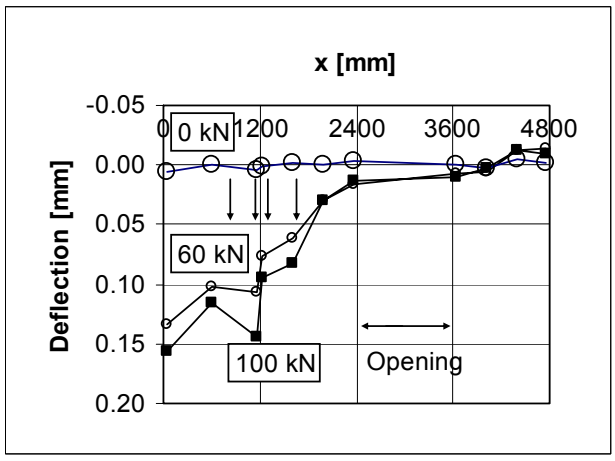

Fig. 41. FT200:2. Deflection measured by transducers 60–70 at 60, 100 and 0 kN.

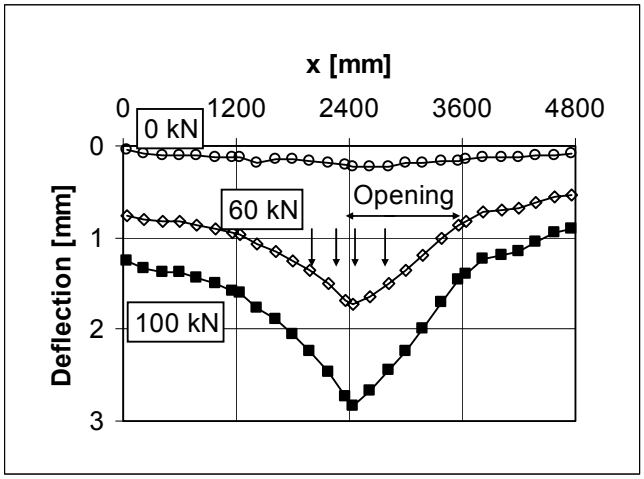

Fig. 42. FT200:3. Deflection measured by transducers 90–117 at 60, 100 and 0 kN.

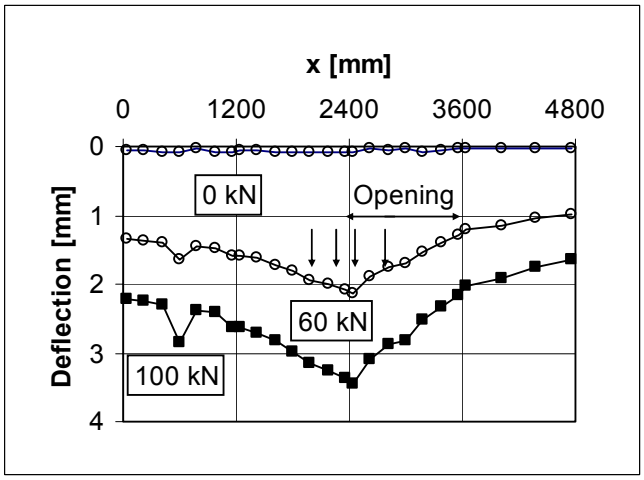

Fig. 43. FT200:3. Deflection measured by transducers 120–144 at 60, 100 and 0 kN.

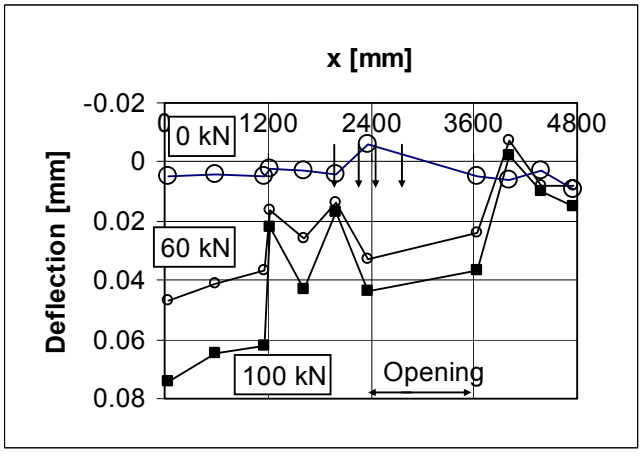

Fig. 44. FT200:3. Deflection measured by transducers 60–70 at 60, 100 and 0 kN.

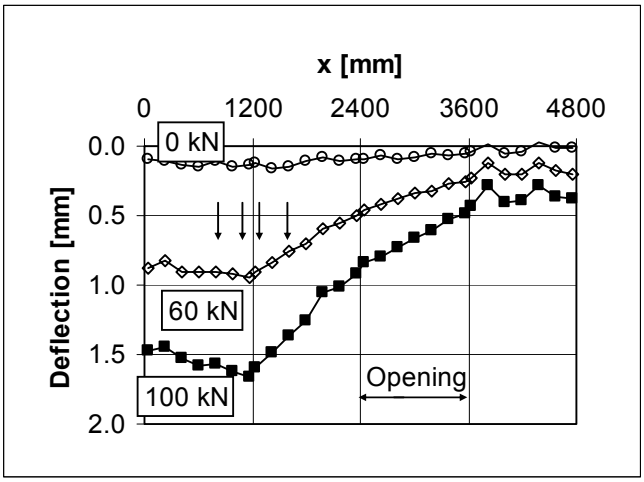

Fig. 45. FT200:4. Deflection measured by transducers 150–177 at 60, 100 and 0 kN.

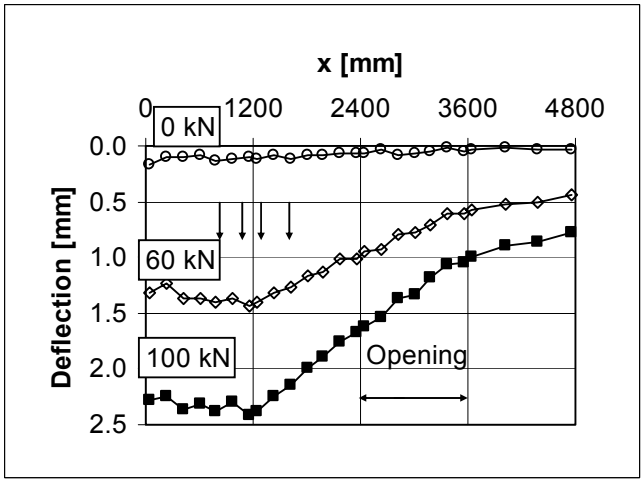

Fig. 46. FT200:4. Deflection measured by transducers 180–204 at 60, 100 and 0 kN.

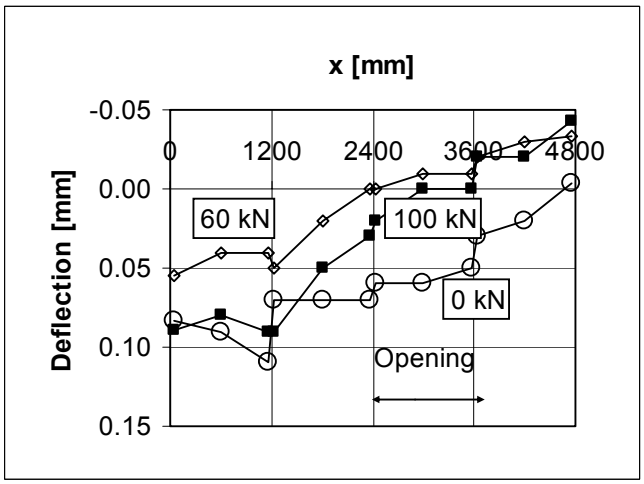

Fig. 47. FT200:4. Deflection measured by transducers 71–82 at 60, 100 and 0 kN.

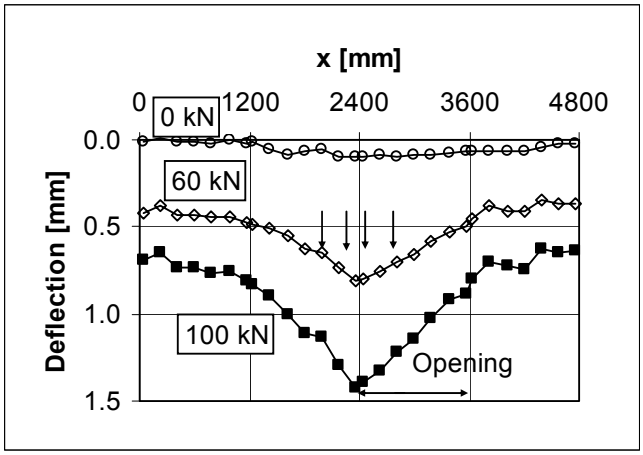

Fig. 48. FT200:5. Deflection measured by transducers 150–177 at 60, 100 and 0 kN.

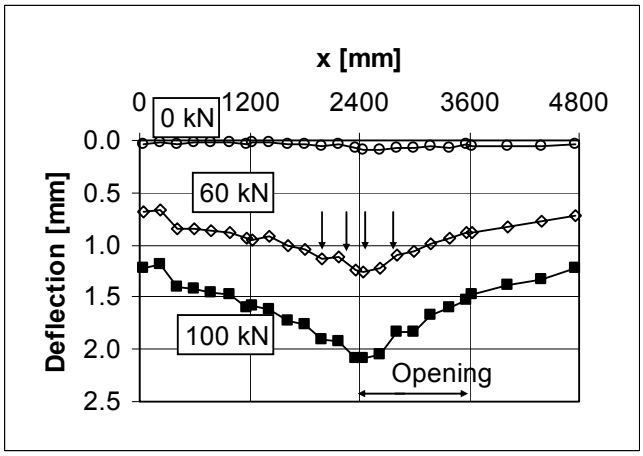

Fig. 49. FT200:5. Deflection measured by transducers 180–204 at 60, 100 and 0 kN.

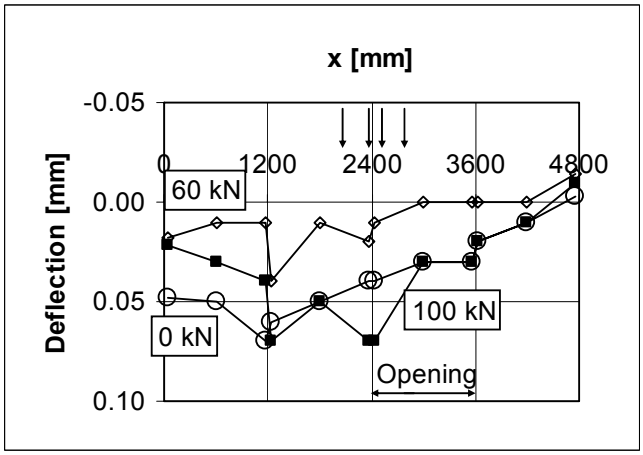

Fig. 50. FT200:5. Deflection measured by transducers 71–82 at 60, 100 and 0 kN.

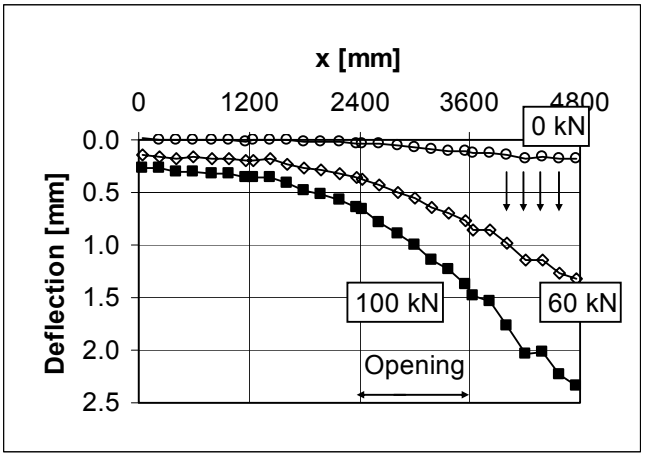

Fig. 51. FT200:6. Deflection measured by transducers 150–177 at 60, 100 and 0 kN.

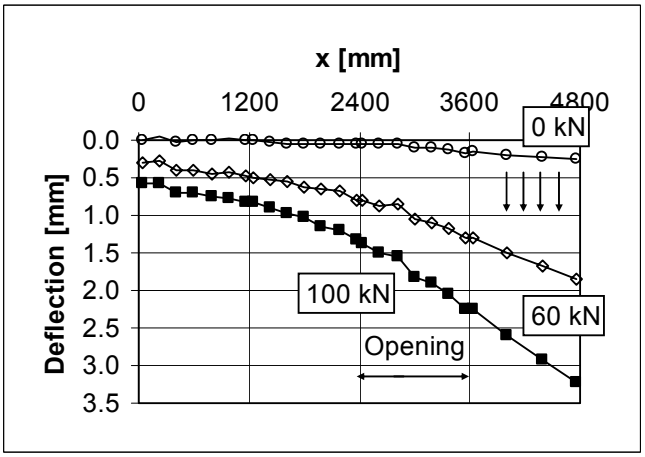

Fig. 52. FT200:6. Deflection measured by transducers 180–204 at 60, 100 and 0 kN.

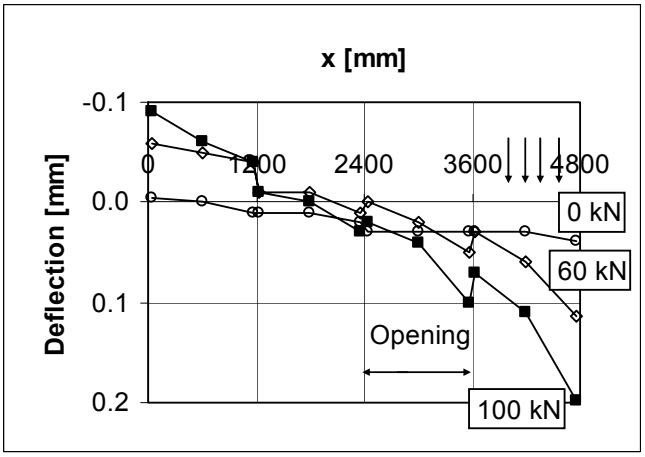

Fig. 53. FT200:6. Deflection measured by transducers 71–82 at 60, 100 and 0 kN.

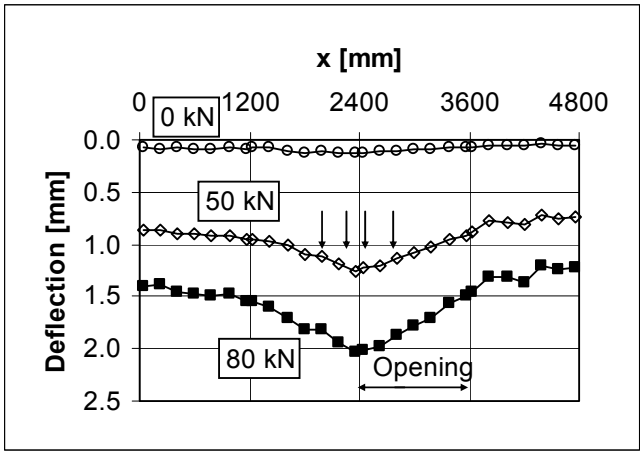

Fig. 54. FT200:7. Deflection measured by transducers 150–177 at 50, 80 and 0 kN.

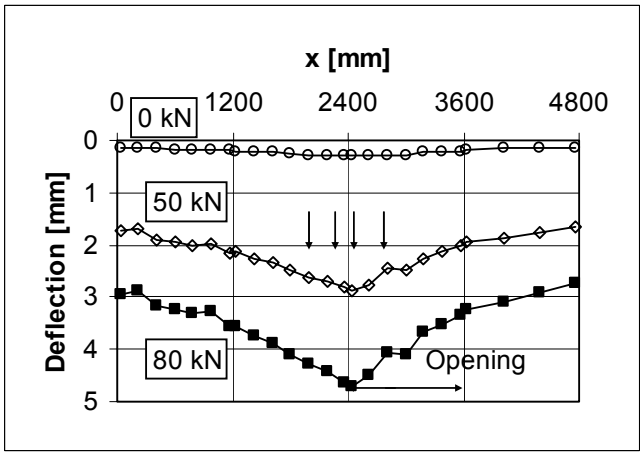

Fig. 55. FT200:7. Deflection measured by transducers 180–204 at 50, 80 and 0 kN.

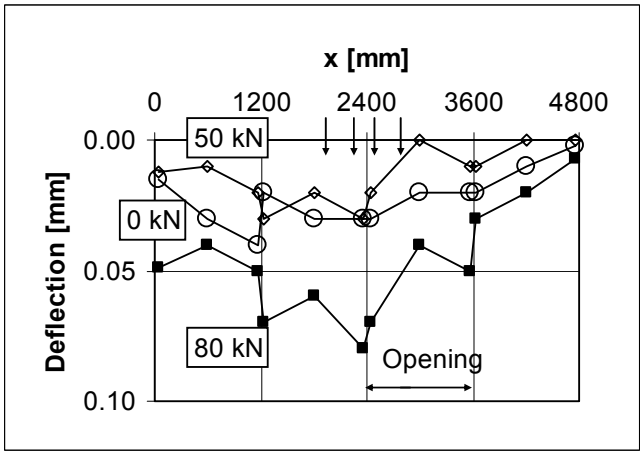

Fig. 56. FT200:7. Deflection measured by transducers 71–82 at 50, 80 and 0 kN.

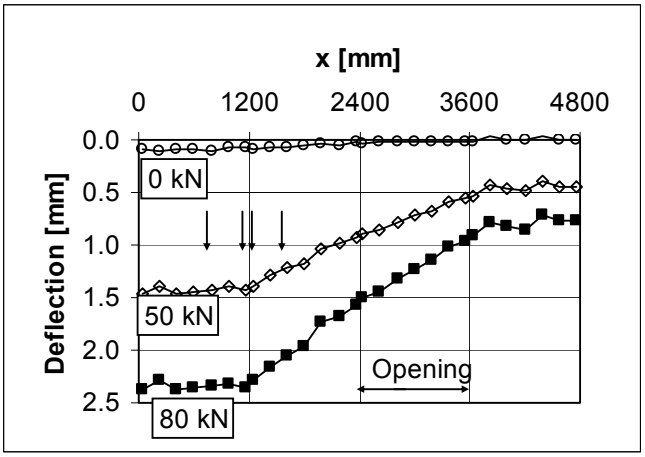

Fig. 57. FT200:8. Deflection measured by transducers 150–177 at 50, 80 and 0 kN.

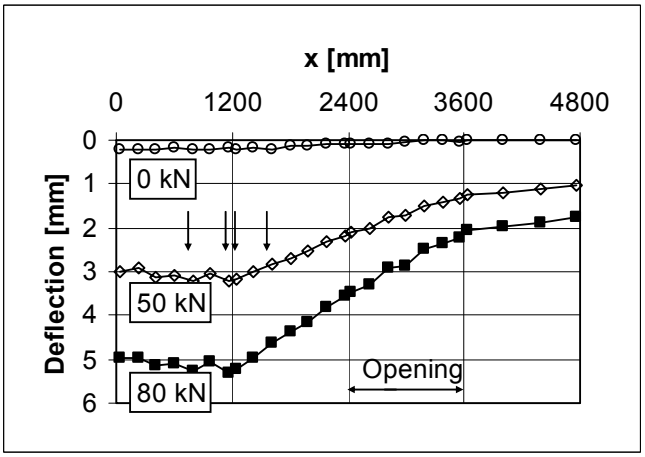

Fig. 58. FT200:8. Deflection measured by transducers 180–204 at 50, 80 and 0 kN.

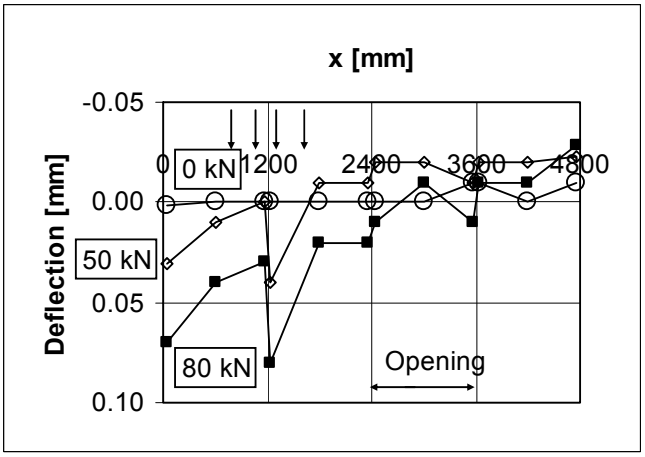

Fig. 59. FT200:8. Deflection measured by transducers 71–82 at 50, 80 and 0 kN.

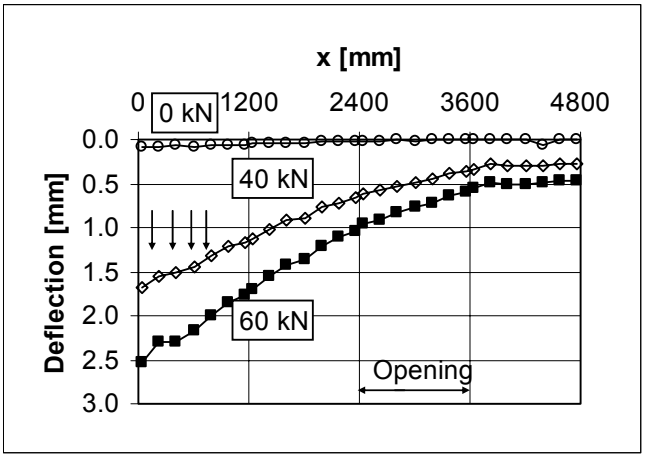

Fig. 60. FT200:9. Deflection measured by transducers 150–177 at 40, 60 and 0 kN.

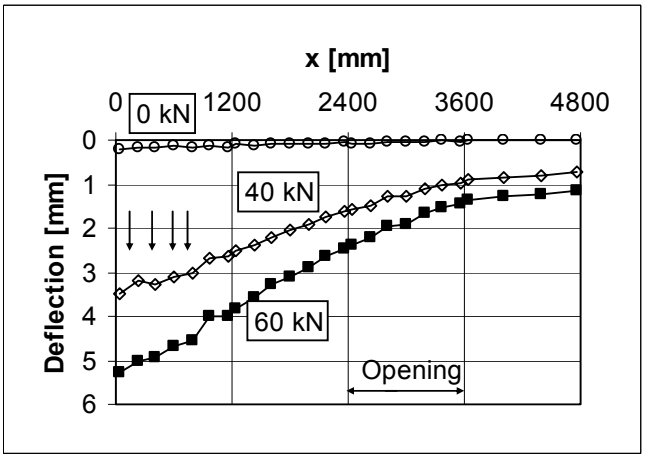

Fig. 61. FT200:9. Deflection measured by transducers 180–204 at 40, 60 and 0 kN.

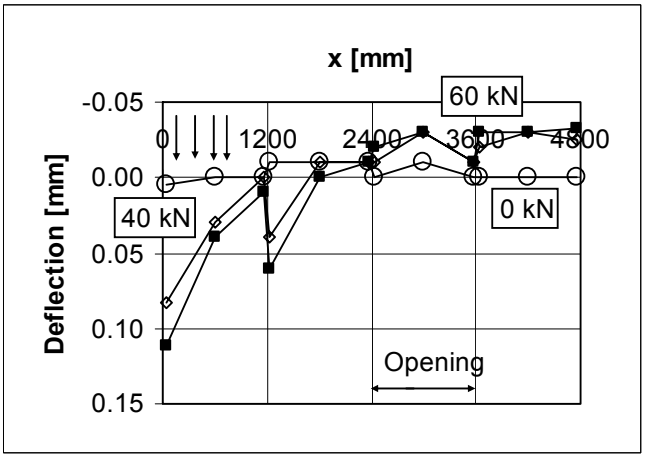

Fig. 62. FT200:9. Deflection measured by transducers 71–82 at 40, 60 and 0 kN.

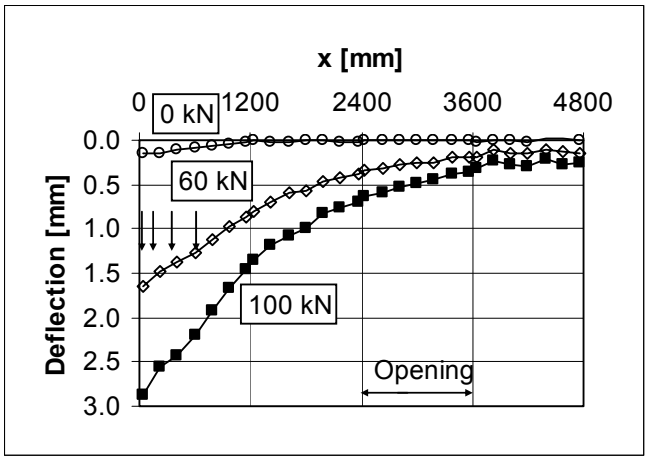

Fig. 63. FT200:10. Deflection measured by transducers 150–177 at 60, 100 and 0 kN.

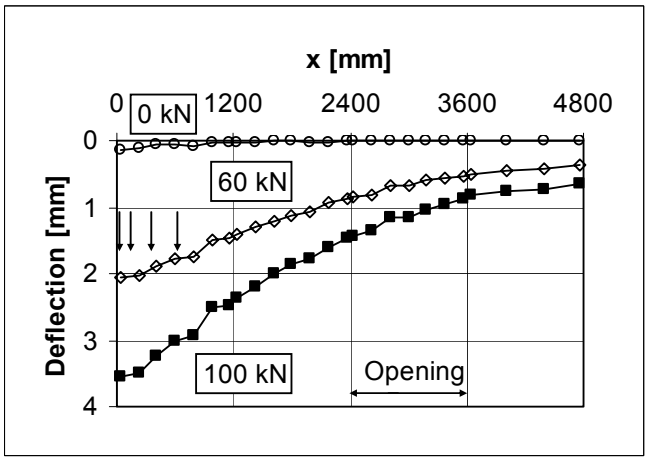

Fig. 64. FT200:10. Deflection measured by transducers 180–204 at 60, 100 and 0 kN.

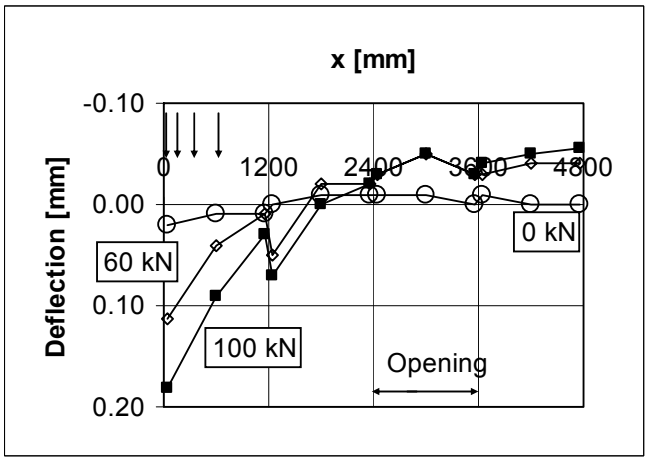

Fig. 65. FT200:10. Deflection measured by transducers 71–82 at 60, 100 and 0 kN.

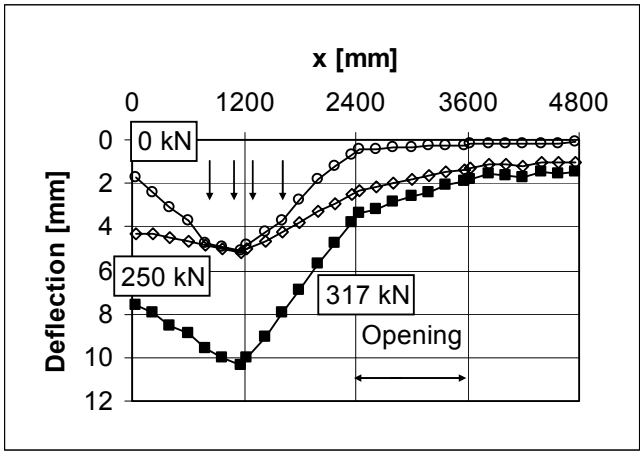

Fig. 66. FT200:11. Deflection measured by transducers 150–177 at 250, 317 (failure load) and 0 kN.

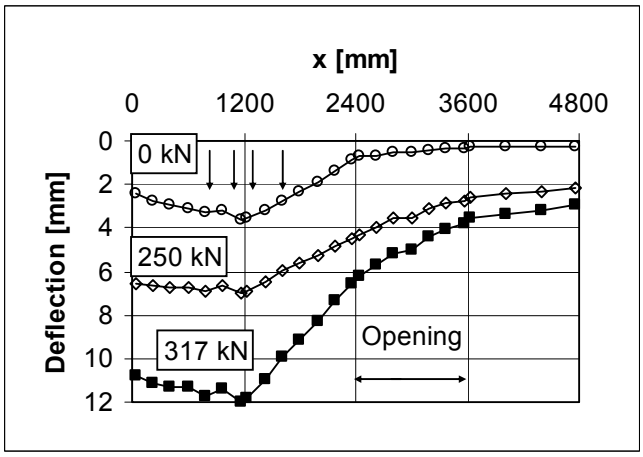

Fig. 67. FT200:11. Deflection measured by transducers 180–204 at 250, 317 (failure load) and 0 kN.

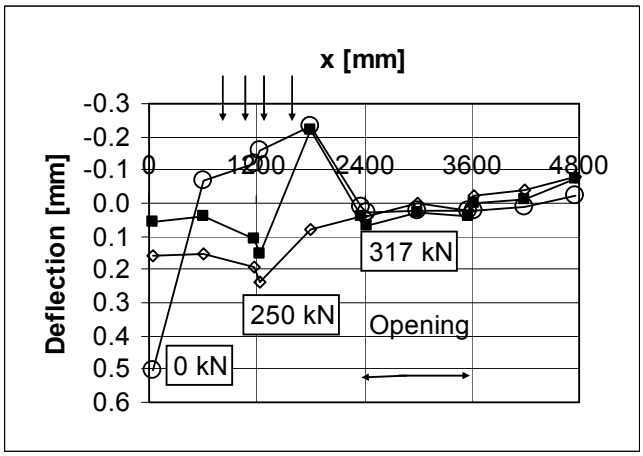

Fig. 68. FT200:11. Deflection measured by transducers 71–82 at 250, 317 (failure load) and 0 kN.

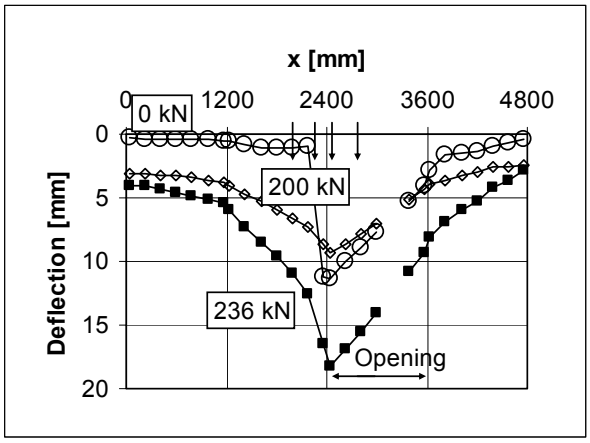

Fig. 69. FT200:12. Deflection measured by transducers 90–117 at 200, 236 (failure load) and 0 kN.

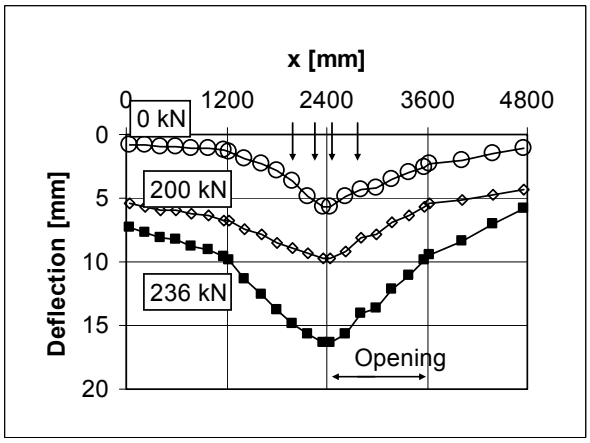

Fig. 70. FT200:12. Deflection measured by transducers 120–144 at 200, 236 (failure load) and 0 kN.

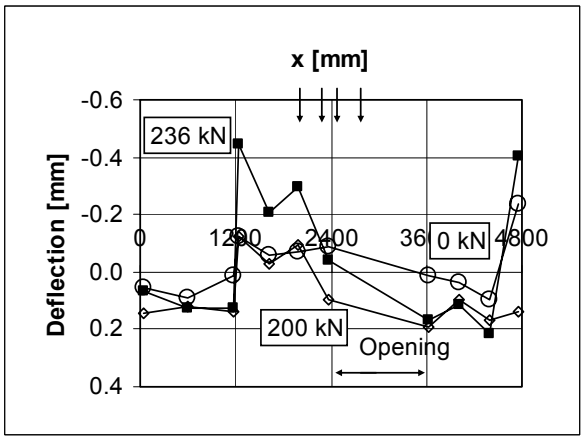

Fig. 71. FT200:12. Deflection measured by transducers 60–70 at loads 200, 236 (failure load) and 0 kN.

In Figs 72–75 the deflection measured in failure tests is compared with the deflection measured in service test. Both deflections correspond to the maximum load in service test. The deflections coincide rather well despite the permanent deformations and cracking which had taken place before the failure tests had been started.

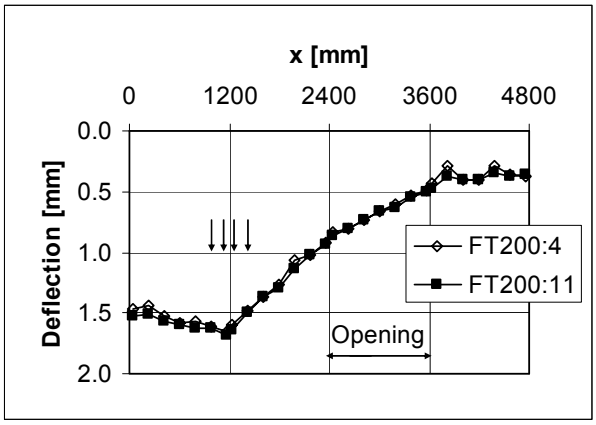

Fig. 72. FT200:4 and FT200:11. Deflection measured by transducers 1500–177 at load 100 kN.

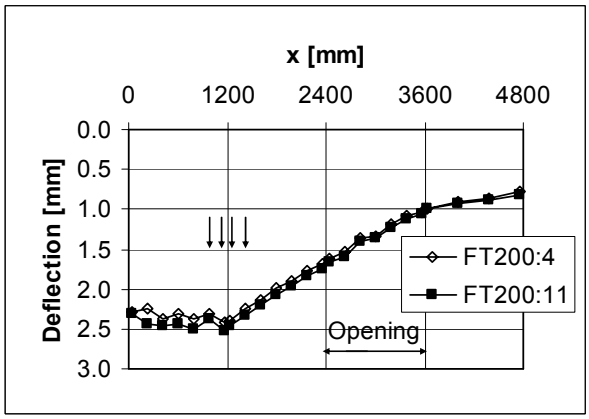

Fig. 73. FT200:4 and FT200:11. Deflection measured by transducers 180–204 at load 100 kN.

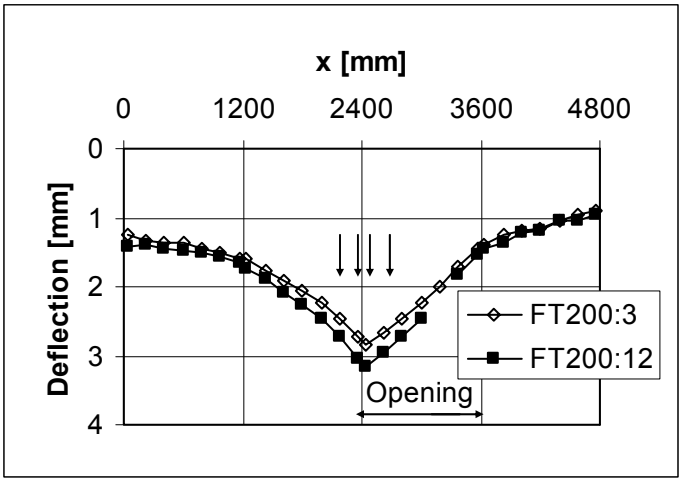

Fig. 74. FT200:3 and FT200:12. Deflection measured by transducers 90–117 at load 100 kN.

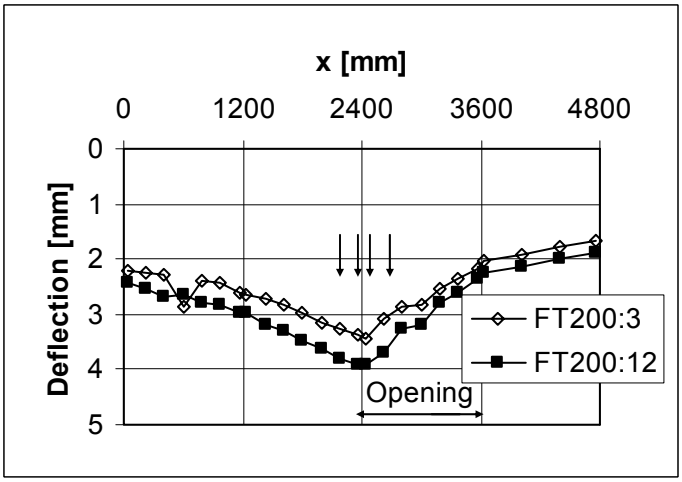

Fig. 75. FT200:3 and FT200:12. Deflection measured by transducers 120–144 at load 100 kN.

4.4.2 Transverse horizontal motion of slab edges

Fig. 76 illustrates how the horizontal motion of the slab edge was measured. A 30x30 mm^2 piece of thin metal sheet was glued to the slab edge. Efforts were made to place the piece as vertical as possible, but it is possible that a deviation of the order of 0.1 mm / 5 mm from the vertical axis remained. This means that the displacements measured by transducers 21–38 cannot be too accurate.

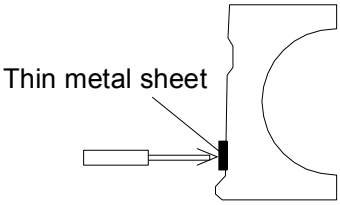

Fig. 76. Measuring horizontal motion of slab edge.

4.4.3 Crack width

The changes in crack width during the service load tests remained smaller or equal to the crack width measured after precracking. In the service load tests the change due to the loading disappeared after unloading almost completely which shows that the response of the floor was almost elastic.

Before failure or yielding in the failure tests the crack widths also remained small, not higher than 0.4 mm. This indicates that the tie beams connecting the slab ends worked as intended.

4.4.4 Settlement of supports

The vertical displacement measured at a distance of 30 mm from slab ends is here called settlement of supports. It is affected at least by four major effects:

1) Vertical compressive strain of the grout below the slab end
2) Compression at the interface between the supporting beam and the floor of the laboratory
3) Rotation of slab end around an axis other than the assumed one at a distance of 30 mm from slab
4) Uplift due to concentrated load.

The measured displacements are small but cannot be totally ignored when verifying computer models with the aid of the measured floor response.

4.4.5 Tilting and sliding of supporting beams

When a floor is loaded as in the tests, see Fig. 77, the soffit of the slab tends to elongate. If this elongation is not free, which was the case in the tests, a horizontal force H is induced into the slab. This horizontal force tends to move the supporting beams apart.

At the same time, the eccentric support reactions of the floor tend to turn the upper ends of the beams inwards closer to each other. Fig. 77.b illustrates the resulting forces which the beams are subjected to. Since the vertical force on support B is much higher than that on support A, so is also the friction force and if one of the beams slides, it will be beam A. Due to the higher bending moment on beam B, if tilting occurs, it tends to be to the left.

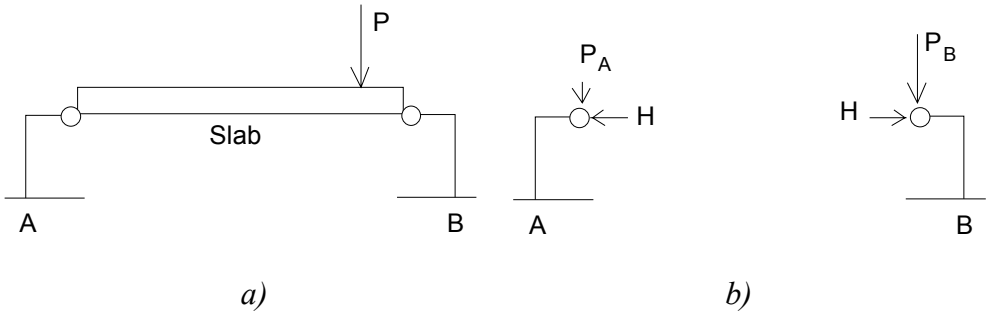

Fig. 77. Schematic diagram about behaviour of supporting beams A and B. a) Mechanical model. b) Forces on beams.

The horizontal motion of the supporting beams in the direction of the slabs was measured by transducers 11–18. The results are illustrated in App. G with figures which show the position of the beam with regard to its position before the test at different load levels. These figures show that in all cases the beam at the loaded end of the floor moved inwards, the opposite beam outwards, i.e. both beams moved to the direction from the loaded end of the slab to the unloaded one as expected.

The figures in App. G show that after unloading the lower transducers showed almost zero displacement in all service load tests but this was not the case in failure tests. It can be deduced that there the beams slided along the floor of the laboratory in failure tests, but they did not slide in the service load tests. Even in the failure tests the major part of the horizontal displacements of the supporting beams was attributable to the tilting.

4.4.6 Load carried by the trimmer beam

When considering the behaviour of the trimmer beam, the most interesting tests were FT200:3 and FT200:12 in which slab 2, supported by the trimmer beam, was loaded close to the opening. Since the response of the test specimen in test FT200:3 was very close to that in the initial part of test FT200:12, only the latter test is considered here.

In Figs 78–81 the strain measured by the strain gauges 211–218 in test FT200:12 and in test on trimmer are shown. The strains in test FT200:12 are so small when compared

with the strains in trimmer beam test, see Chapter 3 and Fig. 81, that the almost linear relationship between the strains and load observed in the latter test can be used for estimation of the load carried by the trimmer beam in test FT200:12.

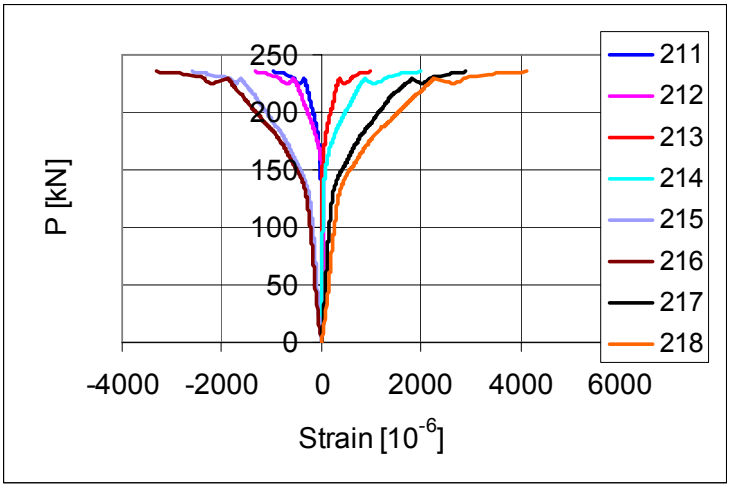

Fig. 78. FT200:12. Strain measured by transducers 211–218 before failure.

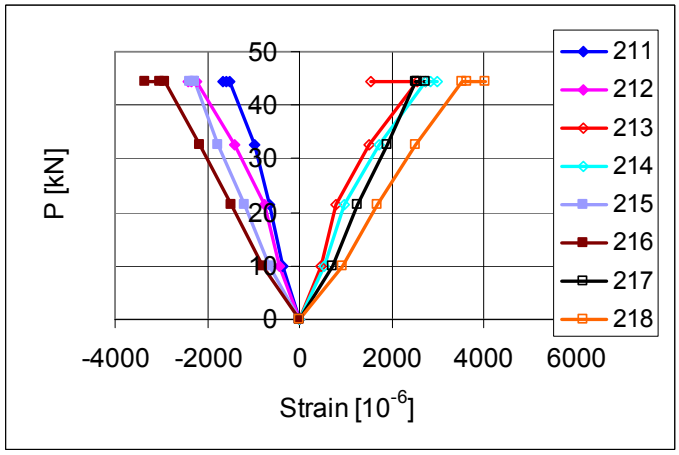

Fig. 79. Test on trimmer beam. Strain measured by transducers 211–218 before unloading.

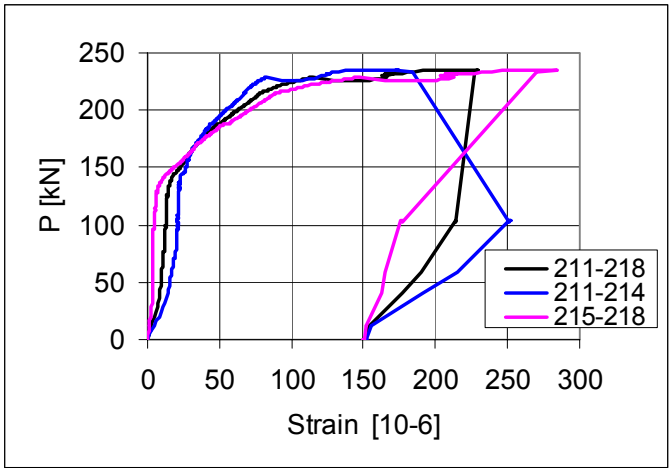

Fig. 80. FT200:12. Average strain measured by transducers 211–218.

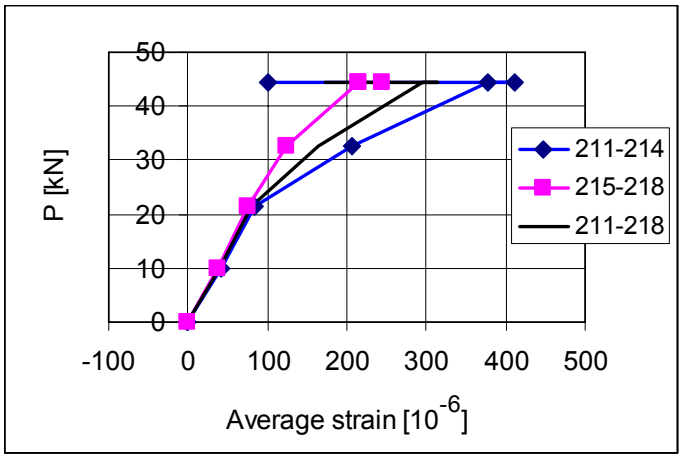

Fig. 81. Test on trimmer beam. Average strain measured by transducers 211–218 before unloading.

To estimate roughly the load carried by the trimmer beam, Figs 80 and 81 are applied using the following assumptions:

1. The reaction force due to the self weight of slab 2 (10 kN) is completely carried by the trimmer beam.
2. The load carried by the trimmer beam follows the measured average strains as curve 211-218 in Fig. 81.
3. In test FT200:12 the average strain corresponding to actuator load P is the one taken from curve 211–218 in Fig. 80.

In this way, Table 6 is obtained. 50% of the total actuator load *P* was directly on slab 2. The share of 0.5*P*, carried by the trimmer beam, is illustrated in Fig. 82. This rough

estimation shows that the longitudinal joints between slabs carry a major part of the load on the slab supported by the trimmer beam.

Table 6. FT200:12. Actuator load P, average strain ε_{P+G} in trimmer beam due to P and self weight of slab G, as well as part of P carried by trimmer beam R_P.

P kN	0.5P kN	ε_{P+G} 10^{-6}	R_{P+G} kN	R_P kN
0	0	40	10	0
100	50	50	12	2
160	80	68	18	8
200	100	105	26	16
229	115	160	33	23
234	117	225	38	28
236	118	280	45	35

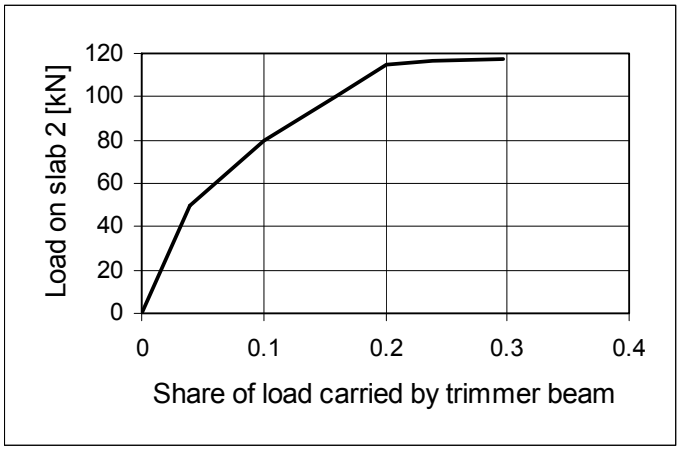

Fig. 82. FT200:12. Contribution of trimmer beam on the load-carrying mechanism.

5. Strength of concrete

The strength of the concrete was measured from 50 x 50 mm cores for the slab units and from 150 mm test cubes for the cast-in-situ concrete. The results are given in Tables 7–9. After drilling the cores were covered with plastic in such a way that they were still wet when tested. The test cubes were kept in the same temperature and relative humidity as the floor test specimen until testing.

Table 7. Strength and density of 50 x 50 mm cores drilled from slab unit 1 and tested on 21th of November 2003.

Specimen	Strength MPa	Density kg/m^3
L1	56.5	2390
L2	56.0	2400
L3	57.0	2380
L4	52.5	2380
L5	53.5	2370
L6	58.0	2380
Mean x	55.6	2383
Standard deviation s	2.1	10
Characteristic strength $f_{ck,C50} = x–1.65s$	52.1	

Table 8. Strength and density of 150 mm test cubes cast from grouting in the longitudinal joints and tested on 18th of November 2003.

Specimen	Strength MPa	Density kg/m3
S2	41.5	2260
S3	40.0	2230
S4	41.0	2240
S5	41.5	2250
S6	42.0	2250
Mean x	41.2	2246
Standard deviation s	0.76	
Characteristic strength $f_{ck,K150} = x–1.65s$	39.9	

Table 9 . Strength and density of 150 mm test cubes cast from the tie beams and tested on 18th of November 2003.

Specimen	Strength MPa	Density kg/m^3
P2	34.0	2220
P3	34.5	2240
P4	34.5	2230
P5	34.5	2230
P6	36.0	2250
Mean x	34.7	2234
Standard deviation s	0.76	5
Characteristic strength $f_{ck,K150} = x - 1.65s$	33.4	

6. Analysis of results

6.1 Error in measured deflections

The deflection of the floor was measured using transducers, a part of which were provided with springs. The transducers were placed on long, relatively flexible steel beams, the ends of which were supported by stands placed on the floor of the laboratory. When the floor was loaded, the spring force in the transducers slightly relaxed and the beam spanning over the floor deflected. In other words, the transducers were fixed to a beam that also moved. Hence they did not measure the absolute deflection of the floor exactly. The error due to this approximation is considered in Appendix F and proved to be small.

6.2 Evaluation of observed resistance in failure tests

It is assumed that the strength measured from 50 mm drilled cores gives directly the cubic strength measured from 150 mm cubes and that the cylinder strength is equal to 85% of the cubic strength. In this way, the lower characteristic cylinder strength $f_{ck,C150}$ (150 x 300 mm cylinders) given in Table 10 is obtained. From this, the mean tensile strength

$$f_{ctm} = 0.30 f_{ck,C150}^{2/3} \tag{1}$$

and the lower characteristic tensile strength

$$f_{ctk} = 0.70 f_{ctm} \tag{2}$$

are obtained according to Eurocode 2 [2].

Table 10. Strength $f_{c,C50}$ measured from 50 mm cores, corresponding cylinder strength $f_{c,C150}$ and mean tensile strength f_{ctm}.

	$f_{c,C50}$ MPa	$f_{c,C150}$ MPa	f_{ctm} MPa
FT200	52.1	44.3	3.76

To give an impression about the shear resistance observed in tests FT200:11–FT200:12, a virtual load test FT200V is analysed according to the product standard EN 1168 [1]. In this test a single slab element, identical to those in floor test and with similar support conditions, is loaded with a transverse line load P at a distance of 830 mm from slab end.

The cross-sectional characteristics of the slab are calculated from the measured cross-section shown in Fig. 83 with the exception that the measured value 276 mm, see App. B, is used for b_w, the sum of the web widths.

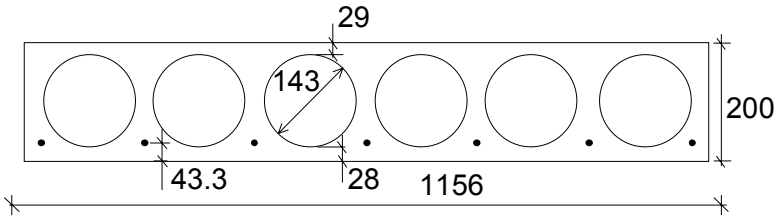

Figure 83. Geometry used for calculating A, S and I.

The transfer length l_{pt} is calculated according to Eurocode 2 from

$$l_{pt} = \frac{1.25 \cdot 0.19 \cdot (12.5\,\text{mm}) \cdot ((900 - 50)\,\text{MPa})}{3.2 \cdot 0.7 \cdot \left(0.30 f_{ck,C150}^{2/3} / \gamma_c\right)} \tag{3}$$

where $f_{ckC,150}$, the strength at the release of the prestress, is assumed to be 70% of the cylinder strength 44.3 MPa. It is also assumed that the steel stress after the release is equal to 850 MPa.

Including γ_c in expression 3 is confusing, because later in the code it is stated that " The design value of transmission length should be taken as the less favourable of two values, depending on the design situation : $l_{pt1} = 0.8 l_{pt}$ or $l_{pt2} = 1.2 l_{pt}$." This suggests that the characteristic value for l_{pt} is obtained using a nationally determined safety factor which cannot be tuned for the transfer length only. Due to this confusion, the transfer length is calculated using two values for $\gamma_c = 1.0$ and 1.5. In this way $l_{pt} = 391$ mm and $l_{pt} = 587$ mm are obtained.

The results of the calculations are given in Table 10. Two values are obtained for the predicted shear resistance: $V_{u,pre} = 185$ kN and 175 kN with transfer length 391 mm and 587 mm, respectively. In Table 11 also the imposed load $P_{u,pre}$ corresponding to the shear resistance is given.

Table 11. Virtual shear test ST200V. Weight of slab per unit length g, distance from centroid of strands to the bottom fibre e_p, distance from centroidal axis to bottom fibre e, sum of web widths b_w, cross-sectional area A, second moment of area I and first moment of area above centroidal axis S, assumed transfer length l_{pt}, predicted shear resistance $V_{u,pre}$ and imposed load $P_{u,pre}$ corresponding to the predicted shear resistance.

g kN/m	e_p mm	e mm	b_w mm	A mm^2	I mm^4	S mm^3	l_b mm	$V_{u,pre}$ kN	$P_{u,pre}$ kN
3.28	43	99	276	138200	$6.581 \cdot 10^8$	$4.412 \cdot 10^6$	391	186	196
"	"	"	"	"	"	"	587	176	186

A reference test with one slab unit and with the same shear span, span of slab , support conditions and loading arrangements as for slab 3 in load test FT200:11 was performed after the floor test, see Fig. 84 and the report [3].

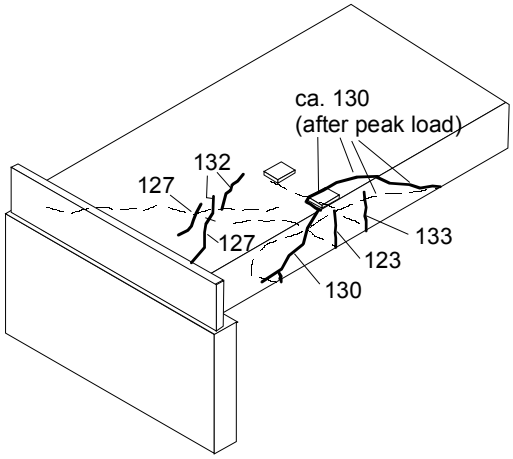

Figure 84. Failure pattern in test ST200E2M [3]. The numbers refer to actuator load.

The ultimate load in the reference test was 133.5 kN. In test FT200:11 the ultimate load on one slab was 159 kN = 0.5 · 317.0 kN (actuator load) + 0.5 · 0.83 kN (weight of loading equipment). So, the neighbouring slabs increased the load-carrying resistance by 19% even though one of the neighbours was loaded with a similar load. On the other hand, the ultimate load on one slab in test FT200:11 was 82–86% of the predicted ultimate load for a single slab with uniformly distributed line load. This difference is explained by the eccentricity of the load.

7. Discussion

The test specimens seemed to be typical of normal production. The strength of the concrete was high enough and the slippage of the strands was small in all elements. The loading and measuring equipment worked as intended with some insignificant exceptions.

In service load tests the response of the floor was nearly elastic. This can be seen from the nearly linear load-deflection relationship and from the fact that in the failure tests the initial part of the deflection curves followed closely the curve obtained in previous service load test with the same arrangements.

In view of the observed resistance in failure test FT200:11 the maximum loads might have been higher in service load tests FT200:4–FT200:10. On the other hand, the response of the floor was so linear in test FT200:11 far above load 100 kN that increasing the maximum loads in the service load tests would not have affected the observed response in the failure test too much.

There was a 1.0 x 1.2 m^2 opening at one end of the floor. A trimmer beam made of steel was used to carry the slab which ended at the opening. Tries were made to measure the contribution of the trimmer beam to the load-carrying mechanism. A rough estimation is that before failure the trimmer beam carried 20% and the grouted joints 80% of the imposed load on the slab.

The deflection of a floor tends to elongate the bottom fibre of the slabs and to push the supporting structures apart. In the present tests the supports were not rigid enough to prevent such an elongation but tilted. The tilting was measured to facilitate the interpretation of numerical simulations.

The main purpose of the tests was to provide experimental data for verification of computer models. In this sense the results look satisfactory.

References

1 EN 1168. Precast concrete products – Hollow core slabs. 2005.

2 EN 1992-1-1. Eurocode 2: Design of concrete structures – Part 1: General rules and rules for buildings. 2004.

3 Pajari, M. Shear-torsion interaction tests on single hollow core slabs. Espoo 2004. VTT Research Notes 2275. 76 p. + app. 122 p. http://www.vtt.fi/inf/pdf/tiedotteet/2004/T2275.pdf

Appendix A: Photographs

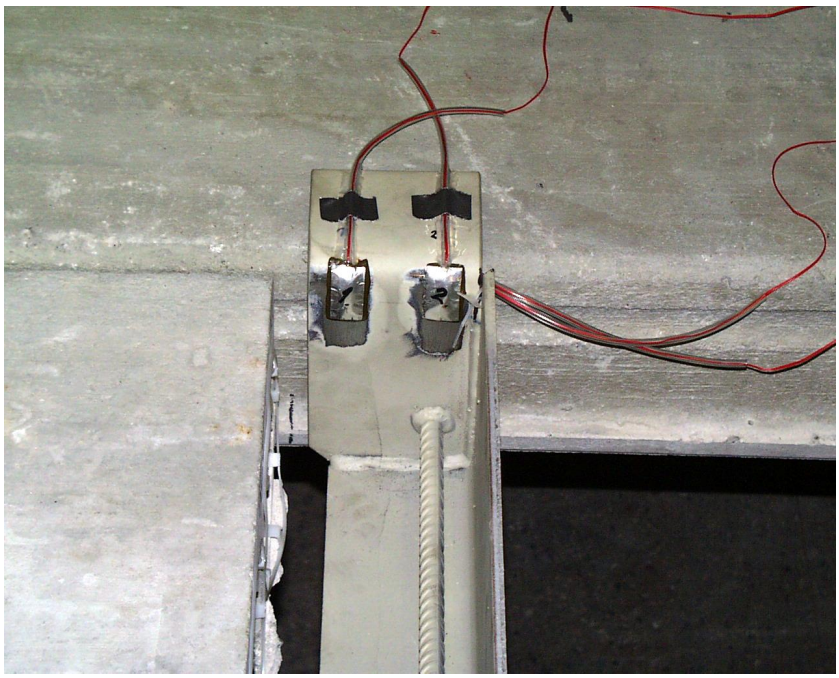

Fig. 1. Strain gauges on trimmer beam.

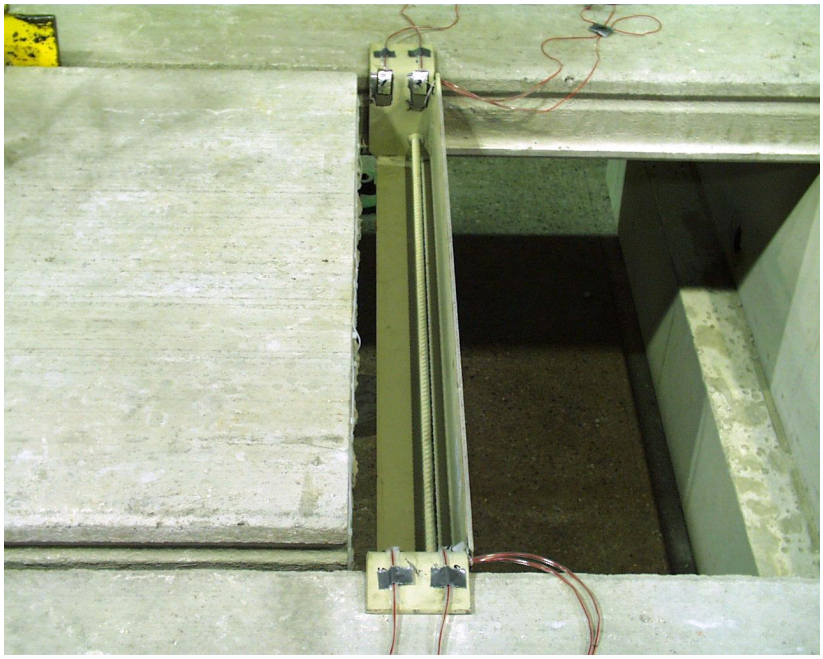

Fig. 2. Trimmer beam.

Fig. 3. Notching of slab to eliminate contact between trimmer beam and edge of slab.

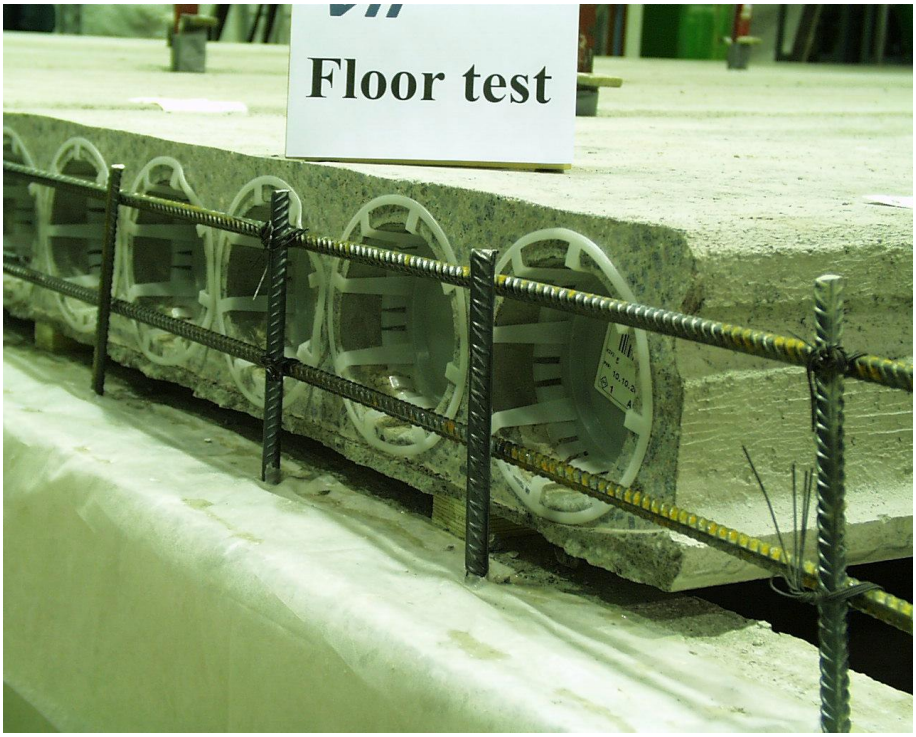

Fig. 4. Tie bars and plywood pads below slab at support.

Fig. 5. Tie bar in longitudinal joint. Note also wrapped wedges in the joint used later for precracking of joint.

Fig. 6. Overview on floor before grouting. The vertical objects in the joints are wedges.

Fig. 7. Overview on floor before grouting.

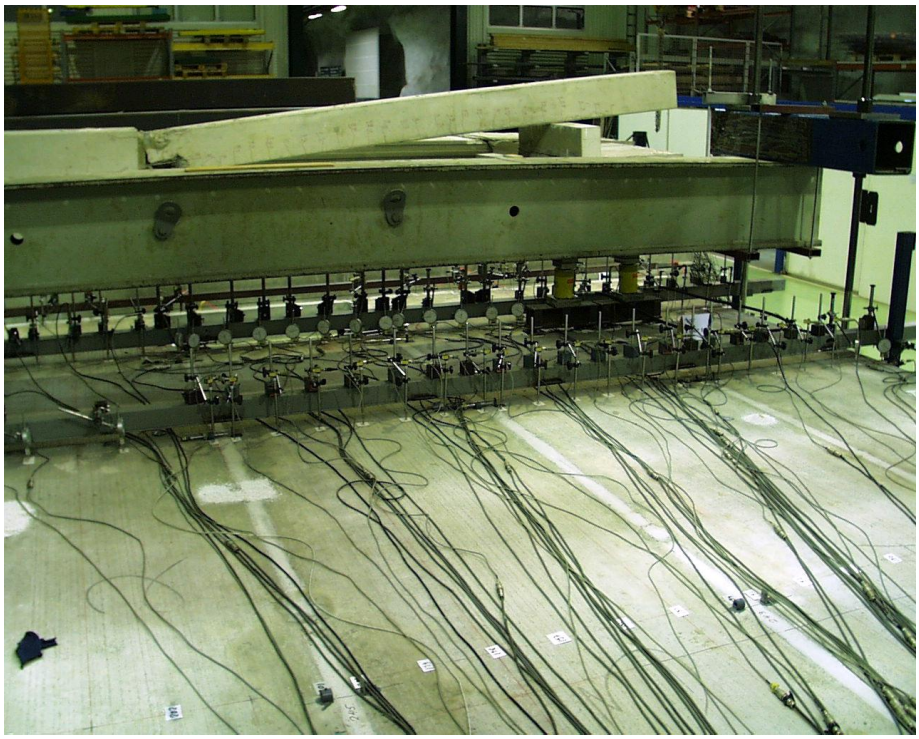

Fig. 8. Overview on floor before first test.

Fig. 9. Transducers for measuring horizontal displacement of outer edges of floor.

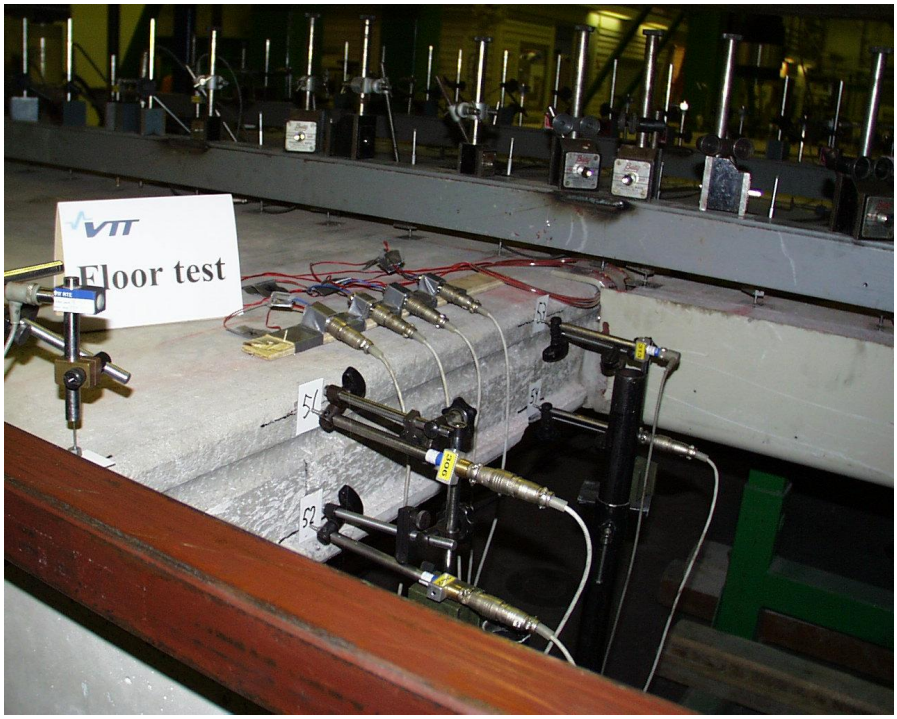

Fig. 10. Transducers for measuring transverse horizontal displacements at an edge of the opening.

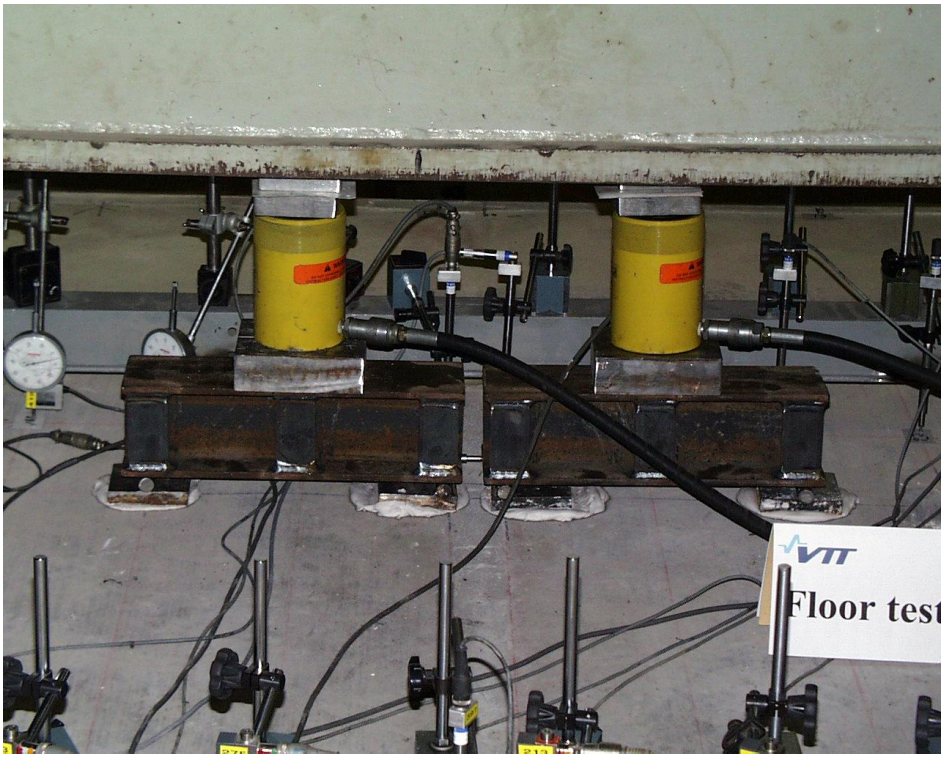

Fig. 11. FT200x:2. Loading arrangements. Note the two teflon sheets to eliminate horizontal friction between steel plates above the actuators.

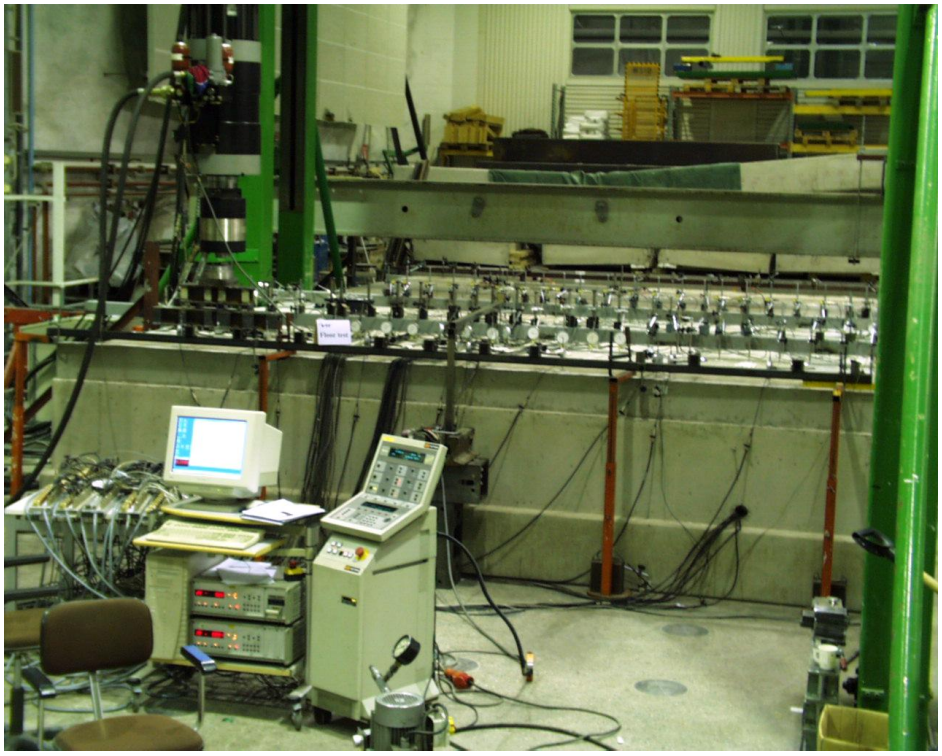

Fig. 12. FT200:6. Loading arrangements. Note the orange stands supporting the beam onto which the transducers are supported.

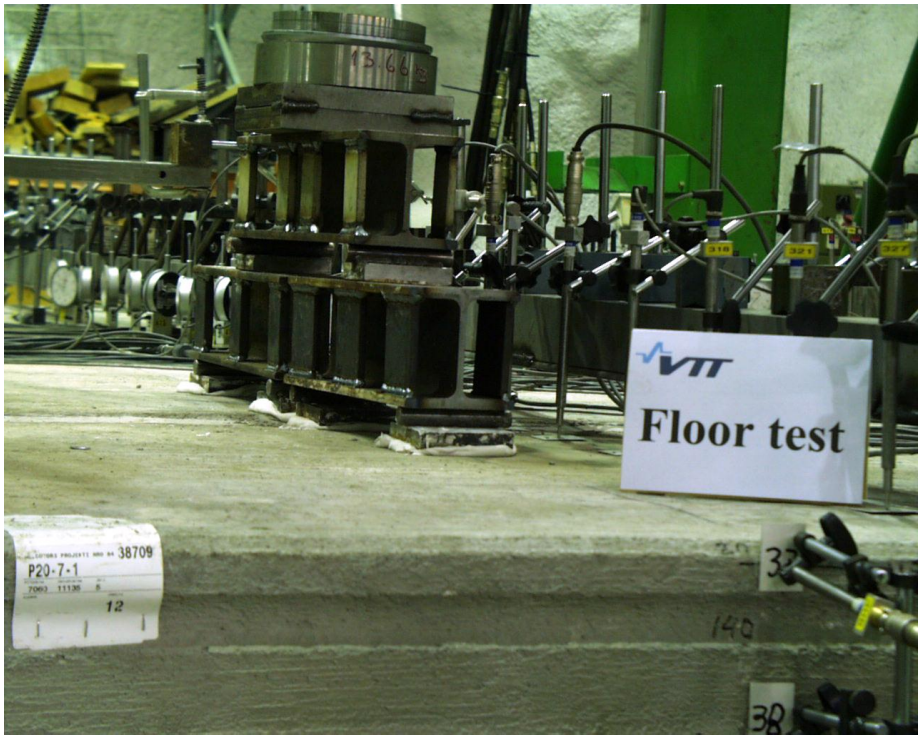

Fig. 13. FT200:4. Loading arrangements.

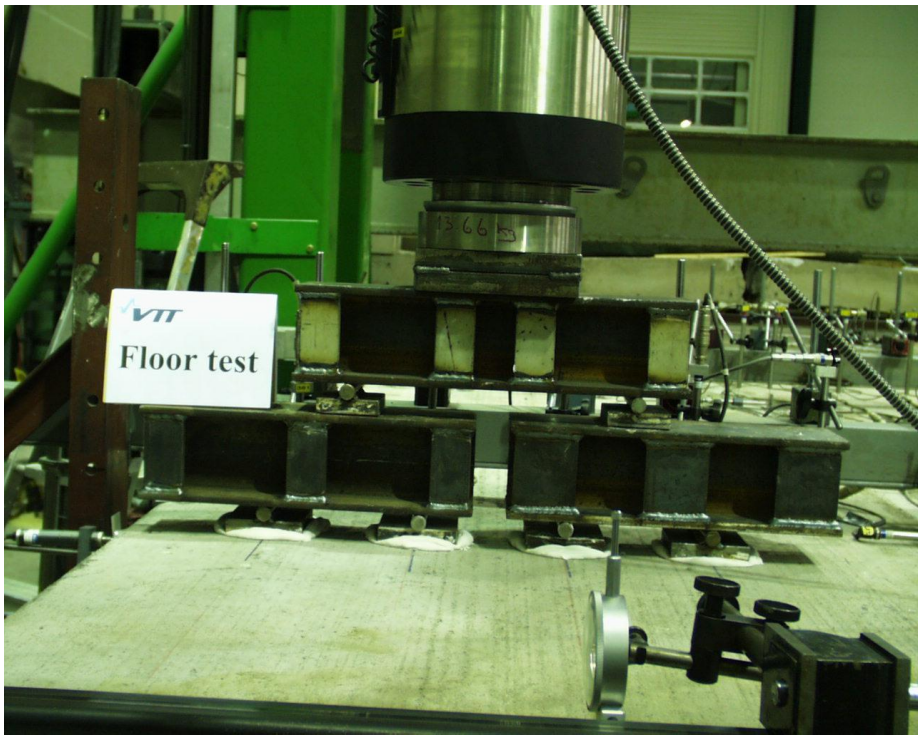

Fig. 14. FT200:6. Loading arrangements.

Fig. 15. FT200:9. Loading arrangements.

Fig. 16. FT200:12. Loading arrangements.

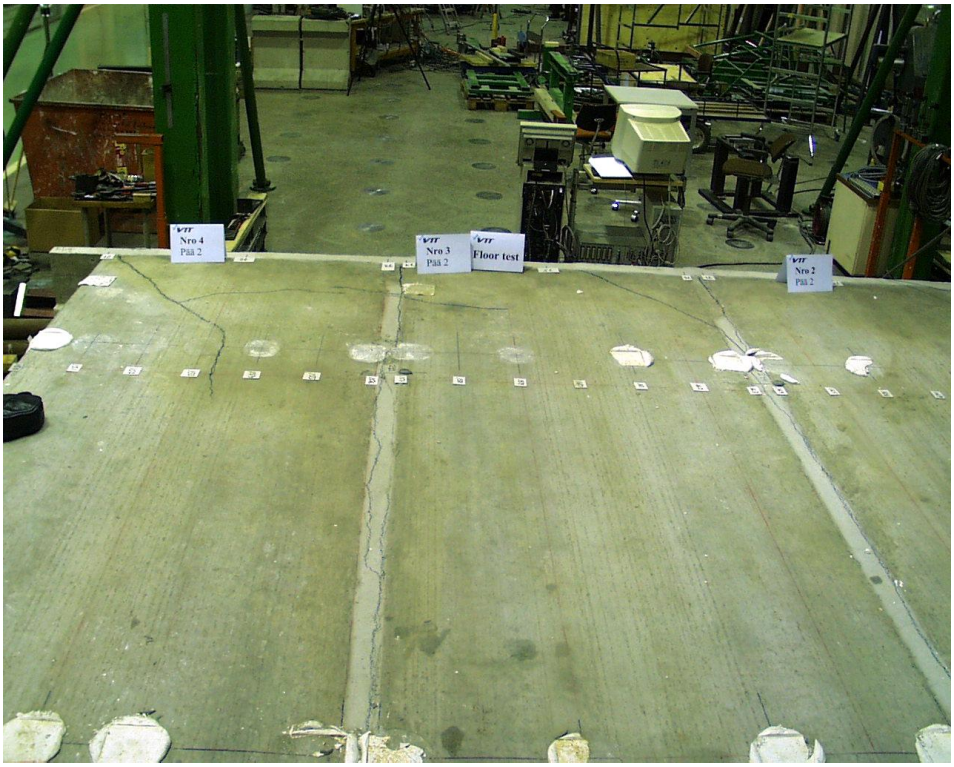

Fig. 17. FT200:11. Overview on cracks on top surface after failure. Slab 4 on the left.

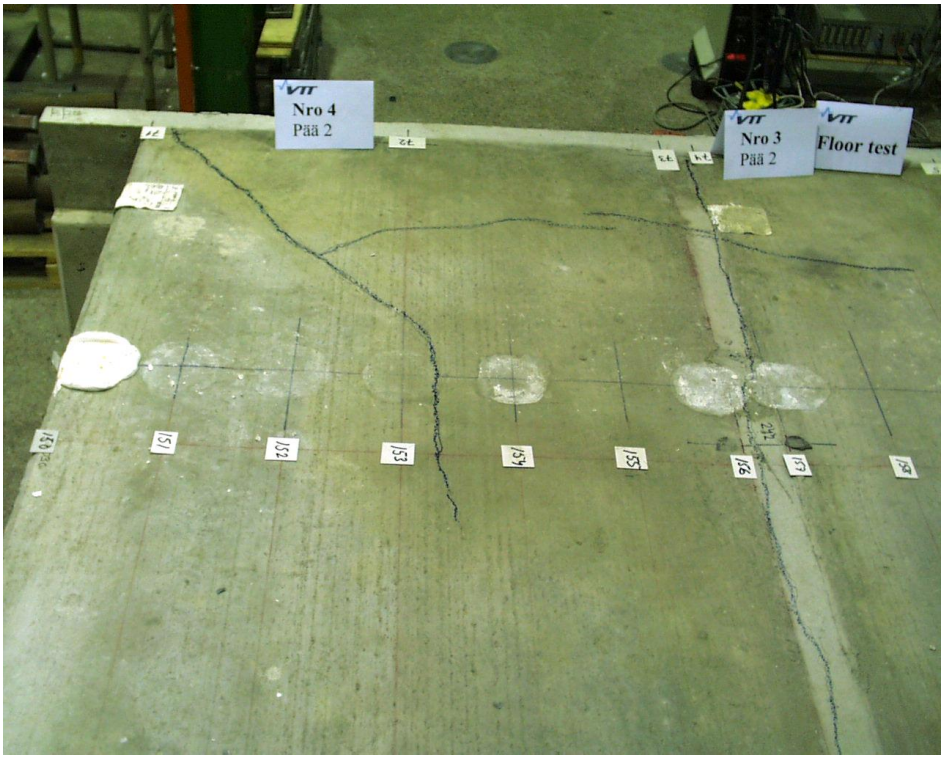

Fig. 18. FT200:11. Cracks on top surface of slabs 3 and 4 (on the left) after failure.

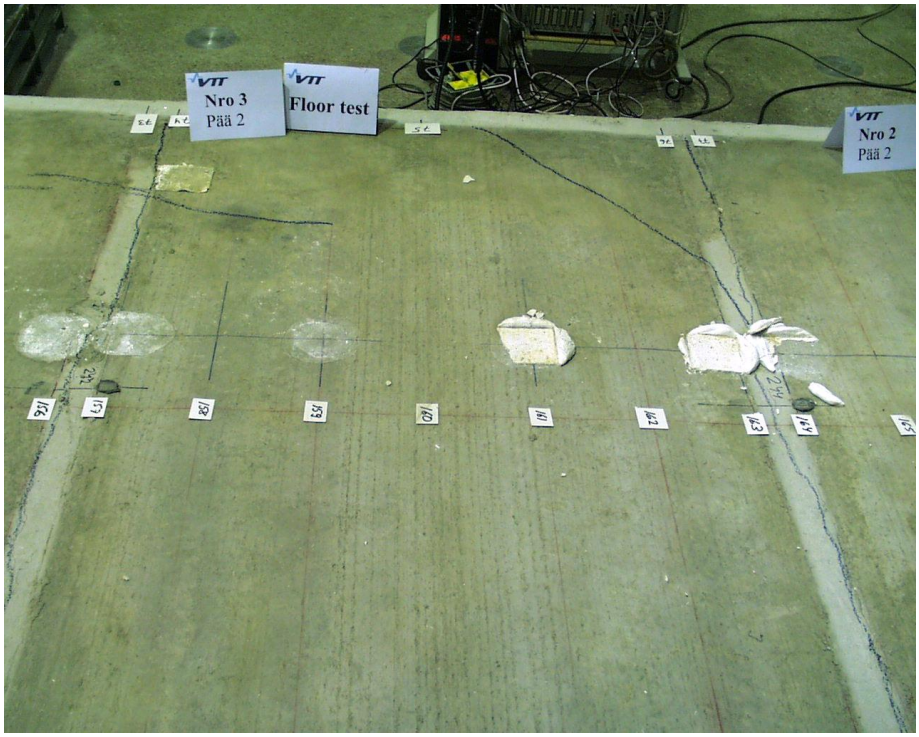

Fig. 19. FT200:11. Cracks on top surface of slab 3 after failure.

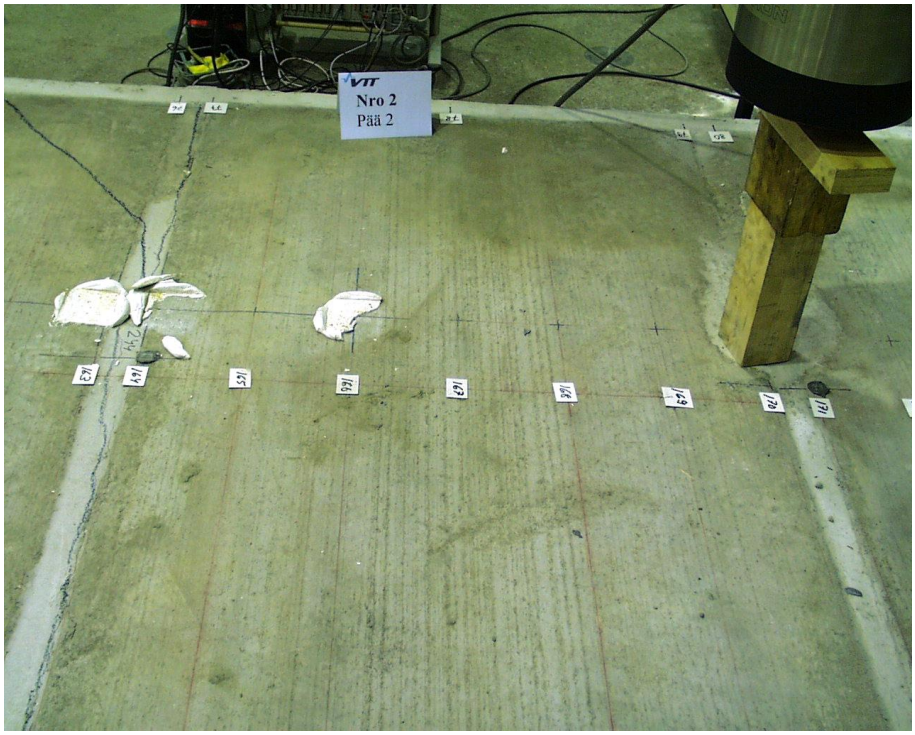

Fig. 20. FT200:11. Uncracked top surface of slab 2 after failure.

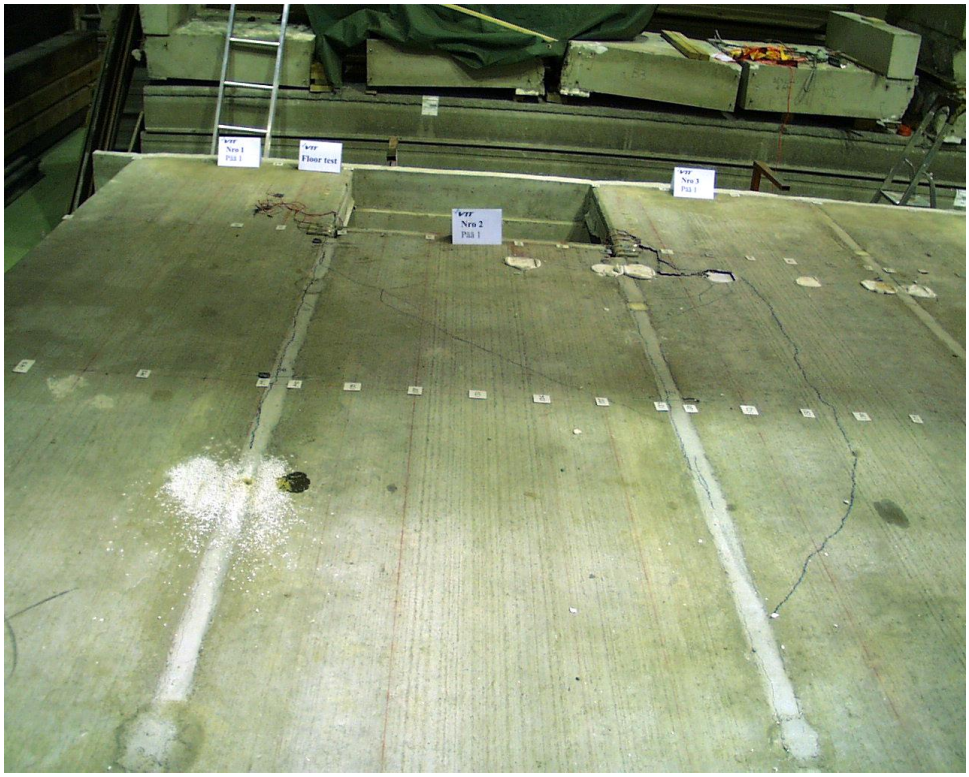

Fig. 21. FT200:12. Overview on cracks on top surface after failure. Slab 1 on the left.

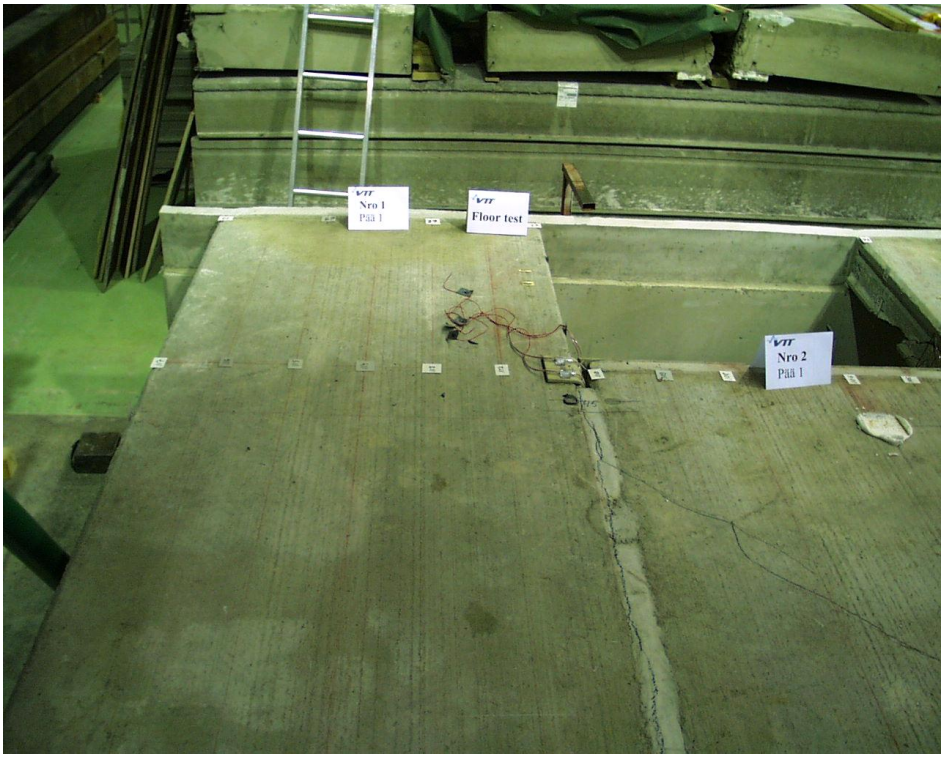

Fig. 22. FT200:12. Cracks on top surface of slab 1 after failure.

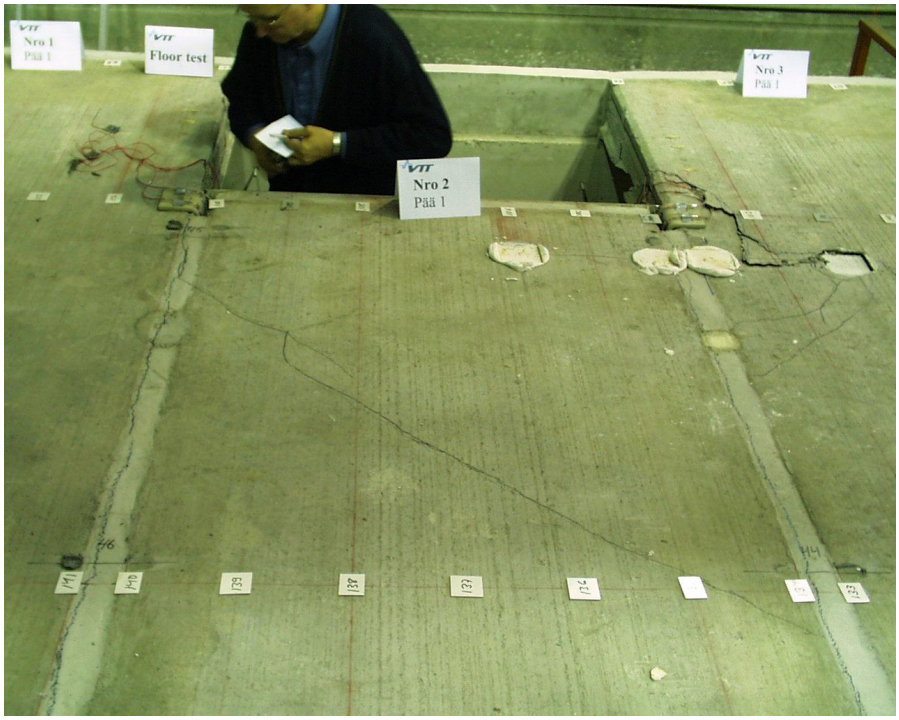

Fig. 23. FT200:12. Cracks on top surface of slab 2 after failure.

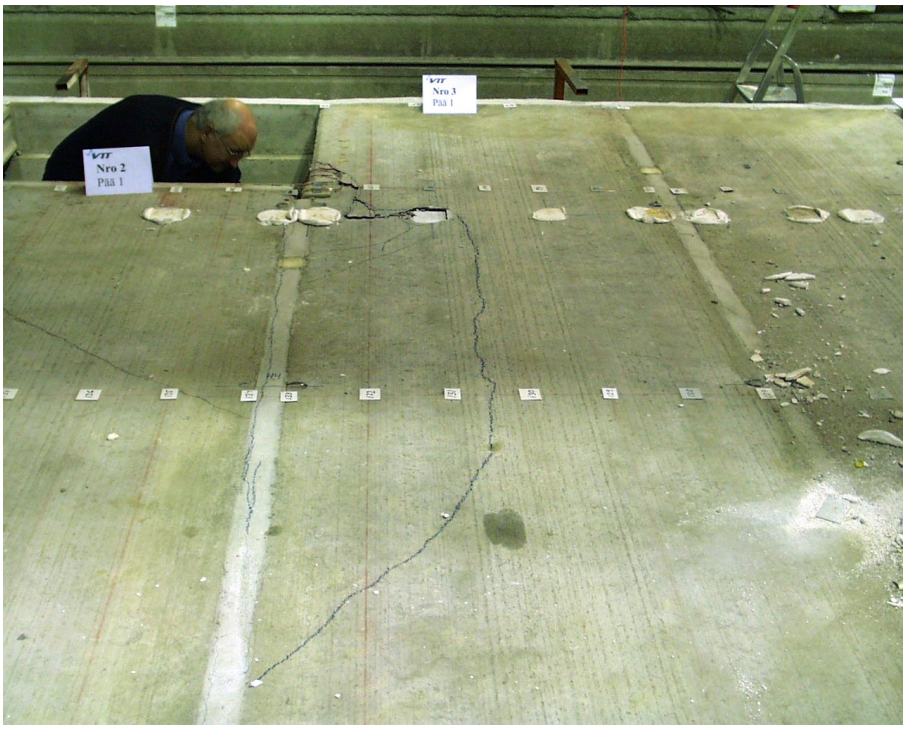

Fig. 24. FT200:12. Cracks on top surface of slab 3 after failure.

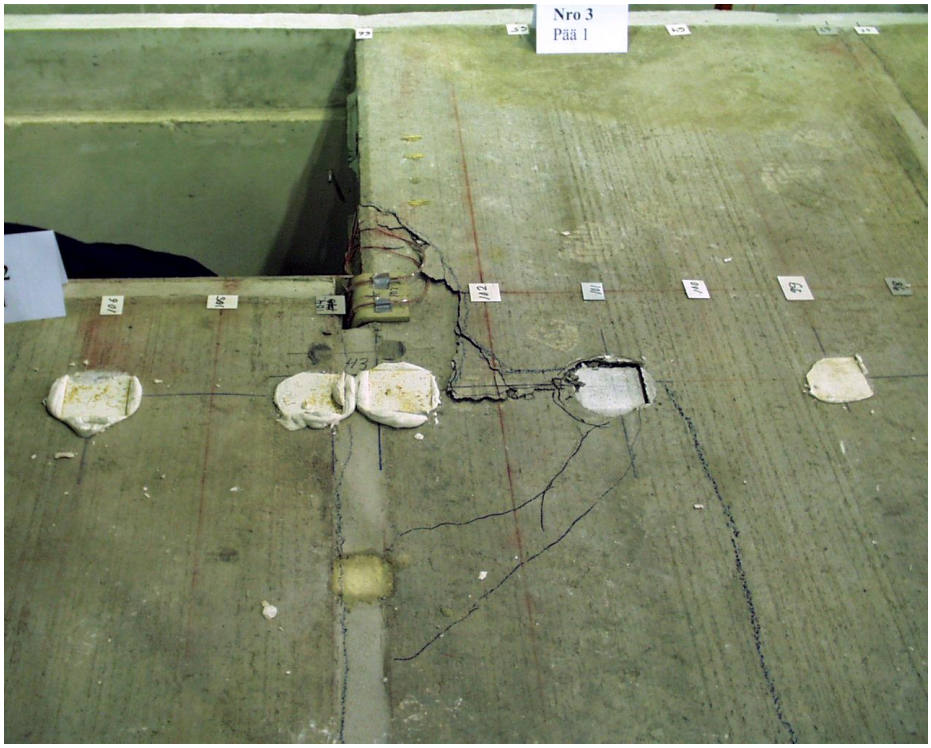

Fig. 25. FT200:12. Cracks on top surface of slab 3 after failure.

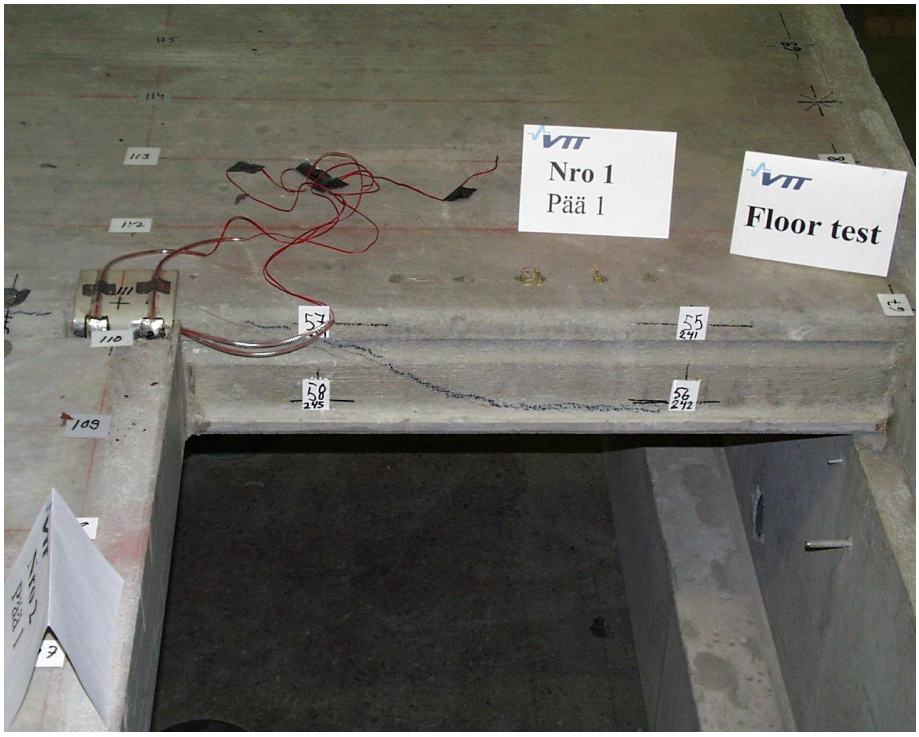

Fig. 26. FT200:12. Cracks on edge of slab 1 next to opening after failure.

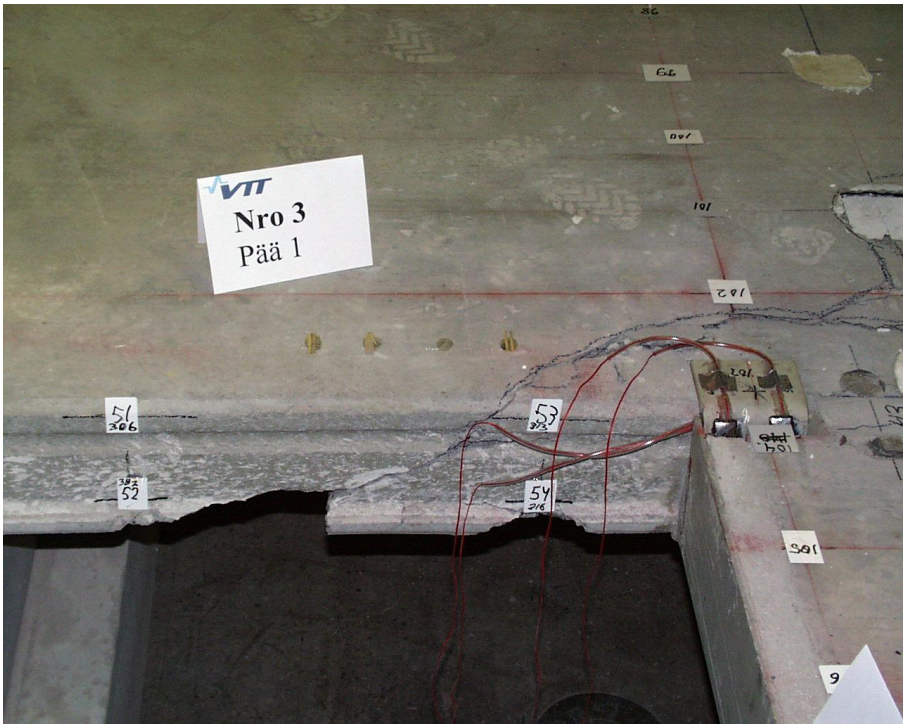

Fig. 27. FT200:12. Cracks on edge of slab 3 after failure.

Fig. 28. FT200:12. Cracks on edge of slab 3 after failure.

Fig. 29. FT200:12. Cracks on soffit of slab 1 after failure.

Fig. 30. FT200:12. Virtually uncracked soffit of slab 2 after failure.

Fig. 31. FT200:12. Cracks on soffit of slab 3 after failure.

Fig. 32. FT200:12. Cracks on soffit of slab 3 after failure.

Fig. 33. FT200:12. Cracks on soffit of slab 3 after failure.

Fig. 34. FT200:11. Cracks on soffit of slab 4 after failure.

Fig. 35. FT200:11. Cracks on soffit of slabs 4 (on the left) and 3 after failure.

Fig. 36. FT200:11. End 2 of slab 4 after demolishing of floor.

Fig. 37. FT200:11. End 2 of slab 4 after demolishing of floor.

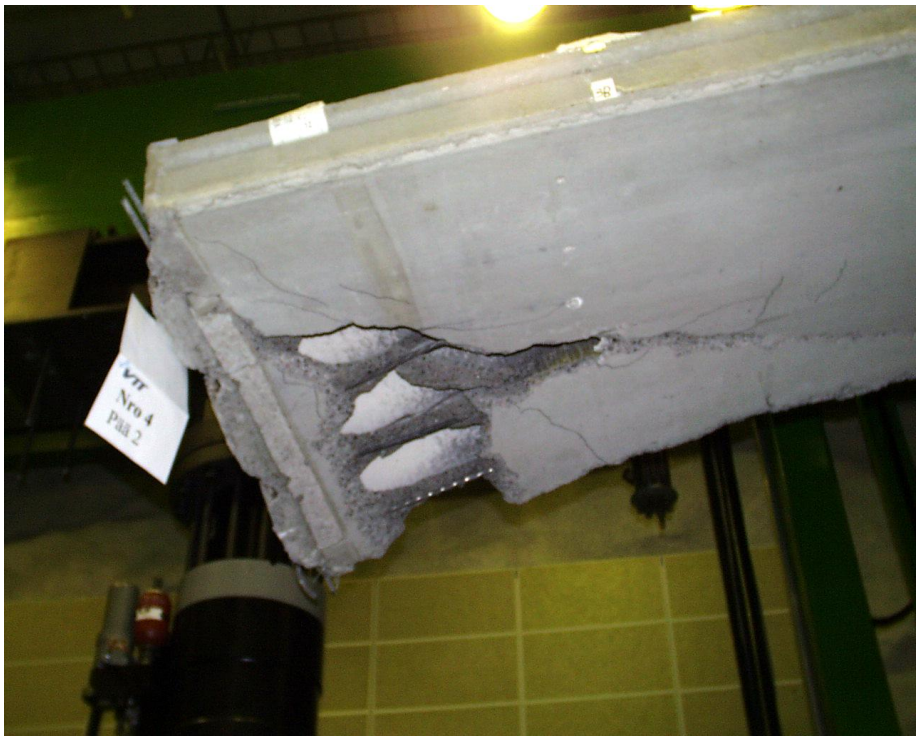

Fig. 38. FT200:11. End 2 of slab 4 after demolishing of floor.

Fig. 39. FT200:11. End 2 of slab 3 after removing slab 4.

Fig. 40. FT200:12. End 1 of slab 3 during removal of slab 2.

Fig. 41. FT200:12. End 1 of slab 3 after demolishing of floor.

Fig. 42. FT200:11. End 2 of slab 3 after demolishing of floor.

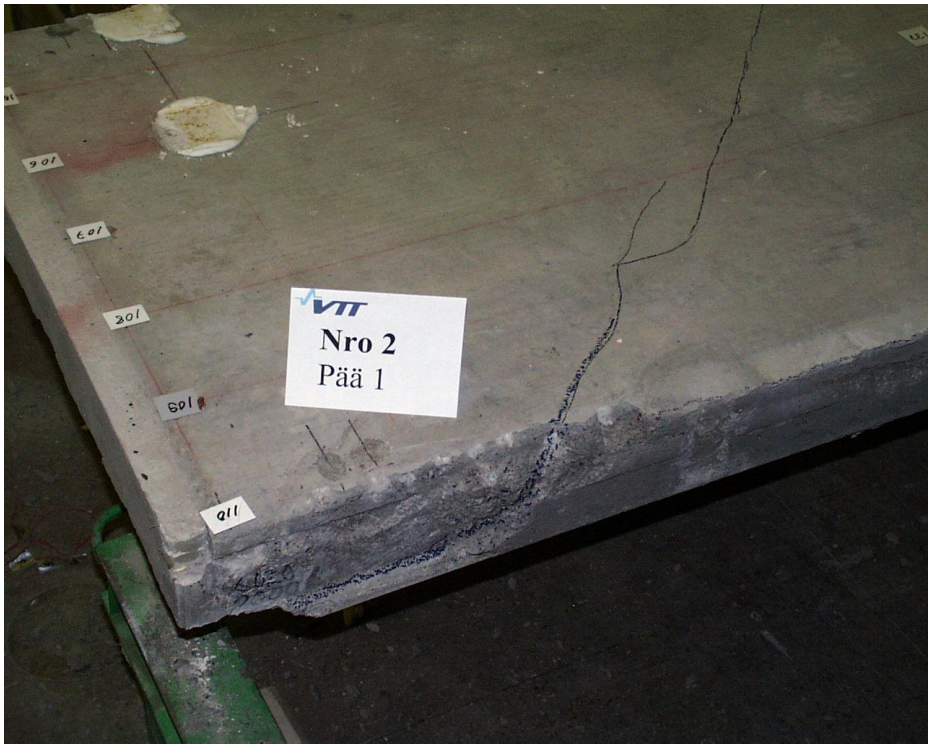

Fig. 43. FT200:12. End 1 of slab 2 after demolishing of floor.

Fig. 44. FT200:12. End 1 of slab 1 after demolishing of floor.

Appendix B: Measured geometry of slabs

In the following figures *prestress* refers to the nominal prestress in the strands after pretensioning (initial prestress). The underlined values refer to initial slippage of the strands. The strands were made of seven smooth wires. The cross-sectional area of a strand is 93 mm^2.

End 1 of each slab was supported on the beam next to the opening of the floor.

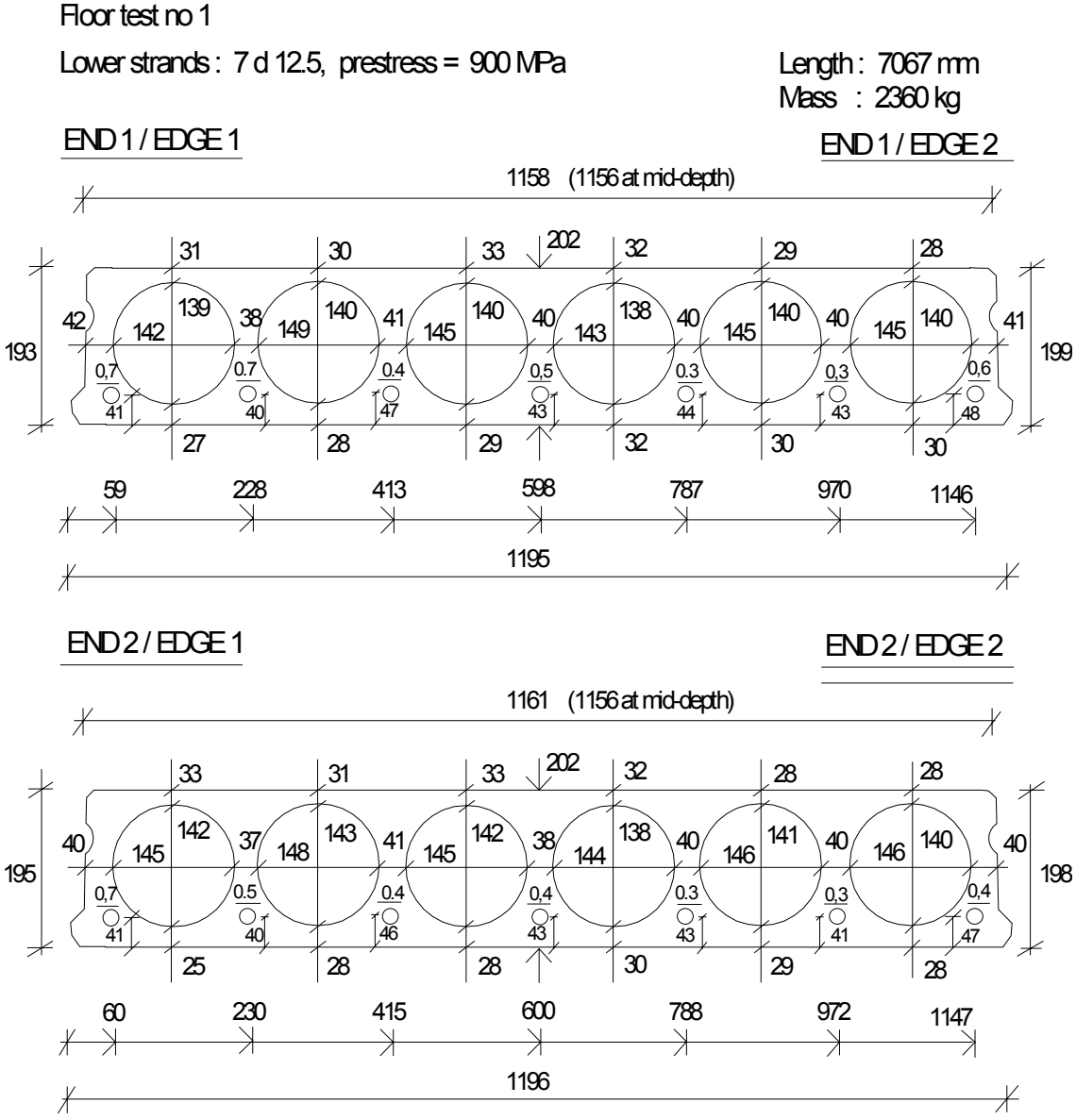

Fig. 1. Slab1.

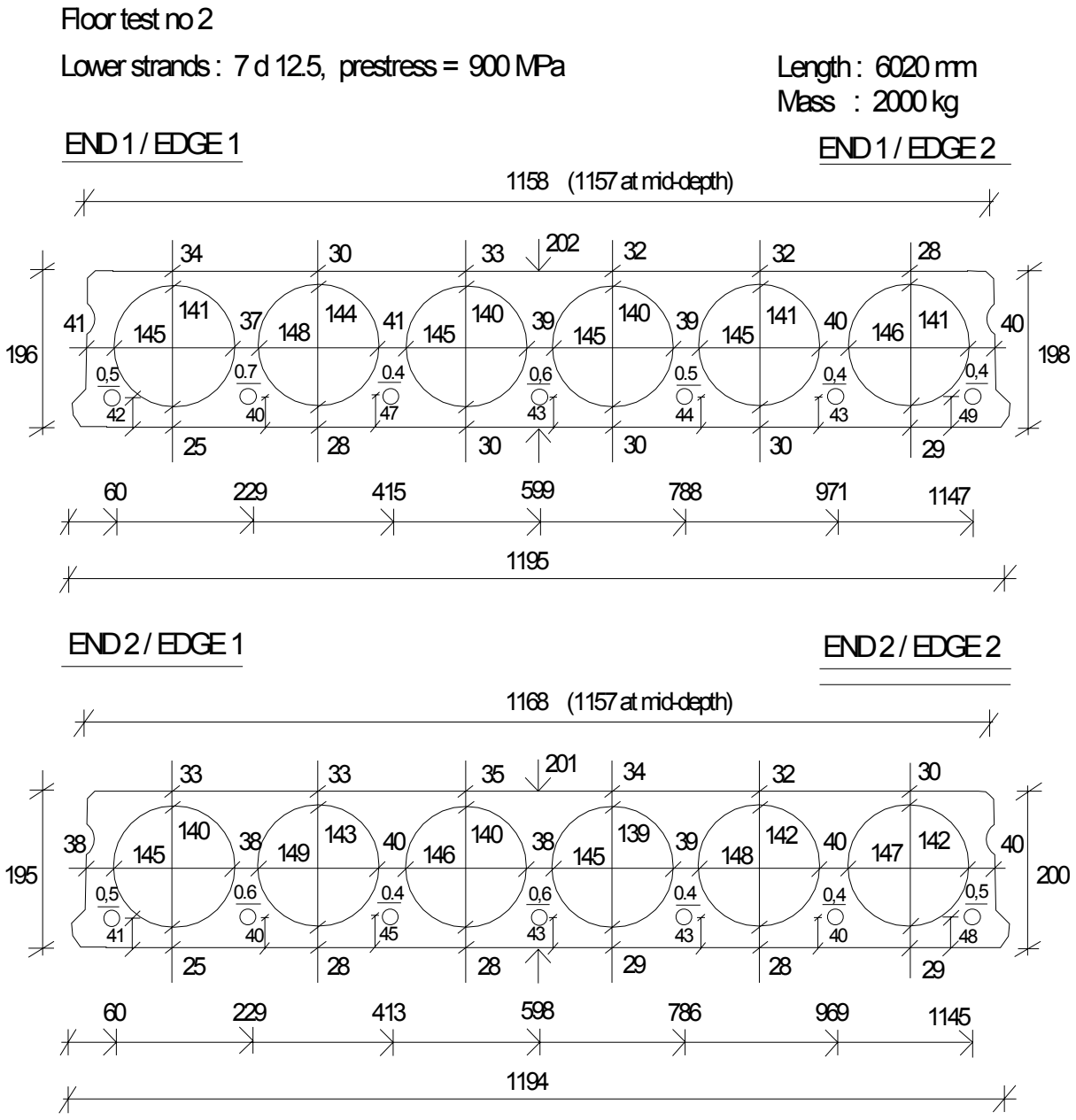
Floor test no 2
Lower strands : 7 d 12.5, prestress = 900 MPa
Length : 6020 mm
Mass : 2000 kg
END 1 / EDGE 1
END 1 / EDGE 2
1158 (1157 at mid-depth)
34 30 33 202 32 32 28
41 145 141 37 148 144 41 145 140 39 145 140 39 145 141 40 146 141 40
196
198
0,5 0.7 0.4 0,6 0.5 0,4 0,4
42 40 47 43 44 43 49
25 28 30 30 30 29
60 229 415 599 788 971 1147
1195
END 2 / EDGE 1
END 2 / EDGE 2
1168 (1157 at mid-depth)
33 33 35 201 34 32 30
38 145 140 38 149 143 40 146 140 38 145 139 39 148 142 40 147 142 40
195
200
0,5 0.6 0.4 0,6 0.4 0,4 0,5
41 40 45 43 43 40 48
25 28 28 29 28 29
60 229 413 598 786 969 1145
1194

Fig. 2. Slab 2.

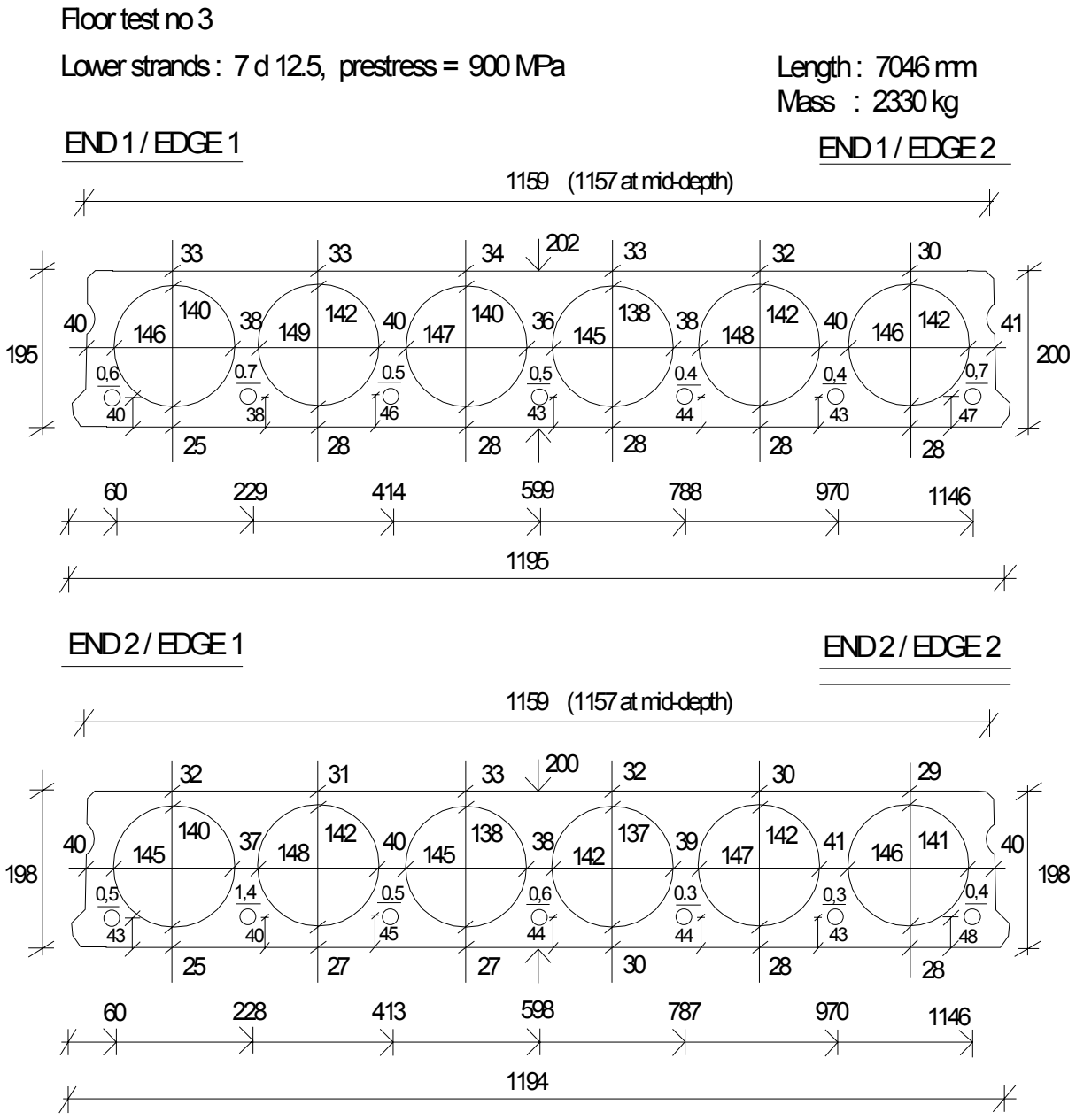
Floor test no 3
Lower strands : 7 d 12.5, prestress = 900 MPa
Length : 7046 mm
Mass : 2330 kg
END 1 / EDGE 1
END 1 / EDGE 2
1159 (1157 at mid-depth)
33 33 34 202 33 32 30
40 146 140 38 149 142 40 147 140 36 145 138 38 148 142 40 146 142 41
195
200
0,6 0.7 0.5 0,5 0.4 0,4 0,7
40 38 46 43 44 43 47
25 28 28 28 28 28
60 229 414 599 788 970 1146
1195
END 2 / EDGE 1
END 2 / EDGE 2
1159 (1157 at mid-depth)
32 31 33 200 32 30 29
40 145 140 37 148 142 40 145 138 38 142 137 39 147 142 41 146 141 40
198
198
0,5 1,4 0.5 0,6 0.3 0,3 0,4
43 40 45 44 44 43 48
25 27 27 30 28 28
60 228 413 598 787 970 1146
1194

Fig. 3. Slab 3.

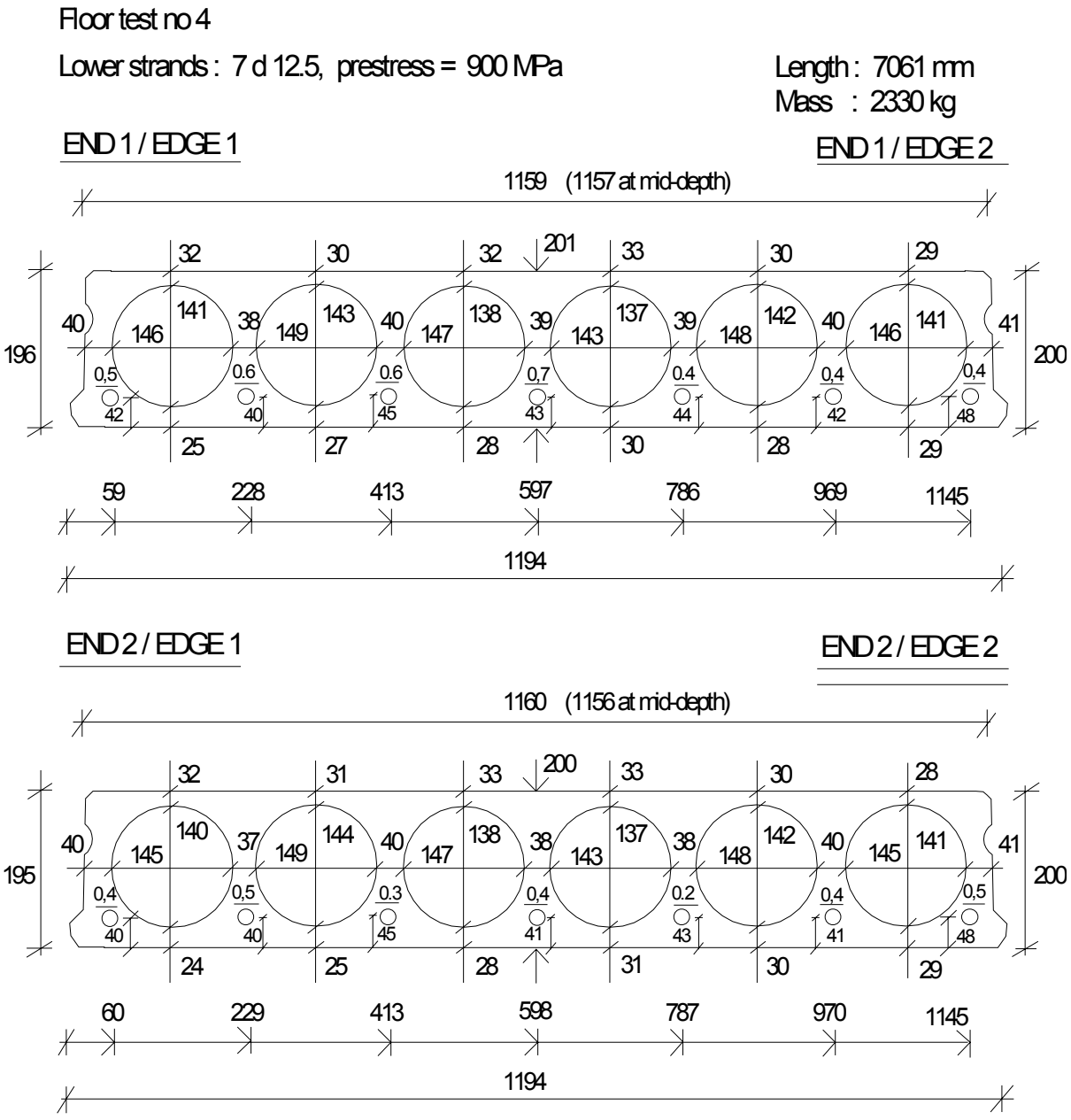
Floor test no 4
Lower strands : 7 d 12.5, prestress = 900 MPa
Length : 7061 mm
Mass : 2330 kg
END 1 / EDGE 1
END 1 / EDGE 2
1159 (1157 at mid-depth)
32 30 32 201 33 30 29
40 141 38 143 40 138 39 137 39 142 40 141 41
146 149 147 143 148 146
196 200
0,5 0.6 0.6 0,7 0.4 0,4 0,4
42 40 45 43 44 42 48
25 27 28 30 28 29
59 228 413 597 786 969 1145
1194
END 2 / EDGE 1
END 2 / EDGE 2
1160 (1156 at mid-depth)
32 31 33 200 33 30 28
40 140 37 144 40 138 38 137 38 142 40 141 41
145 149 147 143 148 145
195 200
0,4 0,5 0.3 0,4 0.2 0,4 0,5
40 40 45 41 43 41 48
24 25 28 31 30 29
60 229 413 598 787 970 1145
1194

Fig. 4. Slab 4.

Appendix C: Measured results in test on trimmer beam

The trimmer beam was subjected to vertical load *P* before grouting of the joints on October 27, 2003. *P,* given at different load steps in Table 1, does not include the self weight of the trimmer beam.

After step 5 the protruding parts of the slab edges at the ends of the trimmer beam were chiseled to make sure that the ends of the trimmer beam were not supported by friction between the trimmer beam and the edge of the hollow core slab. The chiseling was completed after step 6.

Table 1. Measured and average strain.

Step	*P*	Strain gauge								Average strain	
		211	212	213	214	215	216	217	218	211-214	215-218
	kN	10^{-6}	10^{-6}	10^{-6}	10^{-6}	10^{-6}	10^{-6}	10^{-6}	10^{-6}	10^{-6}	10^{-6}
0	0.00	1	1	-1	0	0	0	-1	-2	0.25	-0.75
1	9.82	-380	-428	456	520	-656	-807	700	913	42	37.5
2	21.36	-637	-771	784	956	-1181	-1469	1263	1687	83	75
3	32.46	-993	-1398	1497	1716	-1785	-2150	1910	2524	205.5	124.75
4	44.34	-1531	-2235	2546	2729	-2257	-2928	2520	3523	377.25	214.5
5	44.34	-1588	-2338	2722	2850	-2285	-3030	2551	3624	411.5	215
6	44.34	-1679	-2413	1529	2967	-2399	-3353	2720	4013	101	245.25
7	44.34	-1689	-2422	1482	2975	-2410	-3395	2742	4054	86.5	247.75
8	32.46	-1474	-2172	1216	2627	-2142	-3109	2425	3694	49.25	217
9	21.36	-1244	-1883	924	2239	-1746	-2602	1994	3090	9	184
10	9.82	-922	-1381	406	1626	-1116	-1678	1322	2013	-67.75	135.25
11	0.00	-474	-789	127	946	-381	-650	544	848	-47.5	90.25
12	9.82	-816	-1214	945	1469	-979	-1428	1183	1739	96	128.75

The fictitious stress, calculated from the measured strain assuming linear relationship and E = 210 GPa, is given in Table 2. It is clear that at least on surface of the trimmer beam the steel exceeded the nominal yield stress 355 MPa at an early stage.

Table 2. Fictitious stress calculated from measured strain.

Step	Stress								Average stress		
	P	211	212	213	214	215	216	217	218	211-214	211-218
	kN	MPa	MPa	MPa	MPa	MPa	MPa	MPa	MPa	MPa	MPa
0	0	0	0	0	0	0	0	0	0	0	-0.1
1	-80	-90	96	109	-138	-169	147	192	9	8	21.7
2	-134	-162	165	201	-248	-308	265	354	17	16	43.1
3	-209	-294	314	360	-375	-452	401	530	43	26	90.2
4	-322	-469	535	573	-474	-615	529	740	79	45	161.5
5	-333	-491	572	599	-480	-636	536	761	86	45	171.0
6	-353	-507	321	623	-504	-704	571	843	21	52	94.5
7	-355	-509	311	625	-506	-713	576	851	18	52	91.3
8	-310	-456	255	552	-450	-653	509	776	10	46	72.7
9	-261	-395	194	470	-367	-546	419	649	2	39	52.7
10	-194	-290	85	341	-234	-352	278	423	-14	28	18.4
11	-100	-166	27	199	-80	-137	114	178	-10	19	11.7
12	-171	-255	198	308	-206	-300	248	365	20	27	61.4

Appendix D: Measured strains and displacements in tests FT200:1–FT200:3 and FT200:12

The load *P* is the actuator load without weight of loading equipment. The following terms are used for different measured displacements:

- *deflection*: vertical displacement of slab
- *transverse horizontal displacement*: horizontal displacement perpendicular to the longitudinal xis of the slab
- *longitudinal horizontal displacement*: horizontal displacement of supporting beam parallel to the longitudinal axis of the slab.

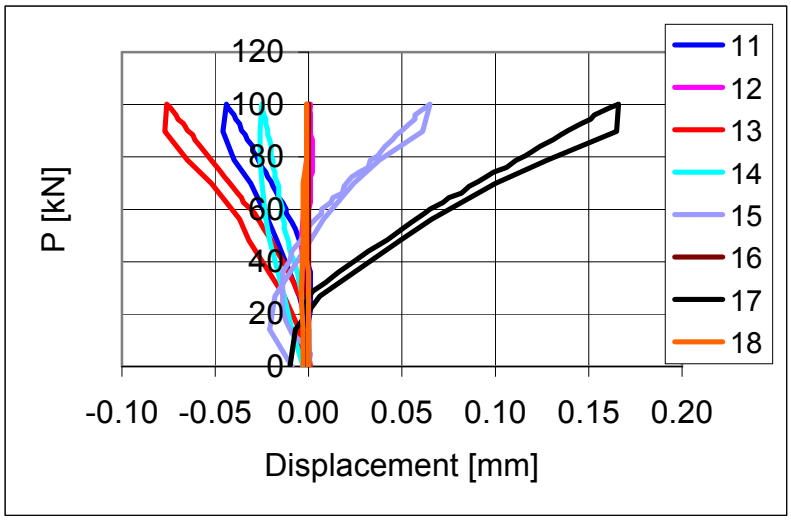

Fig. 1. FT200:1. Longitudinal horizontal displacement. Transducers 11–18.

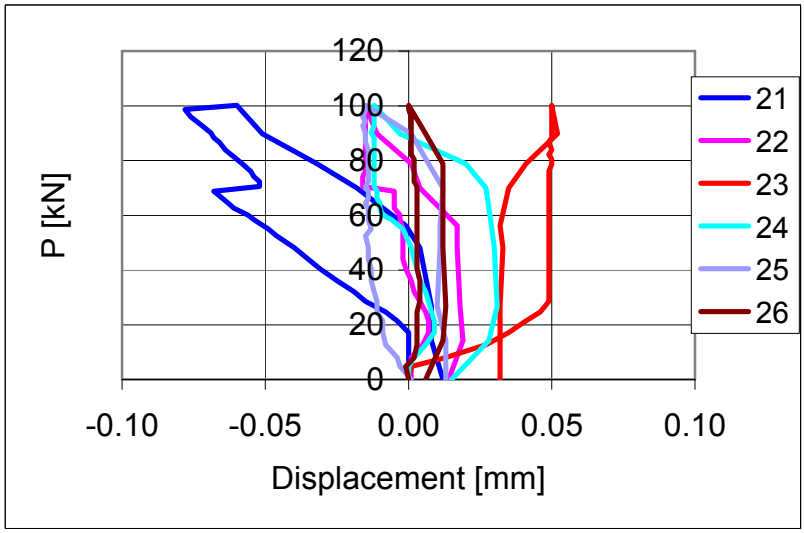

Fig. 2. FT200:1. Transverse horizontal displacement. Transducers 21–26.

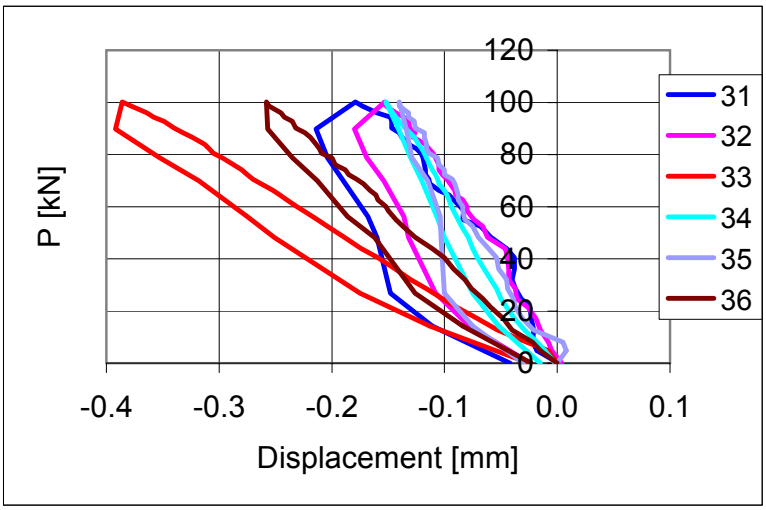

Fig. 3. FT200:1. Transverse horizontal displacement. Transducers 31–36.

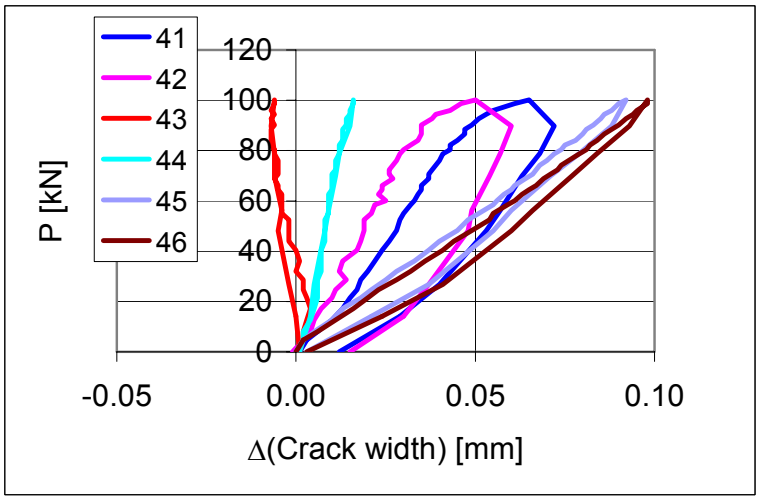

Fig. 4. FT200:1. Change in crack width. Transducers 41–46.

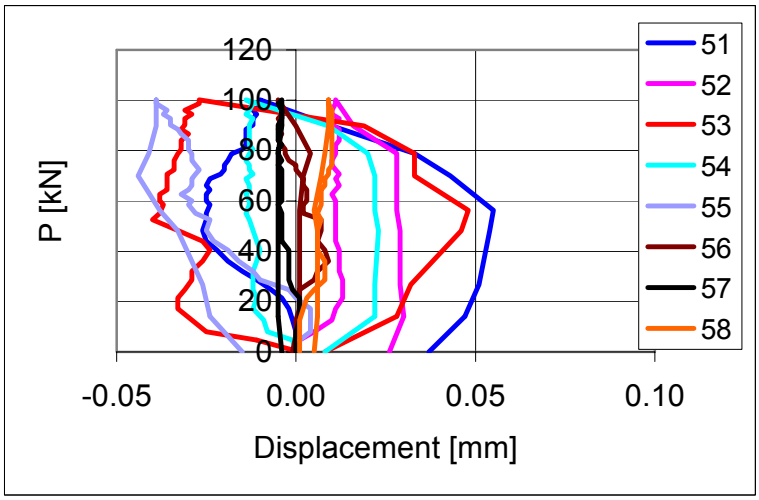

Fig. 5. FT200:1. Transverse horizontal displacement. Transducers 51–58.

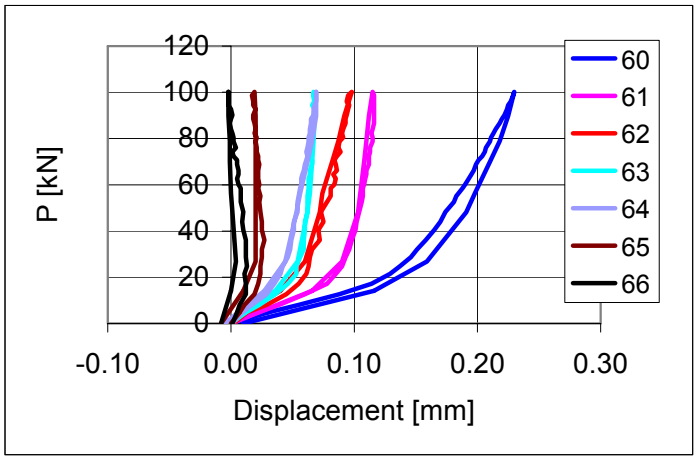

Fig. 6. FT200:1. Settlement of support. Transducers 60–66.

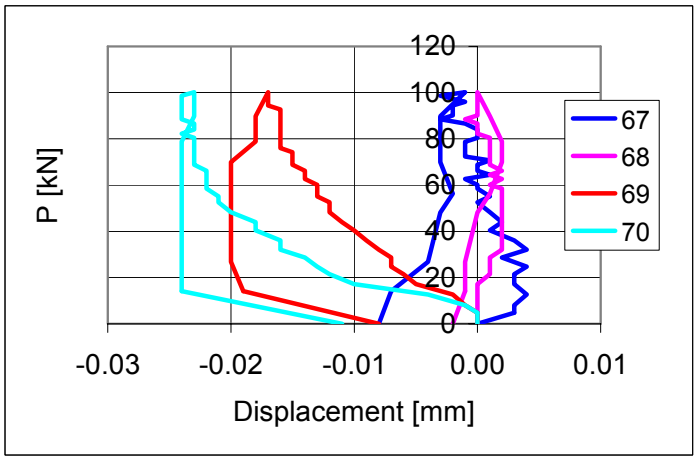

Fig. 7. FT200:1. Settlement of support. Transducers 67–70.

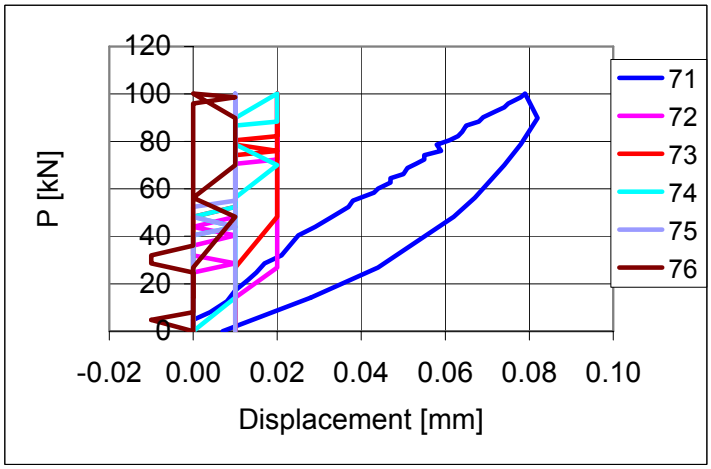

Fig. 8. FT200:1. Settlement of support. Transducers 71–76.

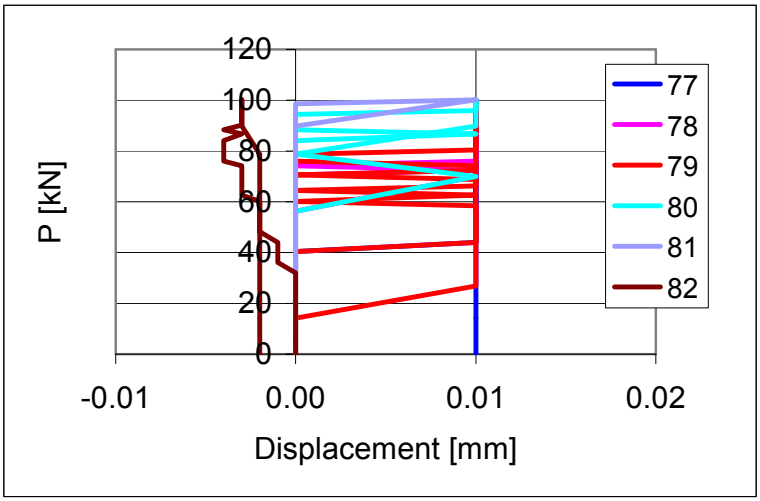

Fig. 9. FT200:1. Settlement of support. Transducers 77–82.

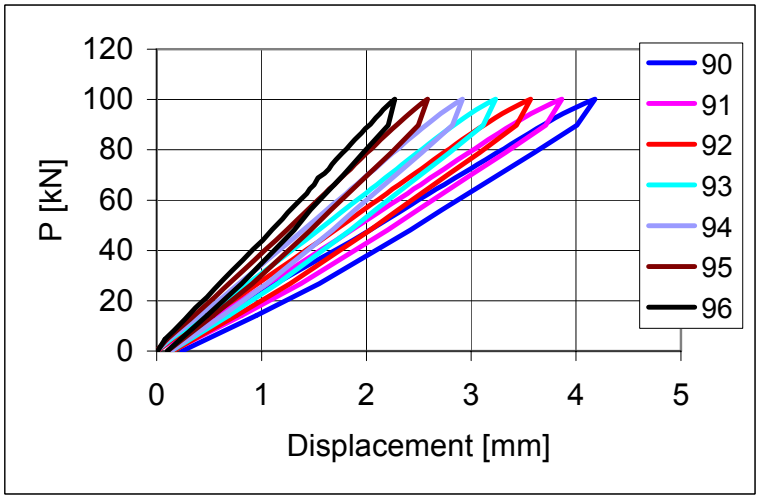

Fig. 10. FT200:1. Deflection. Transducers 90–96.

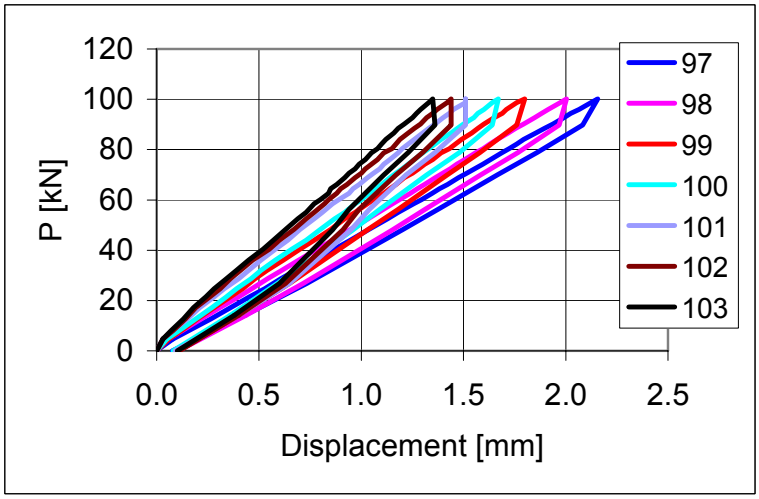

Fig. 11. FT200:1. Deflection. Transducers 97–103.

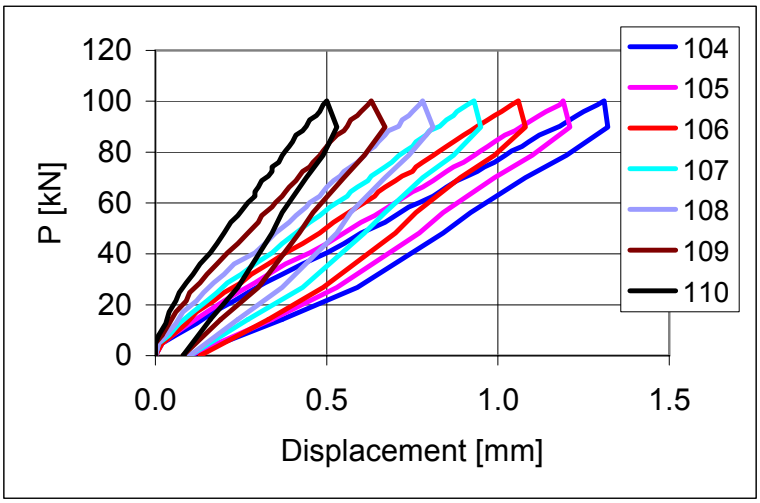

Fig. 12. FT200:1. Deflection. Transducers 104–110.

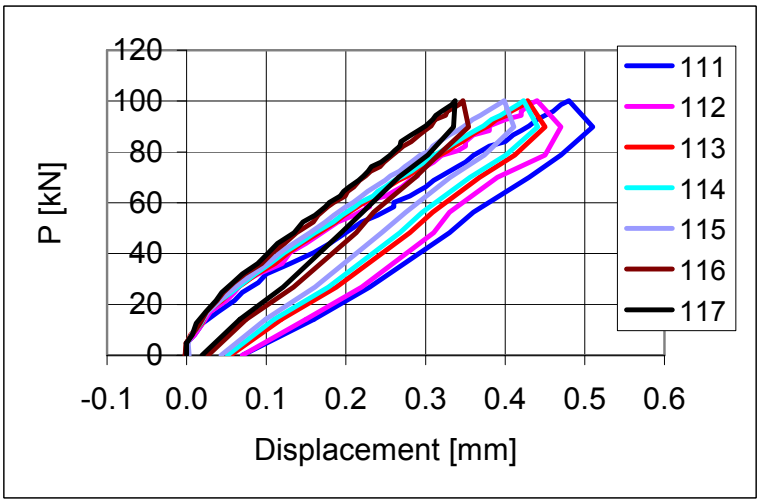

Fig. 13. FT200:1. Deflection. Transducers 111–117.

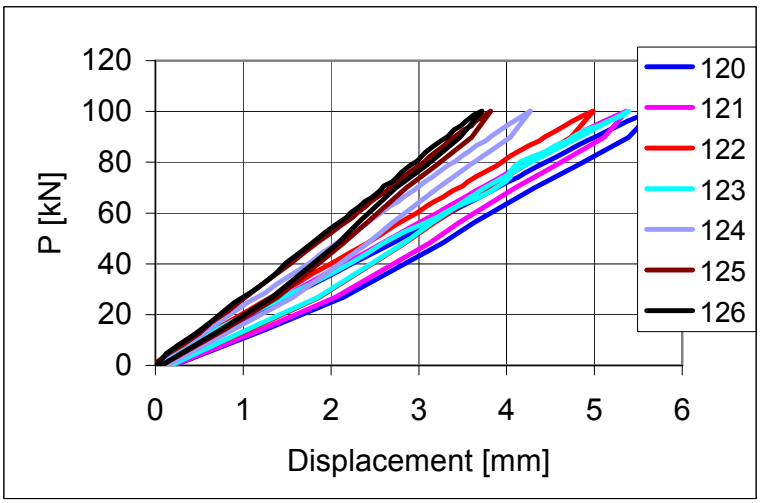

Fig. 14. FT200:1. Deflection. Transducers 120–126. Behaviour of strain 123 seems erroneous.

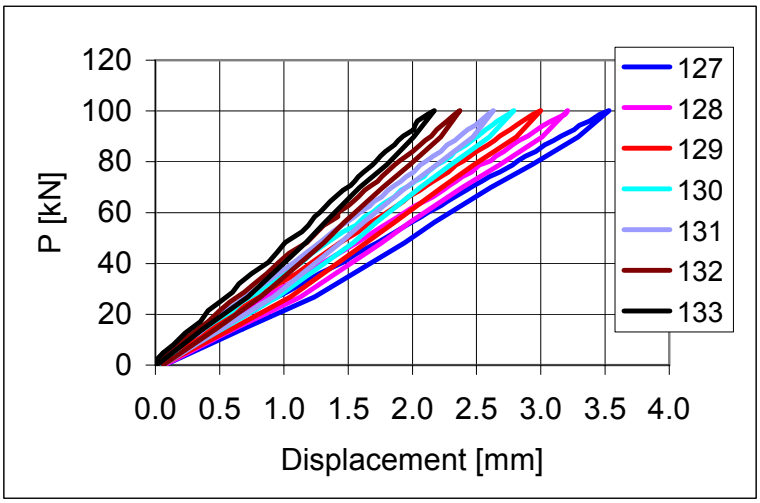

Fig. 15. FT200:1. Deflection. Transducers 127–133.

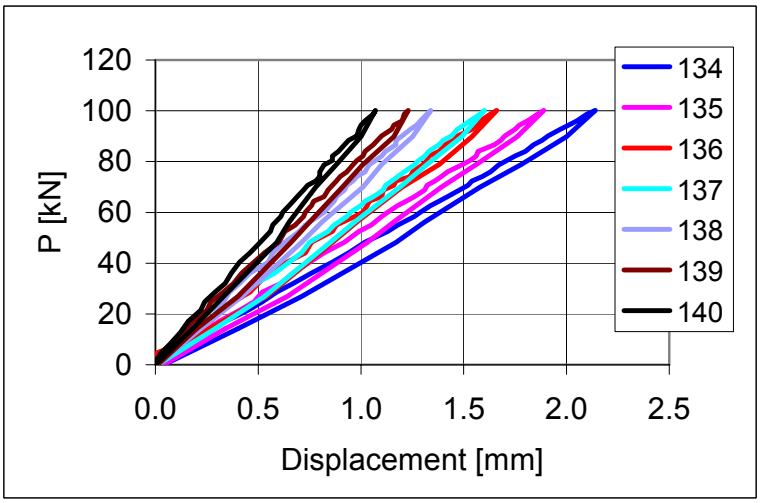

Fig. 16. FT200:1. Deflection. Transducers 134–140.

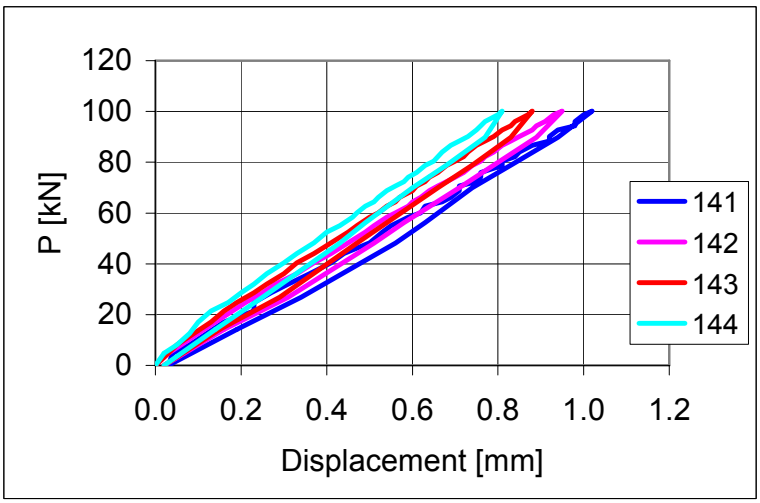

Fig. 17. FT200:1. Deflection. Transducers 141–144.

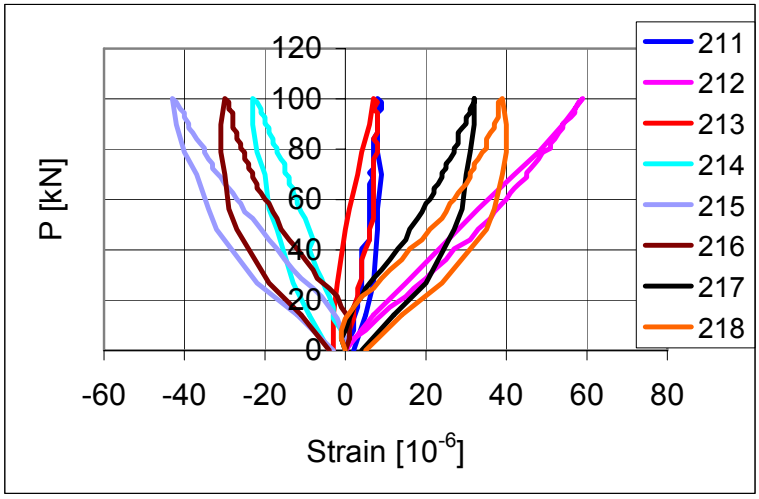

Fig. 18. FT200:1. Strain in trimmer beam. Strain gauges 211–218.

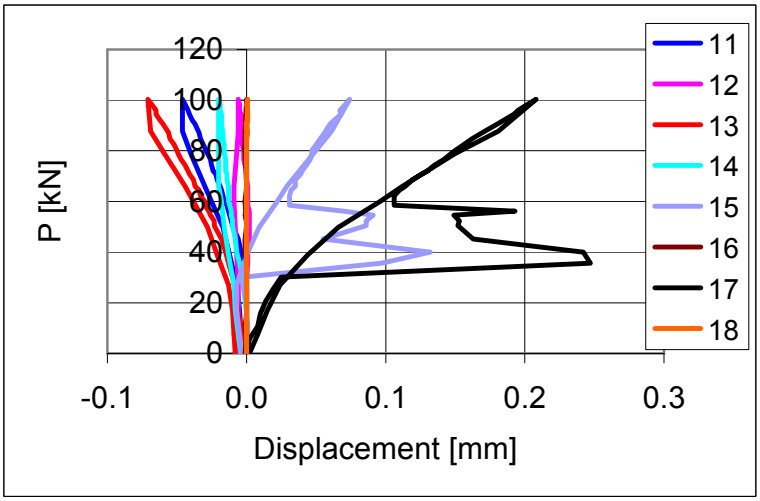

Fig. 19. FT200:2. Longitudinal horizontal displacement. Transducers 11–18.

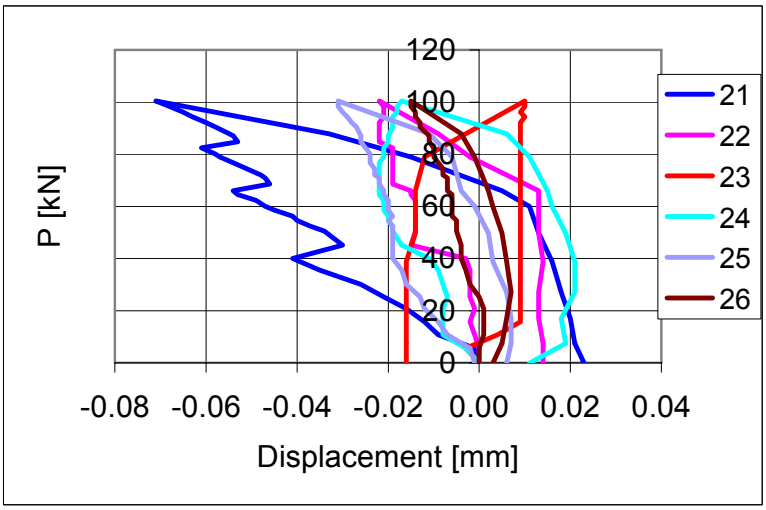

Fig. 20. FT200:2. Transverse horizontal displacement. Transducers 21–26.

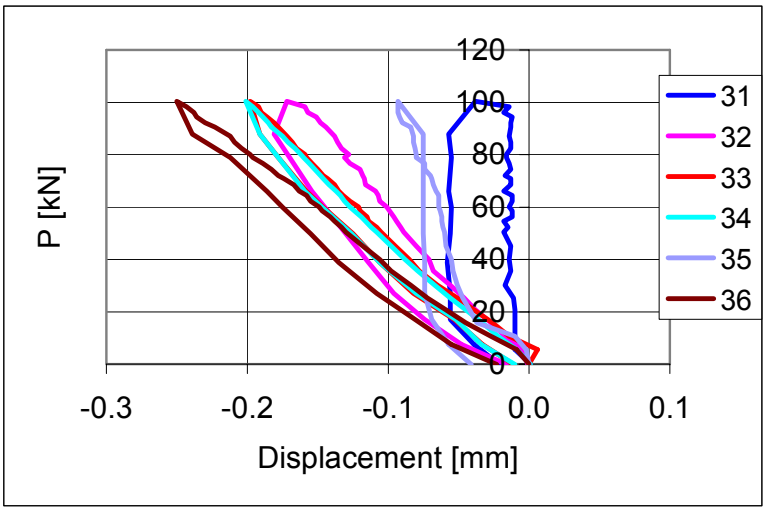

Fig. 21. FT200:2. Transverse horizontal displacement. Transducers 31–36.

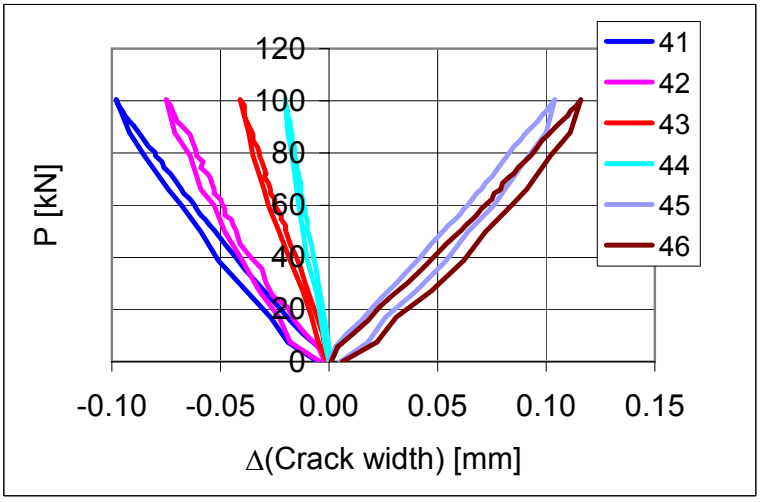

Fig. 22. FT200:2. Change in crack width. Transducers 41–46.

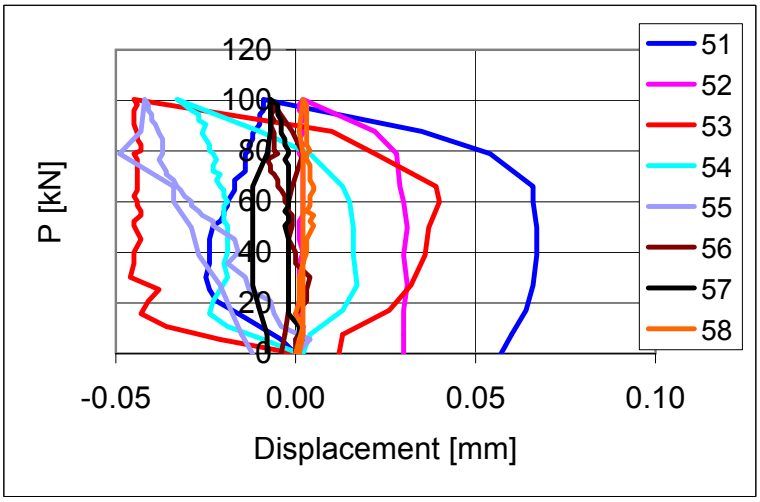

Fig. 23. FT200:2. Transverse horizontal displacement. Transducers 51–58.

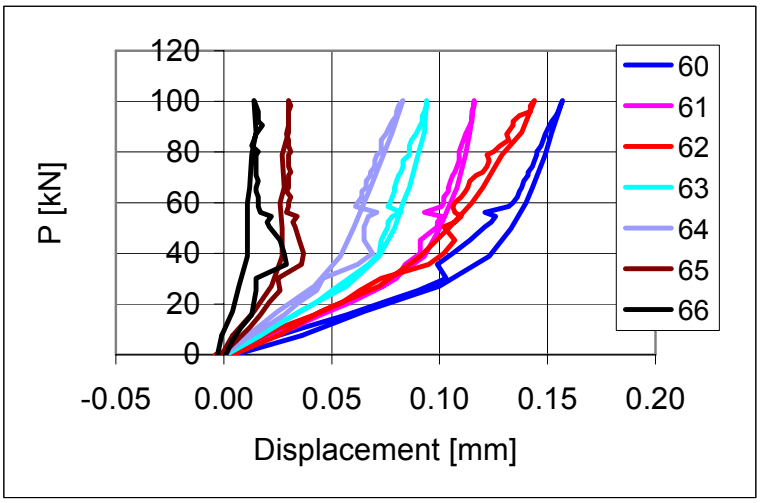

Fig. 24. FT200:2. Settlement of support. Transducers 60–66.

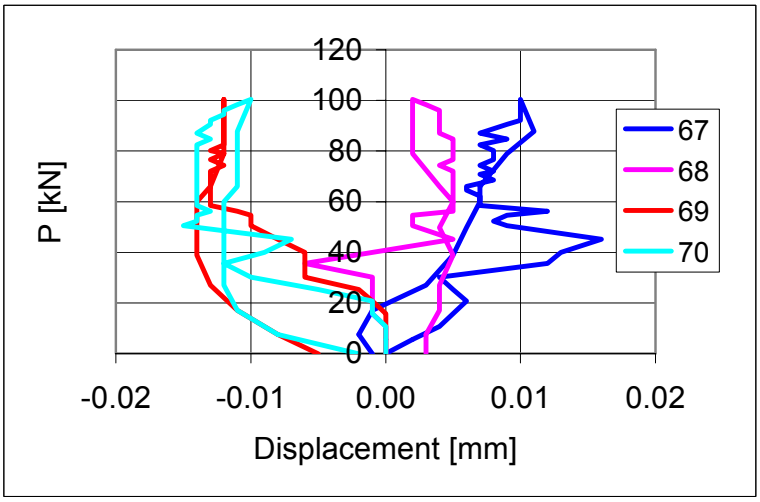

Fig. 25. FT200:2. Settlement of support. Transducers 67–70.

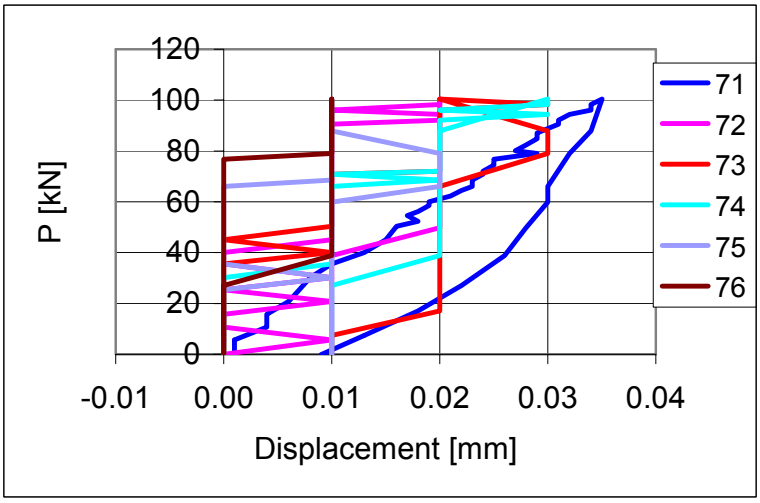

Fig. 26. FT200:2. Settlement of support. Transducers 71–76.

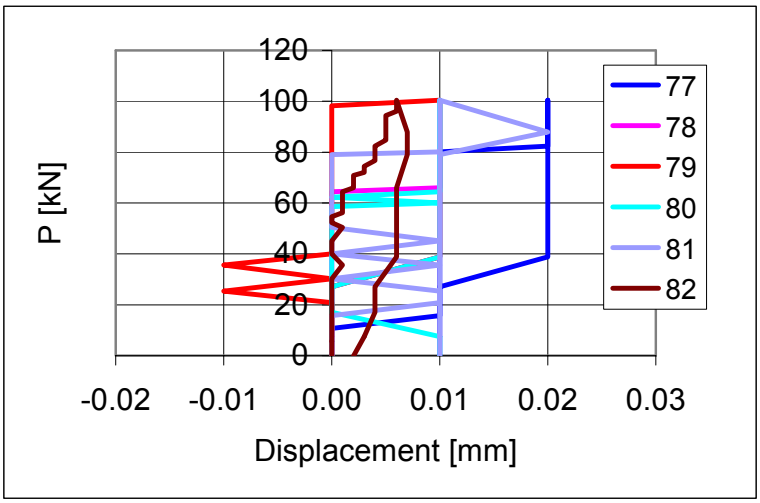

Fig. 27. FT200:2. Settlement of support. Transducers 77–82.

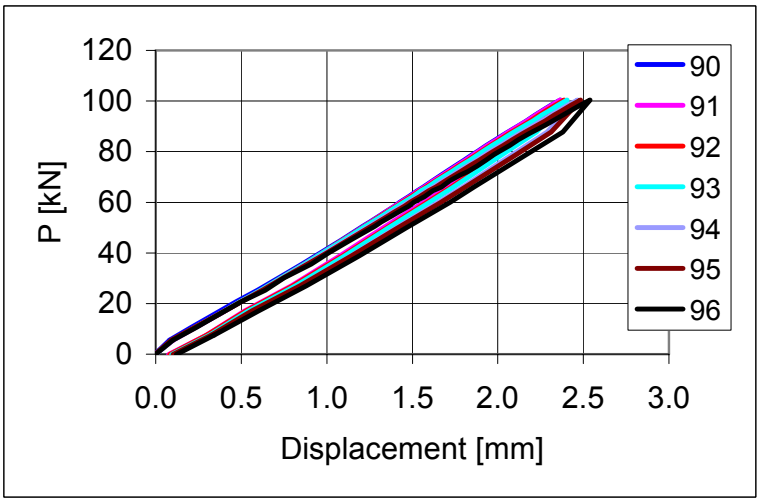

Fig. 28. FT200:2. Deflection. Transducers 90–96.

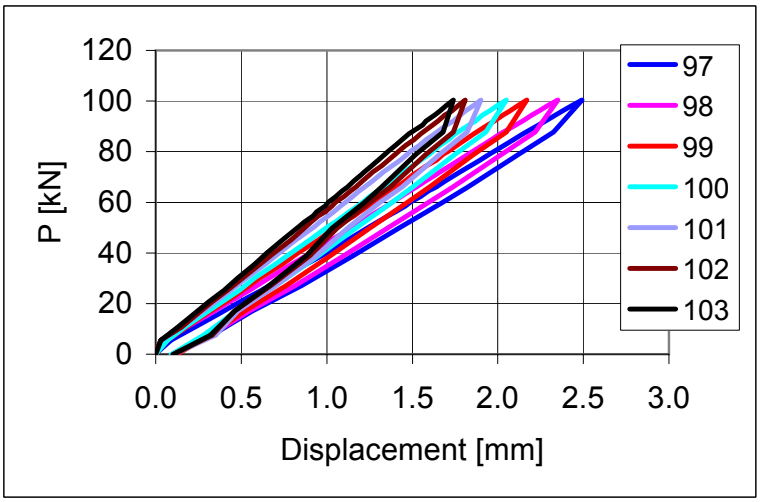

Fig. 29. FT200:2. Deflection. Transducers 97–103.

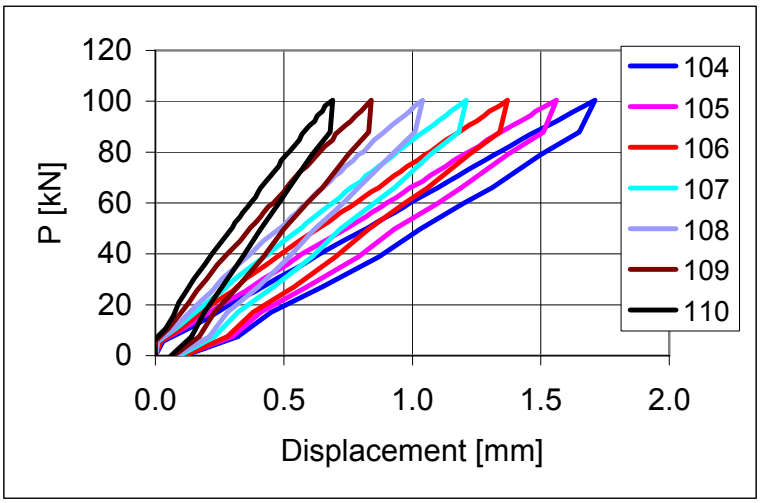

Fig. 30. FT200:2. Deflection. Transducers 104–110.

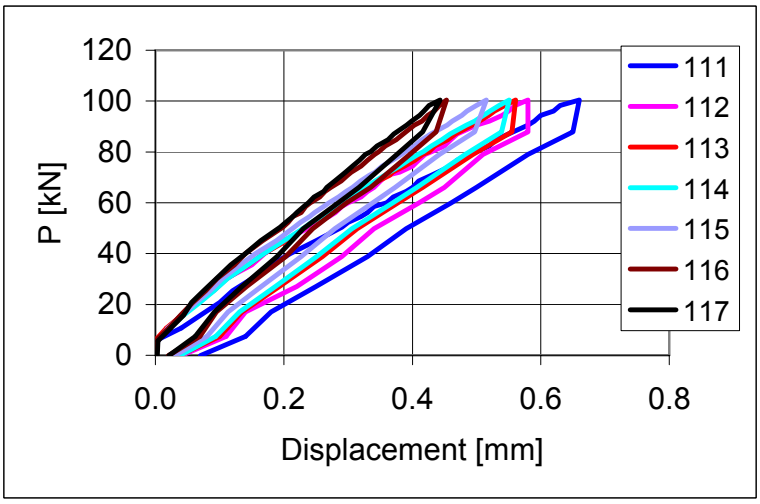

Fig. 31. FT200:2. Deflection. Transducers 111–117.

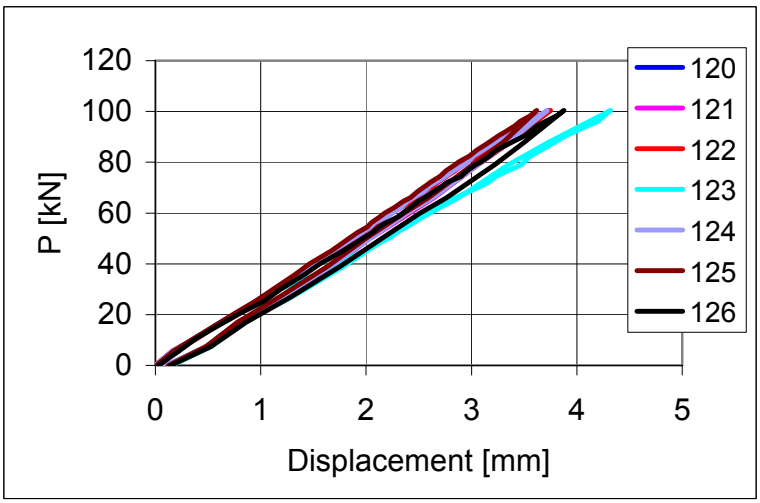

Fig. 32. FT200:2. Deflection. Transducers 120–126.

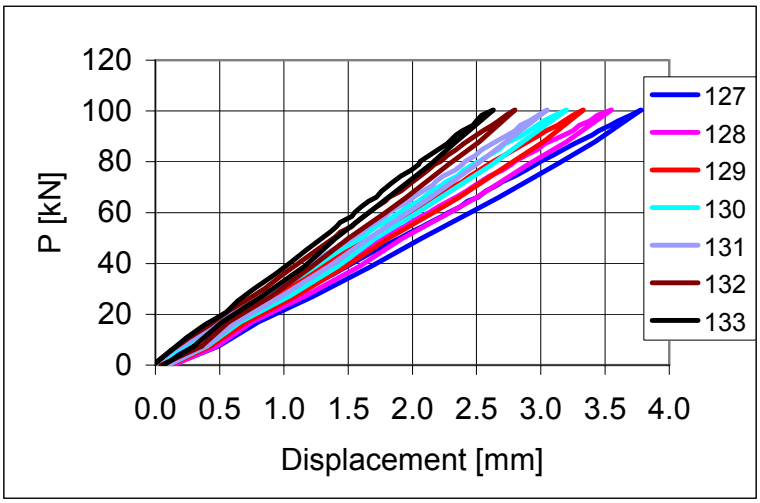

Fig. 33. FT200:2. Deflection. Transducers 127–133.

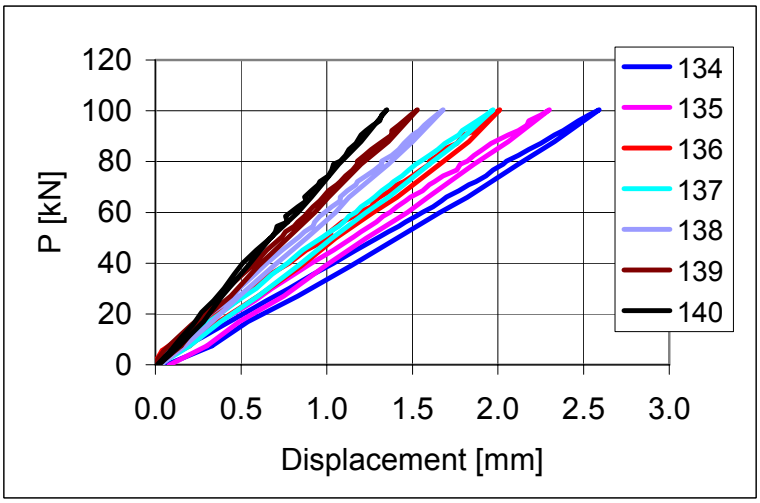

Fig. 34. FT200:2. Deflection. Transducers 134–140.

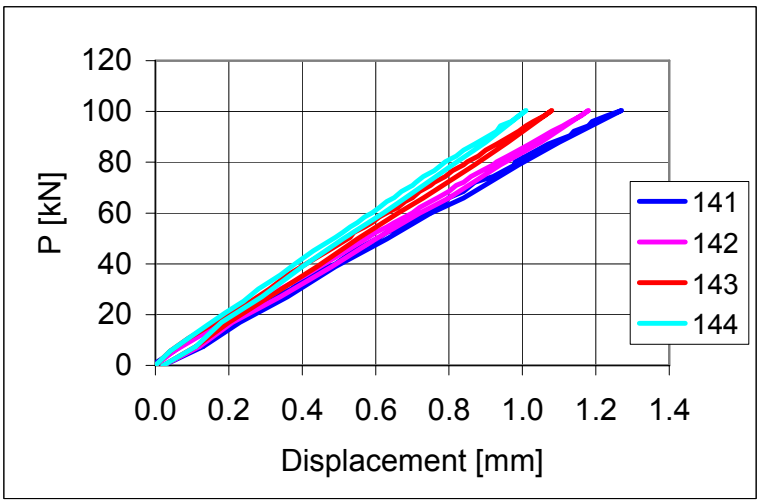

Fig. 35. FT200:2. Deflection. Transducers 141–144.

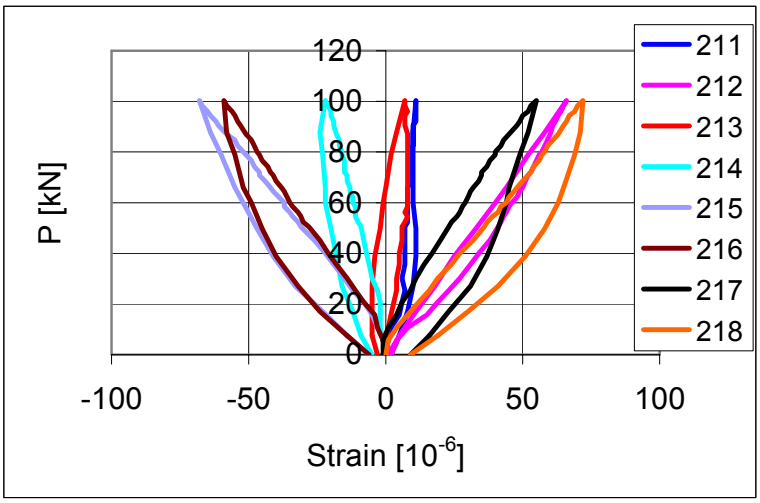

Fig. 36. FT200:2. Strain in trimmer beam. Strain gauges 211–218.

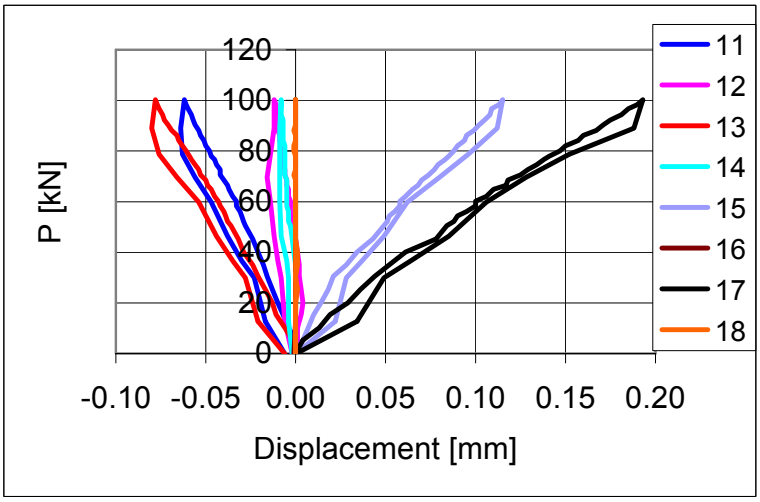

Fig. 37. FT200:3. Longitudinal horizontal displacement. Transducers 11–18.

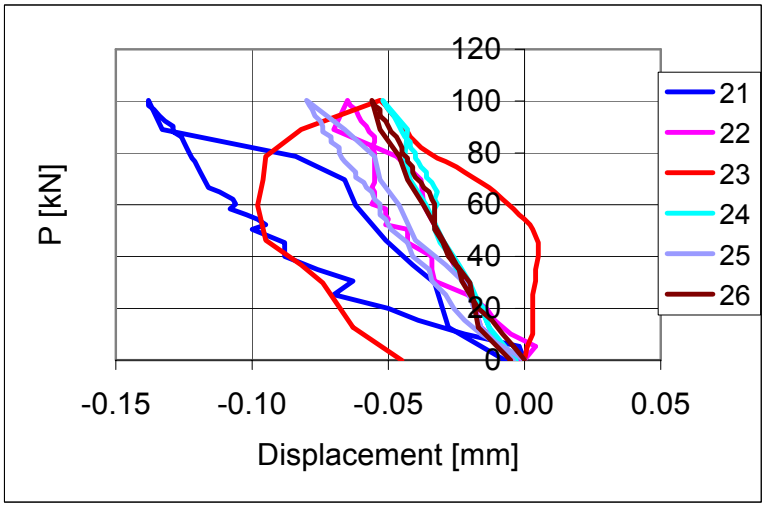

Fig. 38. FT200:2. Transverse horizontal displacement. Transducers 21–26.

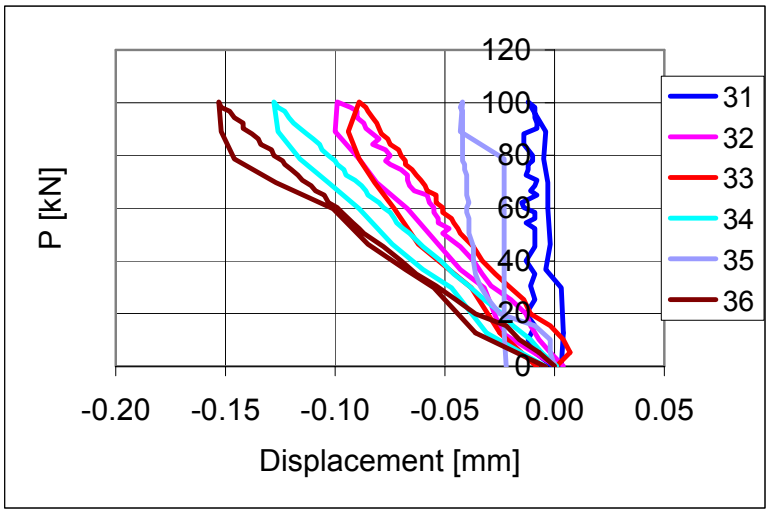

Fig. 39. FT200:3. Transverse horizontal displacement. Transducers 31–36.

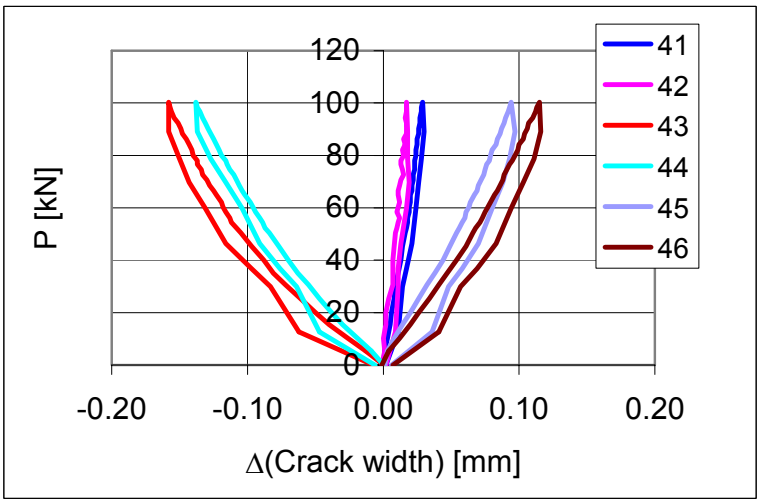

Fig. 40. FT200:3. Change in crack width. Transducers 41–46.

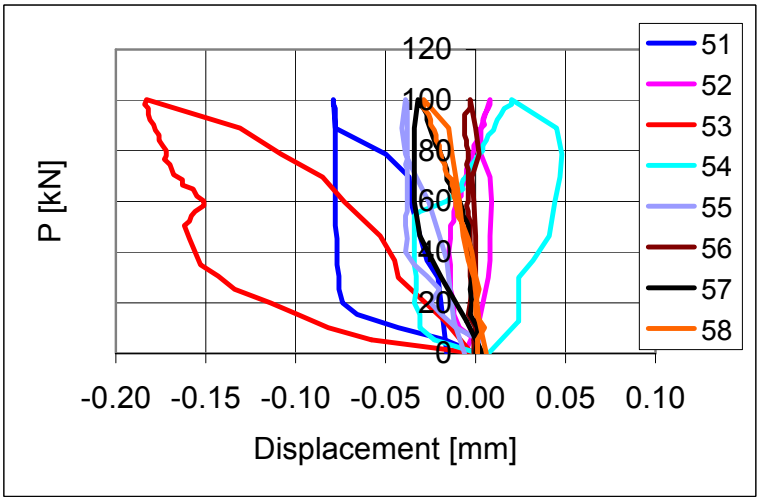

Fig. 41. FT200:3. Transverse horizontal displacement. Transducers 51–58.

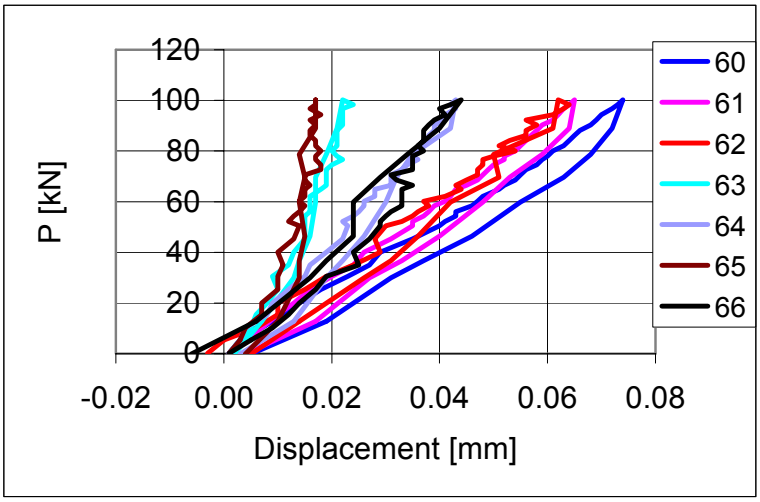

Fig. 42. FT200:3. Settlement of support. Transducers 60–66.

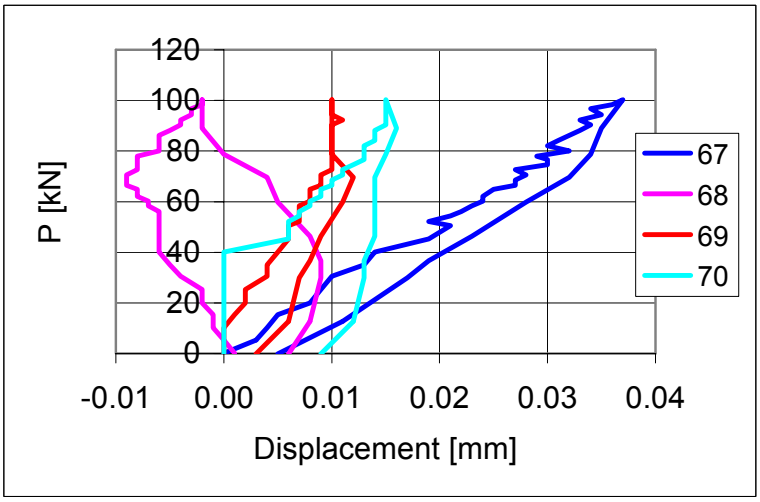

Fig. 43. FT200:3. Settlement of support. Transducers 67–70.

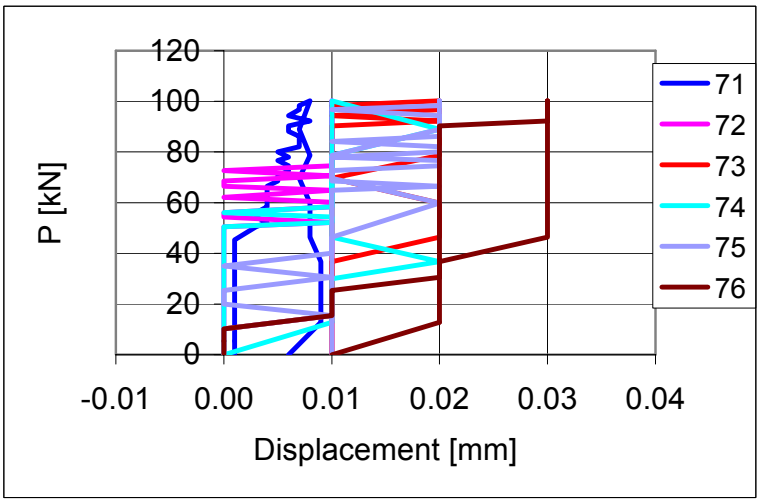

Fig. 44. FT200:3. Settlement of support. Transducers 71–76.

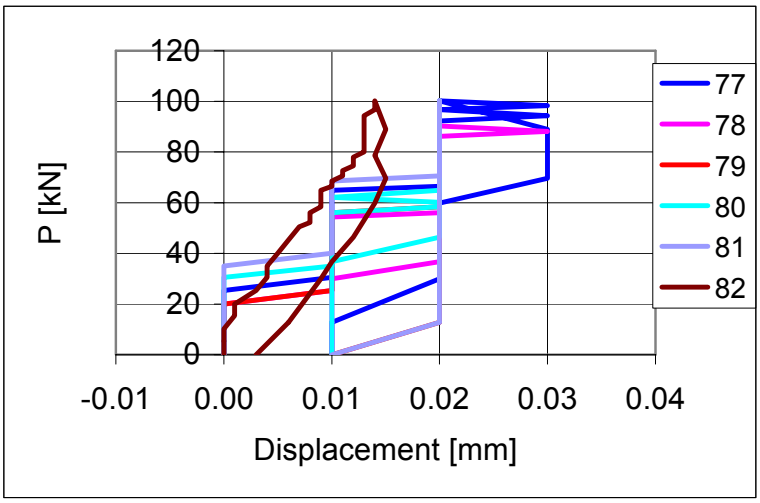

Fig. 45. FT200:3. Settlement of support. Transducers 77–82.

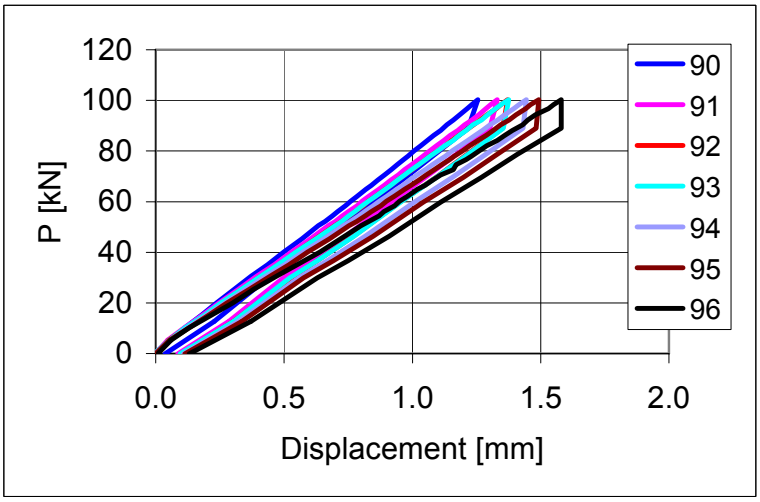

Fig. 46. FT200:3. Deflection. Transducers 90–96.

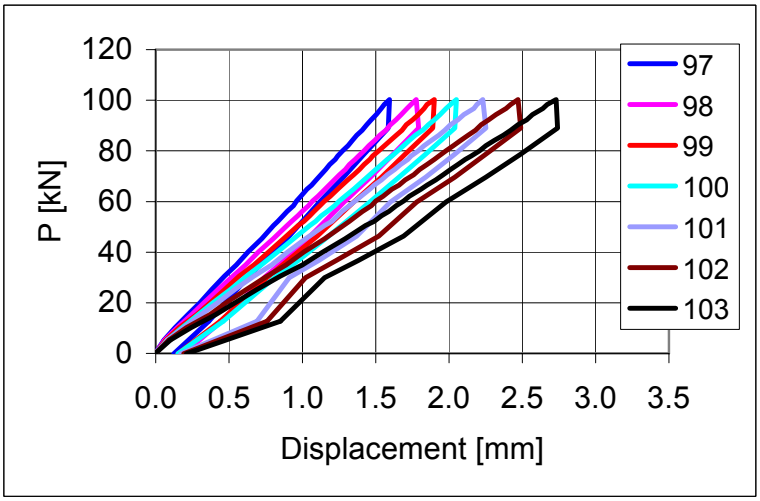

Fig. 47. FT200:3. Deflection. Transducers 97–103.

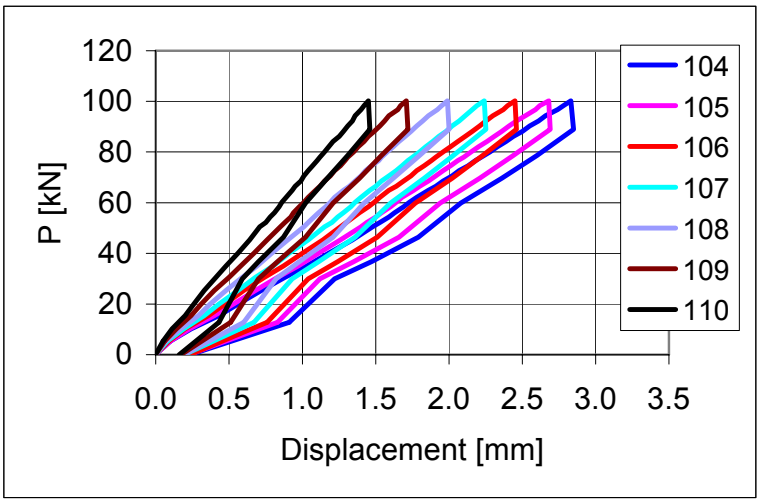

Fig. 48. FT200:3. Deflection. Transducers 104–110.

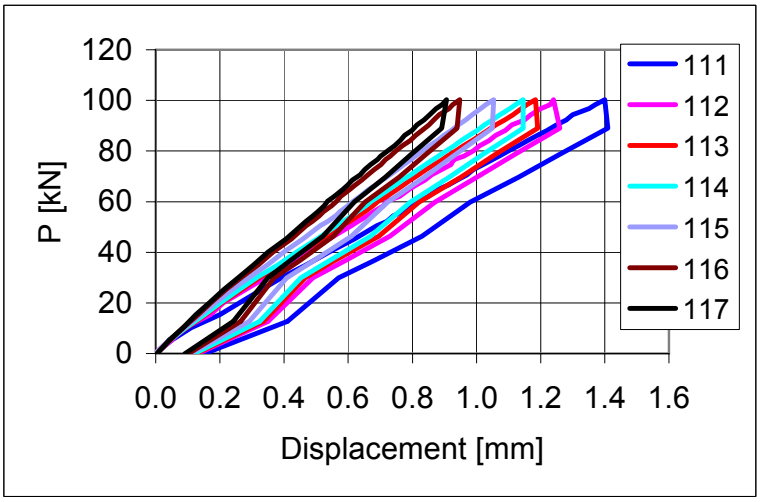

Fig. 49. FT200:3. Deflection. Transducers 111–117.

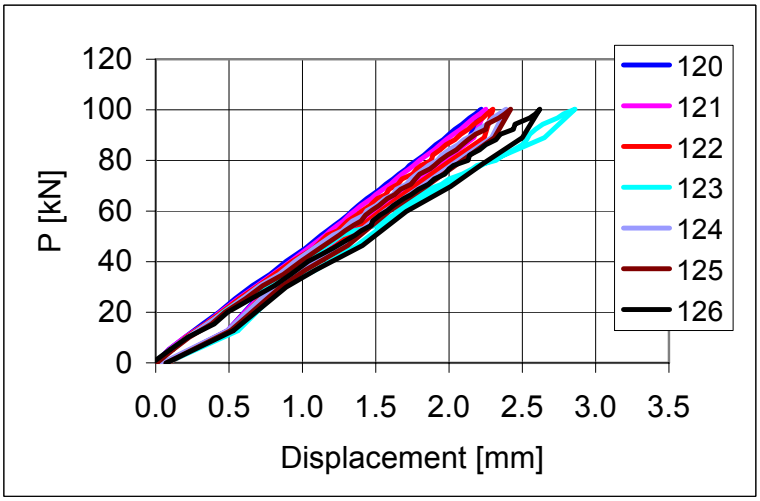

Fig. 50. FT200:3. Deflection. Transducers 120–126.

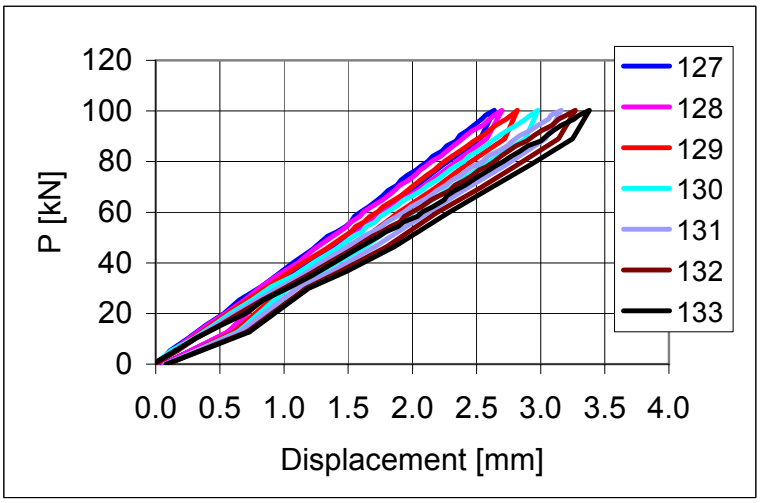

Fig. 51. FT200:3. Deflection. Transducers 127–133.

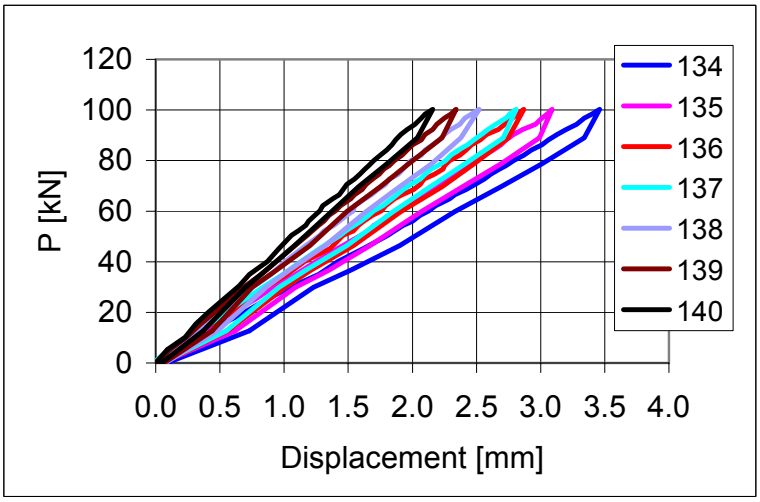

Fig. 52. FT200:3. Deflection. Transducers 134–140.

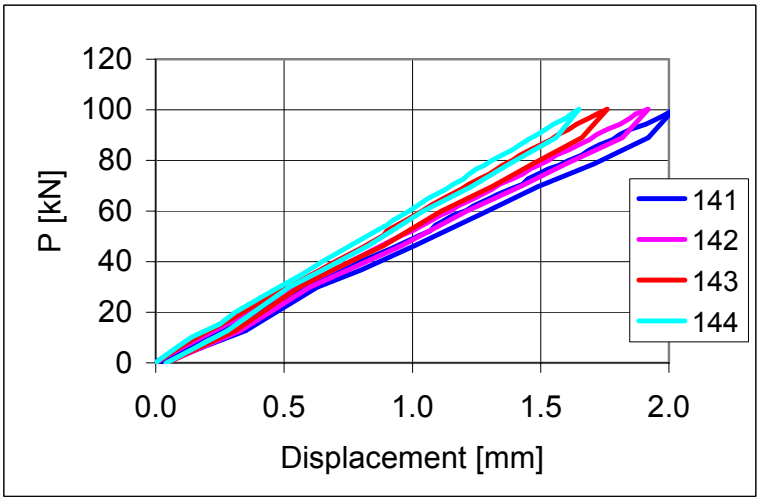

Fig. 53. FT200:3. Deflection. Transducers 141–144.

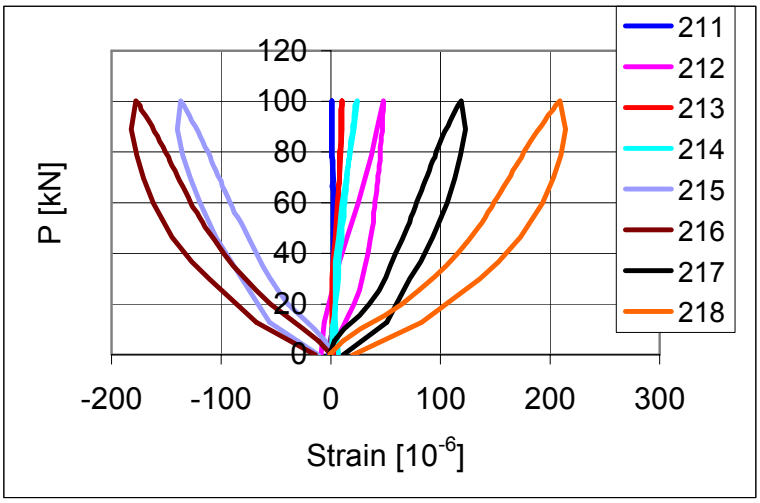

Fig. 54. FT200:3. Strain in trimmer beam. Transducers 211–218.

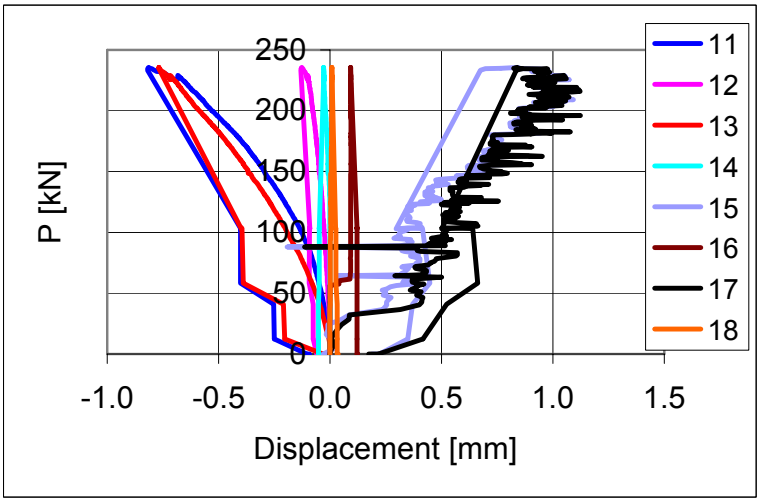

Fig. 55. FT200:12. Longitudinal horizontal displacement. Transducers 11–18.

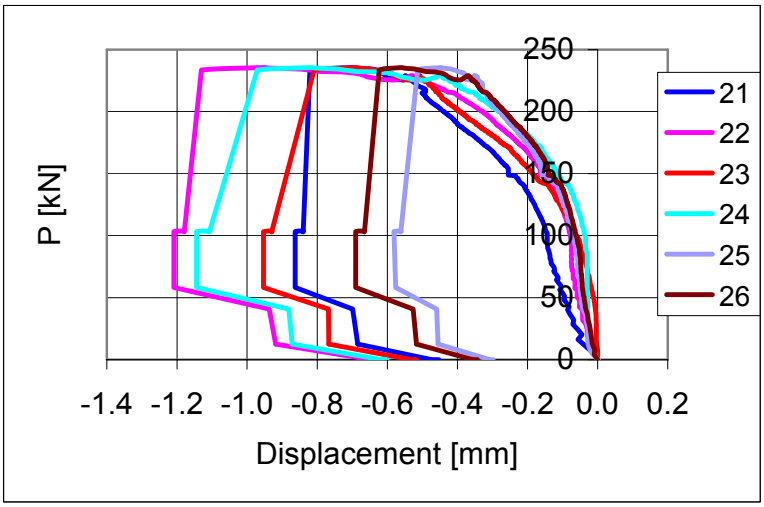

Fig. 56. FT200:12. Transverse horizontal displacement. Transducers 21–26.

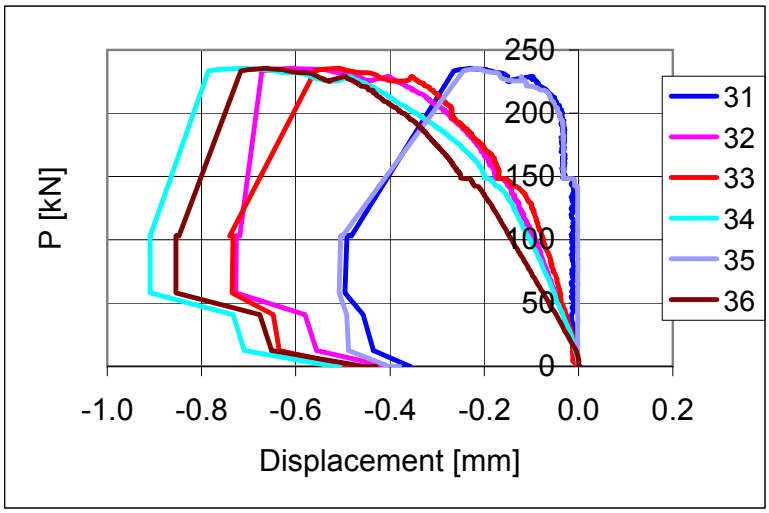

Fig. 57. FT200:12. Transverse horizontal displacement. Transducers 31–36.

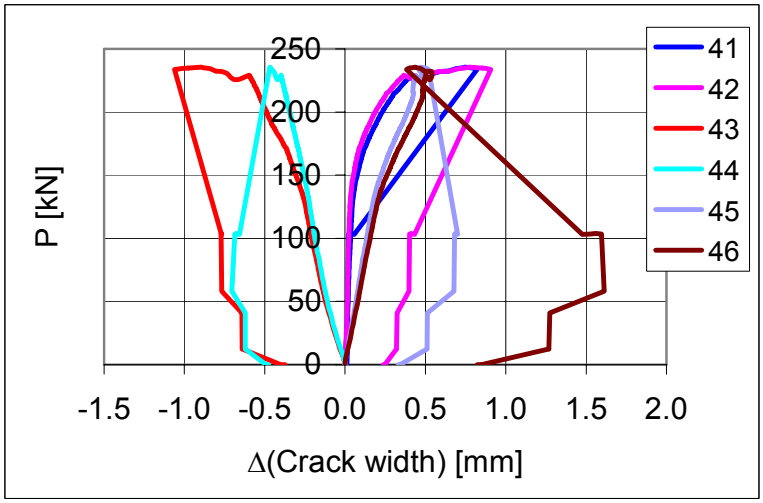

Fig. 58. FT200:12. Change in crack width. Transducers 41–46.

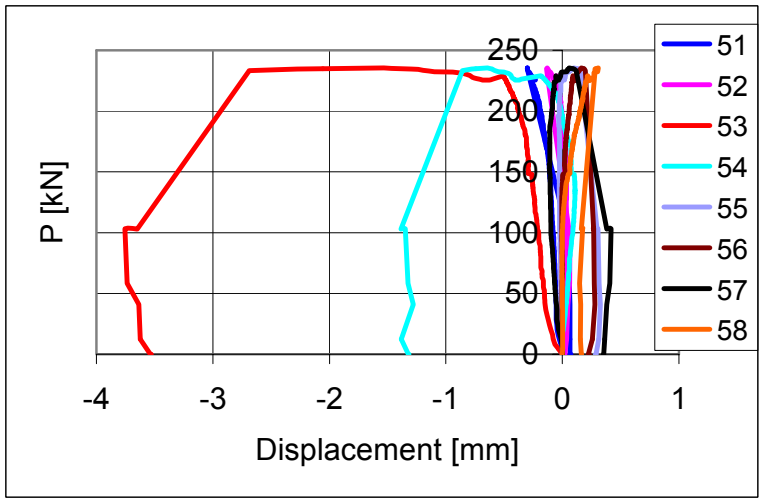

Fig. 59. FT200:12. Transverse horizontal displacement. Transducers 51–58.

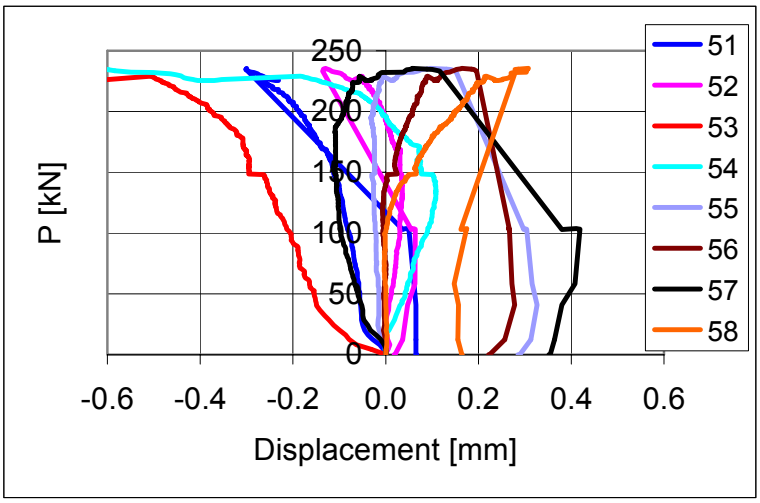

Fig. 60. FT200:12. Transverse horizontal displacement. Transducers 51–58.

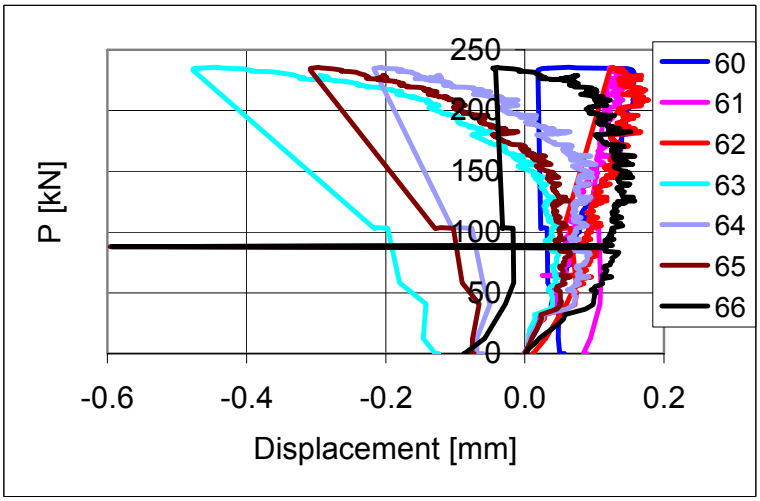

Fig. 61. FT200:12. Settlement of support. Transducers 60–66.

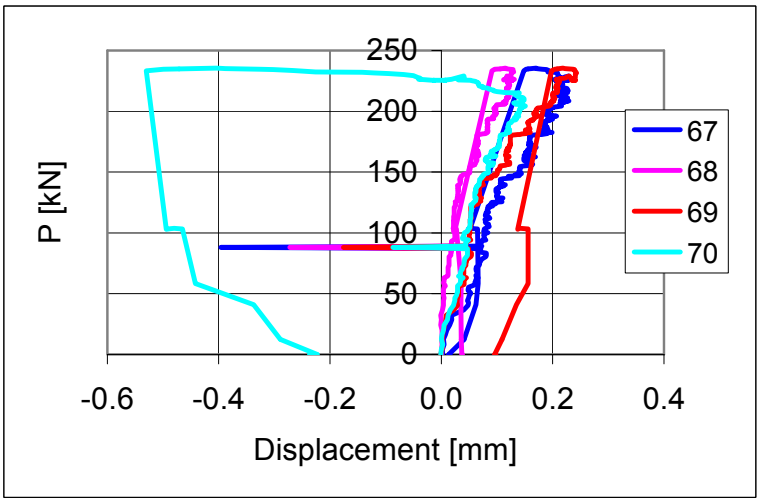

Fig. 62. FT200:12. Settlement of support. Transducers 67–70.

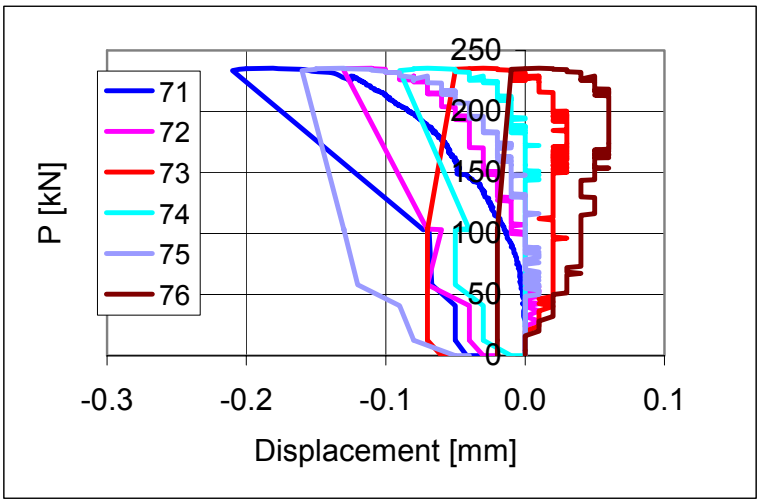

Fig. 63. FT200:12. Settlement of support. Transducers 71–76.

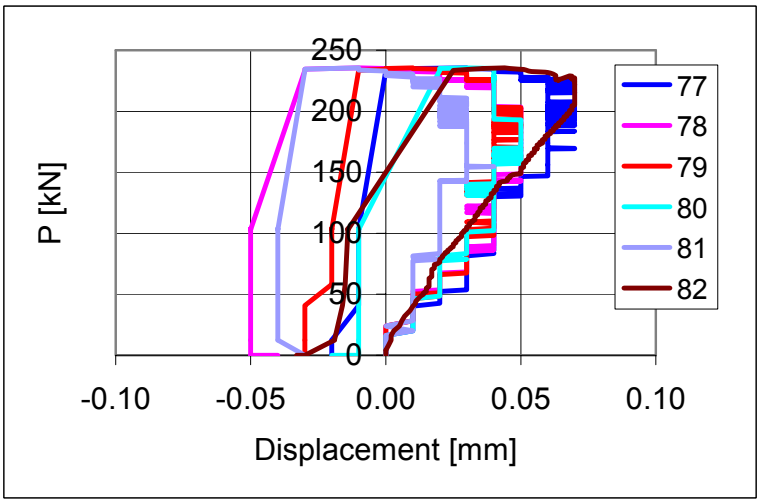

Fig. 64. FT200:12. Settlement of support. Transducers 77–82.

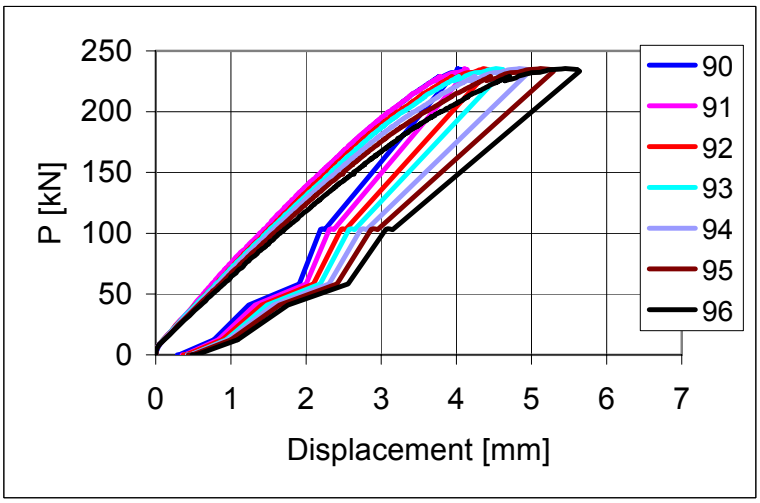

Fig. 65. FT200:12. Deflection. Transducers 90–96.

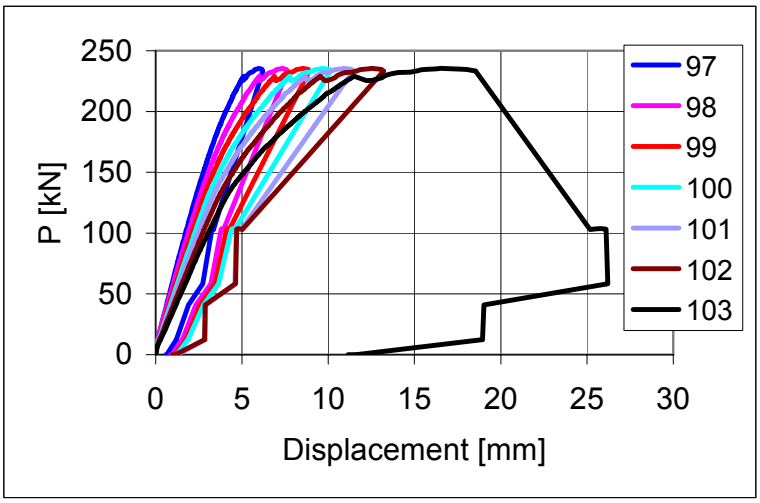

Fig. 66. FT200:12. Deflection. Transducers 97–103.

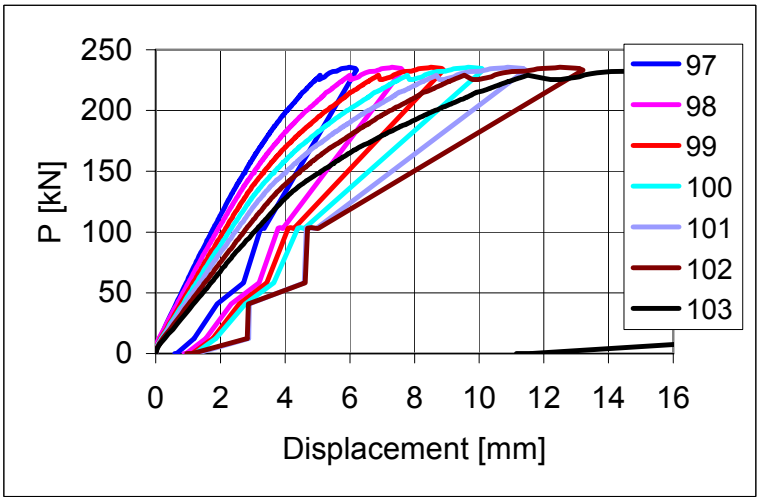

Fig. 67. FT200:12. Deflection. Transducers 97–103.

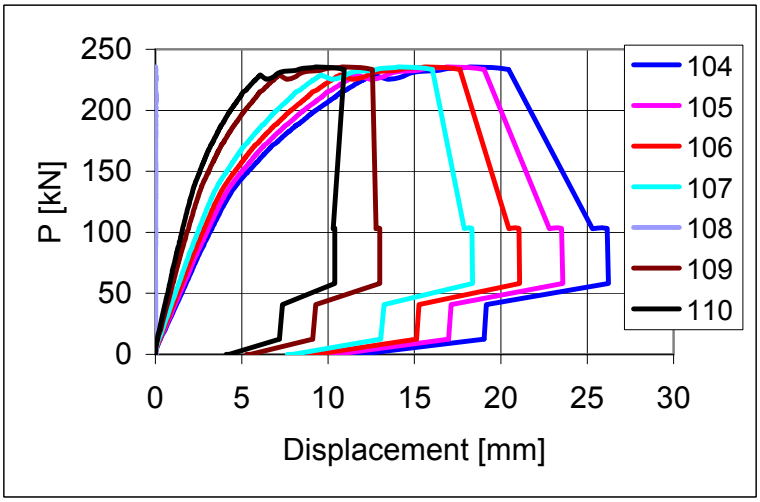

Fig. 68. FT200:12. Deflection. Transducers 104–110.

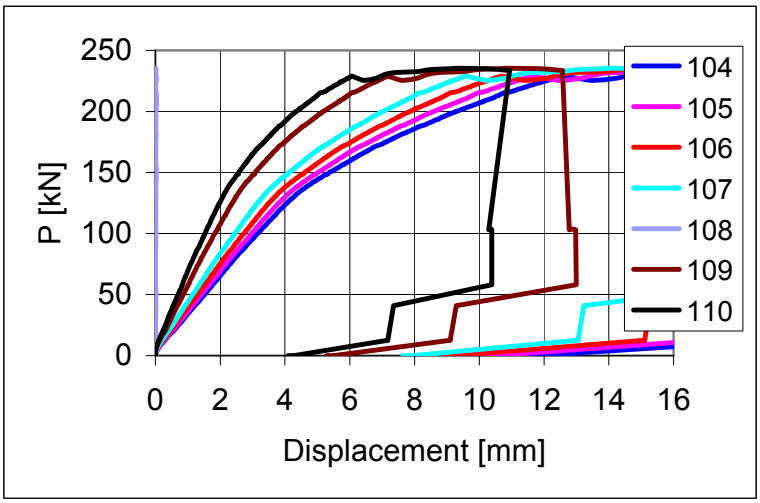

Fig. 69. FT200:12. Deflection. Transducers 104–110. Transducer 108 out of action.

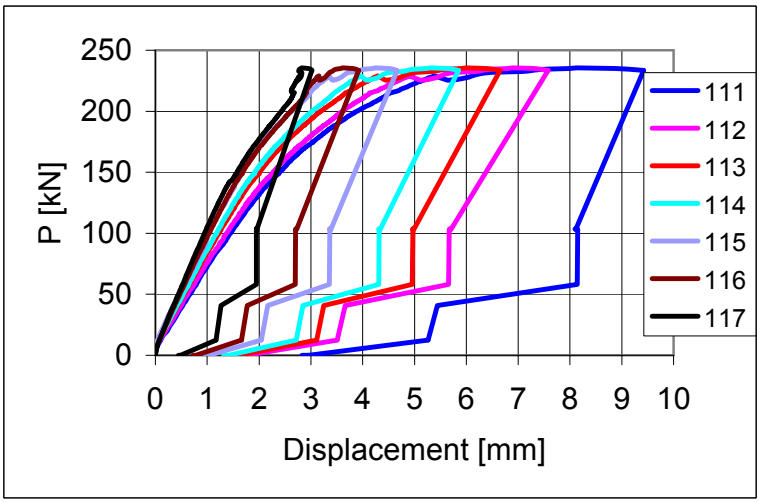

Fig. 70. FT200:12. Deflection. Transducers 111–117.

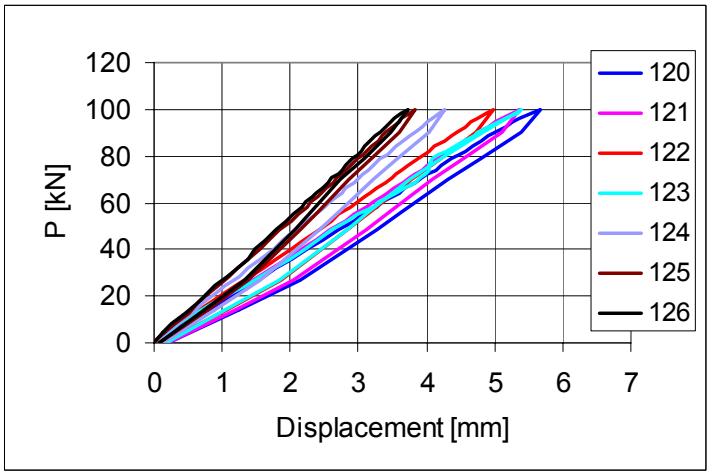

Fig. 71. FT200:12. Deflection. Transducers 120–126.

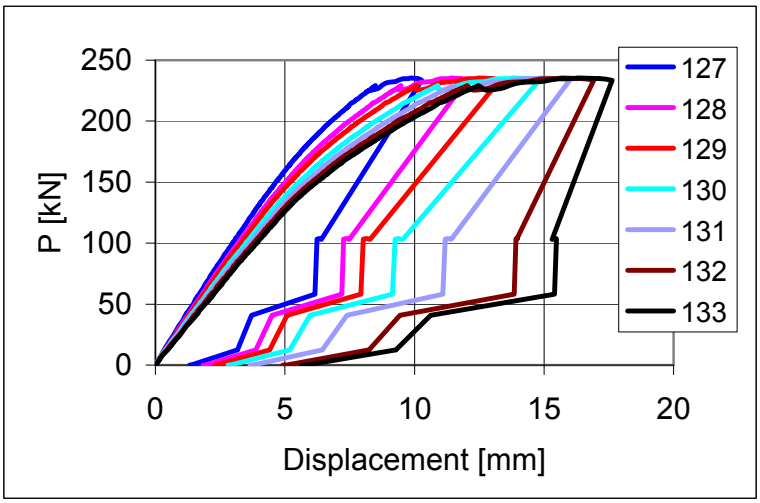

Fig. 72. FT200:12. Deflection. Transducers 127–133.

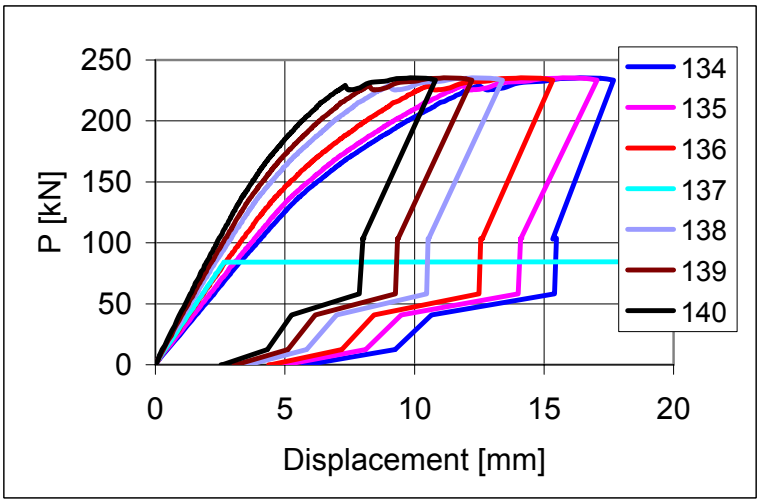

Fig. 73. FT200:12. Deflection. Transducers 134–140.

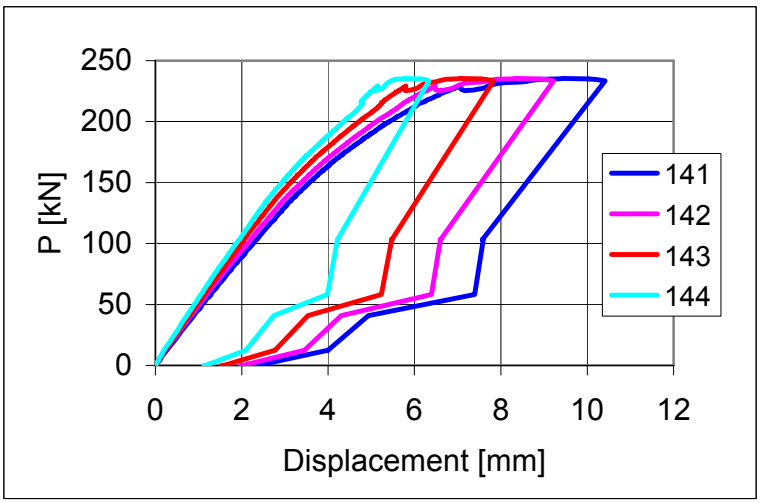

Fig. 74. FT200:12. Deflection. Transducers 141–144.

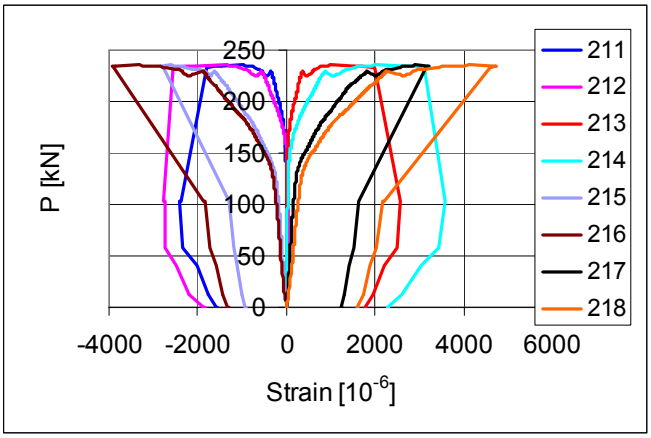

Fig. 75. FT200:12. Strain in trimmer beam. Transducers 211–218.

Appendix E: Measured strains and displacements in tests FT200:4–FT200:11

The load *P* is the actuator load without weight of loading equipment. The following terms are used for different measured displacements:

- *deflection*: vertical displacement of slab
- *transverse horizontal displacement*: horizontal displacement perpendicular to the longitudinal xis of the slab
- *longitudinal horizontal displacement*: horizontal displacement of supporting beam parallel to the longitudinal axis of the slab.

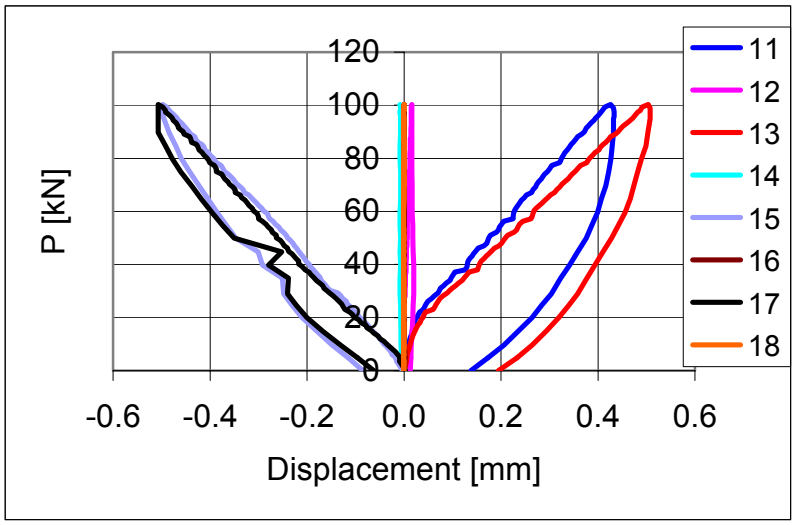

Fig. 1. FT200:4. Longitudinal horizontal displacement. Transducers 11–18.

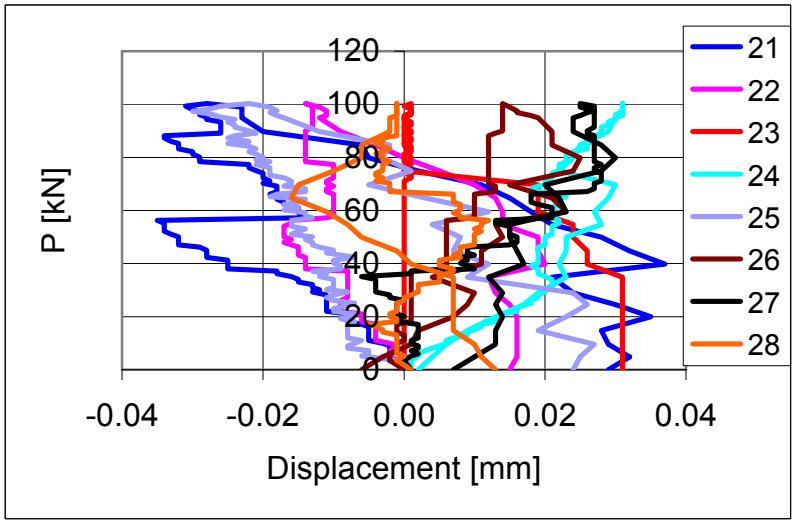

Fig. 2. FT200:4. Transverse horizontal displacement. Transducers 21–28.

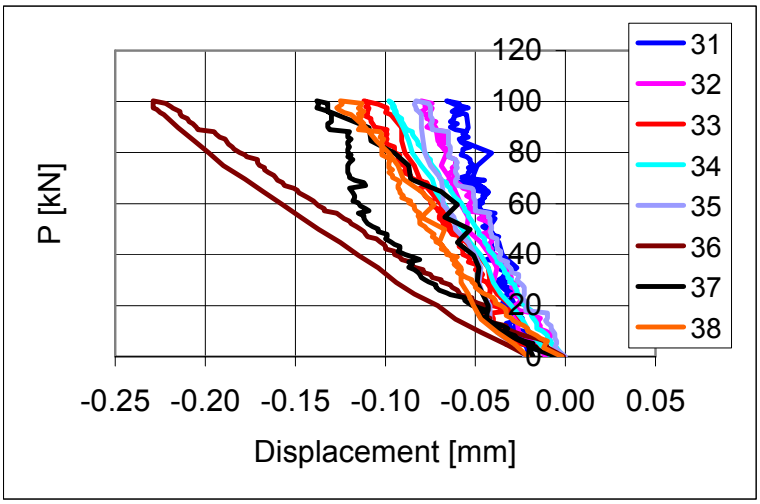

Fig. 3. FT200:4. Transverse horizontal displacement. Transducers 31–38.

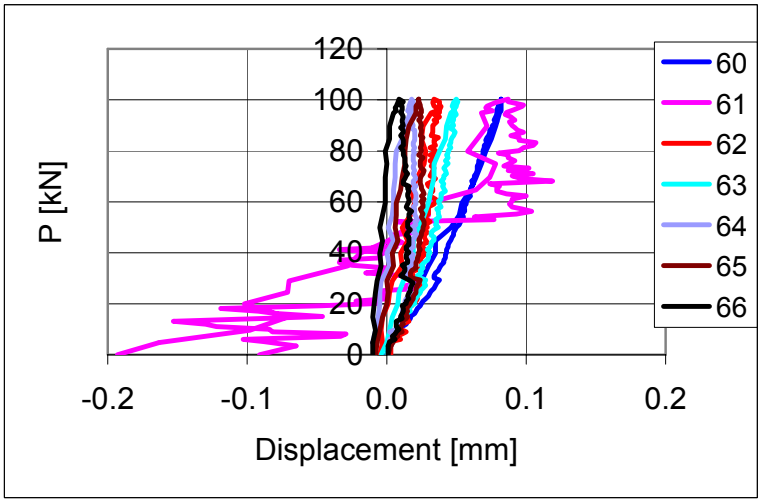

Fig. 4. FT200:4. Settlement of support. Transducers 60–66.

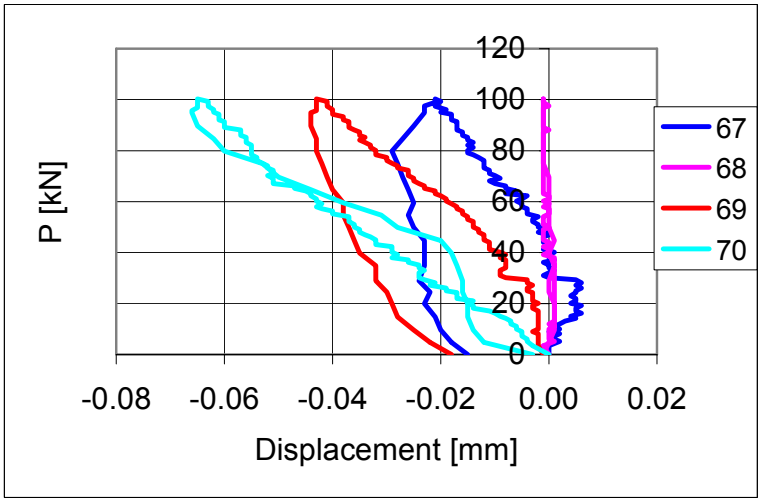

Fig. 5. FT200:4. Settlement of support. Transducers 67–70.

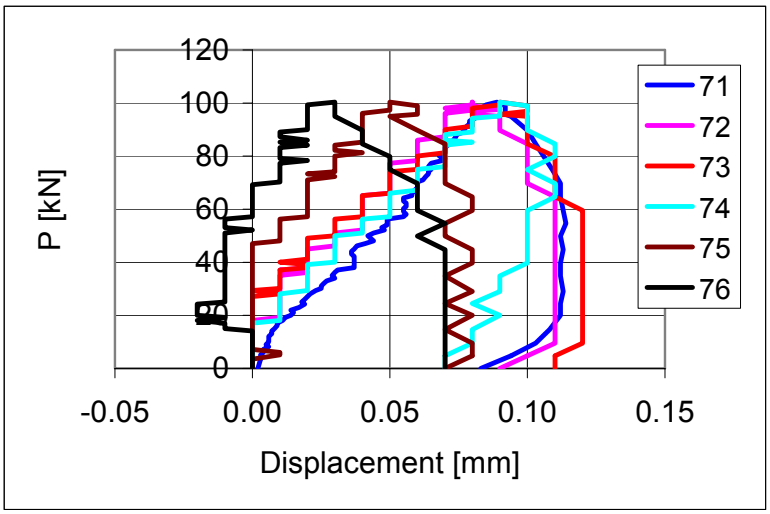

Fig. 6. FT200:4. Settlement of support. Transducers 71–76.

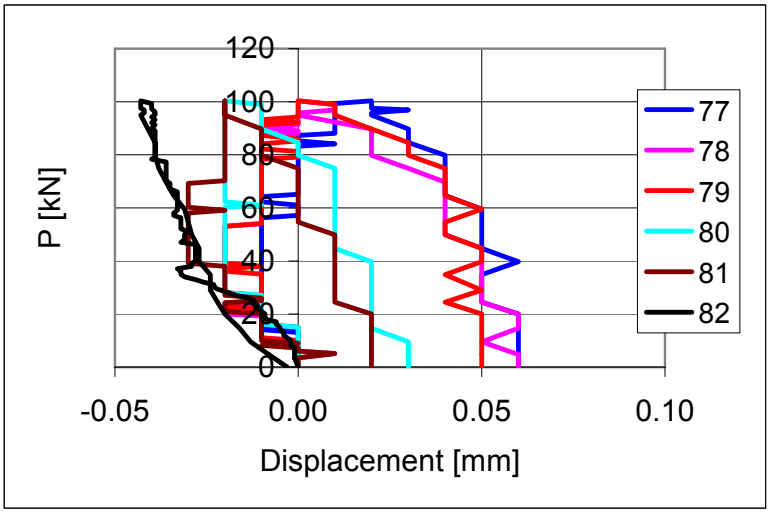

Fig. 7. FT200:4. Settlement of support. Transducers 77–82.

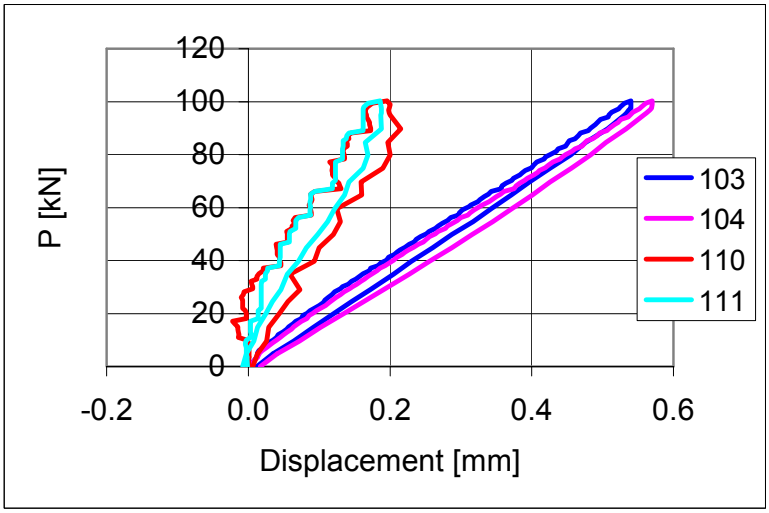

Fig. 8. FT200:4. Deflection. Transducers 103, 104, 110 and 111.

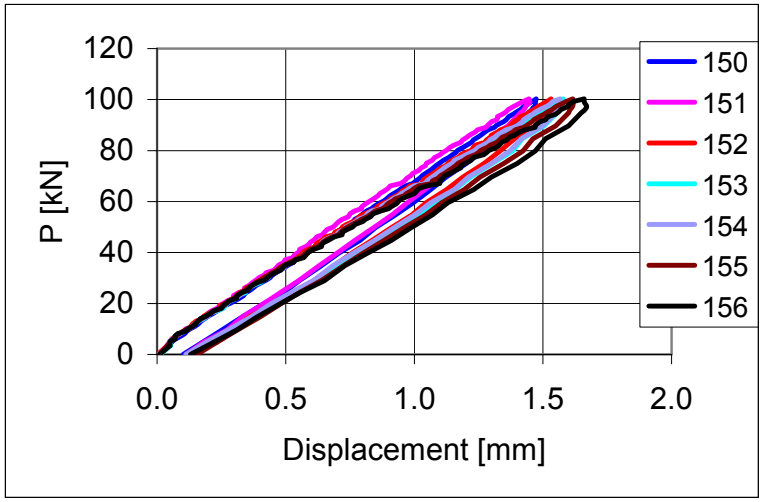

Fig. 9. FT200:4. Deflection. Transducers 150–156.

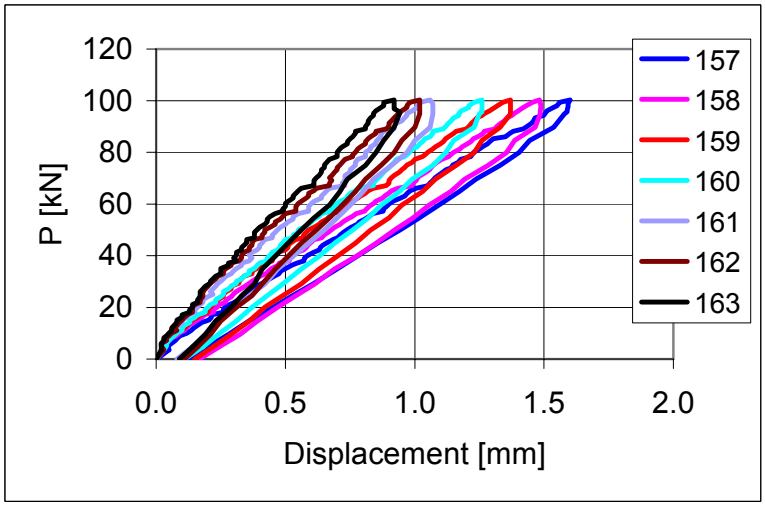

Fig. 10. FT200:4. Deflection. Transducers 157–163.

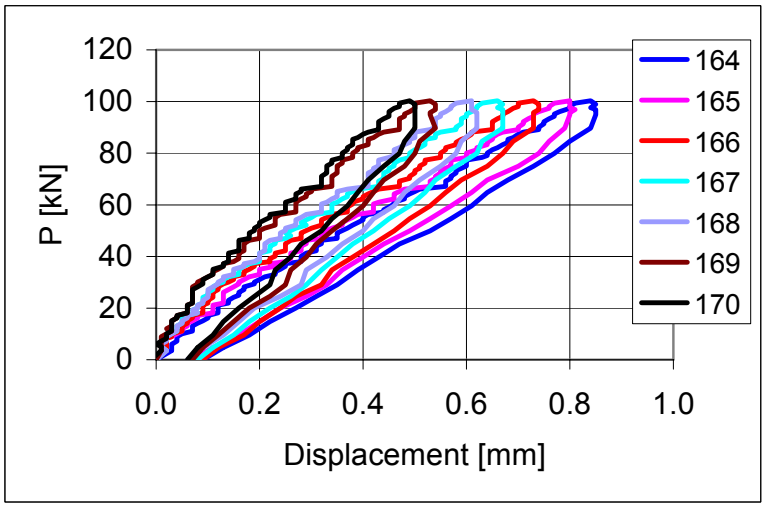

Fig. 11. FT200:4. Deflection. Transducers 164–170.

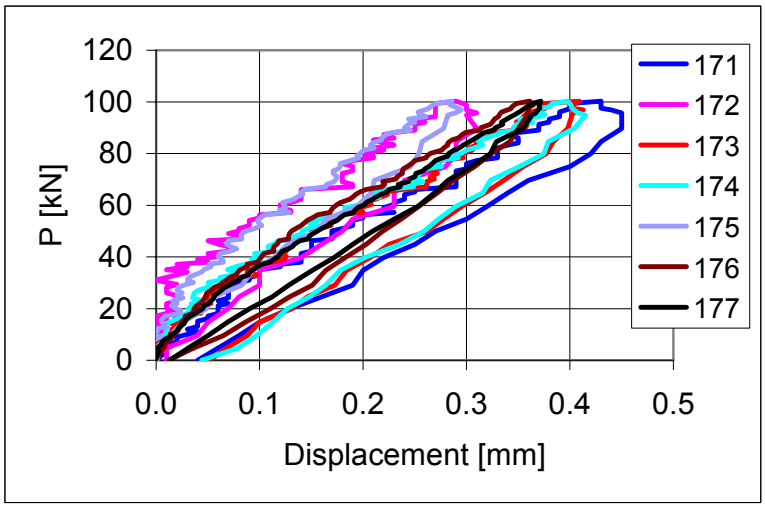

Fig. 12. FT200:4. Deflection. Transducers 171–177.

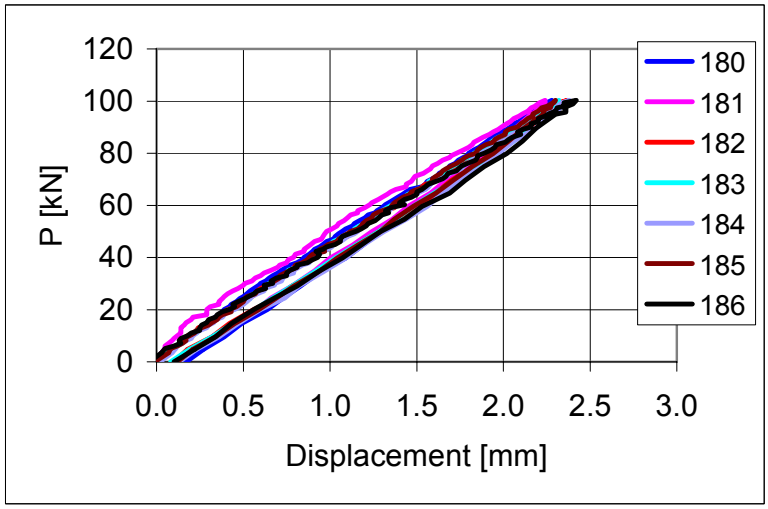

Fig. 13. FT200:4. Deflection. Transducers 180–186.

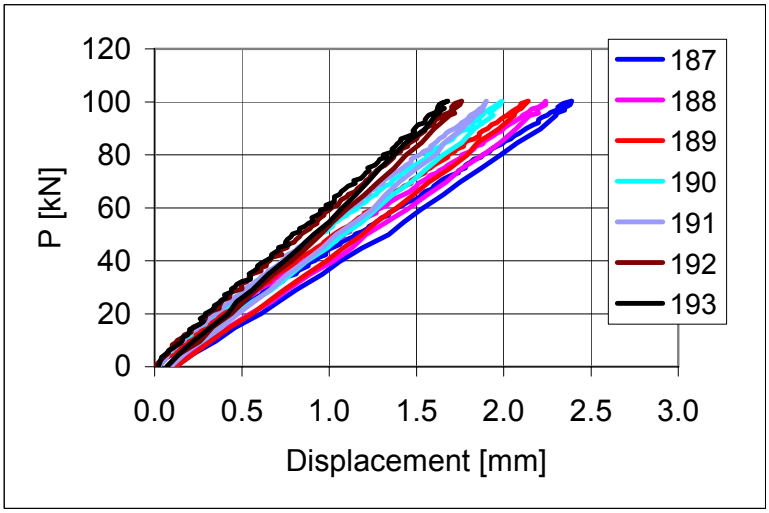

Fig. 14. FT200:4. Deflection. Transducers 187–193.

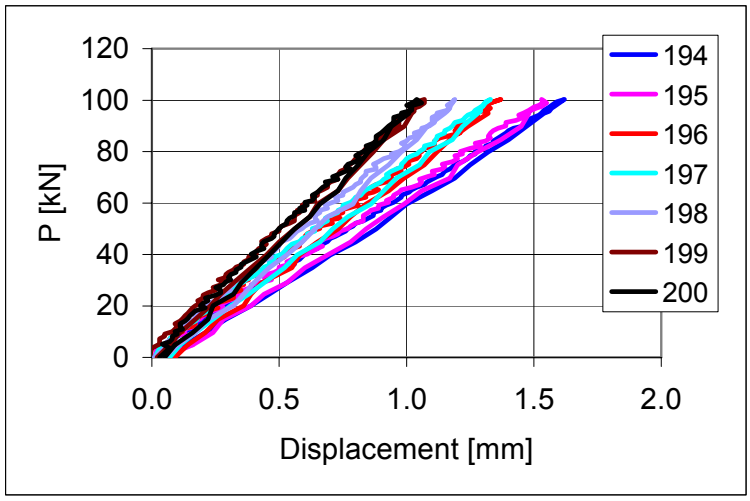

Fig. 15. FT200:4. Deflection. Transducers 194–200.

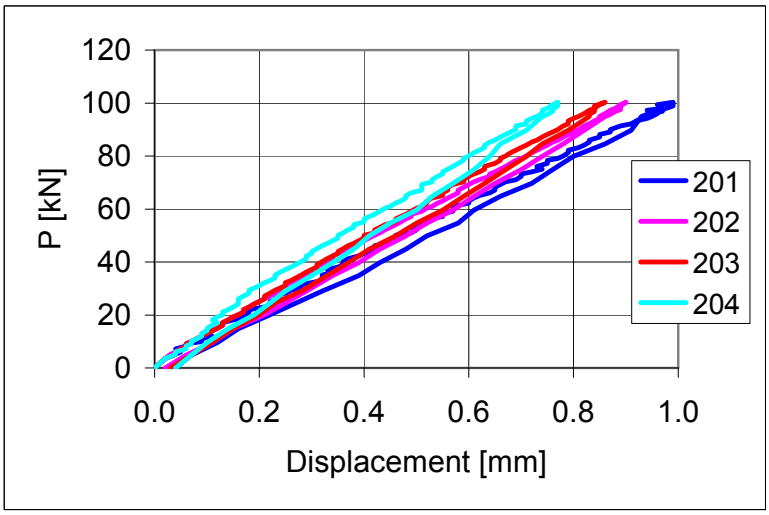

Fig. 16. FT200:4. Deflection. Transducers 201–204.

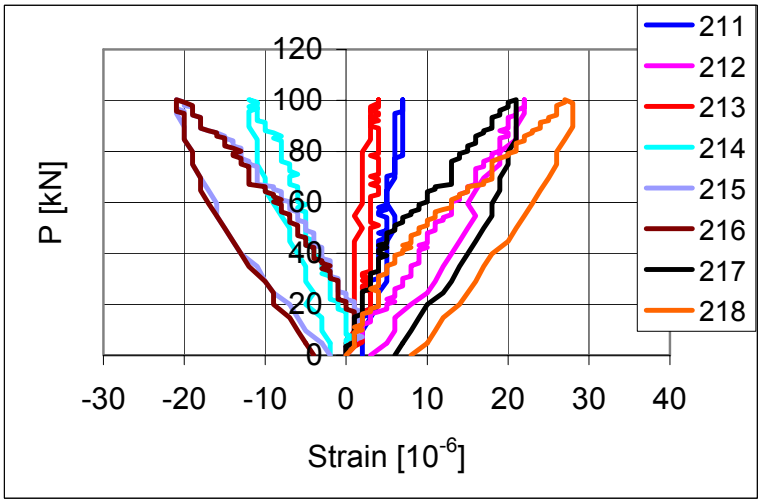

Fig. 17. FT200:4. Strain in trimmer beam. Strain gauges 211–218.

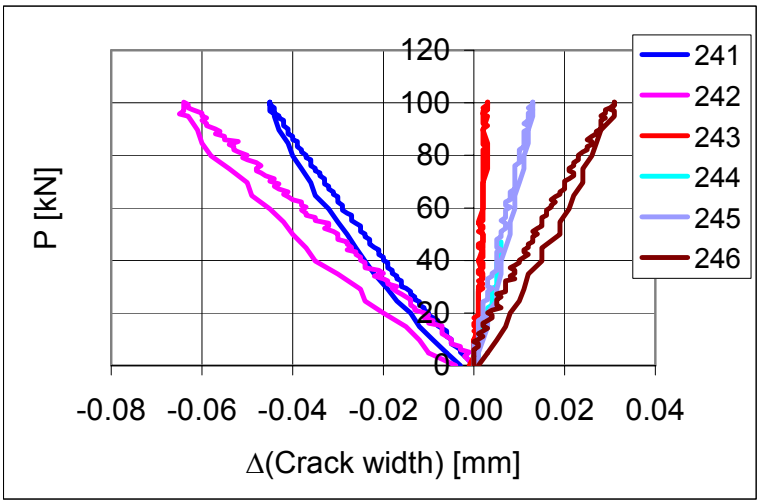

Fig. 18. FT200:4. Change in crack width. Transducers 241–246.

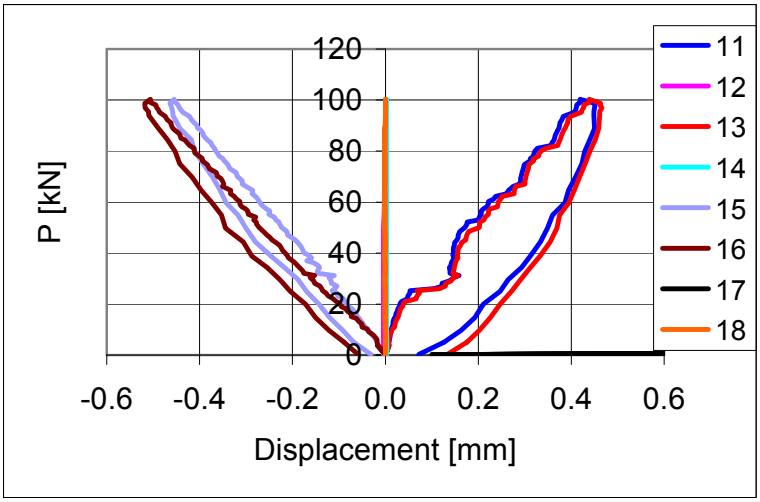

Fig. 19. FT200:5. Longitudinal horizontal displacement. Transducers 11–18.

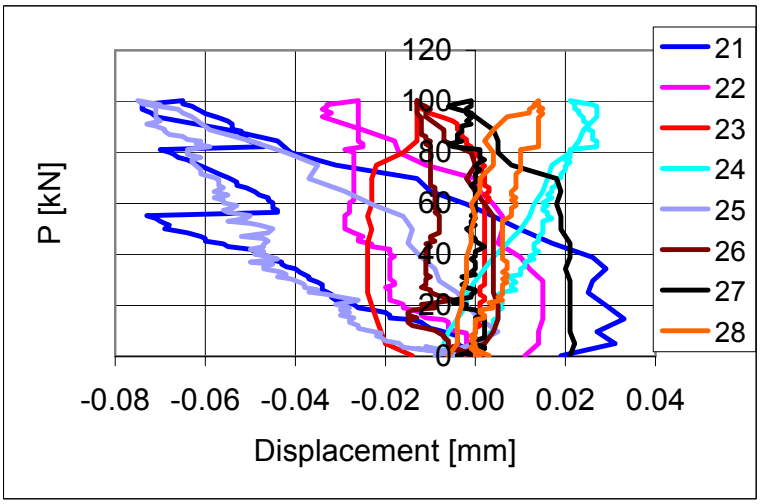

Fig. 20. FT200:5. Transverse horizontal displacement. Transducers 21–28.

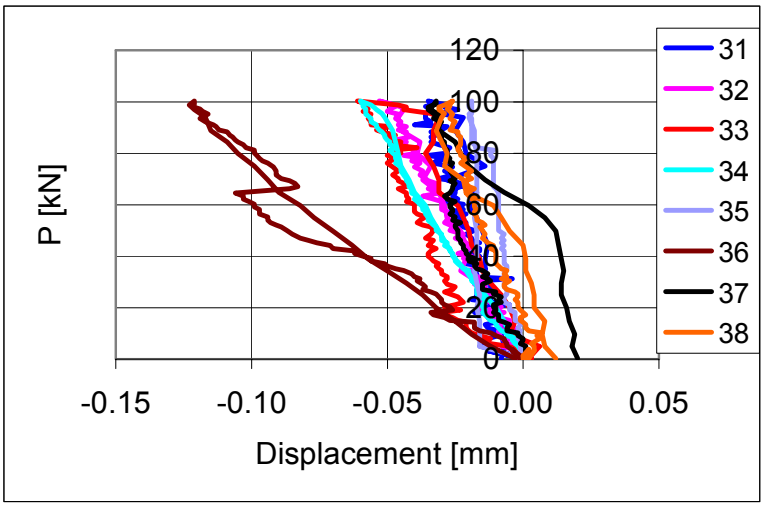

Fig. 21. FT200:5. Transverse horizontal displacement. Transducers 31–38.

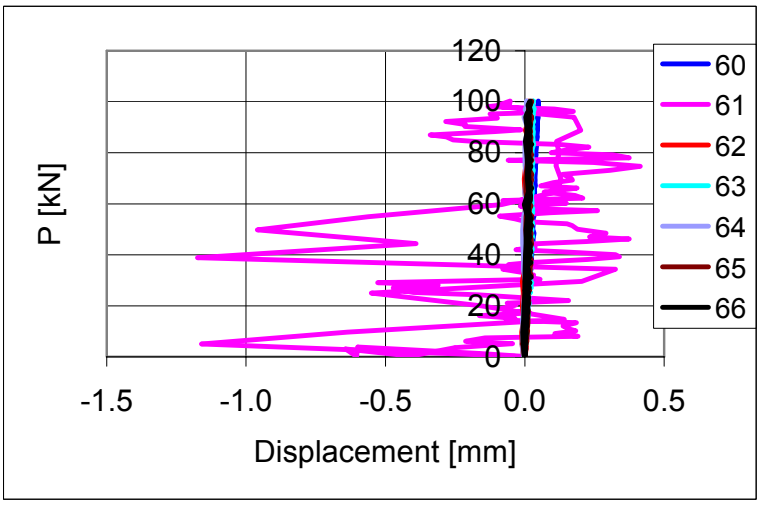

Fig. 22. FT200:5. Settlement of support. Transducers 60–66. Transducer 61 out of action.

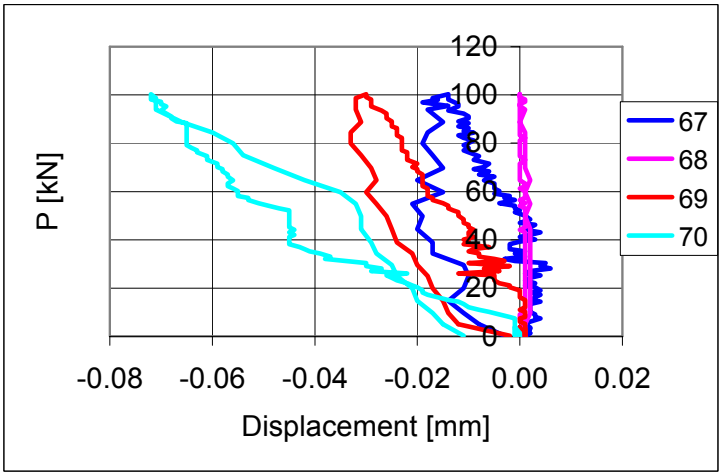

Fig. 23. FT200:5. Settlement of support. Transducers 67–70.

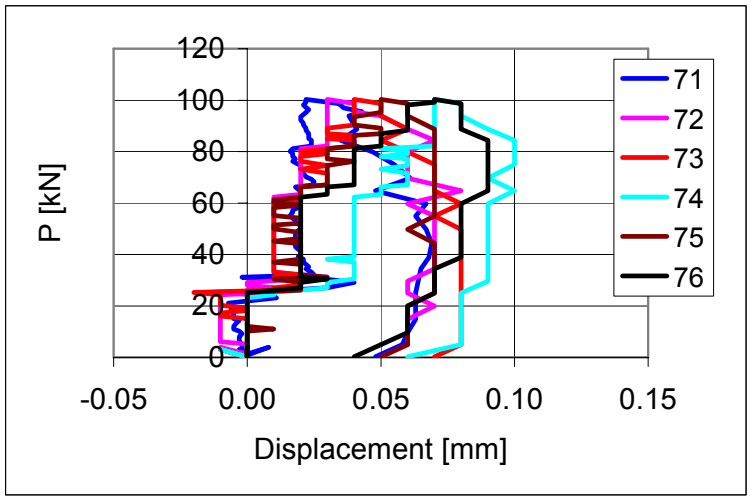

Fig. 24. FT200:5. Settlement of support. Transducers 71–76.

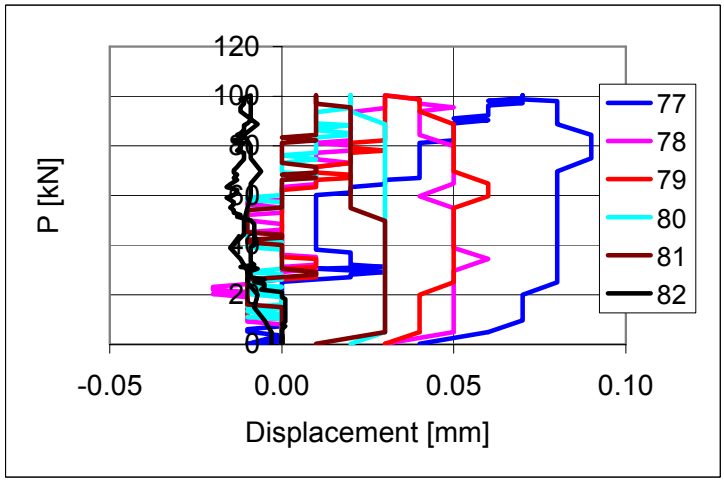

Fig. 25. FT200:5. Settlement of support. Transducers 77–82.

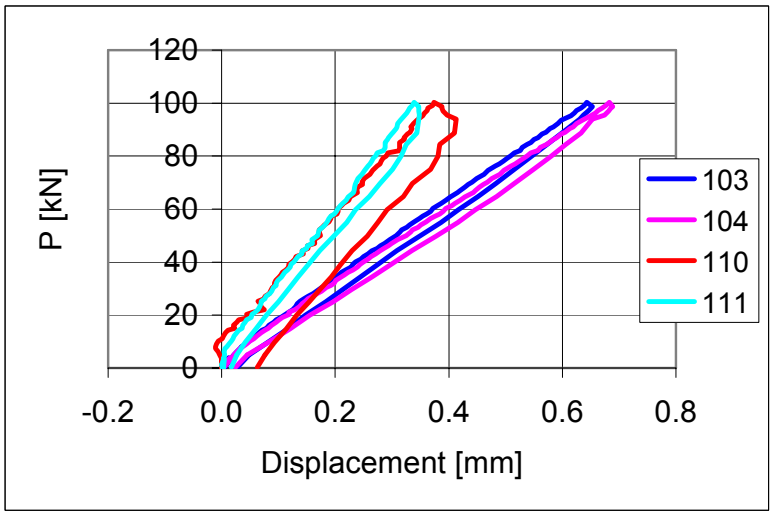

Fig. 26. FT200:5. Deflection. Transducers 103, 104, 110 and 111.

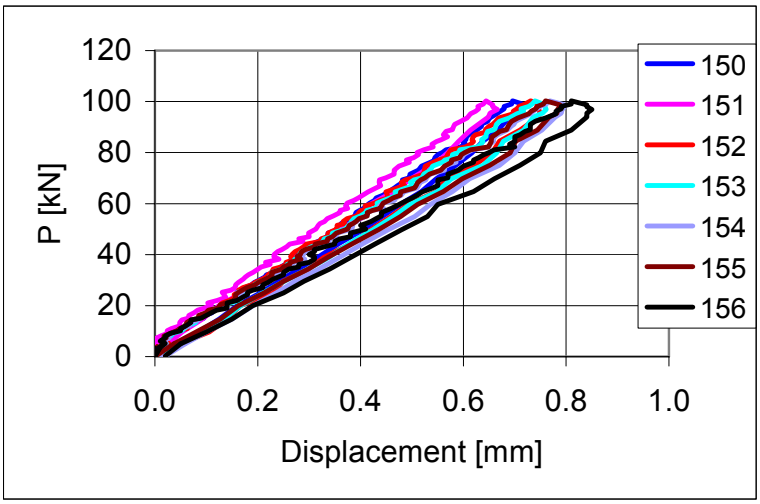

Fig. 27. FT200:5. Deflection. Transducers 150–156.

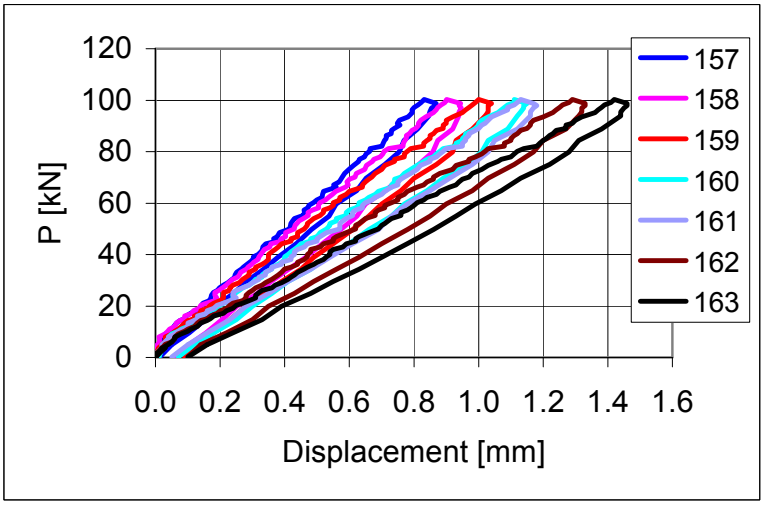

Fig. 28. FT200:5. Deflection. Transducers 157–163.

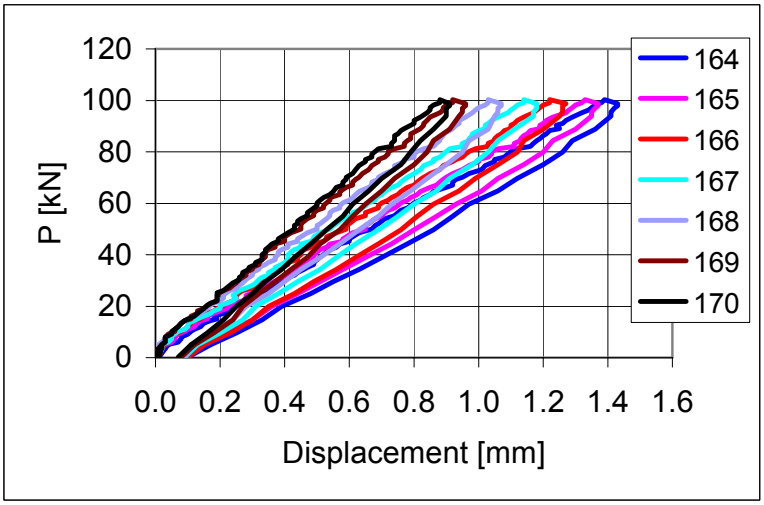

Fig. 29. FT200:5. Deflection. Transducers 164–170.

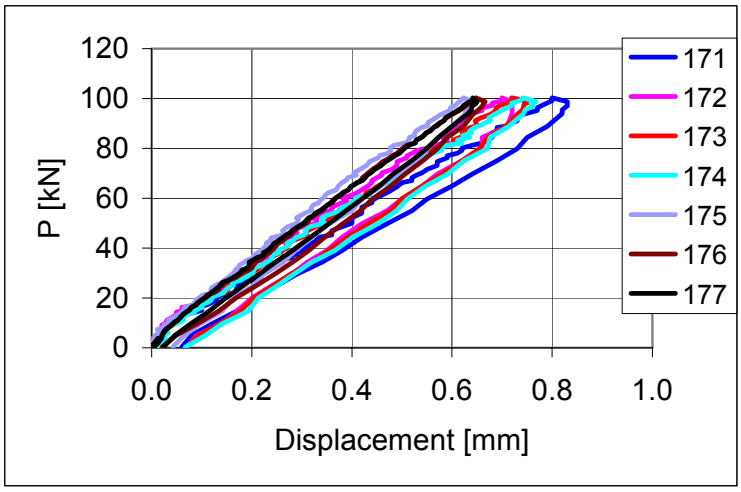

Fig. 30. FT200:5. Deflection. Transducers 171–177.

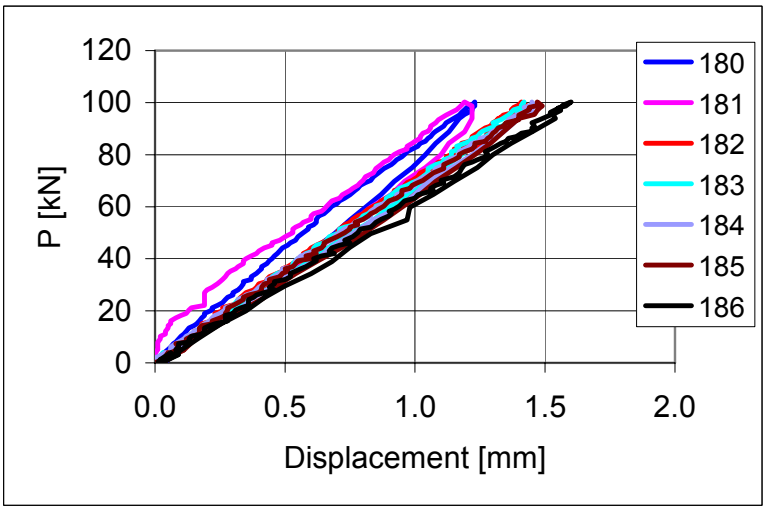

Fig. 31. FT200:5. Deflection. Transducers 180–186.

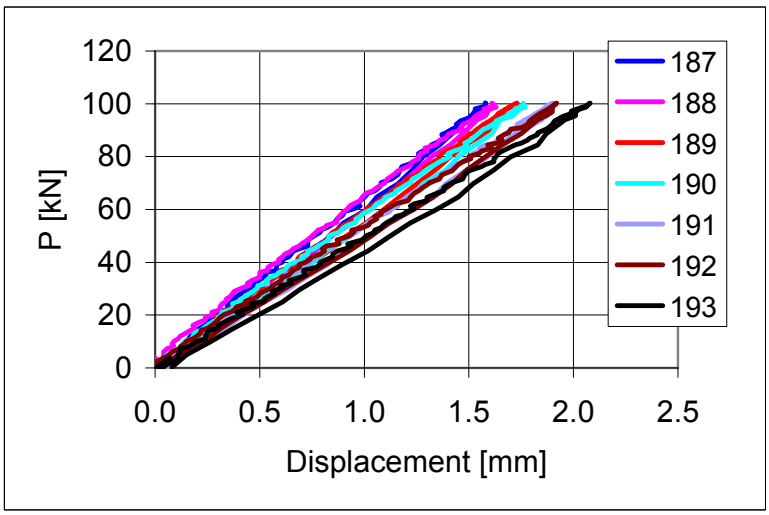

Fig. 32. FT200:5. Deflection. Transducers 187–193.

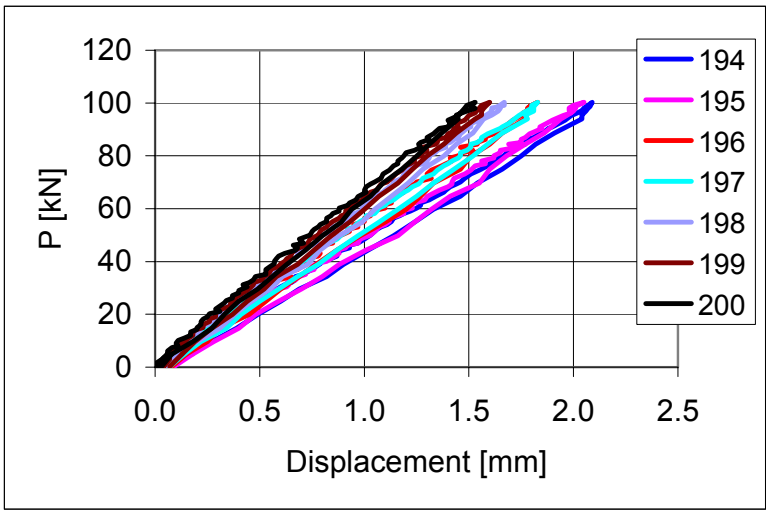

Fig. 33. FT200:5. Deflection. Transducers 194–200.

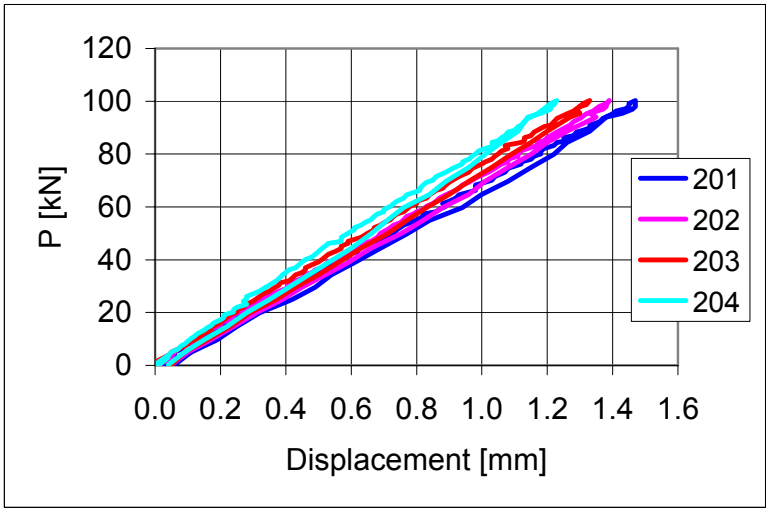

Fig. 34. FT200:5. Deflection. Transducers 201–204.

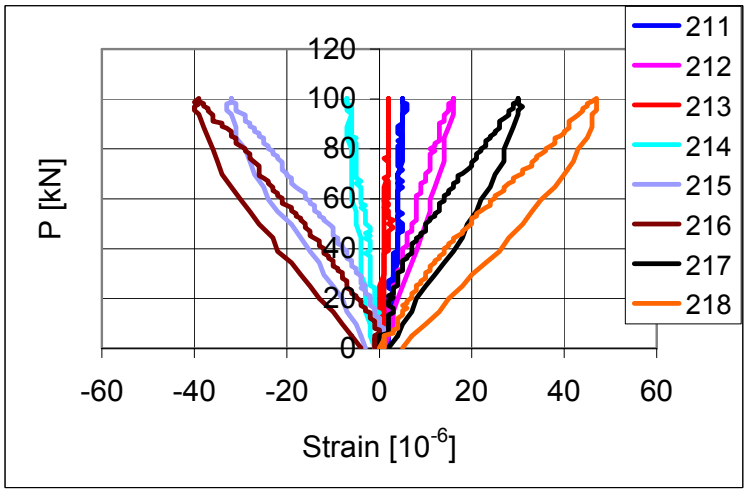

Fig. 35. FT200:5. Strain in trimmer beam. Strain gauges 211–218.

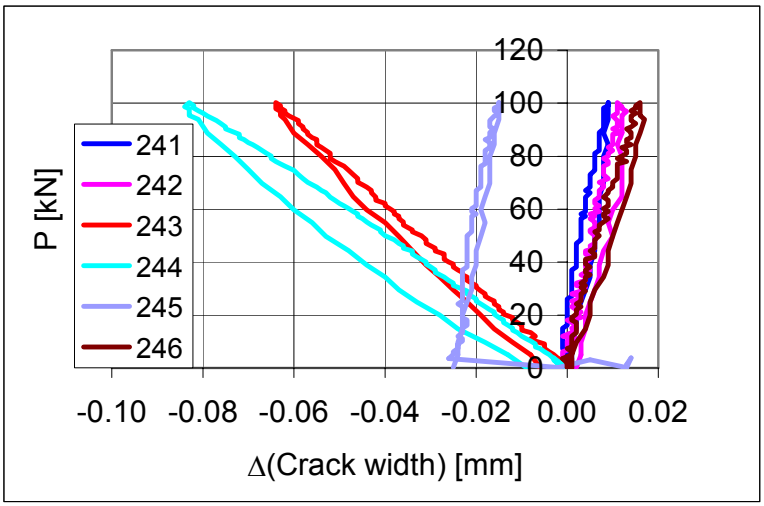

Fig. 36. FT200:5. Change in crack width. Transducers 241–246.

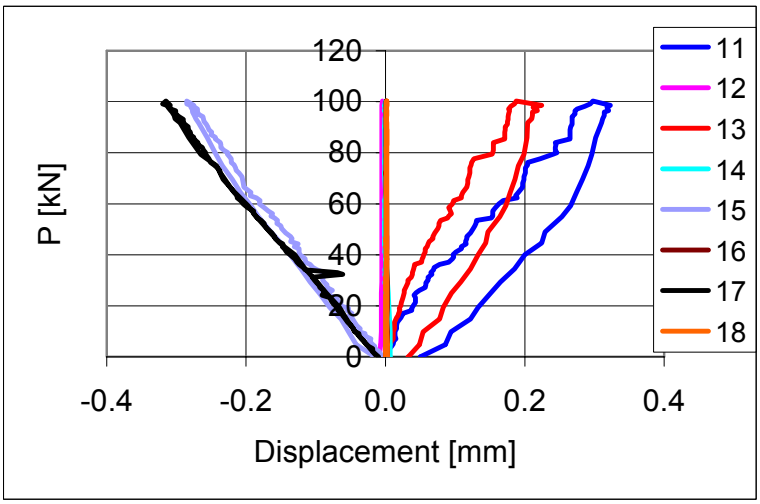

Fig. 37. FT200:6. Longitudinal horizontal displacement. Transducers 11–18.

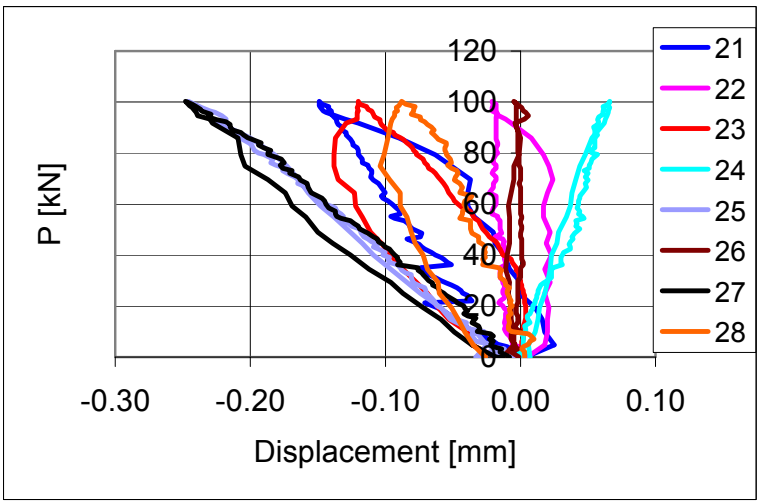

Fig. 38. FT200:6. Transverse horizontal displacement. Transducers 21–28.

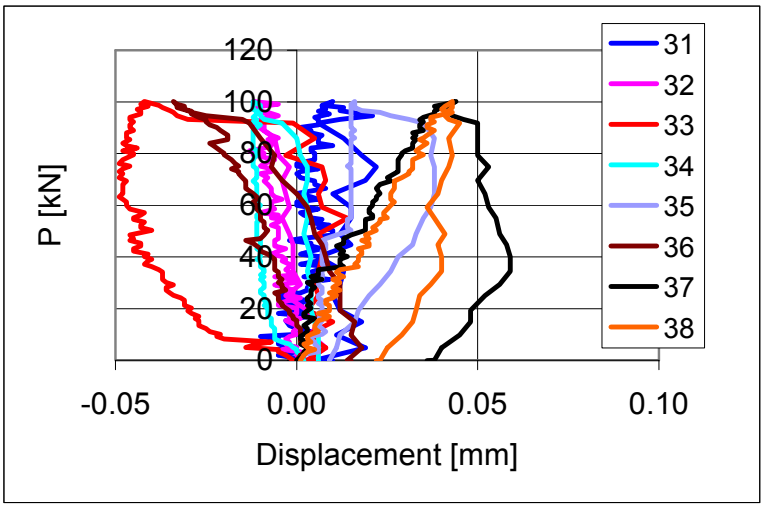

Fig. 39. FT200:6. Transverse horizontal displacement. Transducers 31–38.

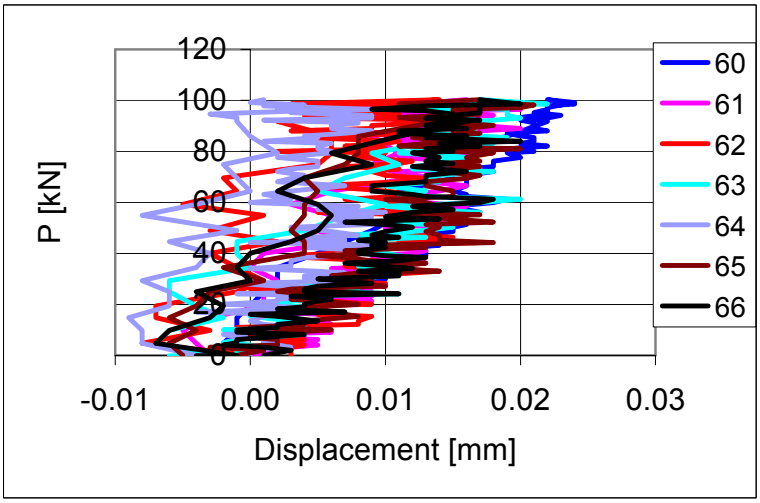

Fig. 40. FT200:6. Settlement of support. Transducers 60–66.

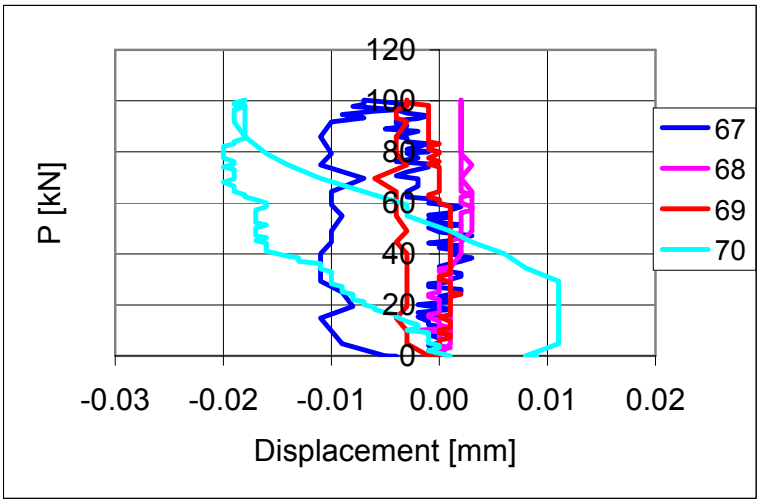

Fig. 41. FT200:6. Settlement of support. Transducers 67–70.

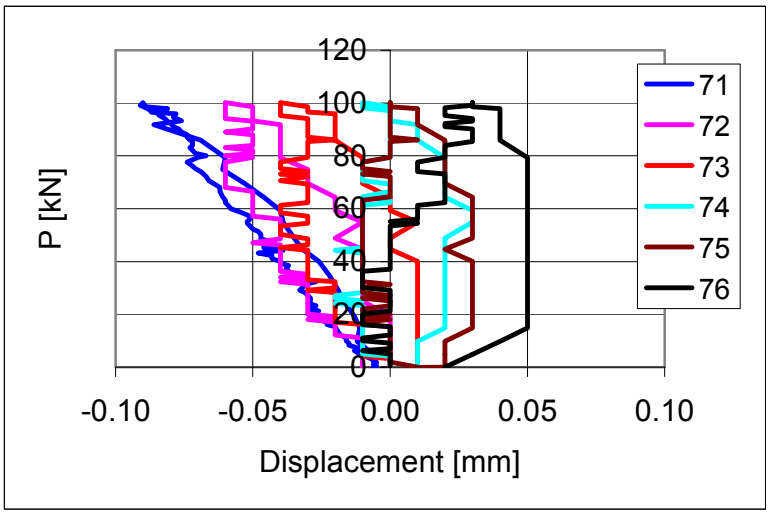

Fig. 42. FT200:6. Settlement of support. Transducers 71–76.

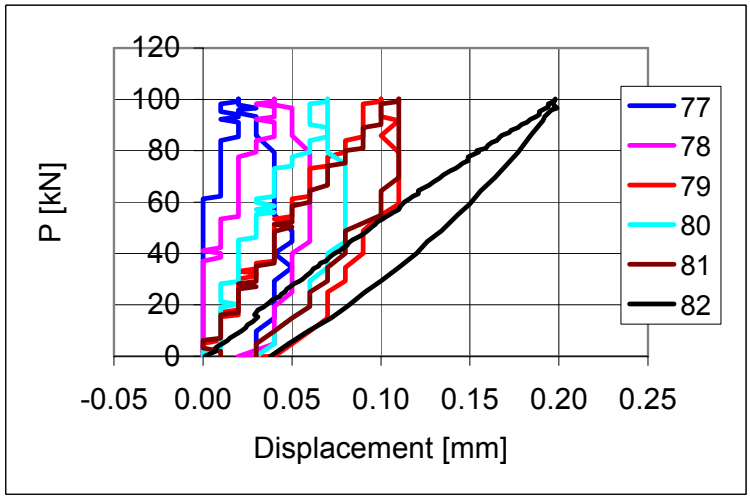

Fig. 43. FT200:6. Settlement of support. Transducers 77–82.

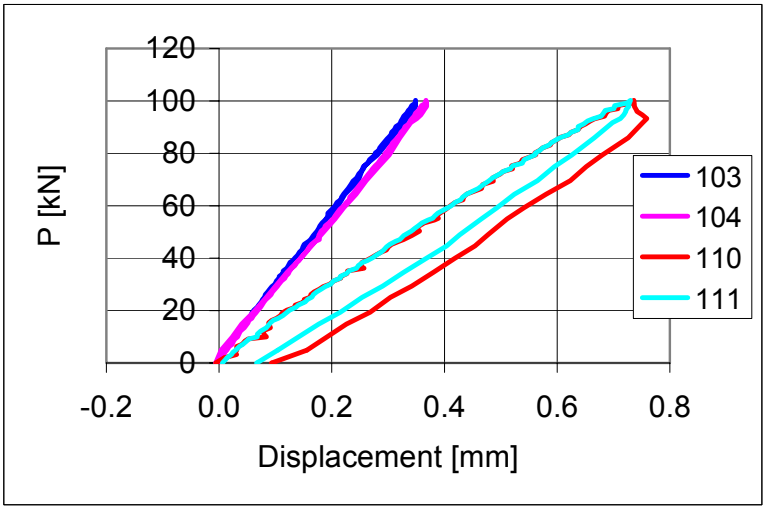

Fig. 44. FT200:6. Deflection. Transducers 103, 104, 110 and 111.

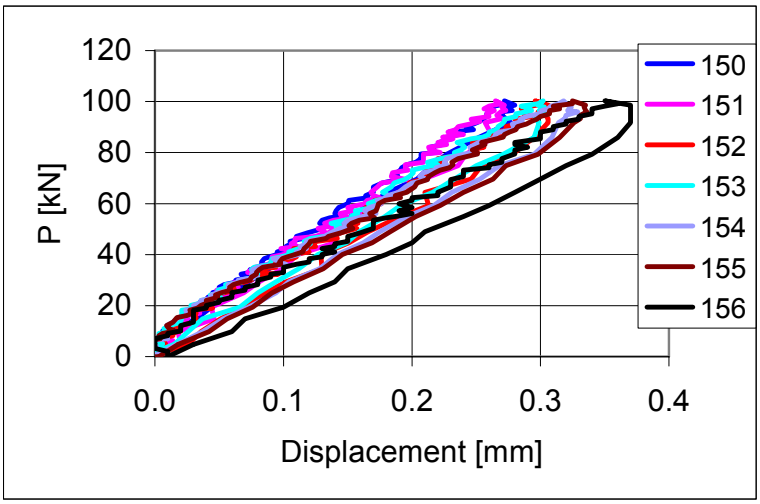

Fig. 45. FT200:6. Deflection. Transducers 150–156.

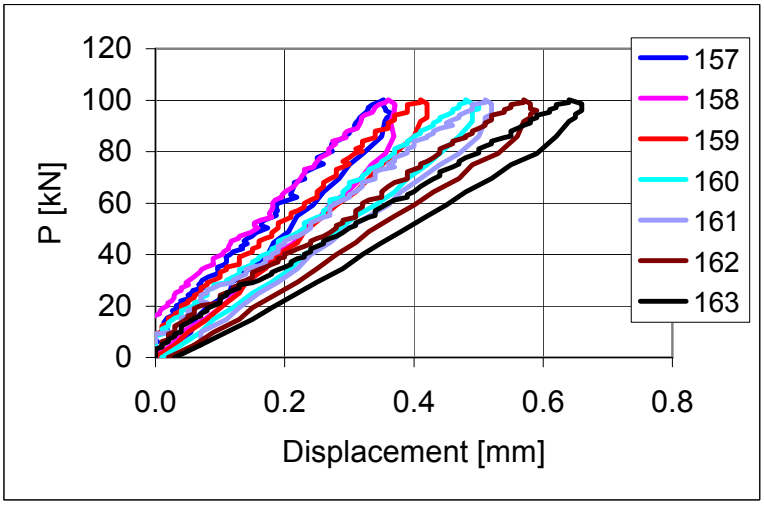

Fig. 46. FT200:6. Deflection. Transducers 157–163.

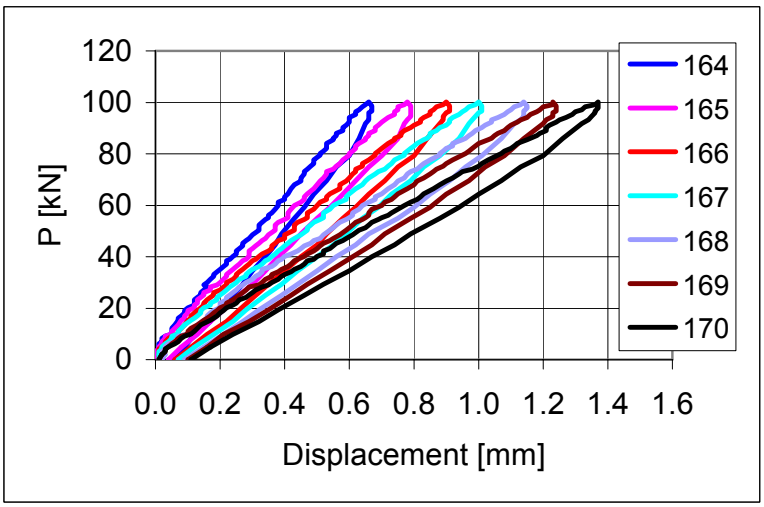

Fig. 47. FT200:6. Deflection. Transducers 164–170.

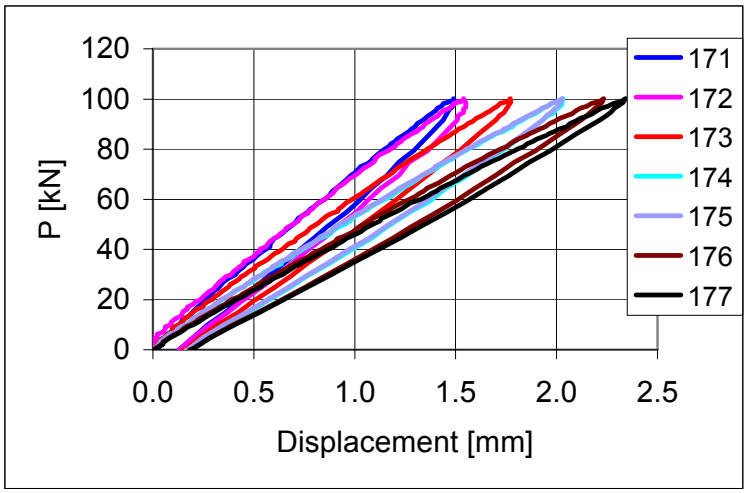

Fig. 48. FT200:6. Deflection. Transducers 171–177.

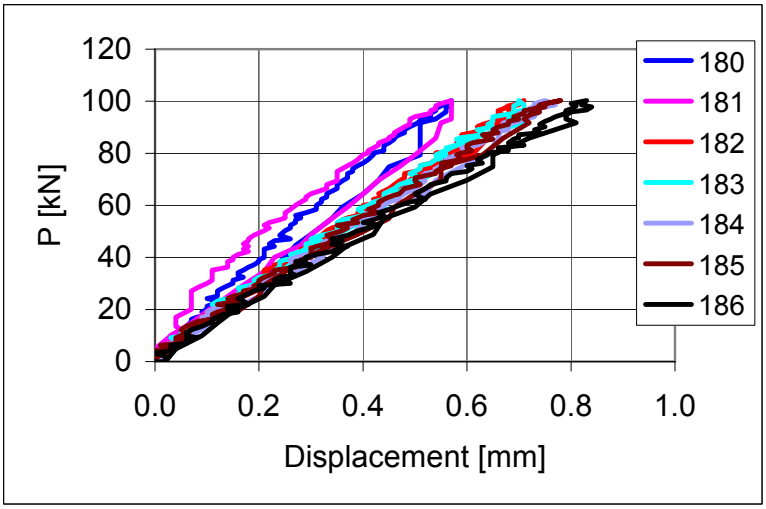

Fig. 49. FT200:6. Deflection. Transducers 180–186.

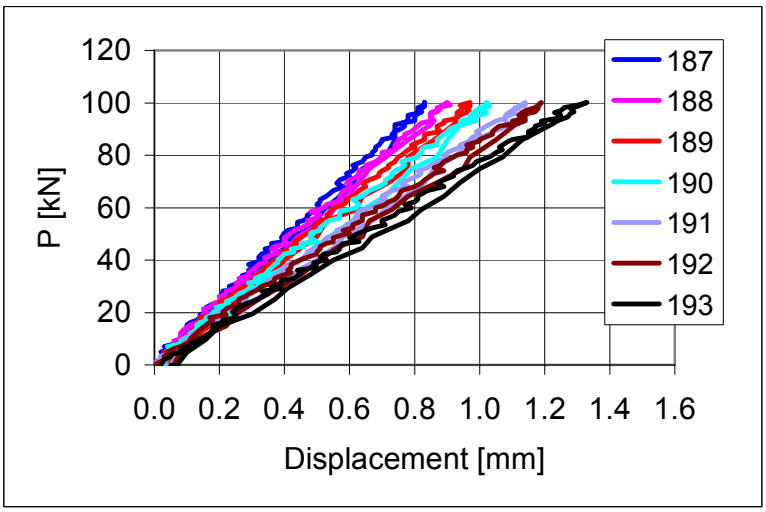

Fig. 50. FT200:6. Deflection. Transducers 187–193.

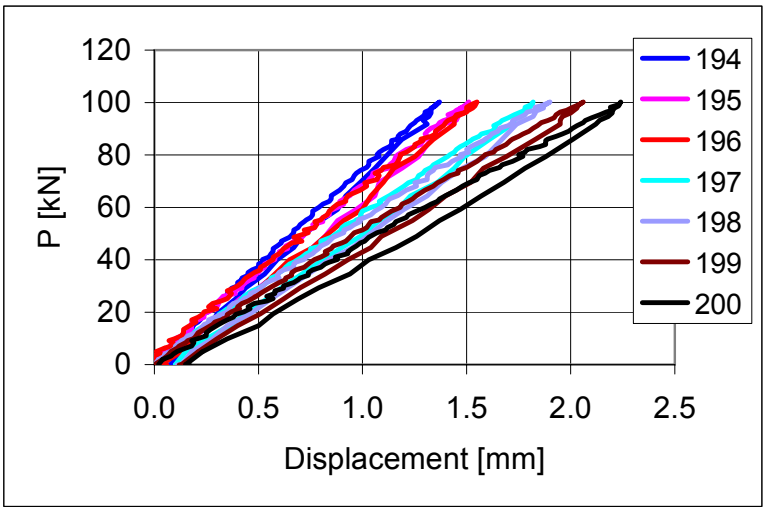

Fig. 51. FT200:6. Deflection. Transducers 194–200.

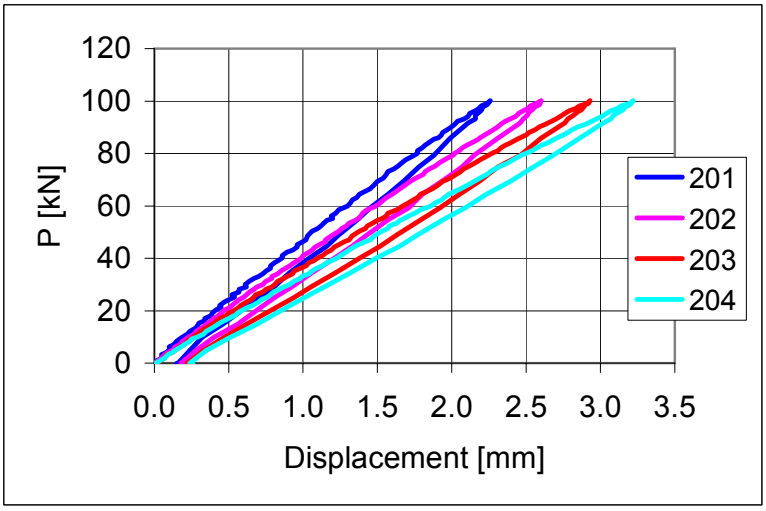

Fig. 52. FT200:6. Deflection. Transducers 201–204.

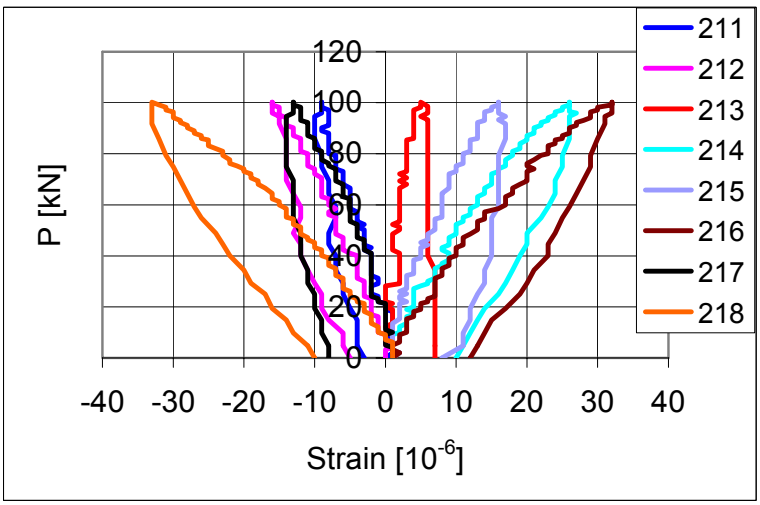

Fig. 53. FT200:6. Strain in trimmer beam. Strain gauges 211–218.

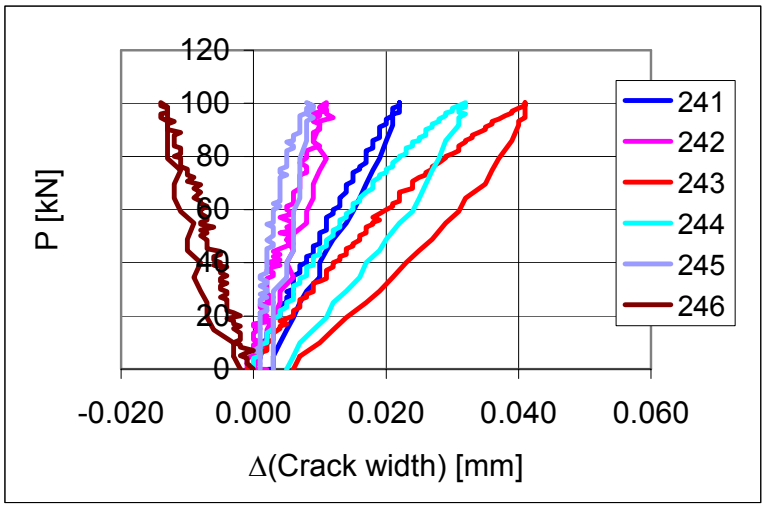

Fig. 54. FT200:6. Change in crack width. Transducers 241–246.

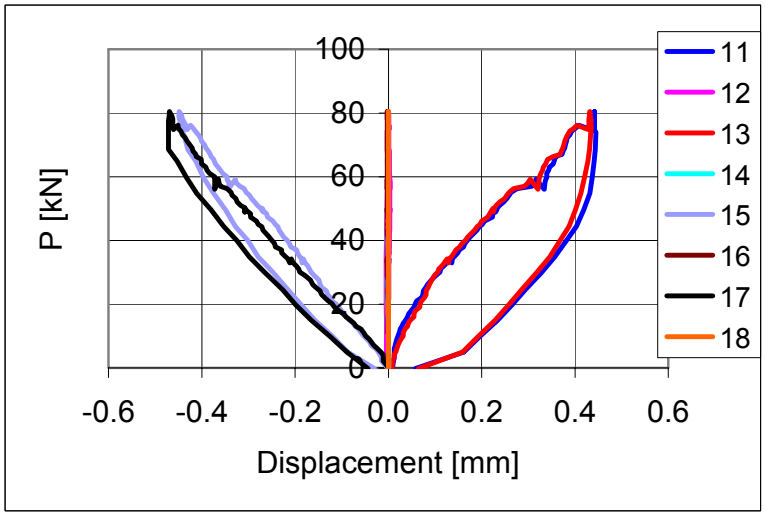

Fig. 55. FT200:7. Longitudinal horizontal displacement. Transducers 11–18.

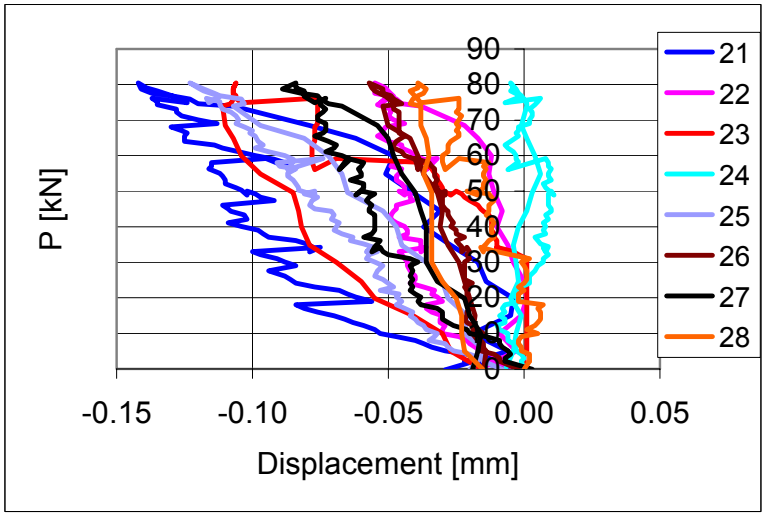

Fig. 56. FT200:7. Transverse horizontal displacement. Transducers 21–28.

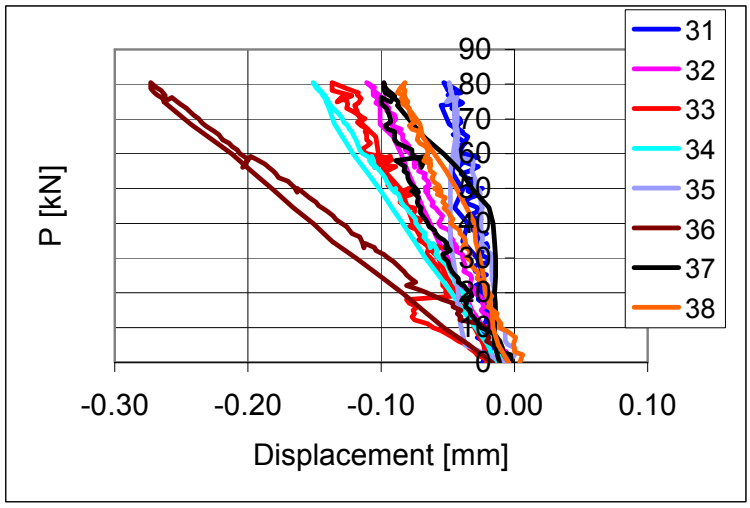

Fig. 57. FT200:7. Transverse horizontal displacement. Transducers 31–38.

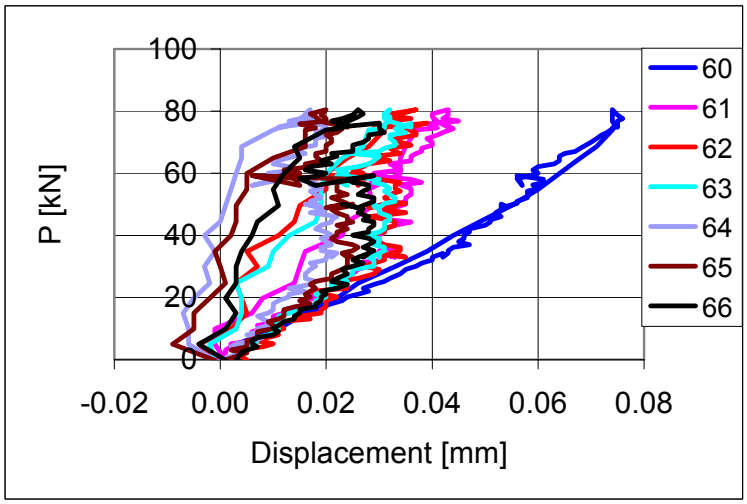

Fig. 58. FT200:7. Settlement of support. Transducers 60–66.

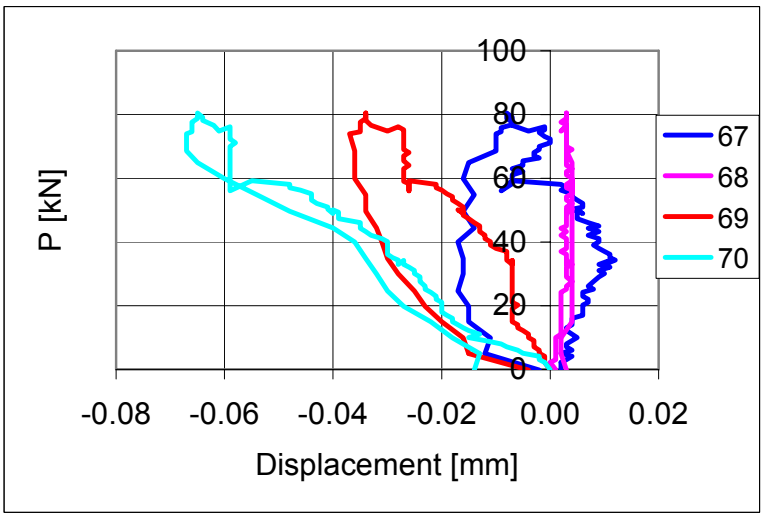

Fig. 59. FT200:7. Settlement of support. Transducers 67–70.

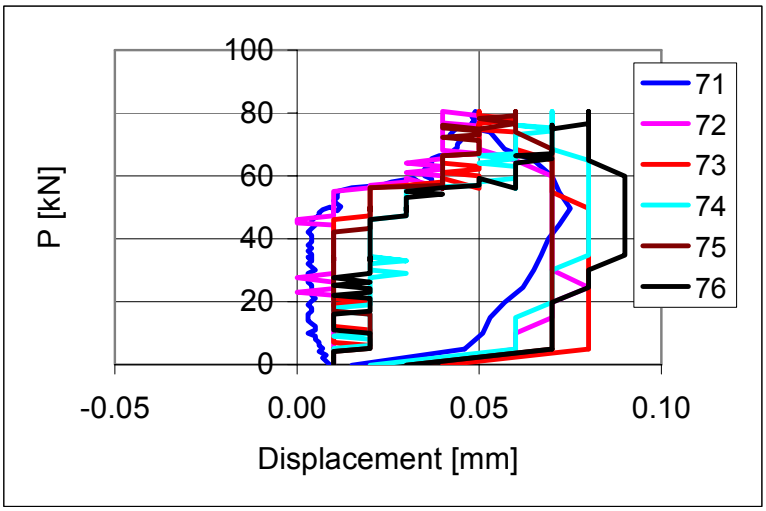

Fig. 60. FT200:7. Settlement of support. Transducers 71–76.

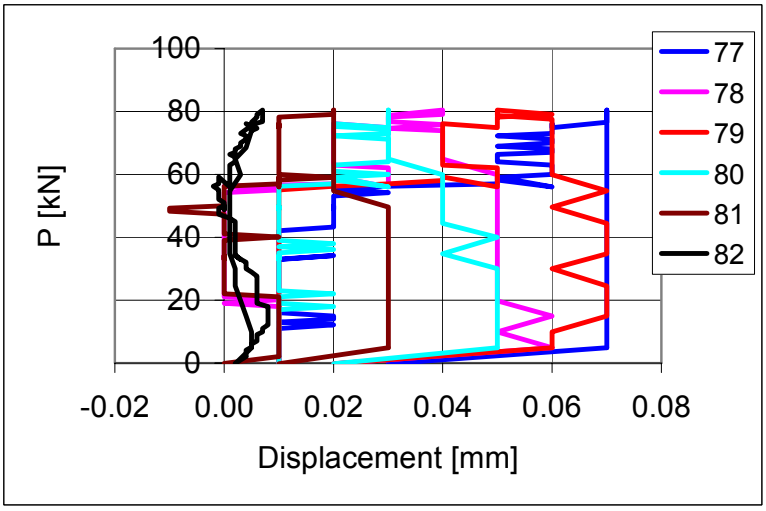

Fig. 61. FT200:7. Settlement of support. Transducers 77–82.

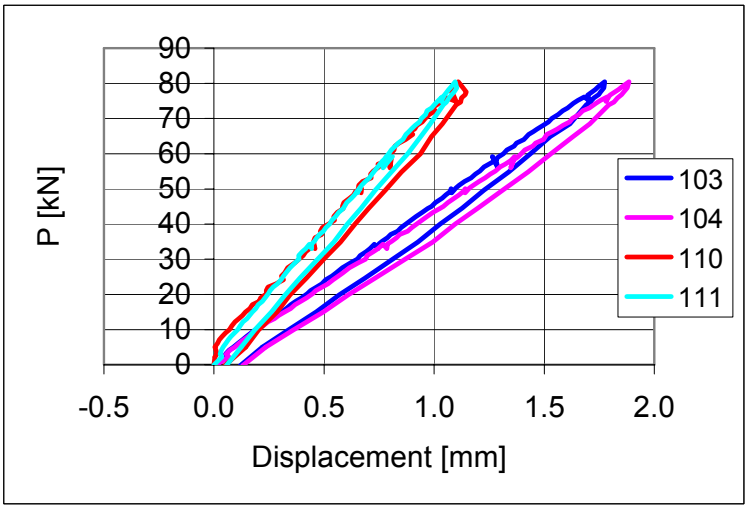

Fig. 62. FT200:7. Deflection. Transducers 103, 104, 110 and 111.

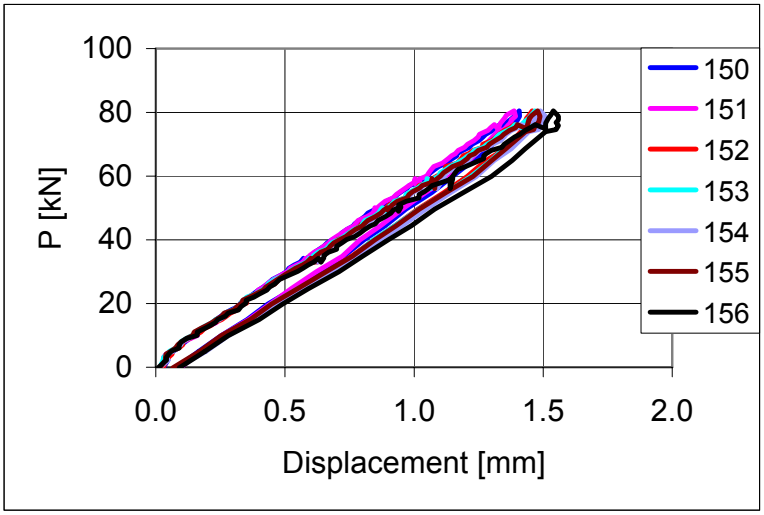

Fig. 63. FT200:7. Deflection. Transducers 150–156.

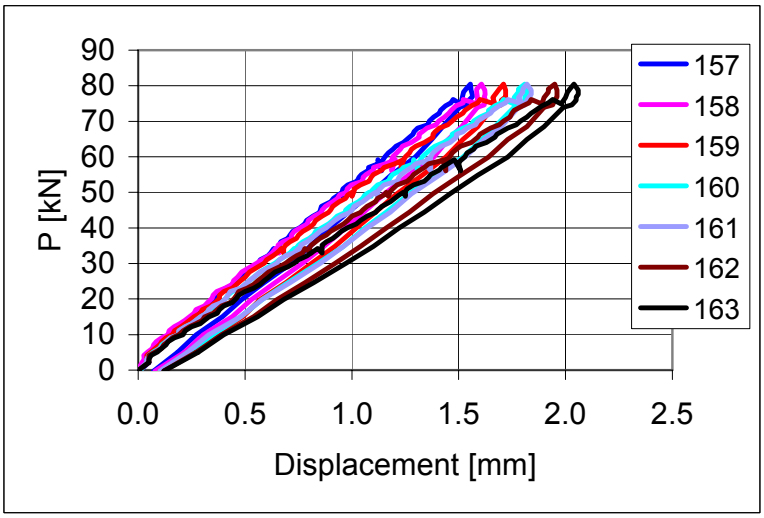

Fig. 64. FT200:7. Deflection. Transducers 157–163.

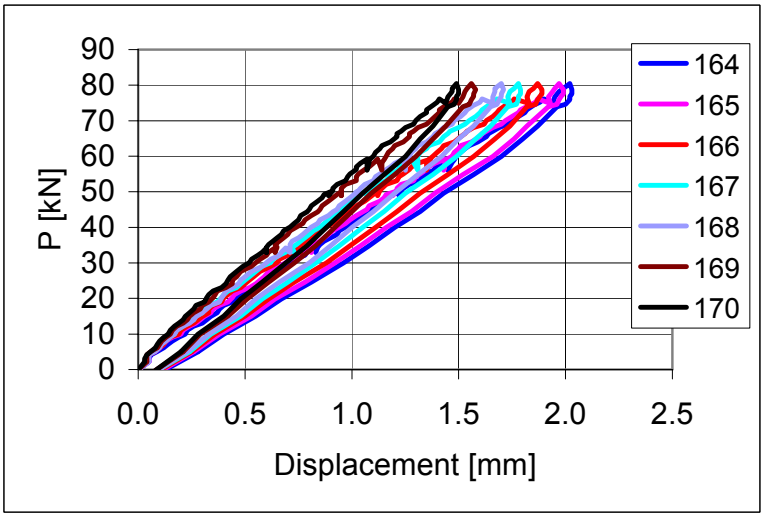

Fig. 65. FT200:7. Deflection. Transducers 164–170.

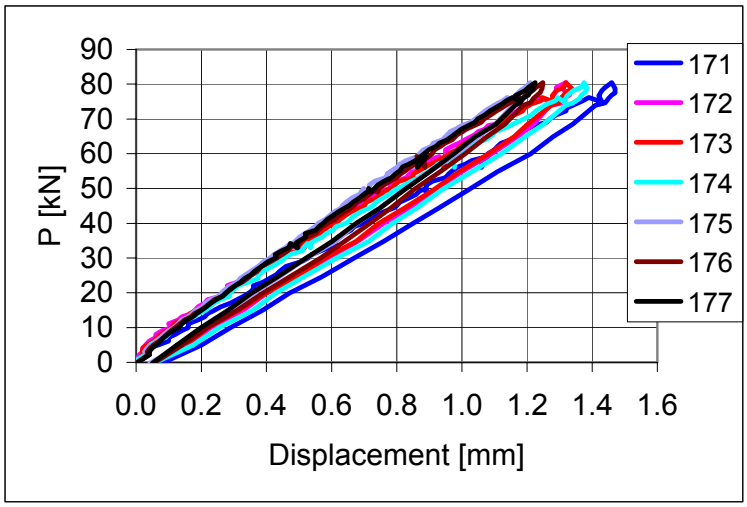

Fig. 66. FT200:7. Deflection. Transducers 171–177.

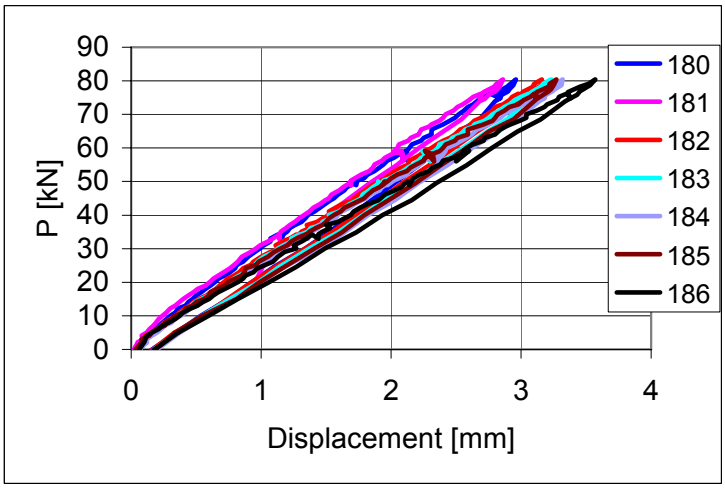

Fig. 67. FT200:7. Deflection. Transducers 180–186.

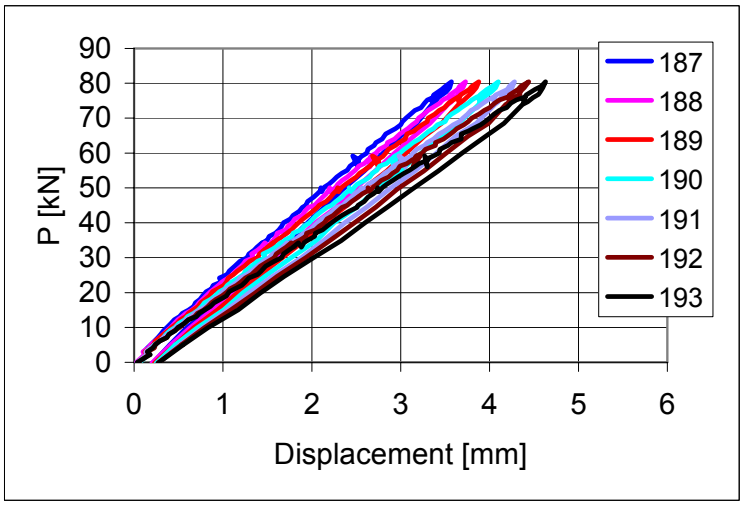

Fig. 68. FT200:7. Deflection. Transducers 187–193.

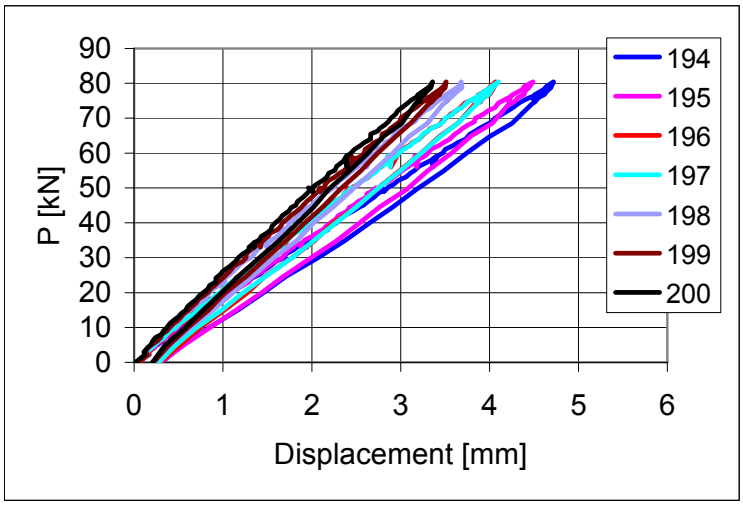

Fig. 69. FT200:7. Deflection. Transducers 194–200.

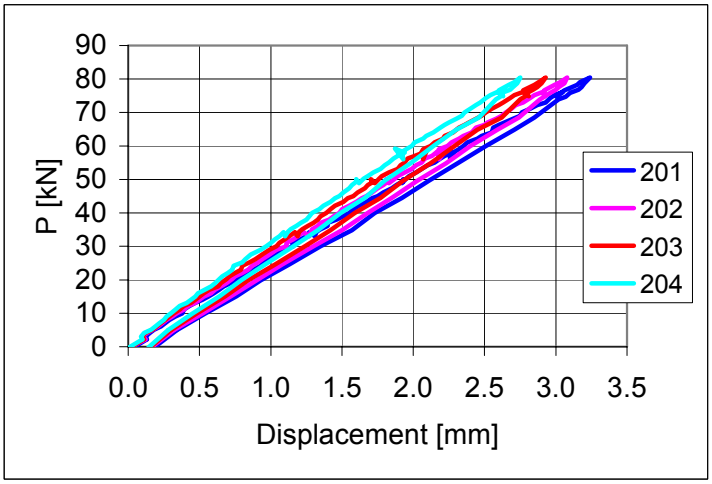

Fig. 70. FT200:4. Deflection. Transducers 201–204.

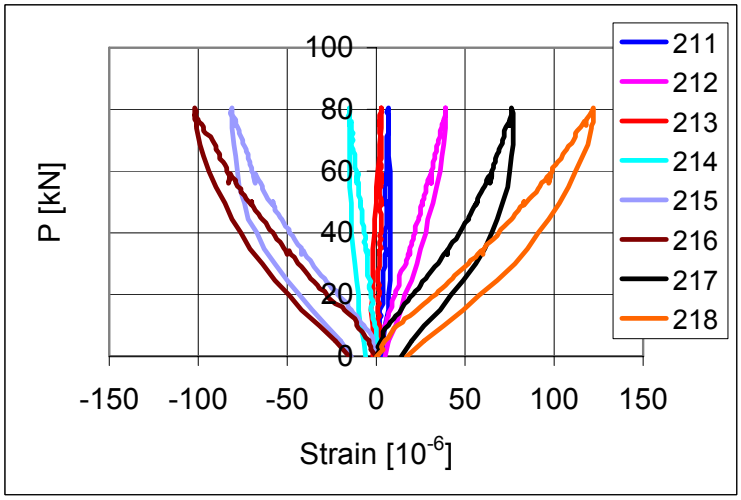

Fig. 71. FT200:7. Strain in trimmer beam. Strain gauges 211–218.

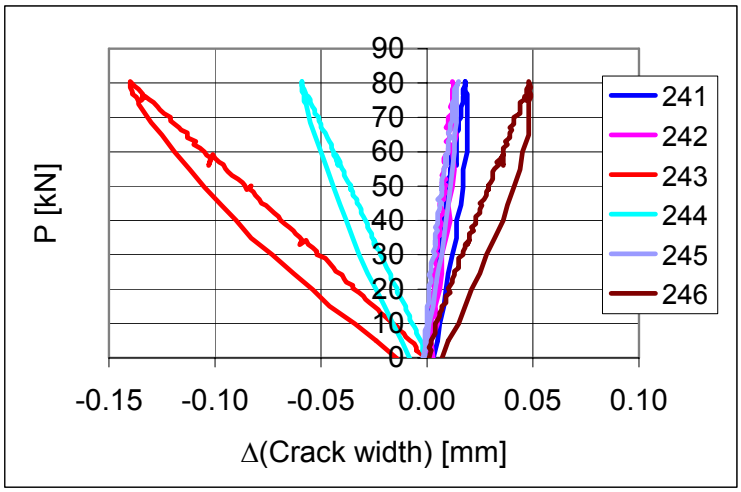

Fig. 72. FT200:7. Change in crack width. Transducers 241–246.

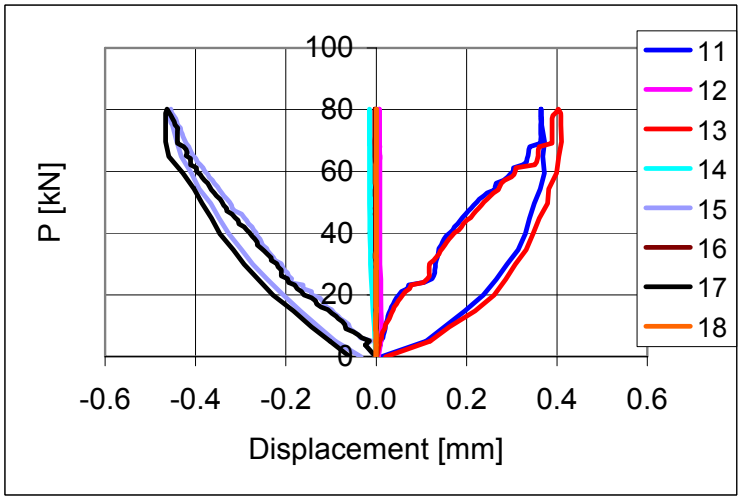

Fig. 73. FT200:8. Longitudinal horizontal displacement. Transducers 11–18.

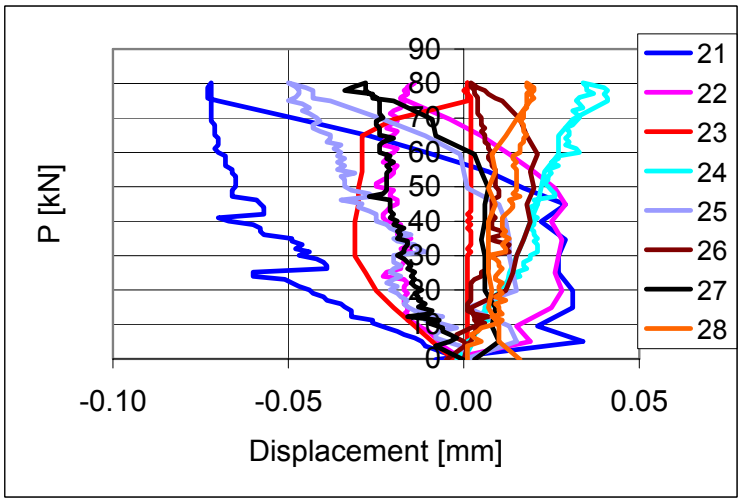

Fig. 74. FT200:8. Transverse horizontal displacement. Transducers 21–28.

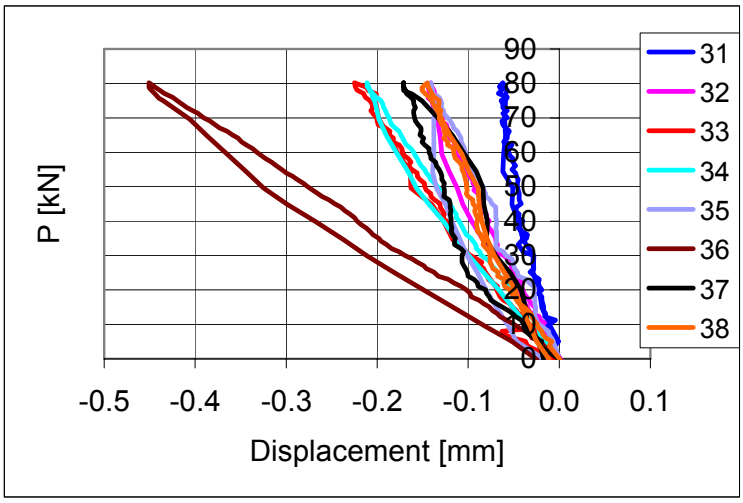

Fig. 75. FT200:8. Transverse horizontal displacement. Transducers 31–38.

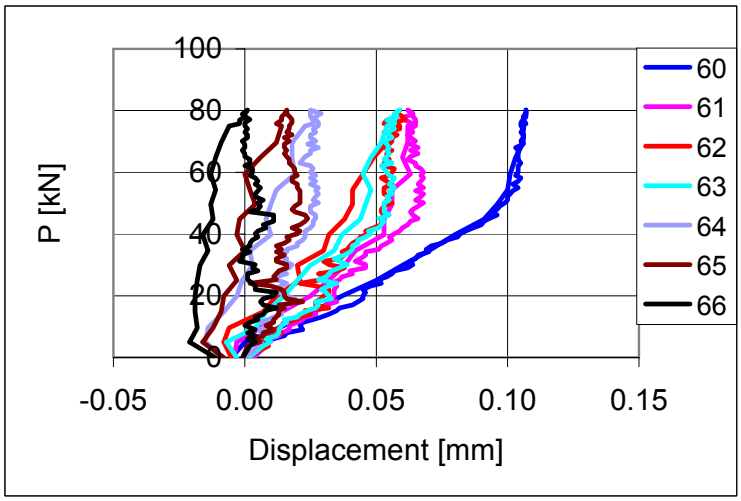

Fig. 76. FT200:8. Settlement of support. Transducers 60–66.

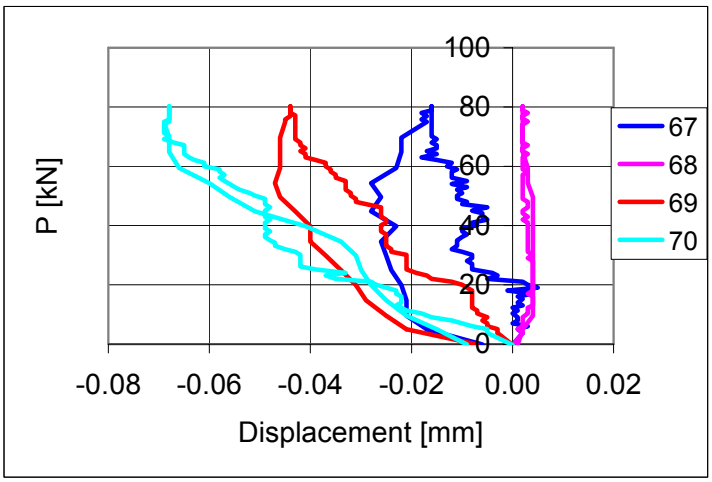

Fig. 77. FT200:8. Settlement of support. Transducers 67–70.

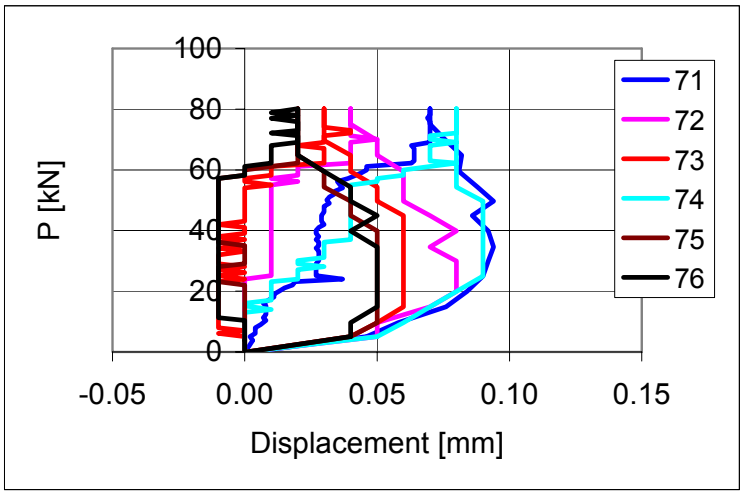

Fig. 78. FT200:8. Settlement of support. Transducers 71–76.

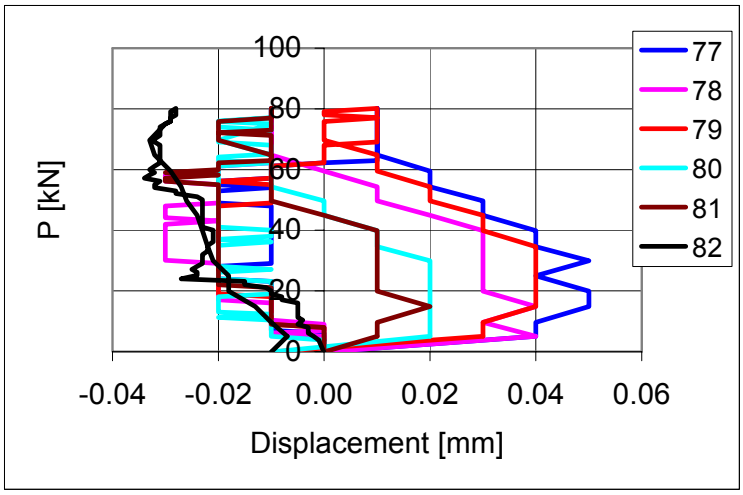

Fig. 79. FT200:8. Settlement of support. Transducers 77–82.

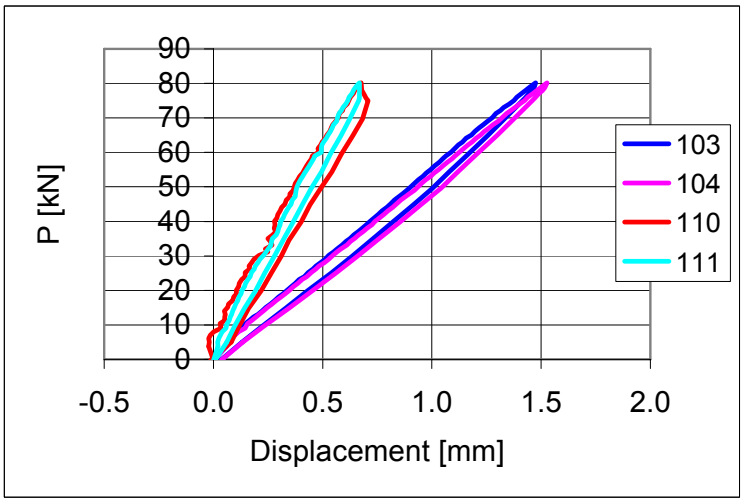

Fig. 80. FT200:8. Deflection. Transducers 103, 104, 110 and 111.

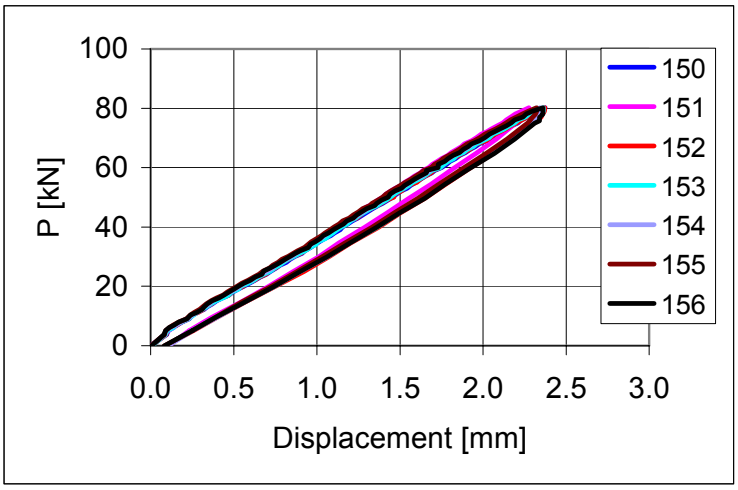

Fig. 81. FT200:8. Deflection. Transducers 150–156.

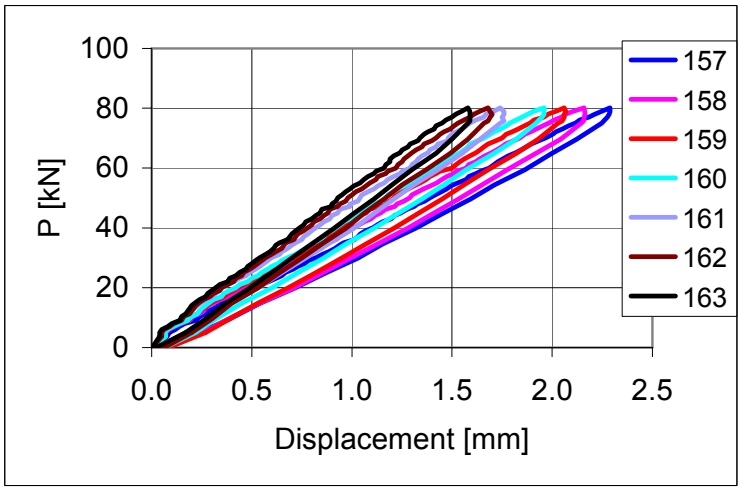

Fig. 82. FT200:8. Deflection. Transducers 157–163.

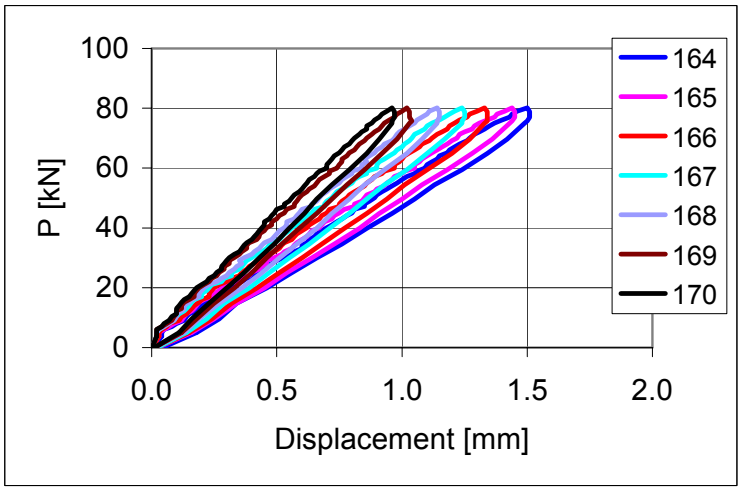

Fig. 83. FT200:8. Deflection. Transducers 164–170.

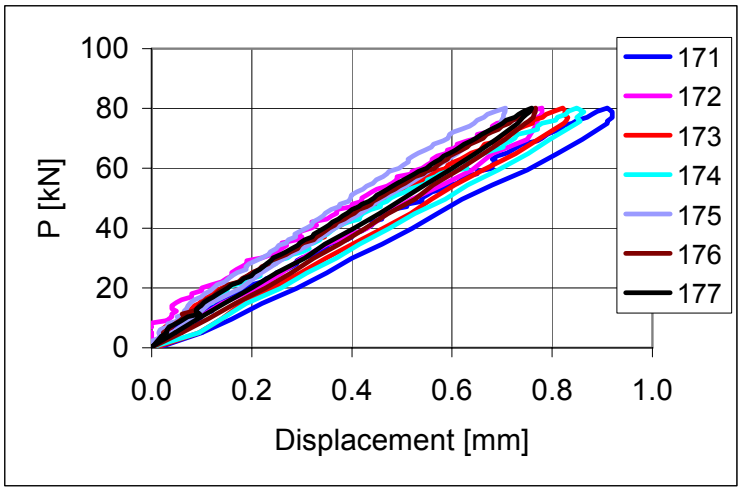

Fig. 84. FT200:8. Deflection. Transducers 171–177.

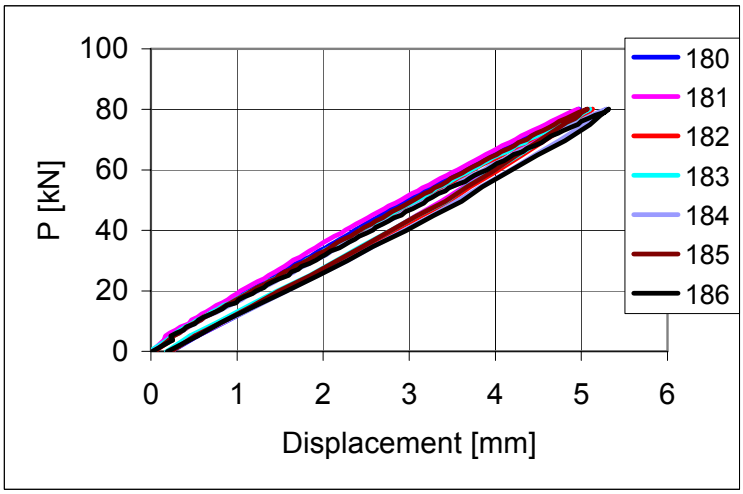

Fig. 85. FT200:8. Deflection. Transducers 180–186.

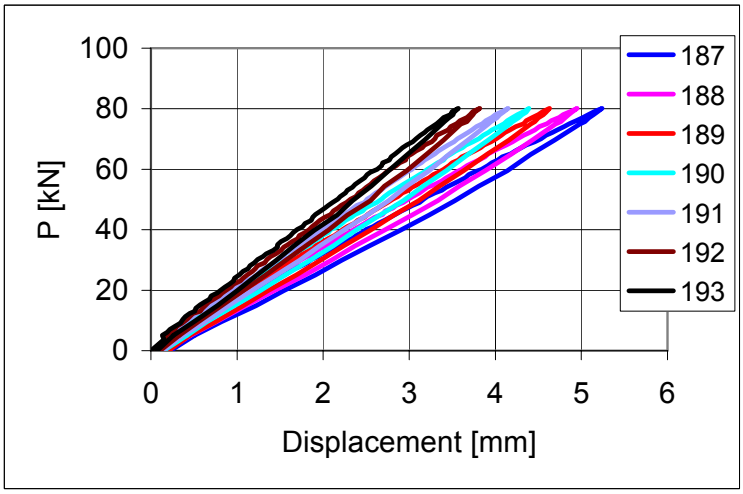

Fig. 86. FT200:8. Deflection. Transducers 187–193.

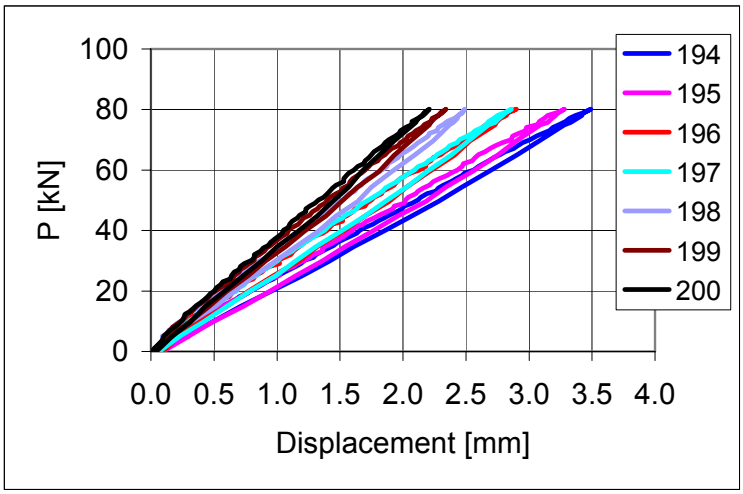

Fig. 87. FT200:8. Deflection. Transducers 194–200.

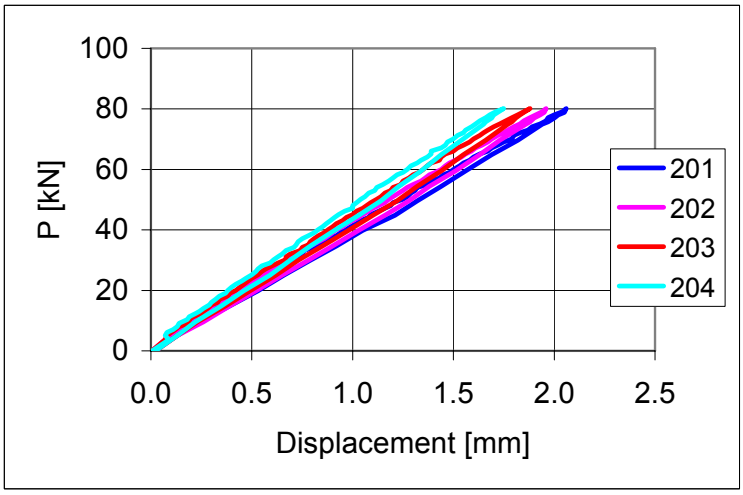

Fig. 88. FT200:8. Deflection. Transducers 201–204.

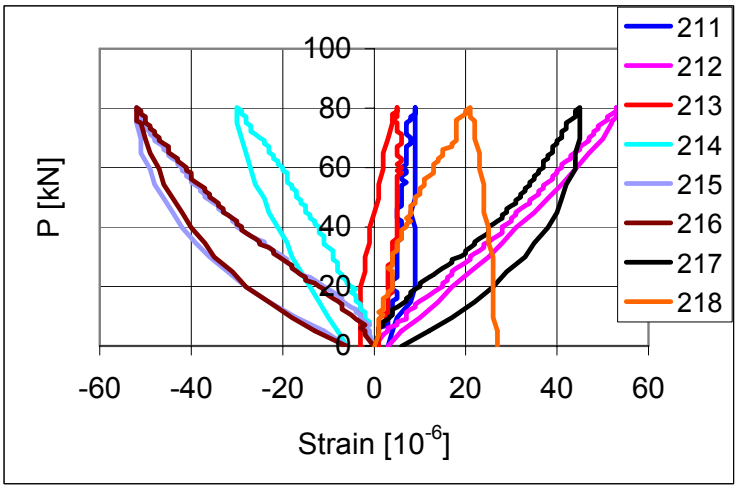

Fig. 89. FT200:8. Strain in trimmer beam. Strain gauges 211–218.

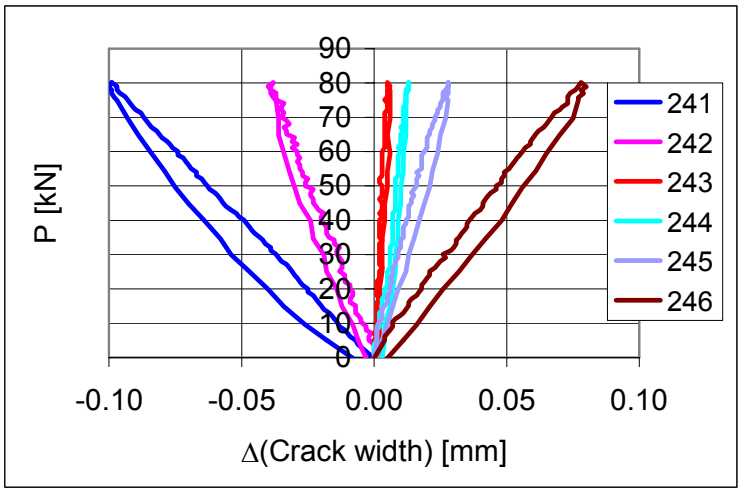

Fig. 90. FT200:8. Change in crack width. Transducers 241–246.

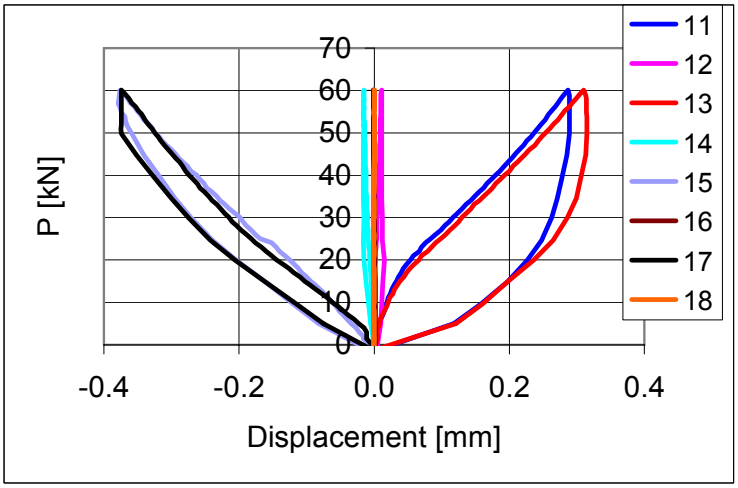

Fig. 91. FT200:9. Longitudinal horizontal displacement. Transducers 11–18.

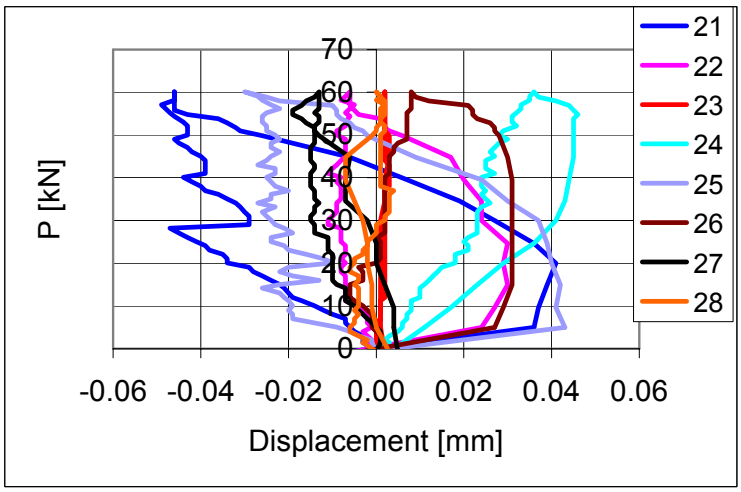

Fig. 92. FT200:9. Transverse horizontal displacement. Transducers 21–28.

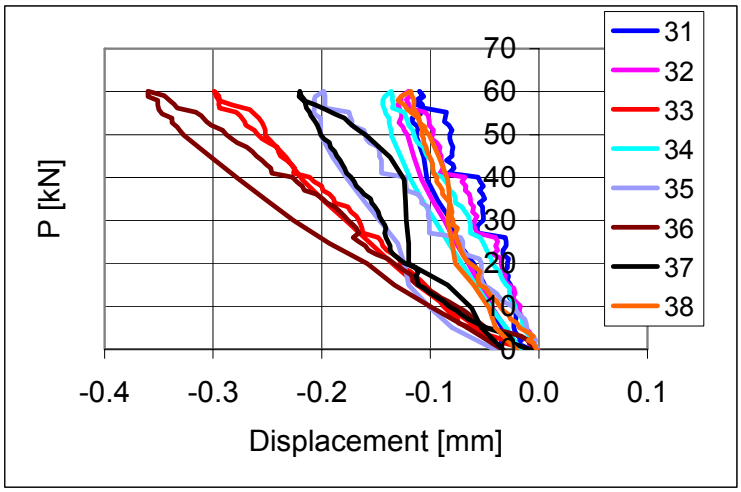

Fig. 93. FT200:9. Transverse horizontal displacement. Transducers 31–38.

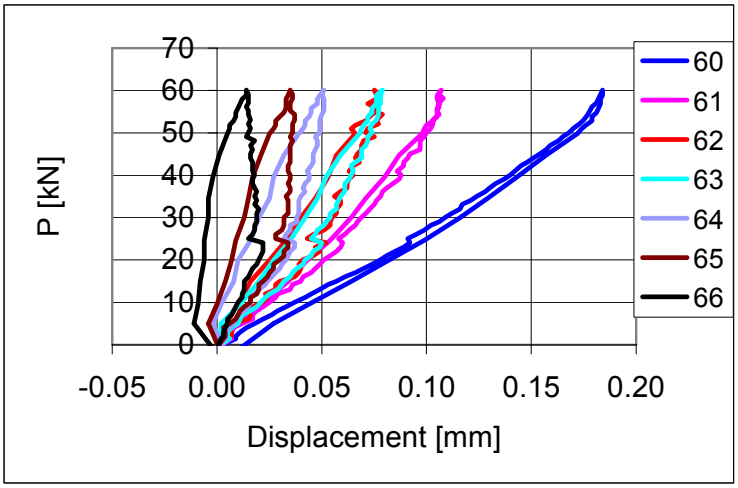

Fig. 94. FT200:9. Settlement of support. Transducers 60–66.

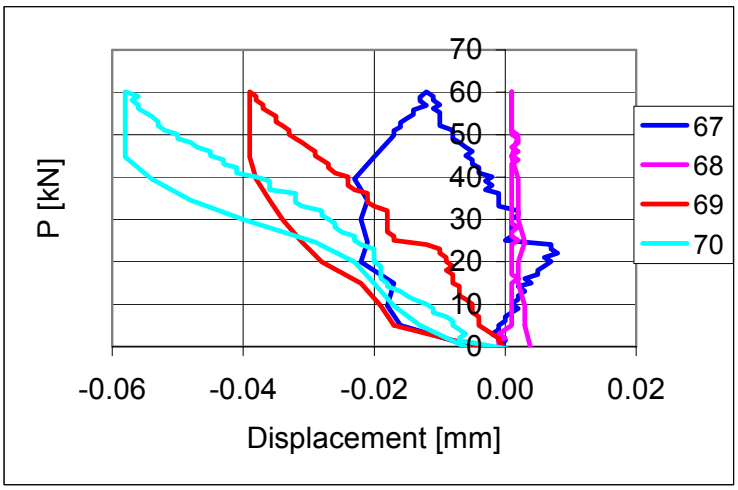

Fig. 95. FT200:9. Settlement of support. Transducers 67–70.

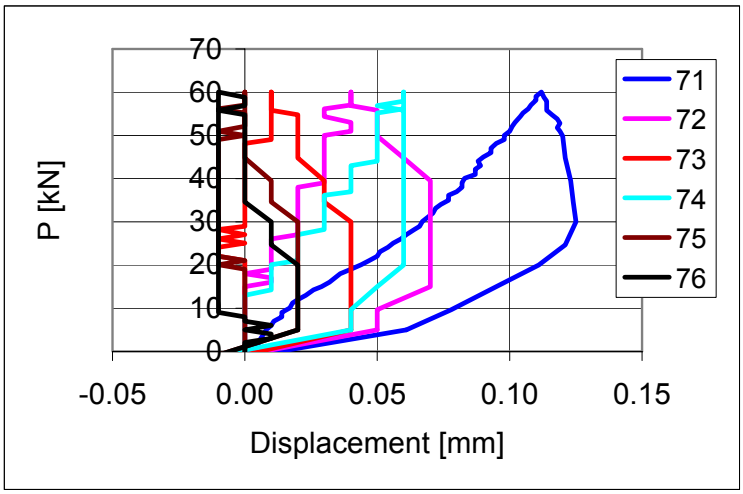

Fig. 96. FT200:9. Settlement of support. Transducers 71–76.

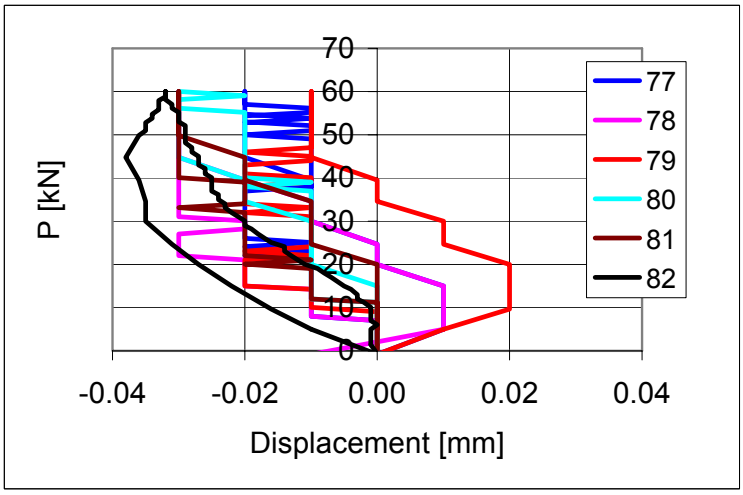

Fig. 97. FT200:9. Settlement of support. Transducers 77–82.

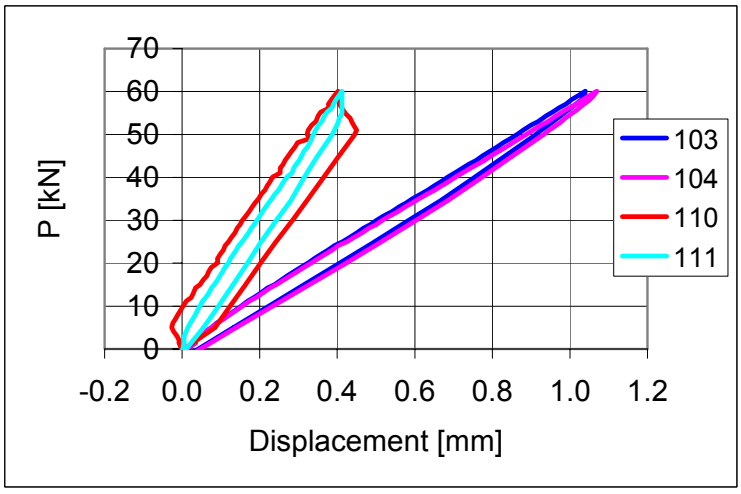

Fig. 98. FT200:9. Deflection. Transducers 103, 104, 110 and 111.

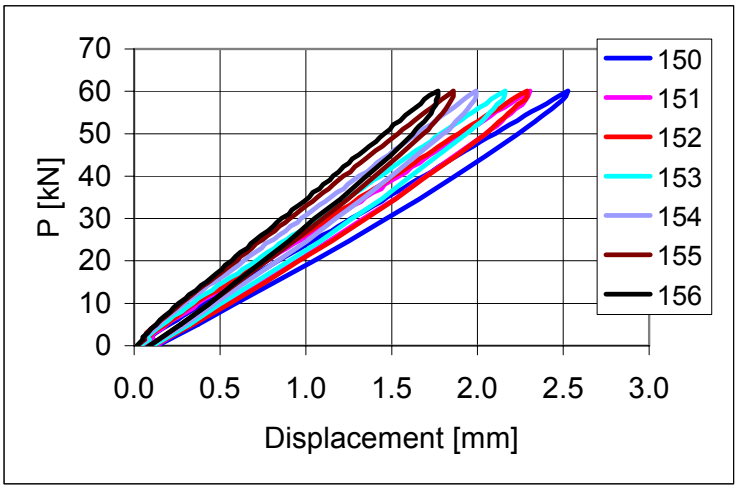

Fig. 99. FT200:9. Deflection. Transducers 150–156.

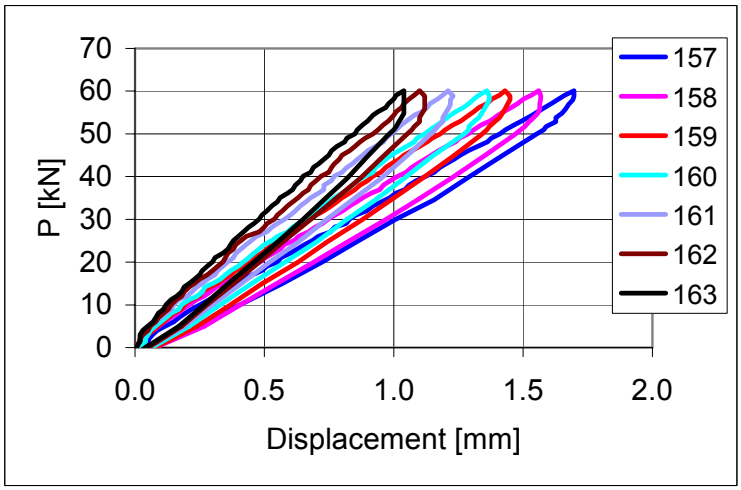

Fig. 100. FT200:9. Deflection. Transducers 157–163.

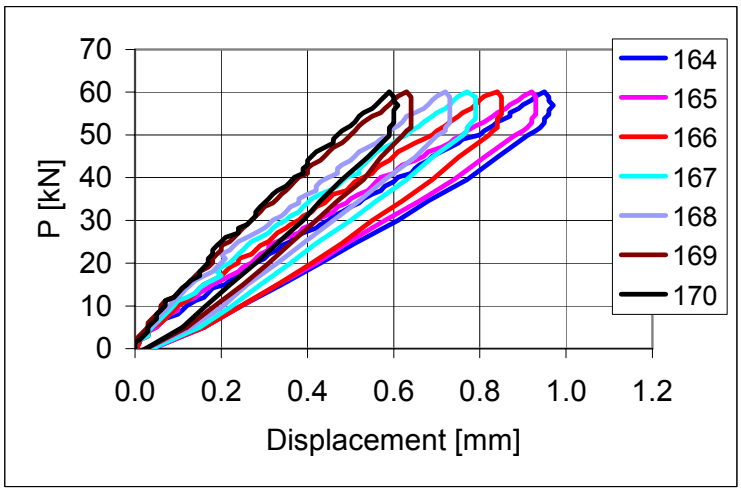

Fig. 101. FT200:9. Deflection. Transducers 164–170.

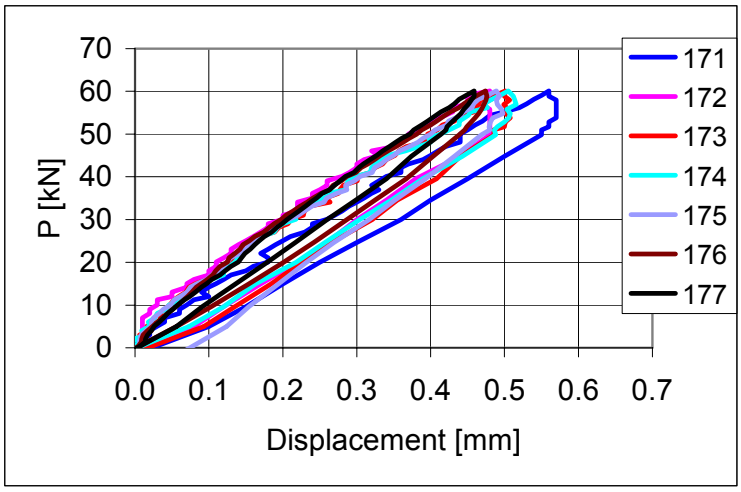

Fig. 102. FT200:9. Deflection. Transducers 171–177.

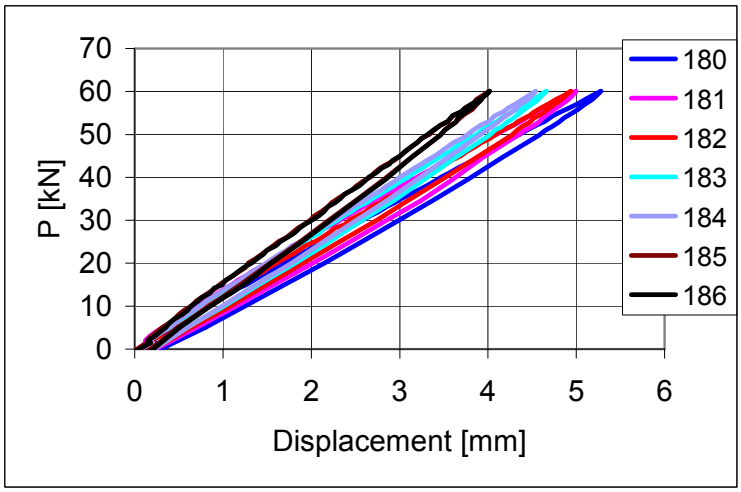

Fig. 103. FT200:9. Deflection. Transducers 180–186.

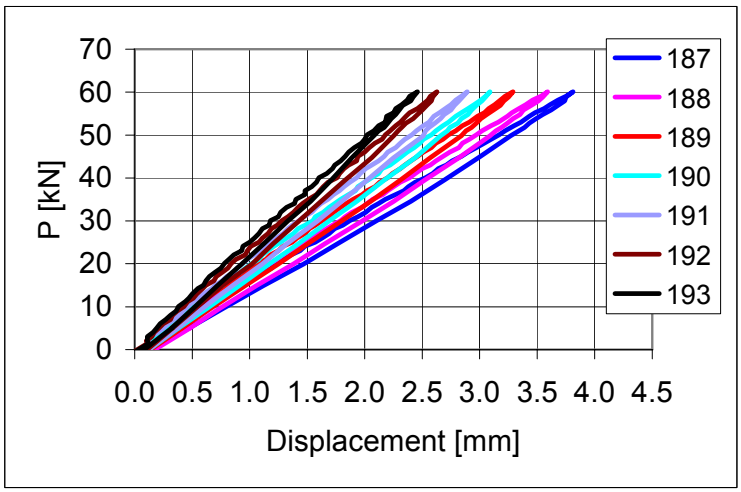

Fig. 104. FT200:9. Deflection. Transducers 187–193.

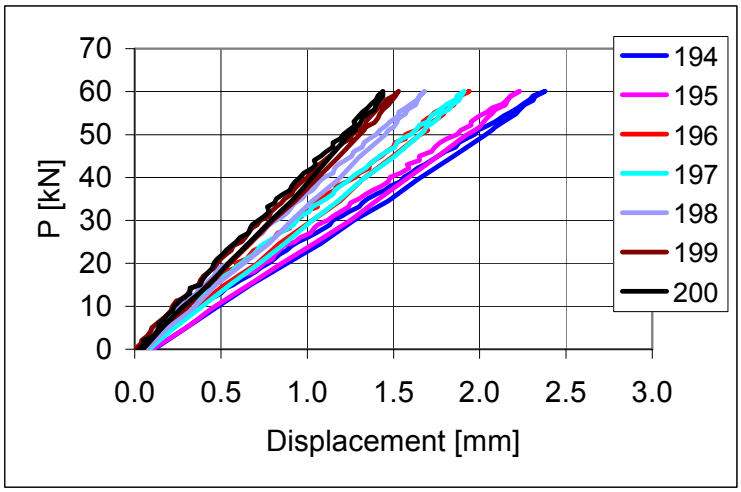

Fig. 105. FT200:9. Deflection. Transducers 194–200.

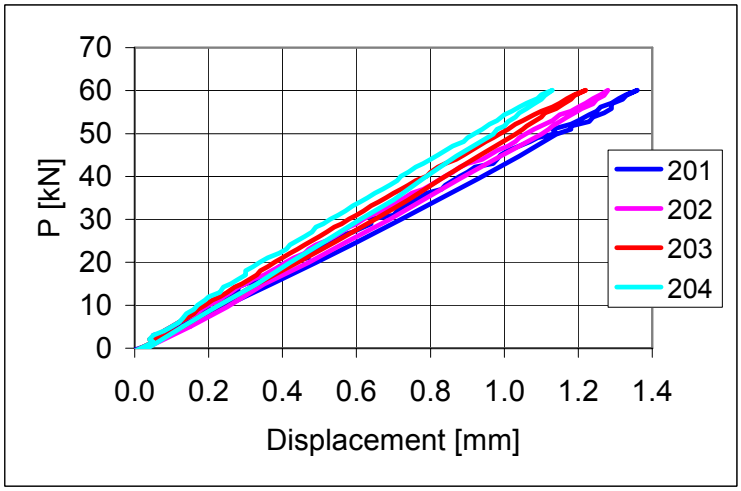

Fig. 106. FT200:9. Deflection. Transducers 201–204.

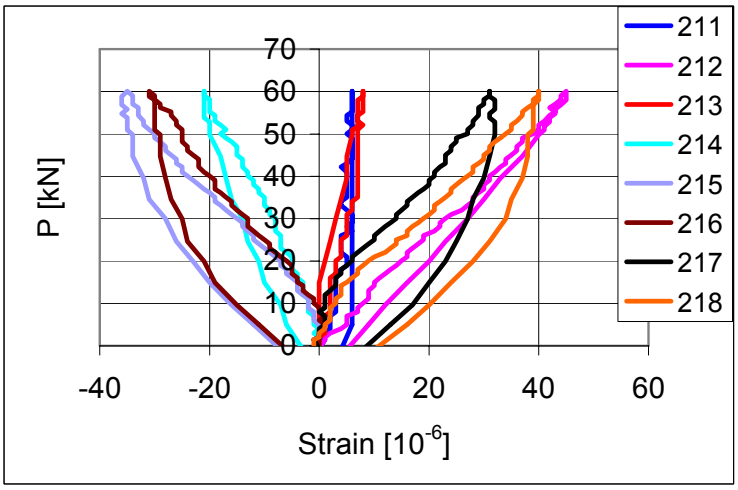

Fig. 107. FT200:9. Strain in trimmer beam. Strain gauges 211–218.

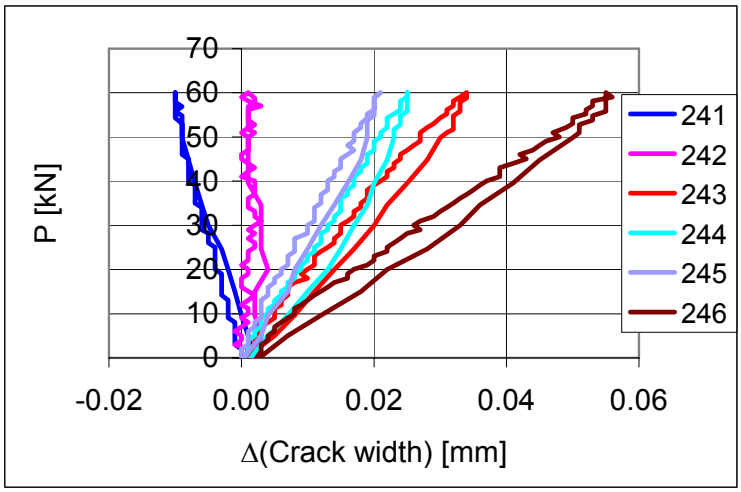

Fig. 108. FT200:9. Change in crack width. Transducers 241–246.

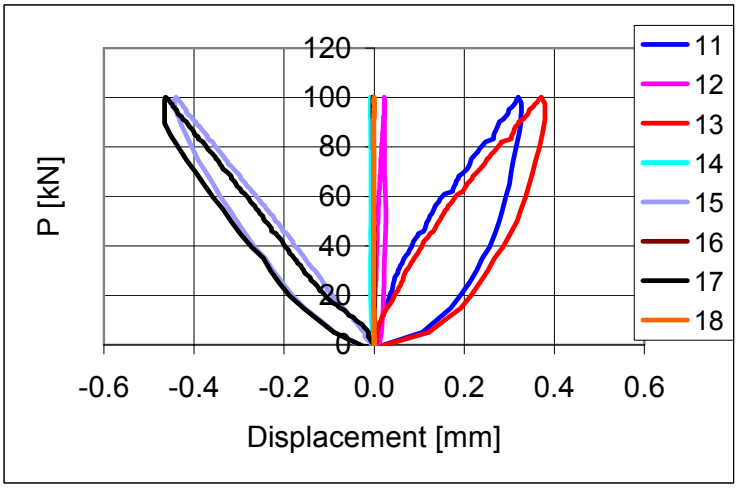

Fig. 109. FT200:10. Longitudinal horizontal displacement. Transducers 11–18.

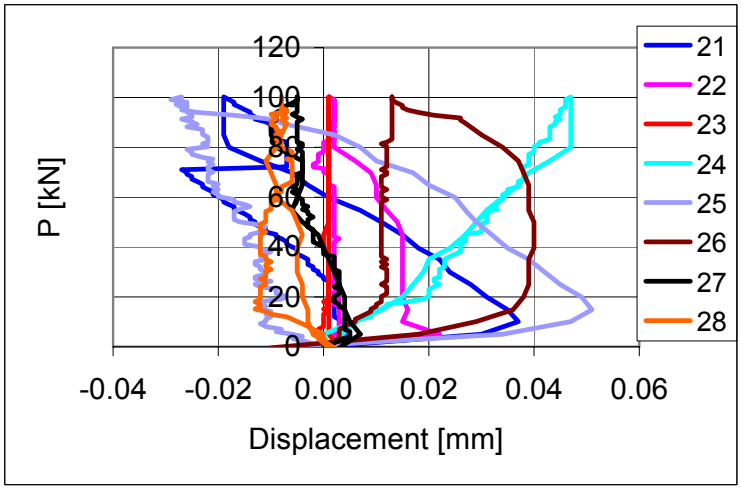

Fig. 110. FT200:10. Transverse horizontal displacement. Transducers 21–28.

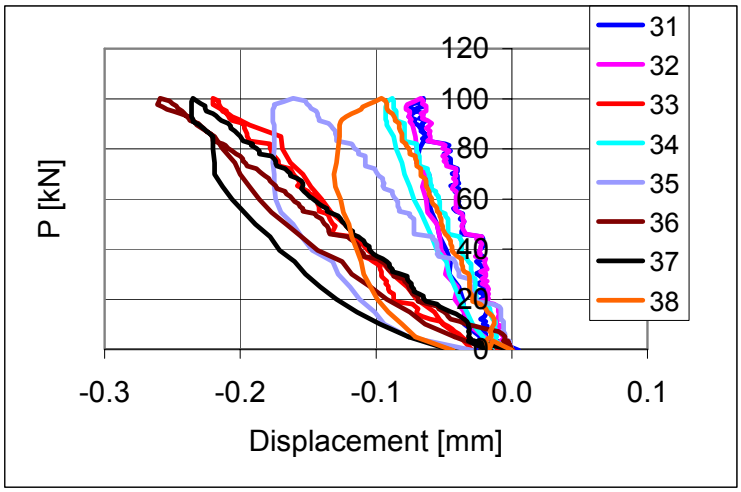

Fig. 111. FT200:10. Transverse horizontal displacement. Transducers 31–38.

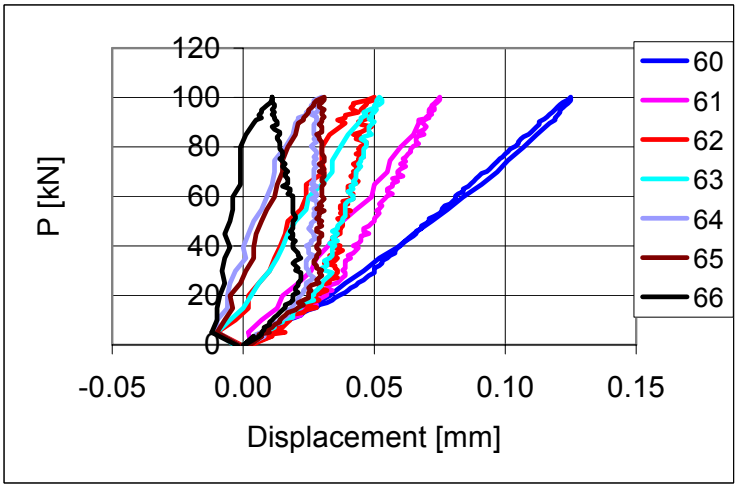

Fig. 112. FT200:10. Settlement of support. Transducers 60–66.

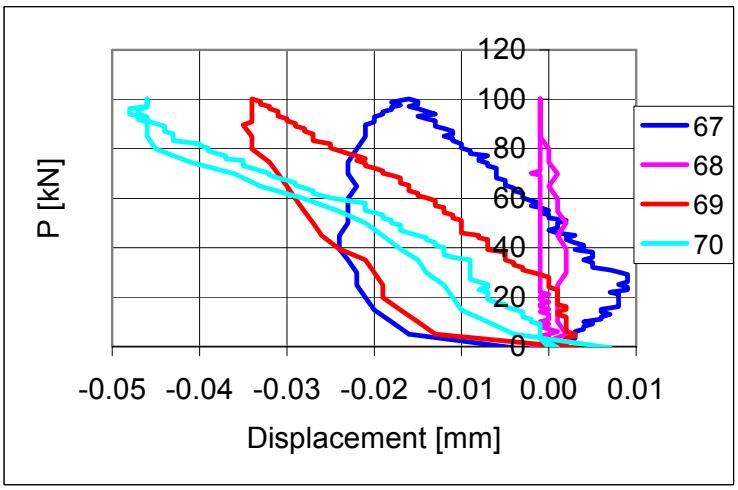

Fig. 113. FT200:10. Settlement of support. Transducers 67–70.

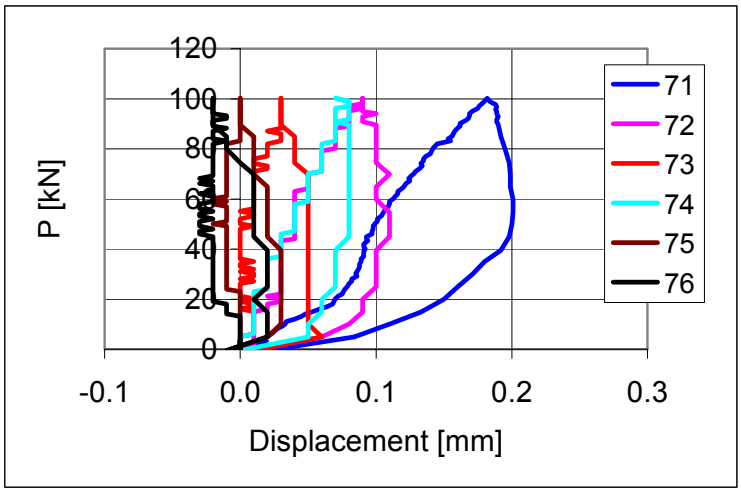

Fig. 114. FT200:10. Settlement of support. Transducers 71–76.

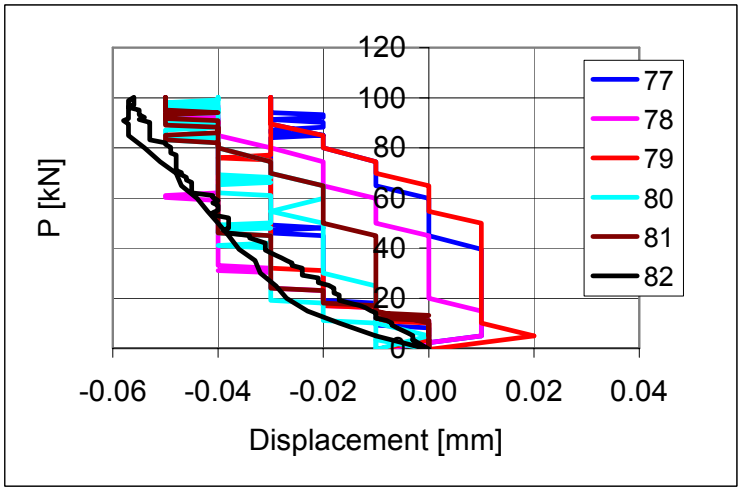

Fig. 115. FT200:10. Settlement of support. Transducers 77–82.

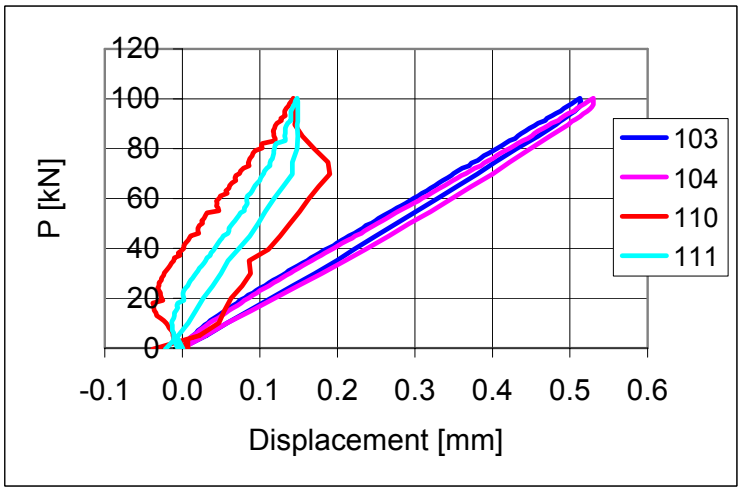

Fig. 116. FT200:10. Deflection. Transducers 103, 104, 110 and 111.

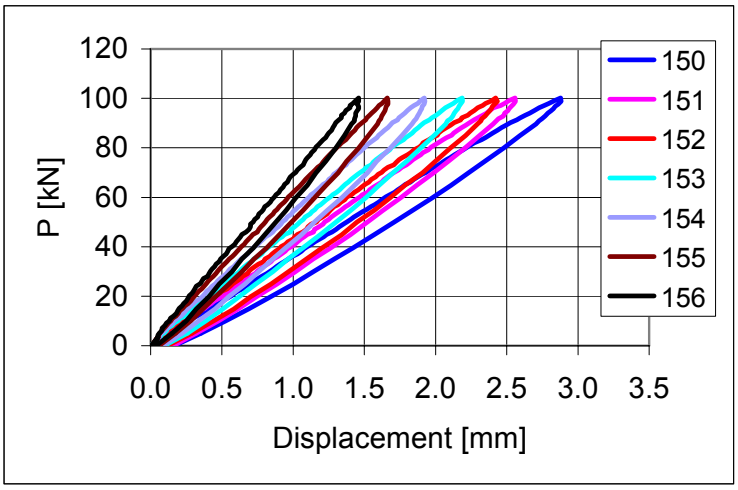

Fig. 117. FT200:10. Deflection. Transducers 150–156.

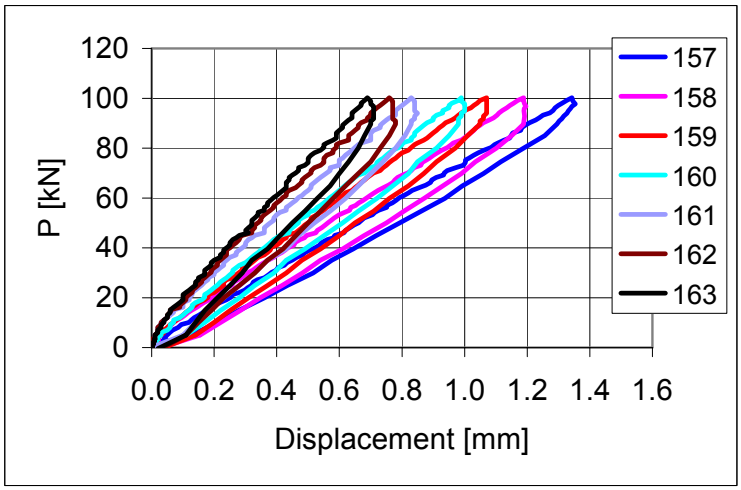

Fig. 118. FT200:10. Deflection. Transducers 157–163.

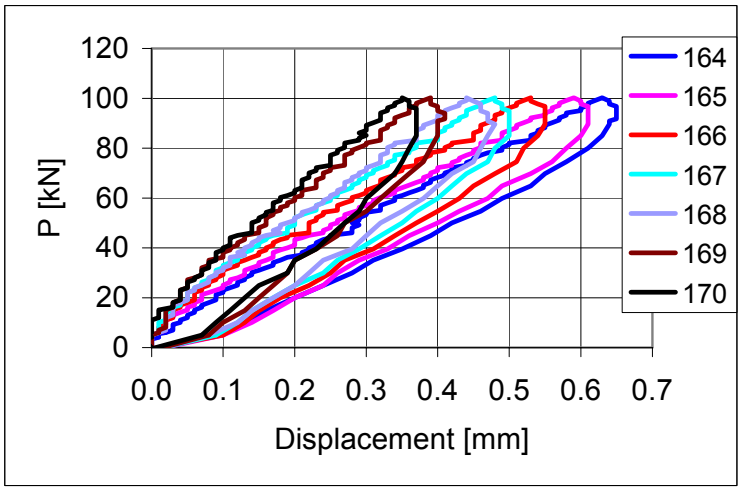

Fig. 119. FT200:10. Deflection. Transducers 164–170.

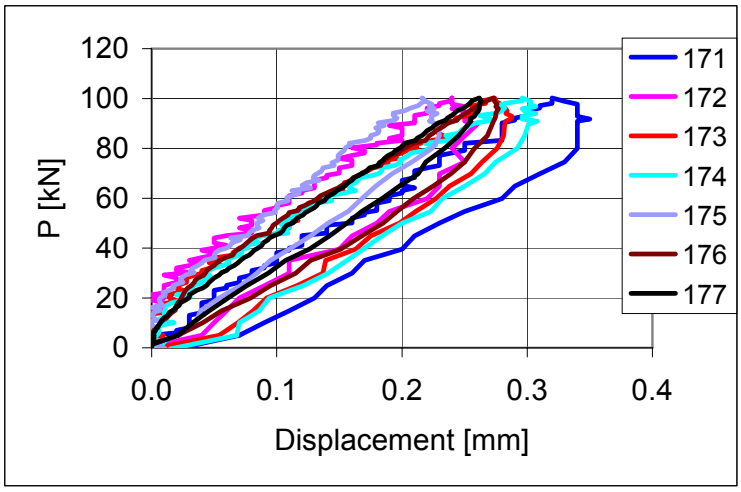

Fig. 120. FT200:10. Deflection. Transducers 171–177.

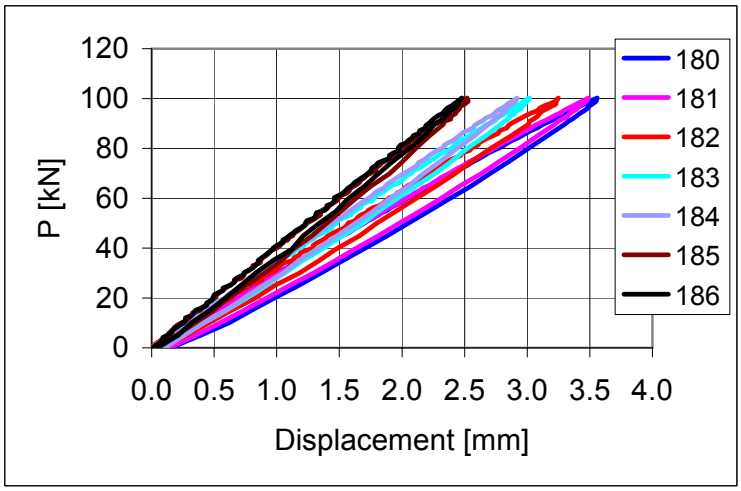

Fig. 121. FT200:10. Deflection. Transducers 180–186.

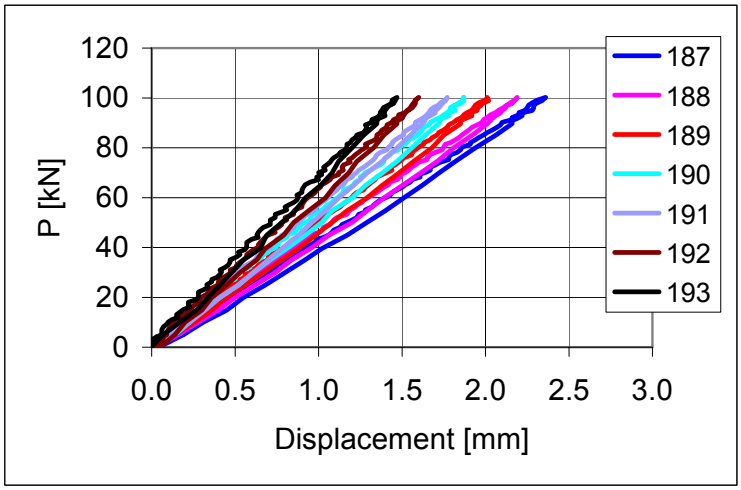

Fig. 122. FT200:10. Deflection. Transducers 187–193.

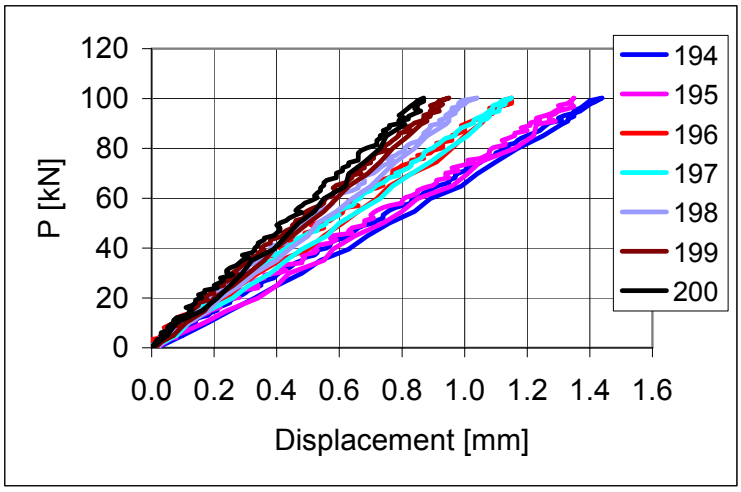

Fig. 123. FT200:10. Deflection. Transducers 194–200.

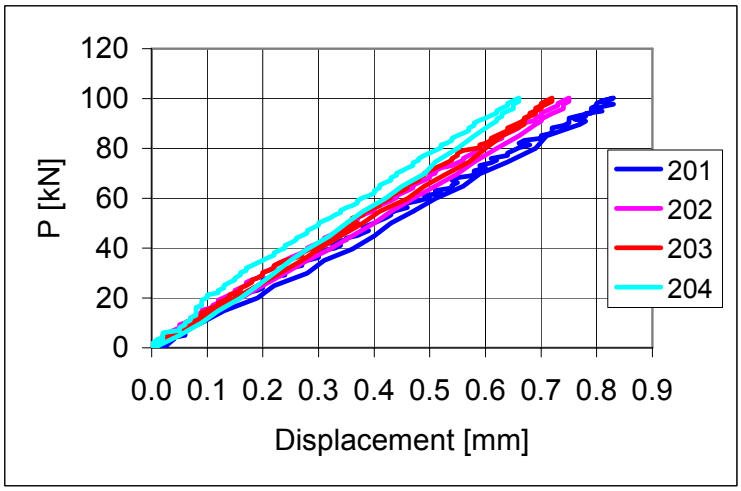

Fig. 124. FT200:4. Deflection. Transducers 201–204.

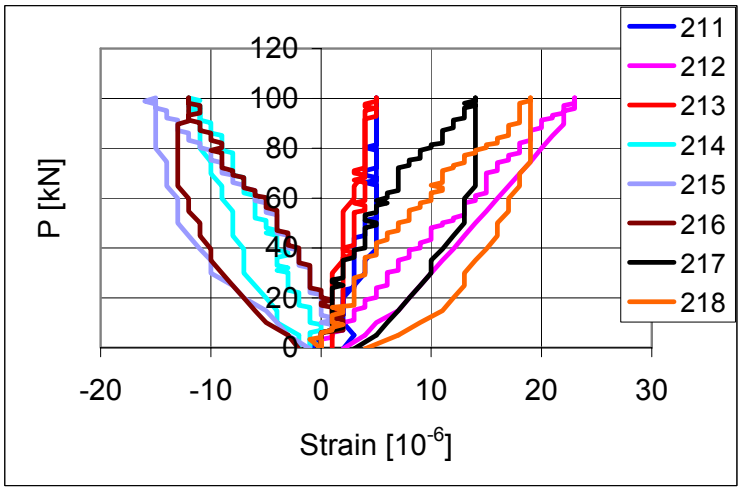

Fig. 125. FT200:10. Strain in trimmer beam. Strain gauges 211–218.

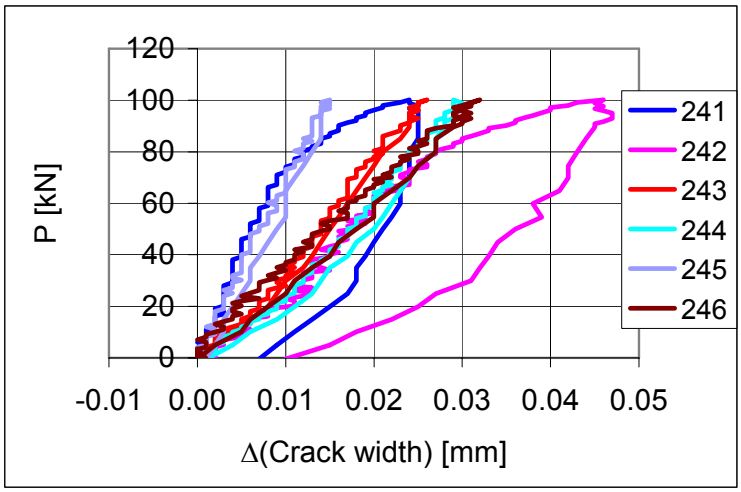

Fig. 126. FT200:10. Change in crack width. Transducers 241–246.

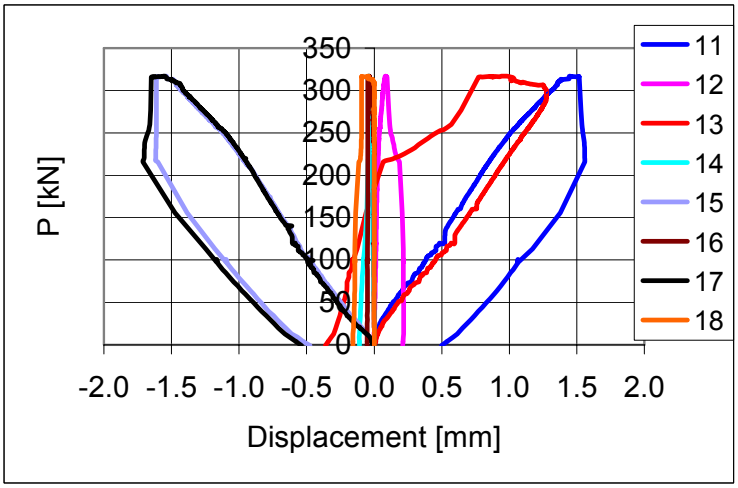

Fig. 127. FT200:11. Longitudinal horizontal displacement. Transducers 11–18.

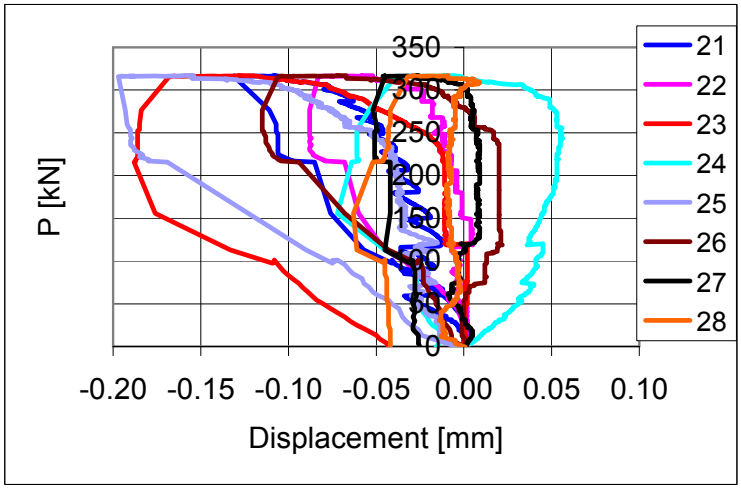

Fig. 128. FT200:11. Transverse horizontal displacement. Transducers 21–28.

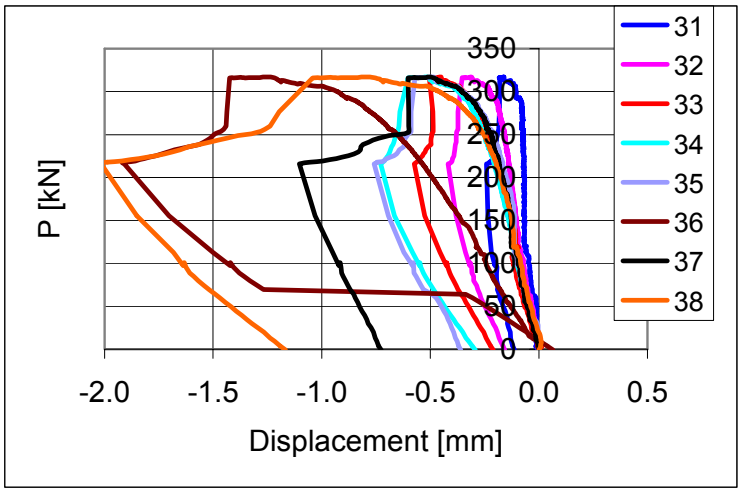

Fig. 129. FT200:11. Transverse horizontal displacement. Transducers 31–38.

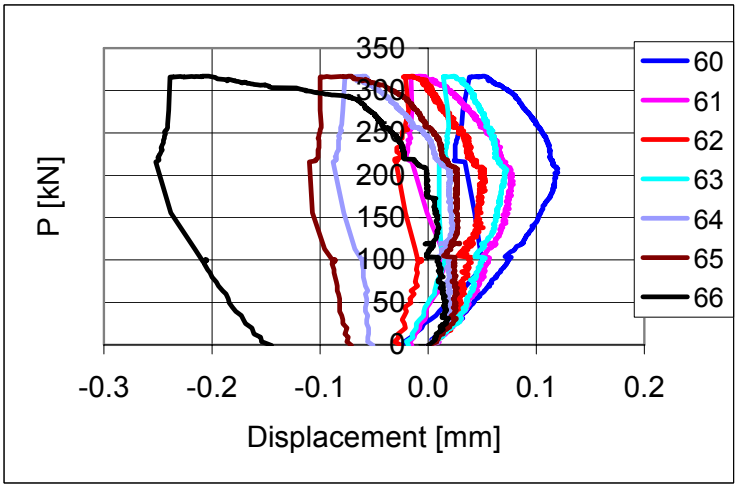

Fig. 130. FT200:11. Settlement of support. Transducers 60–66.

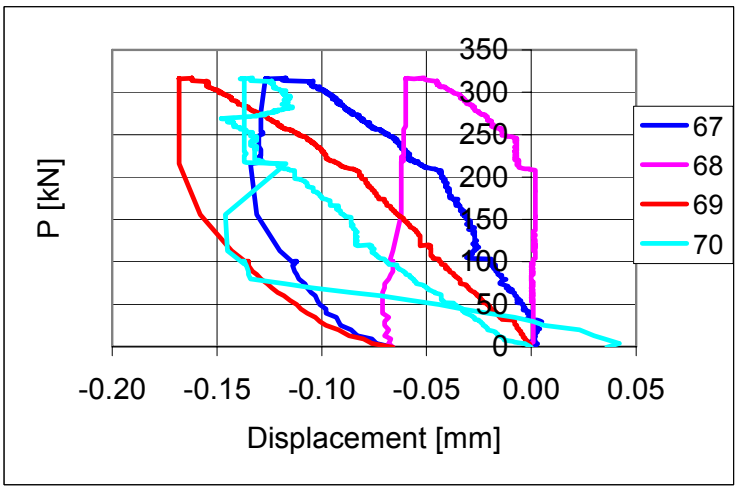

Fig. 131. FT200:11. Settlement of support. Transducers 67–70.

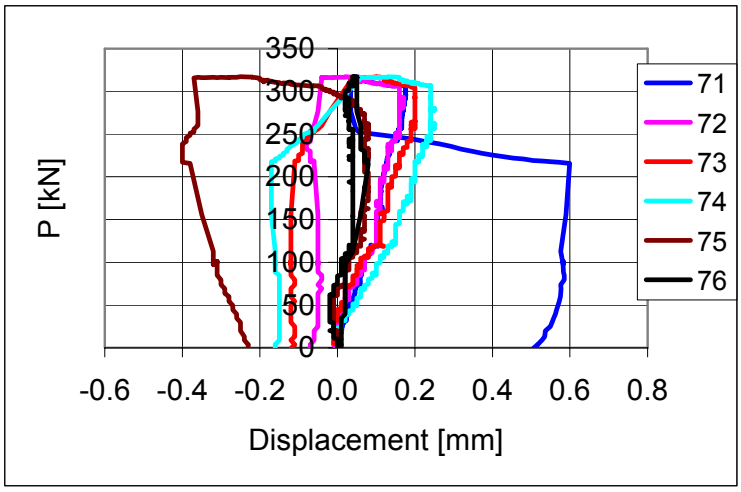

Fig. 132. FT200:11. Settlement of support. Transducers 71–76.

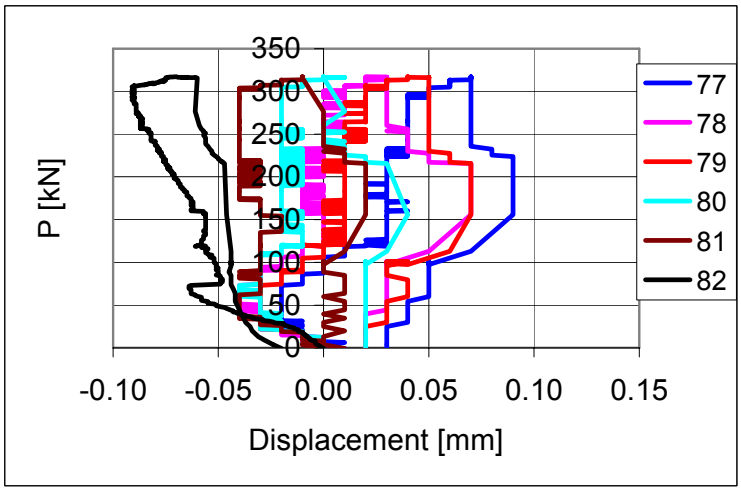

Fig. 133. FT200:11. Settlement of support. Transducers 77–82.

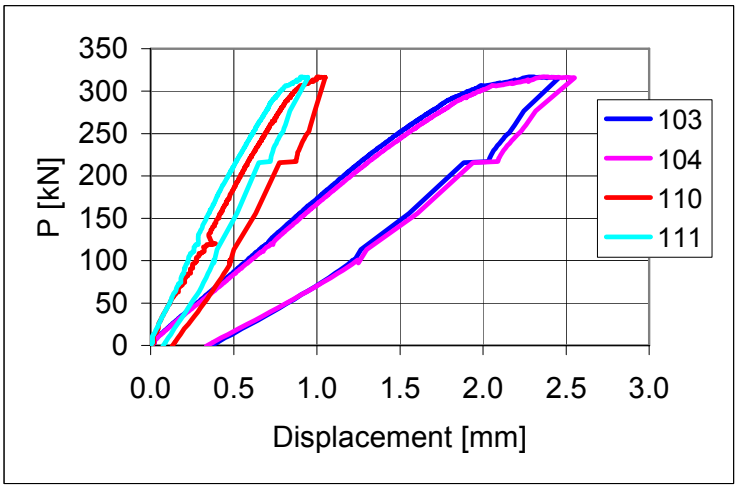

Fig. 134. FT200:11. Deflection. Transducers 103, 104, 110 and 111.

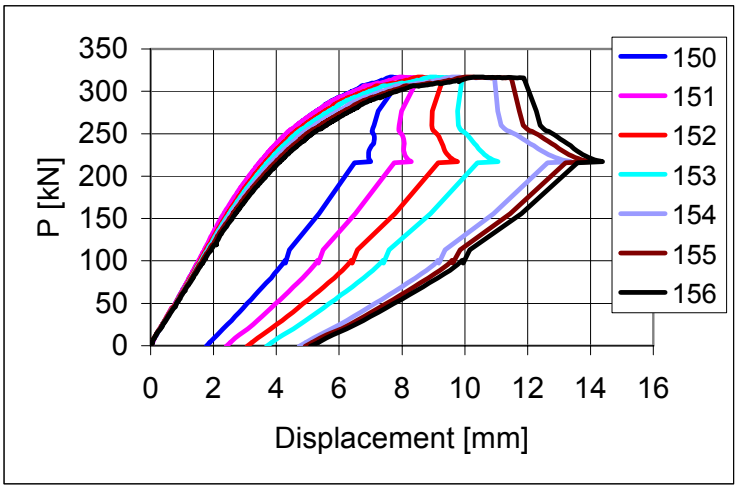

Fig. 135. FT200:11. Deflection. Transducers 150–156.

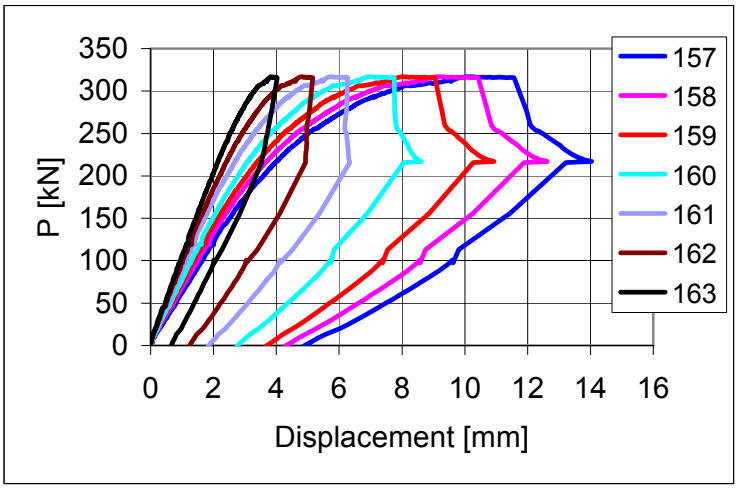

Fig. 136. FT200:11. Deflection. Transducers 157–163.

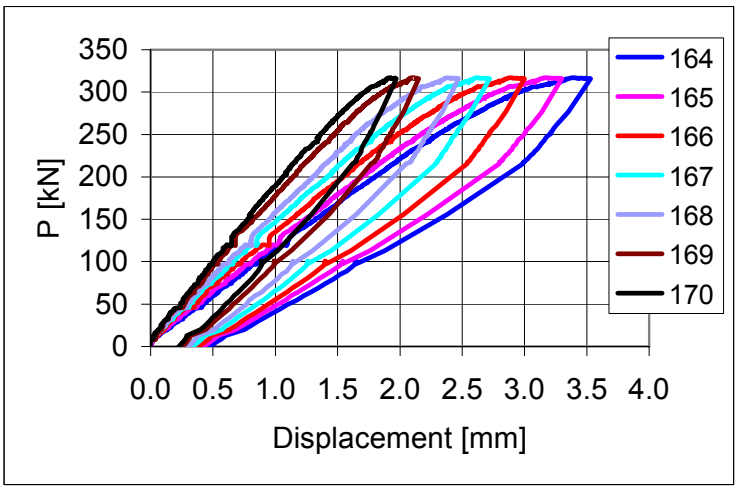

Fig. 137. FT200:11. Deflection. Transducers 164–170.

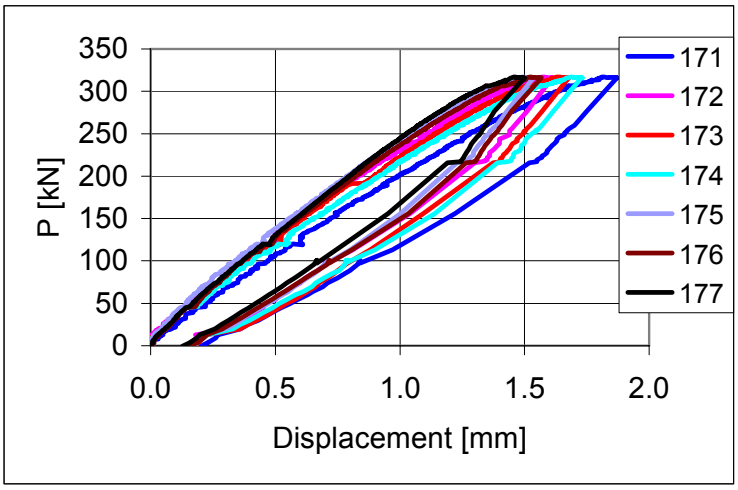

Fig. 138. FT200:11. Deflection. Transducers 171–177.

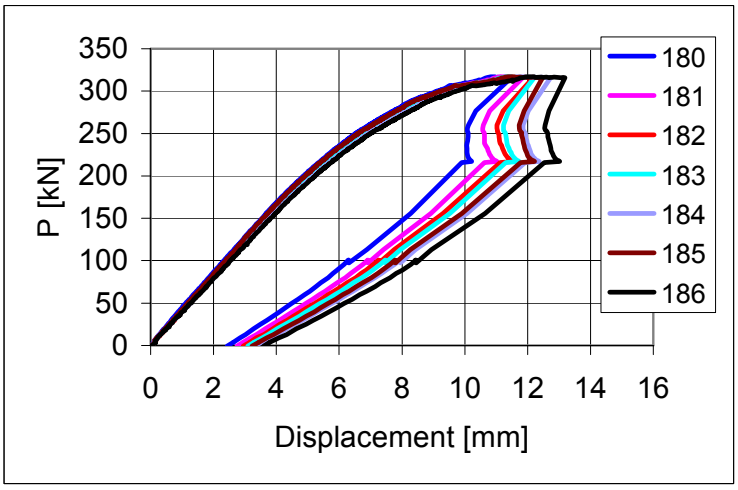

Fig. 139. FT200:11. Deflection. Transducers 180–186.

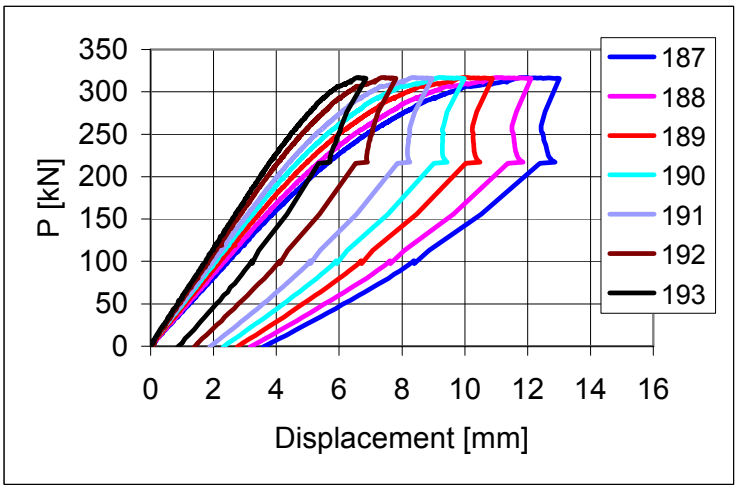

Fig. 140. FT200:11. Deflection. Transducers 187–193.

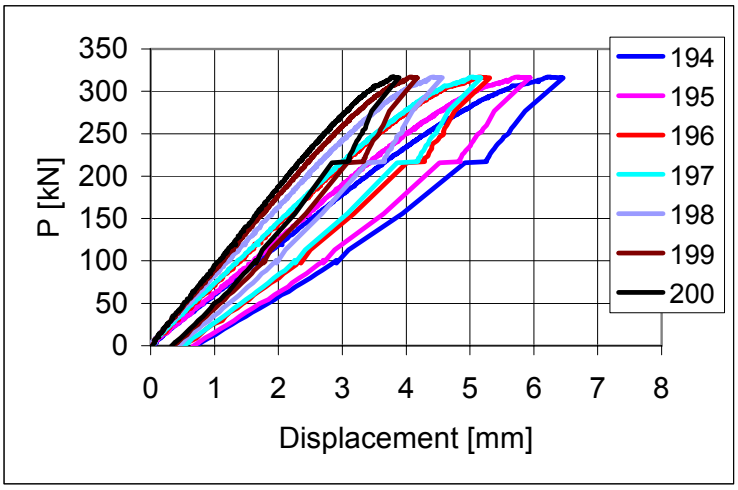

Fig. 141. FT200:11. Deflection. Transducers 194–200.

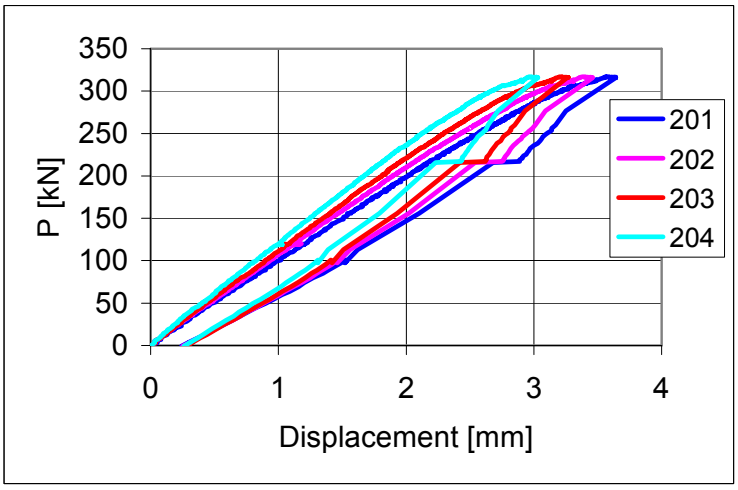

Fig. 142. FT200:11. Deflection. Transducers 201–204.

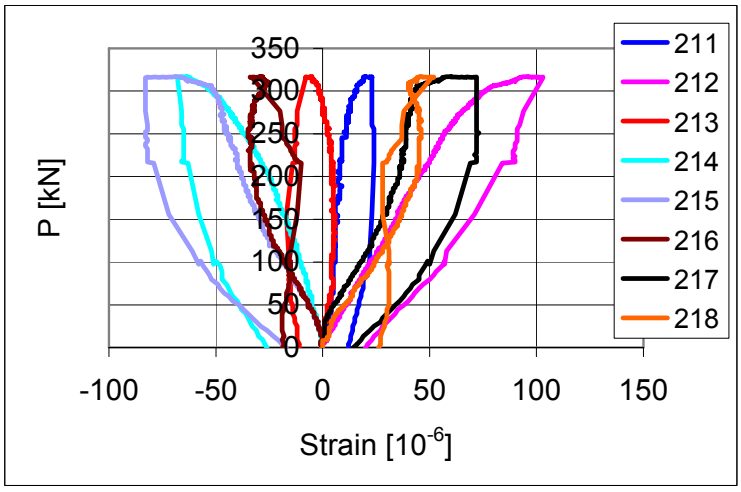

Fig. 143. FT200:11. Strain in trimmer beam. Strain gauges 211–218.

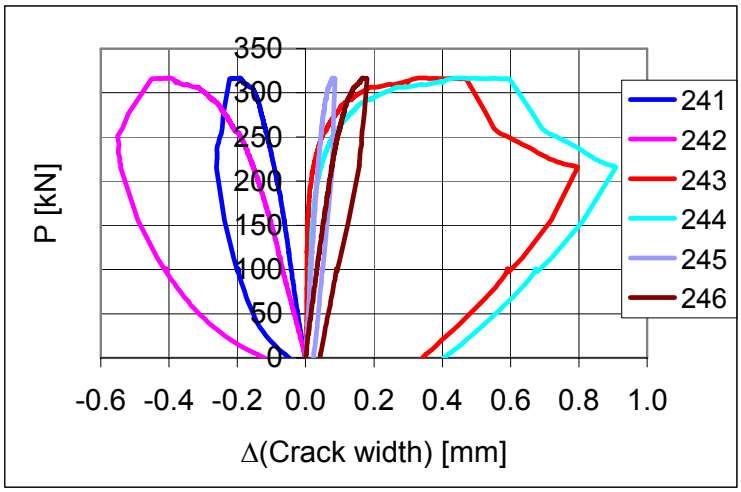

Fig. 144. FT200:11. Change in crack width. Transducers 241–246.

Appendix F: Error in vertical displacements

Some of the transducers for measuring vertical displacement of the floor were provided with a spring. When starting a test, the spring was in compression. The spring force decreased when the floor deflected. For this reason, the structure which the transducer was fixed to, had to be stiff enough. At the ends of the floor this was no major problem because the beams carrying the transducers 60–70 and 71–82 could be provided with any number of intermediate supports. On the other hand, the beams carrying the transducers 90–144 and 150–204 could only be supported at their ends. Therefore, they had to be quite stiff. The errors due to the flexibility of these beams are considered in the following.

The transducers were fixed to stands carried by supporting beams as shown in Fig. 1. The beam was simply or almost simply supported. (The twisting of the beam at supports had to be prevented. This resulted in some friction in bending hinge.)

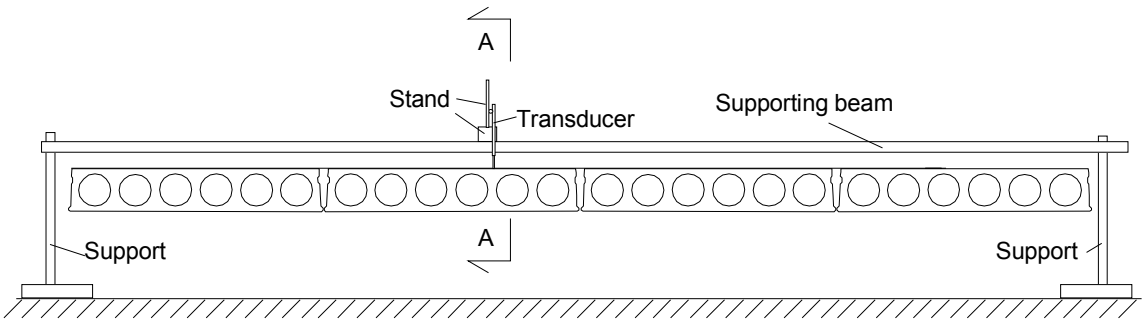

a)

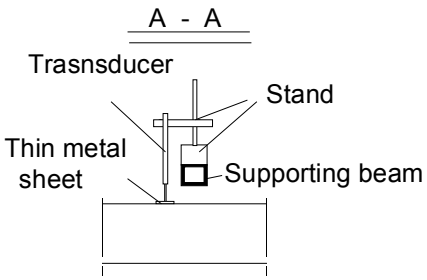

b)

Fig. 1. a) Arrangement to measure deflection of the floor. b) Section A–A.

The transducers provided with springs are shown in Fig. 2. Even though the spring constant was small (= 0.080 N/mm) the flexibility of the supporting beam ($EI = 5.7 \cdot 10^{11}$) made the beam deflect when the floor was loaded. To monitor the error in measured displacements due to this effect, the absolute (relative to the earth) displacement of the supporting beam itself was also measured by transducer 300 (see Fig. 3). The results are shown in Figs 4–9.

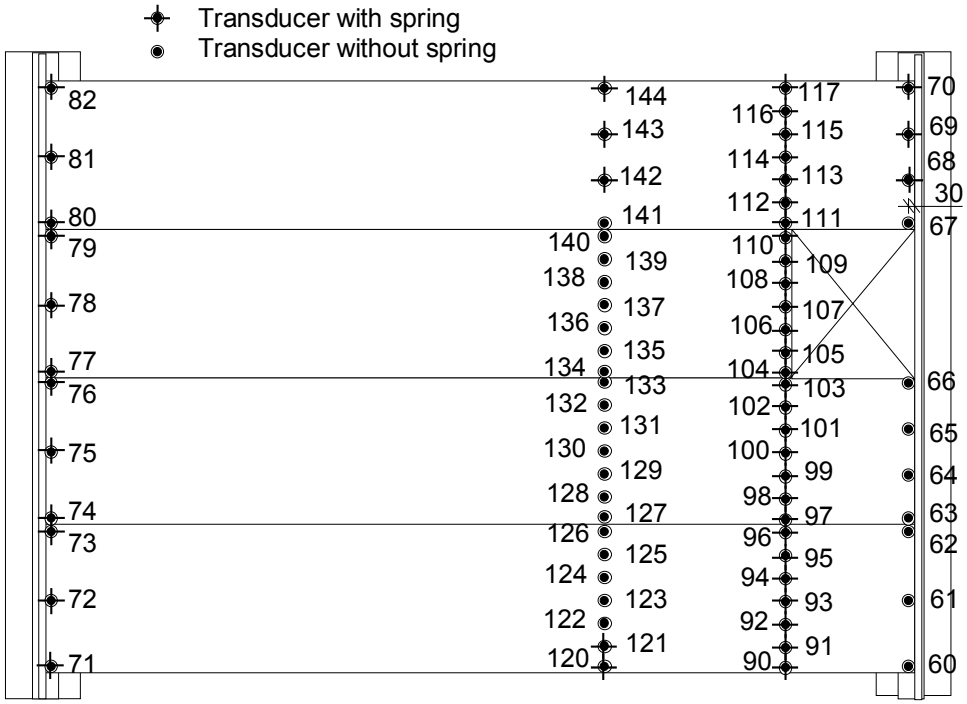

a)

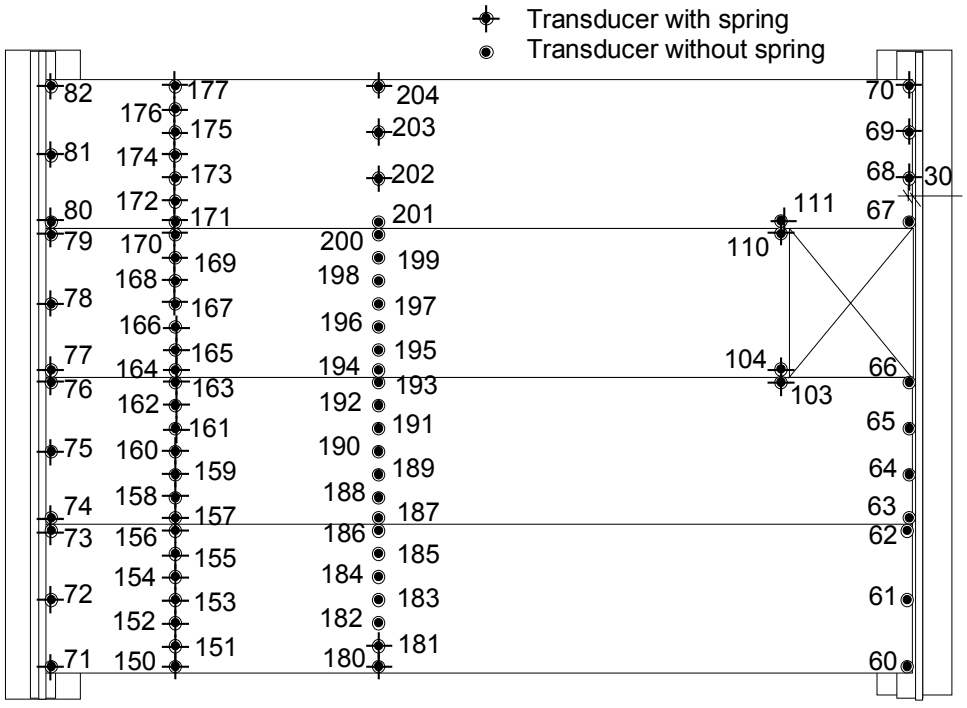

b)

Fig. 2. a) Type of transducers in tests FT200:1–FT200:3 and FT200:12. b) Type of transducers in other tests.

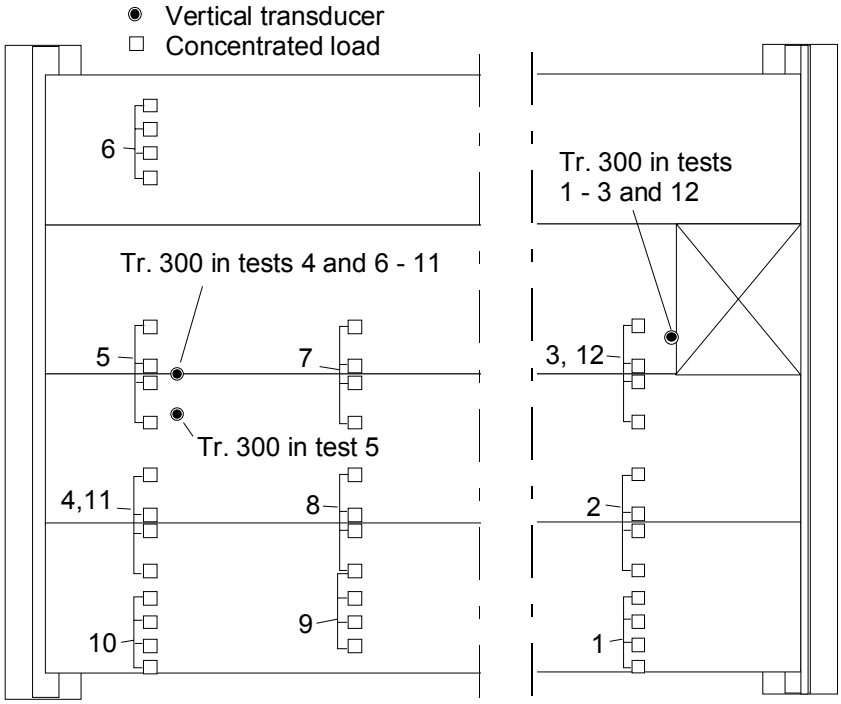

Fig. 3. Location of transducer 300 in different tests.

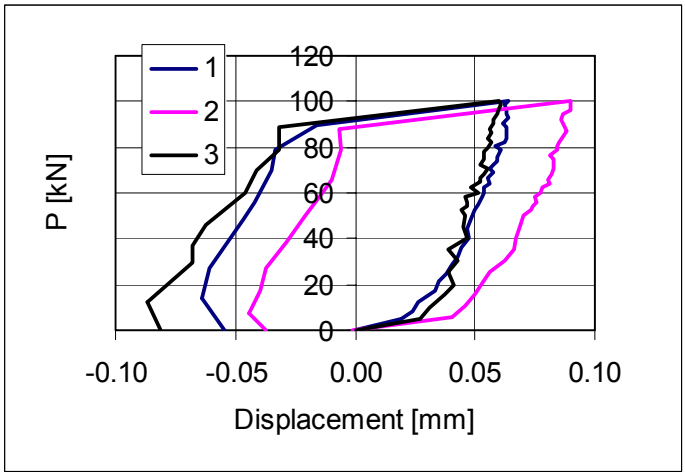

Fig. 4. FT:1–FT:3. Deflection of supporting beam measured by transducer 300.

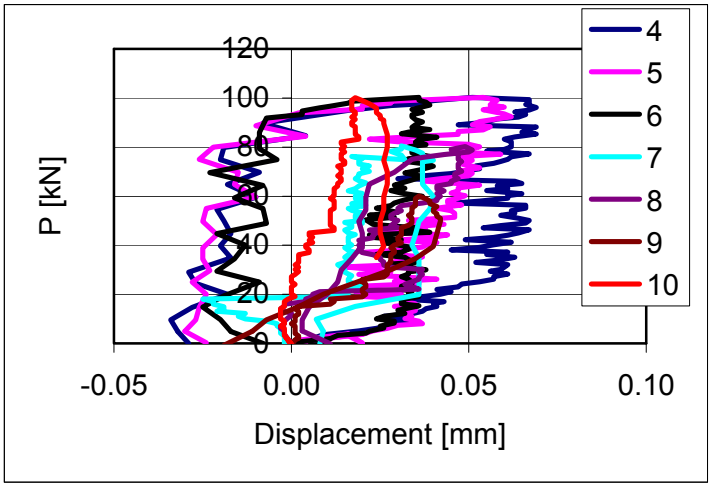

Fig. 5. FT:4–FT:10. Deflection of supporting beam measured by transducer 300.

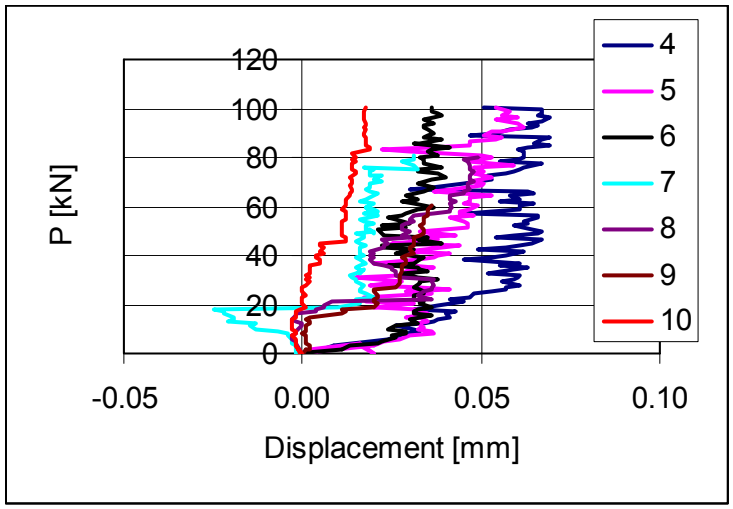

Fig. 6. FT:4–FT:10. Deflection of supporting beam measured by transducer 300 until maximum load.

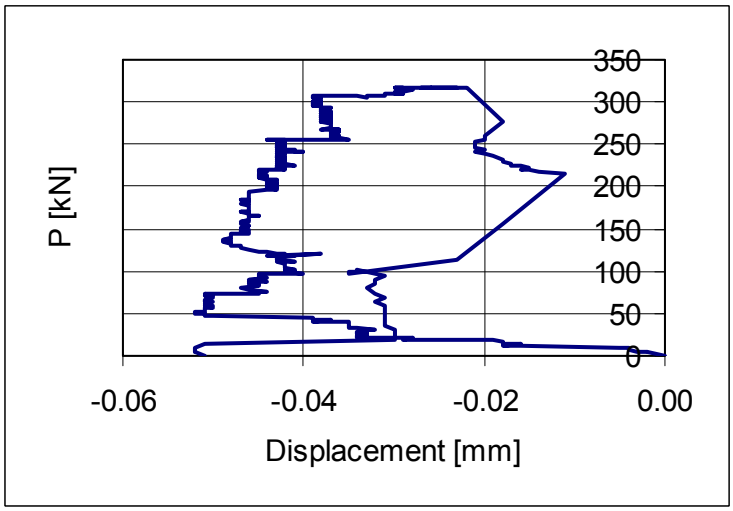

Fig. 7. FT:11. Deflection of supporting beam measured by transducer 300.

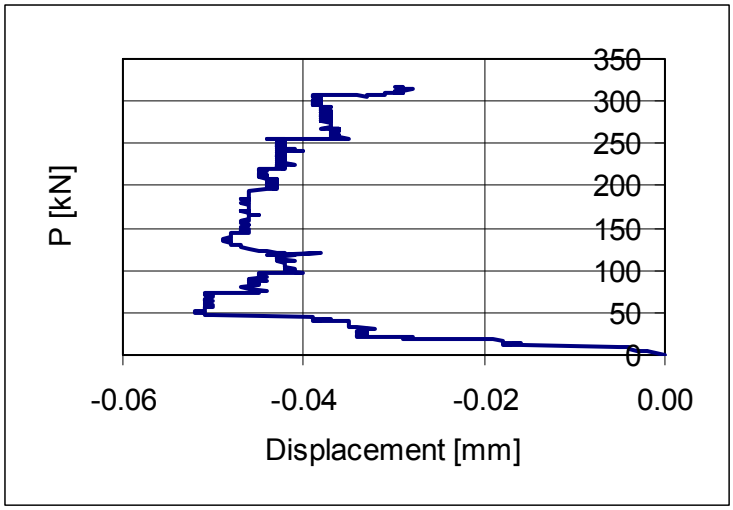

Fig. 8. FT:11. Deflection of supporting beam measured by transducer 300 until maximum load.

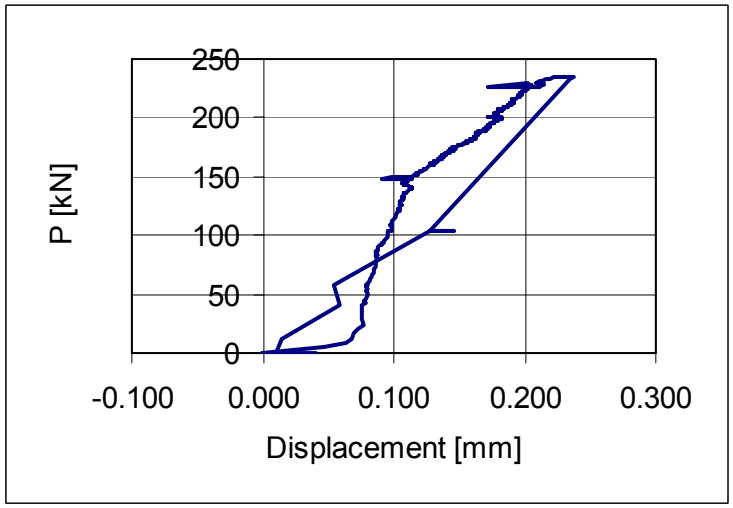

Fig. 9. FT:12. Deflection of supporting beam measured by transducer 300.

The measured deflections of the supporting beam are small when compared with the measured displacements of the floor below the beam.

To give an impression about the effect of the spring forces in the transducers on the measured deflection, three load tests are considered. FT200:3, FT200:5 and FT200:12 are chosen because in these tests the load was close to the mid-span of the supporting beam and the absolute error due to the deflection of the supporting beam was at maximum.

The deflection of the floor measured by transducers 90–117 in tests FT200:3 and FT200:12 and that measured by transducers 150–177 in test FT200:5 is similar to that shown in Fig. 10 but Fig. 10 slightly overestimates the real deflection.

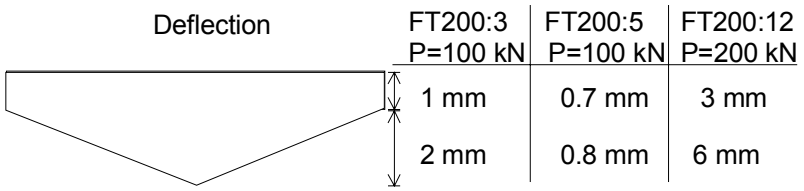

Fig. 10. Approximated deflection pattern in tests FT200:3, FT200:5 and FT200:12.

The change in spring force per unit length due to deflection δ is obtained from

$$\Delta q = 7 \cdot \frac{0.08\ N/mm}{1200\ mm}\delta$$

From this and deflection taken from Fig. 10 an upper limit for the deflection of the supporting beam due to the varying spring force is obtained, see Table 1.

Table 1. Maximum deflection of beam supporting transducers above the loaded floor. Observed deflection (v_{obs}) and approximated upper limit for deflection (v_{appr}).

Test	v_{obs} mm	v_{appr} mm	v_{obs} / v_{appr}
PT200:3	0.060	0.015	0.250
PT200:5	0.060	0.0081	0.135
PT200:12	0.182	0.0046	0.025

The results show that only a small part of the observed deflection of the supporting beam was caused by the relaxing spring forces in the transducers if the springs worked in an ideal way. Calculations also show that the twist of the supporting beam due to the relaxing spring forces is so small that the deflection due to it is only a small part of the deflection calculated from the bending.

Transducer 300, used for measuring the absolute deflection of the supporting beam, proved to work accurately after the tests. The cables connected to the transducers were too light to cause the observed deflection of the considered beam. Therefore, it remains that some kind of instability in the vertical supports and their connections to the supporting beam have caused the major part of the observed absolute deflection. In any case the errors in the measured deflections of the floor are small, less than 0.23 mm in test FT200:12, less than 0.09 mm in test FT200:2 and less than 0.06 in other serviceability tests. In tests FT200:11, FT200:12 and FT200:1-FT200:10 the maximum error was 0.5%, 1.3% and less than 4% of the maximum measured deflection, respectively.

Appendix G: Measured tilting and sliding of supporting beams

In the following the horizontal displacement of the supporting beams is illustrated in figures which show the tilting and sliding (actually position) with respect to the position before the test:

- at a load which is smaller than the maximum load
- at maximum load and
- after unloading.

The figures on the left and right hand side show the displacement measured by transducers 11–14 and 15–18, respectively. *z* denotes the distance from the floor of the hall to a transducer.

A positive displacement means that the beam is moving away from the transducer. To facilitate the interpretation, the scale in the figures on the right hand side is in reverse order. Hence, a marker on the right and left from the vertical axis means motion of the beam from its original position to the right and left, respectively.

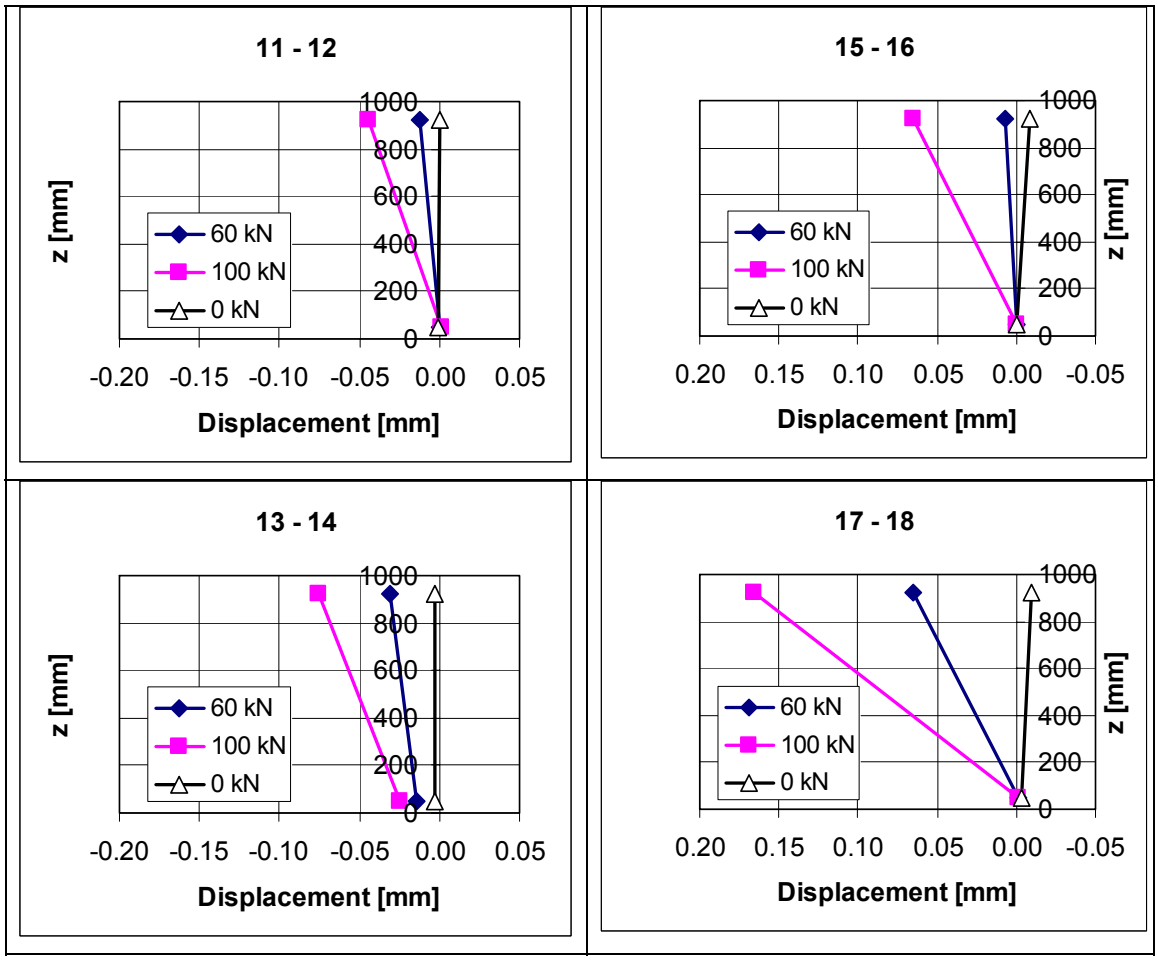

Fig. 1. FT200:1.

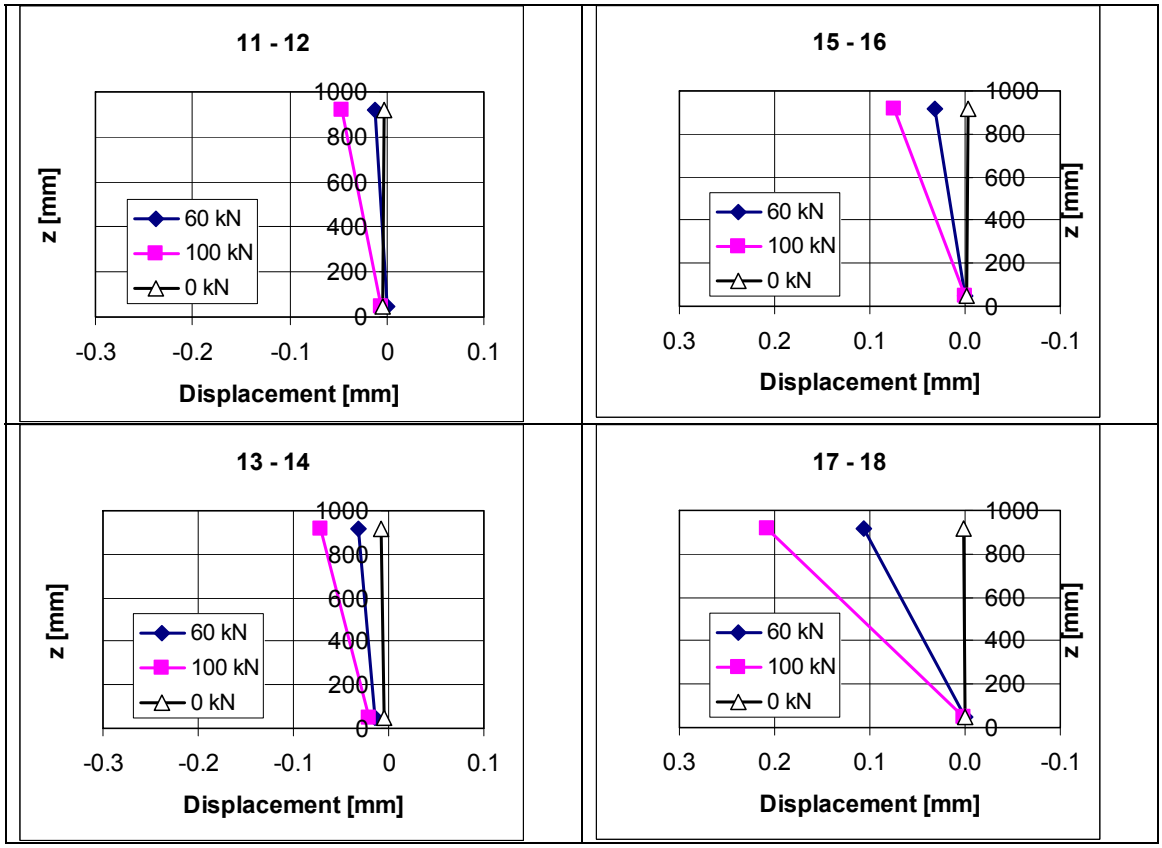

Fig. 2. FT200:2.

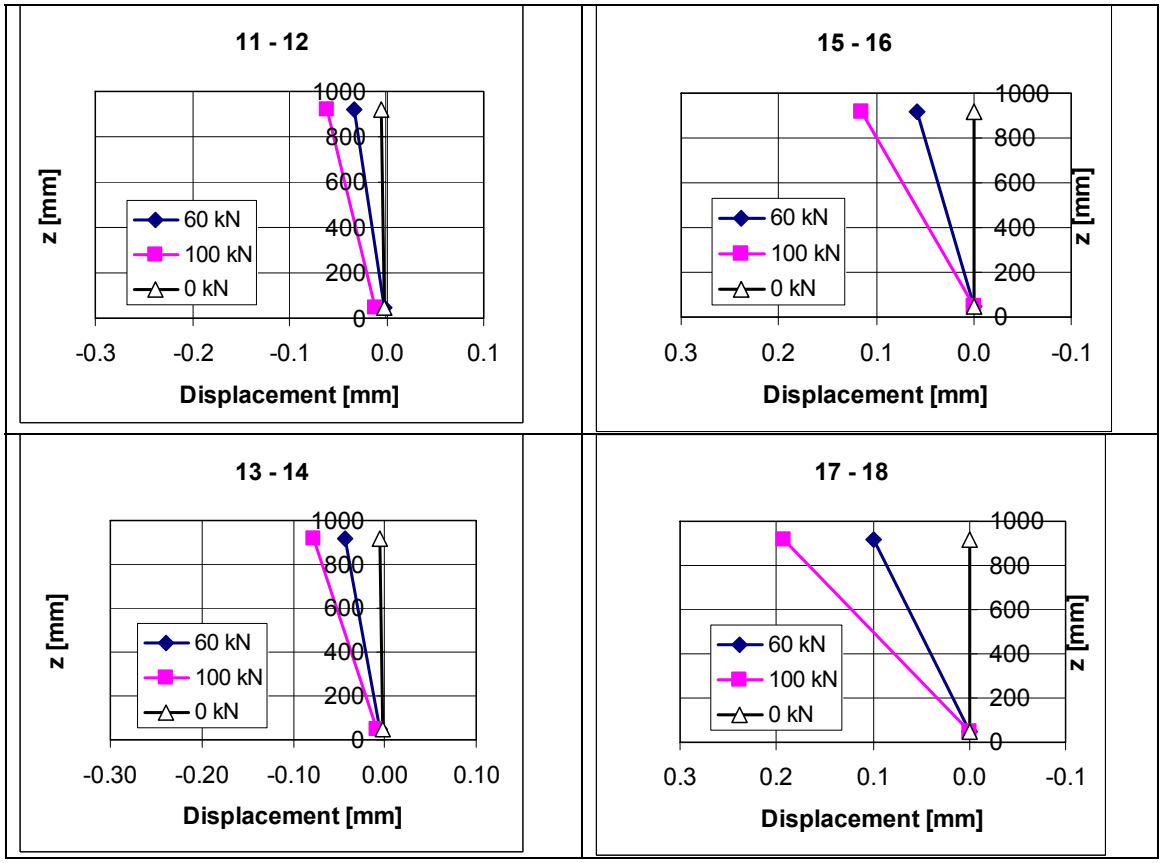

Fig. 3. FT200:3.

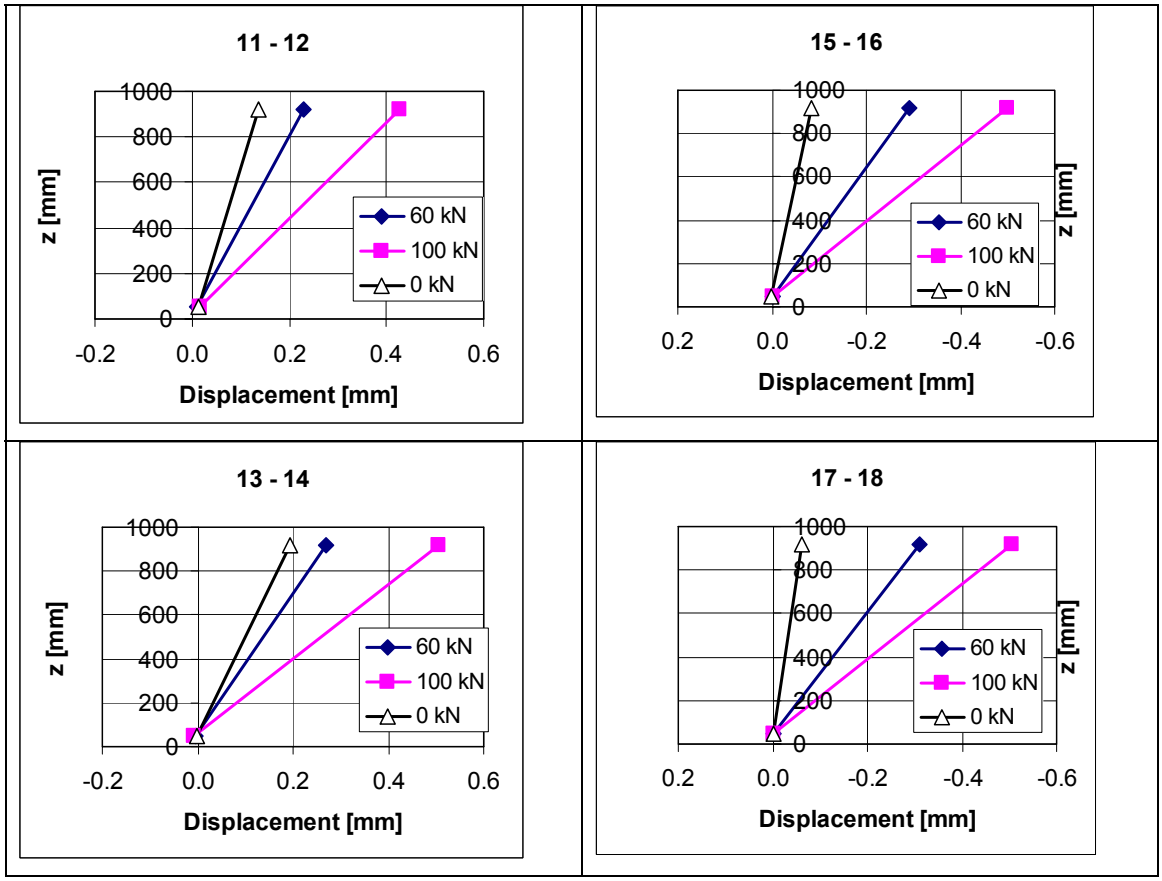

Fig. 4. FT200:4.

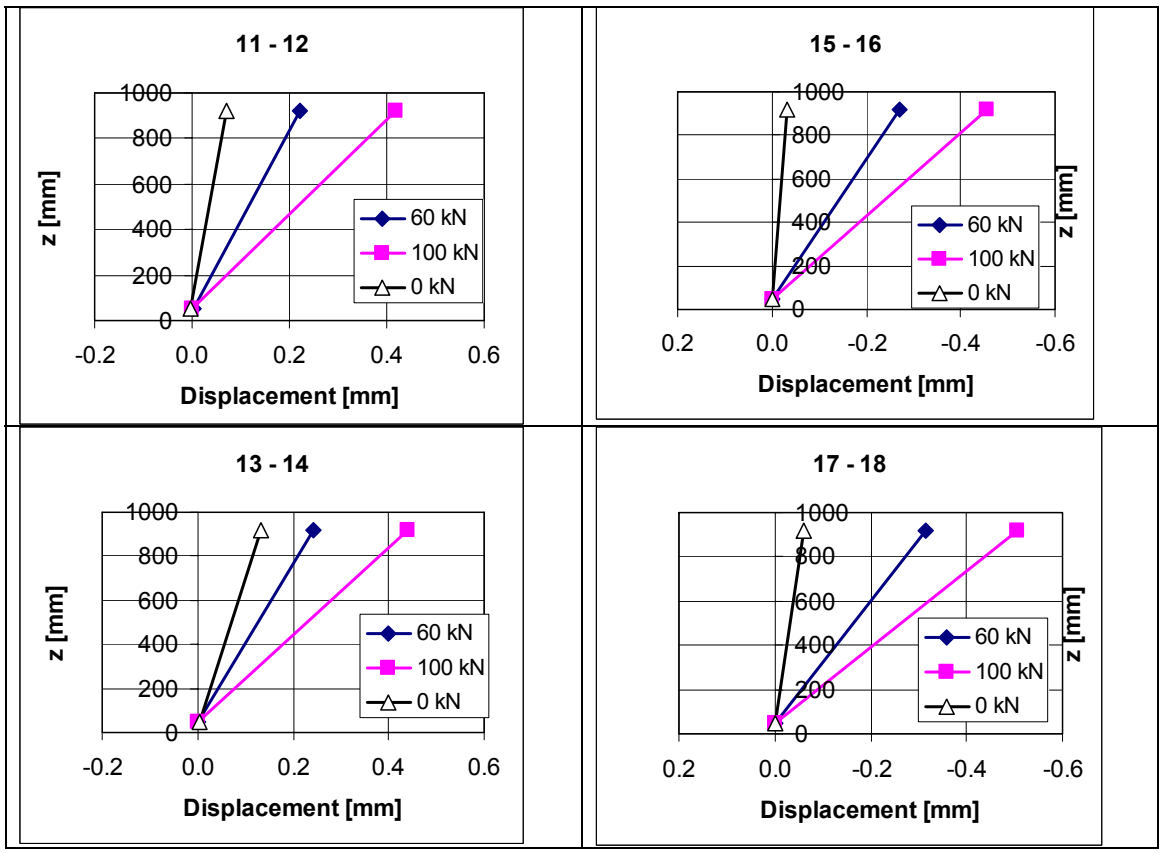

Fig. 5. FT200:5.

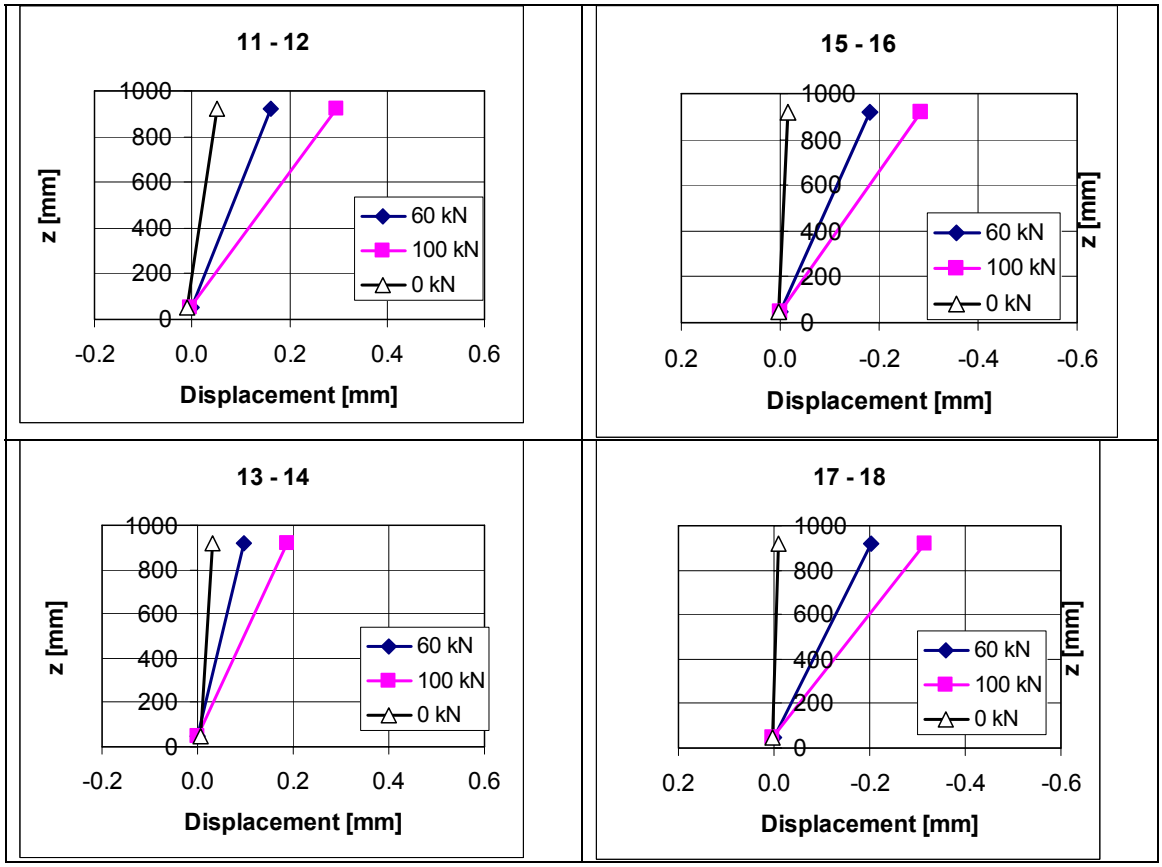

Fig. 6. FT200:6.

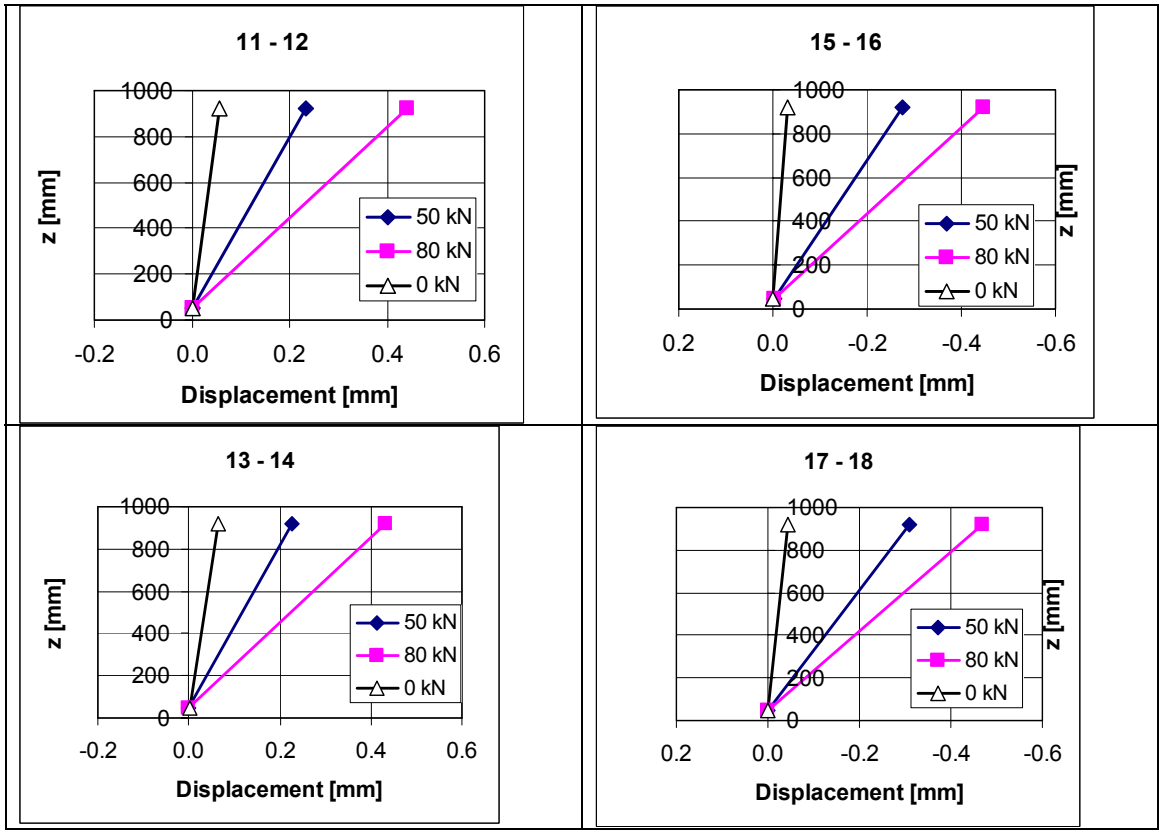

Fig. 7. FT200:7.

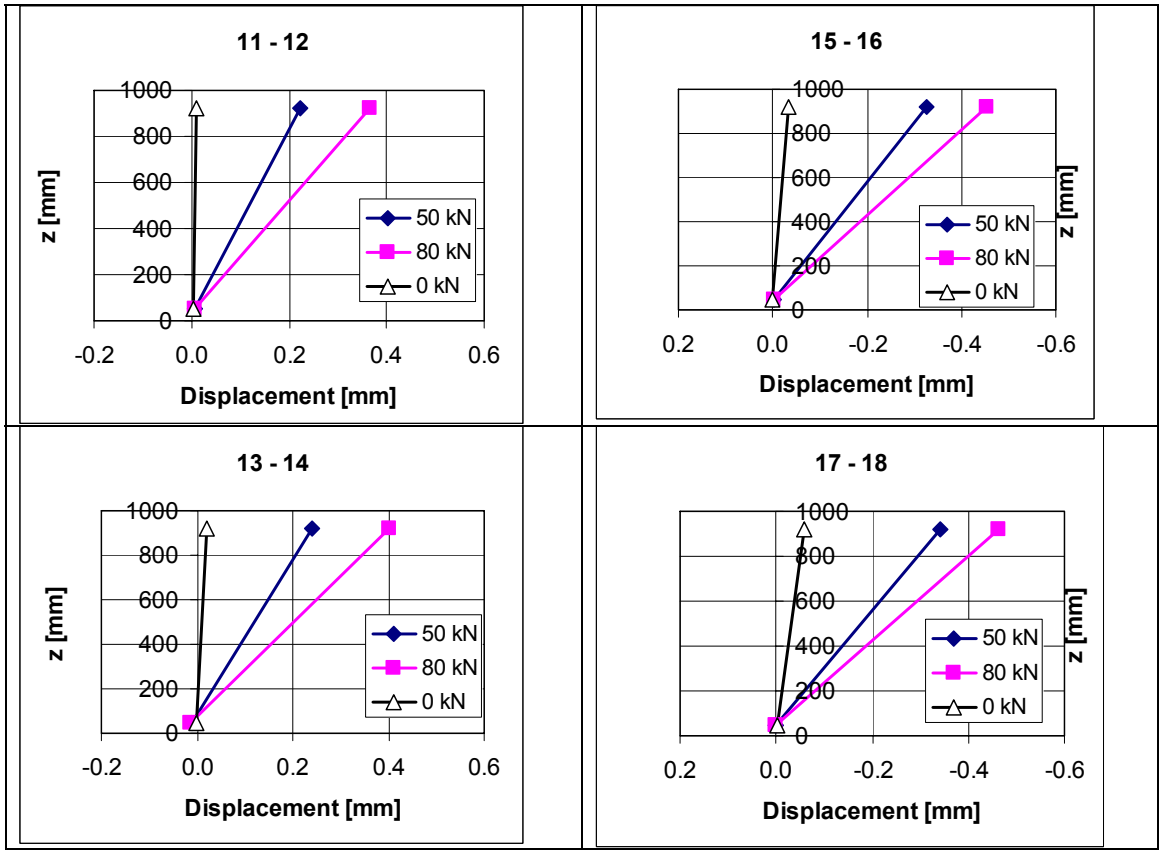

Fig. 8. FT200:8.

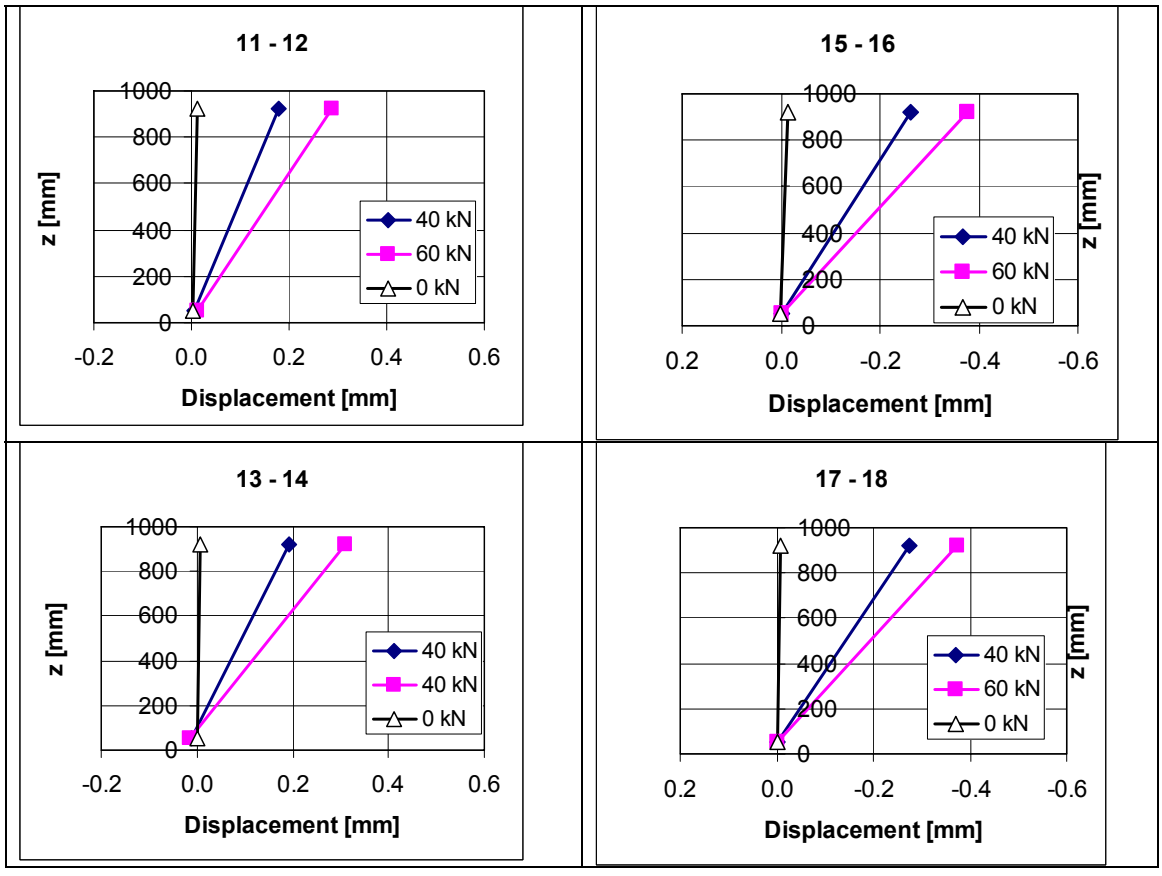

Fig. 9. FT200:9.

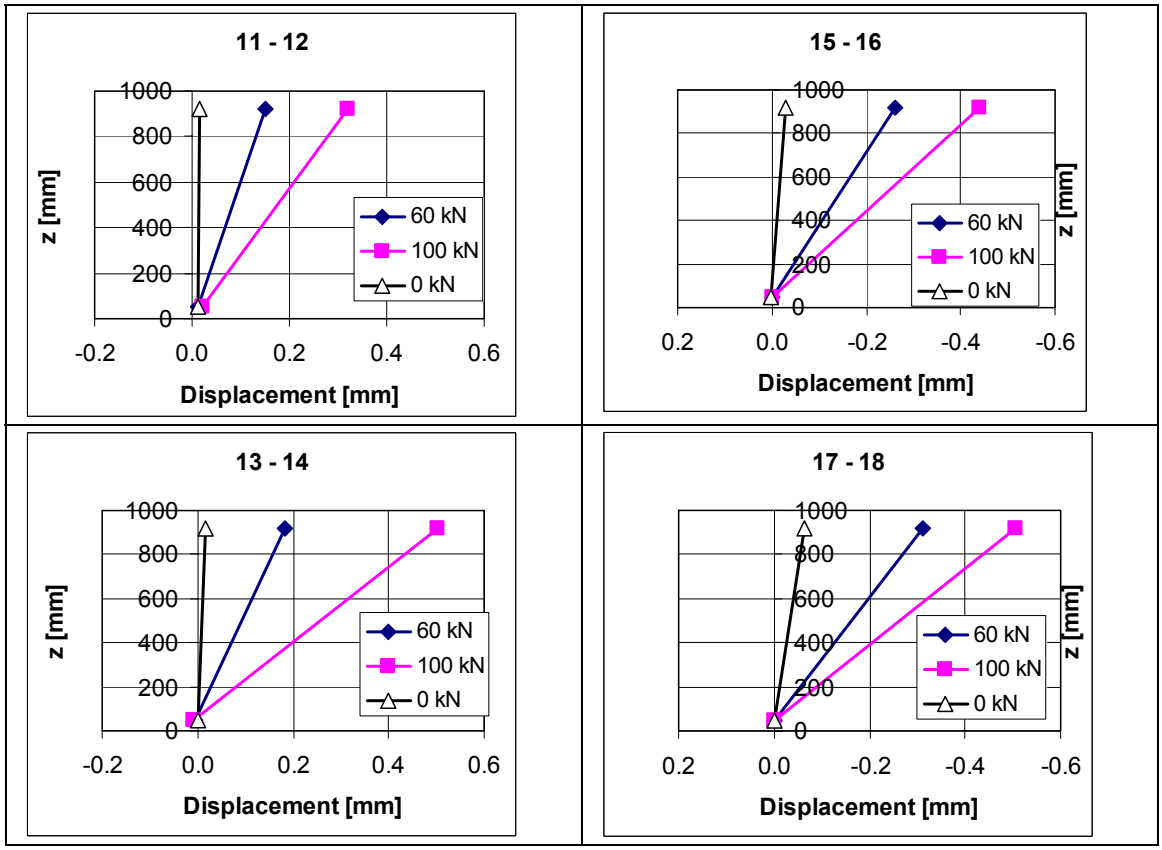

Fig. 10. FT200:10.

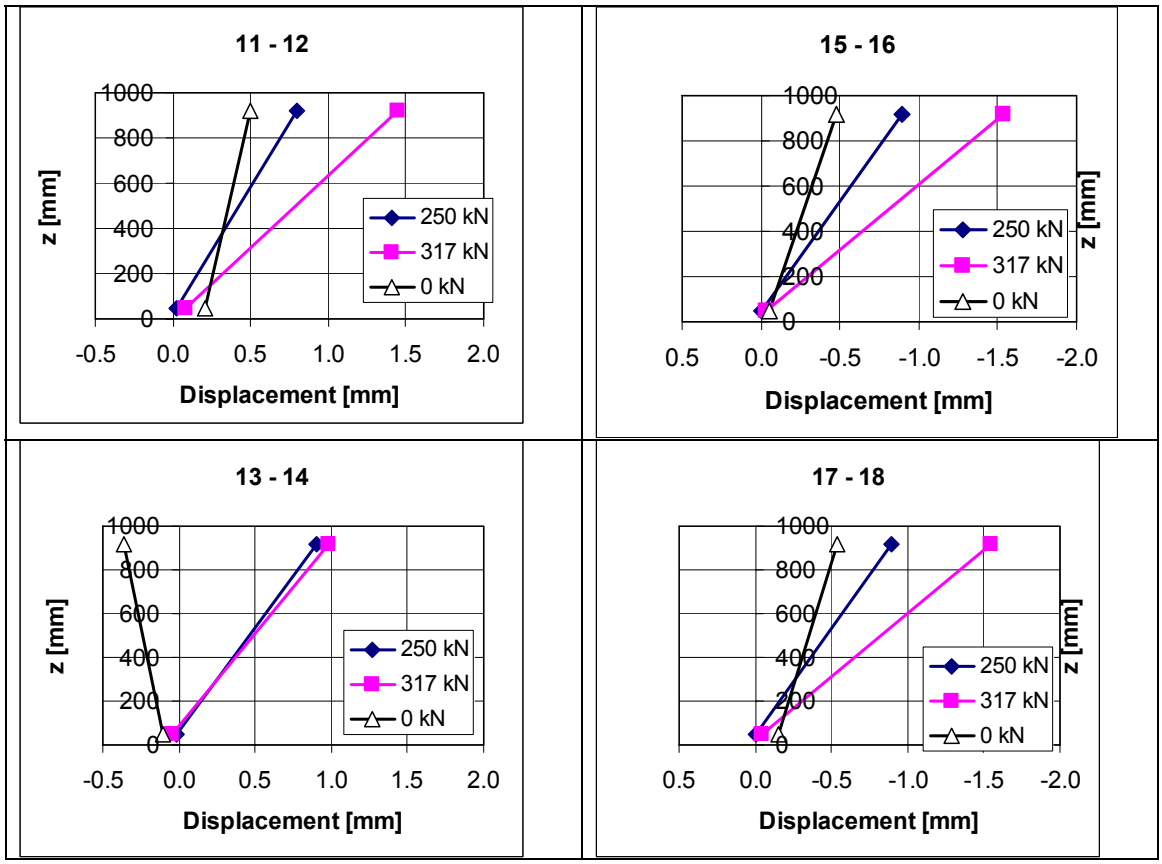

Fig. 11. FT200:11.

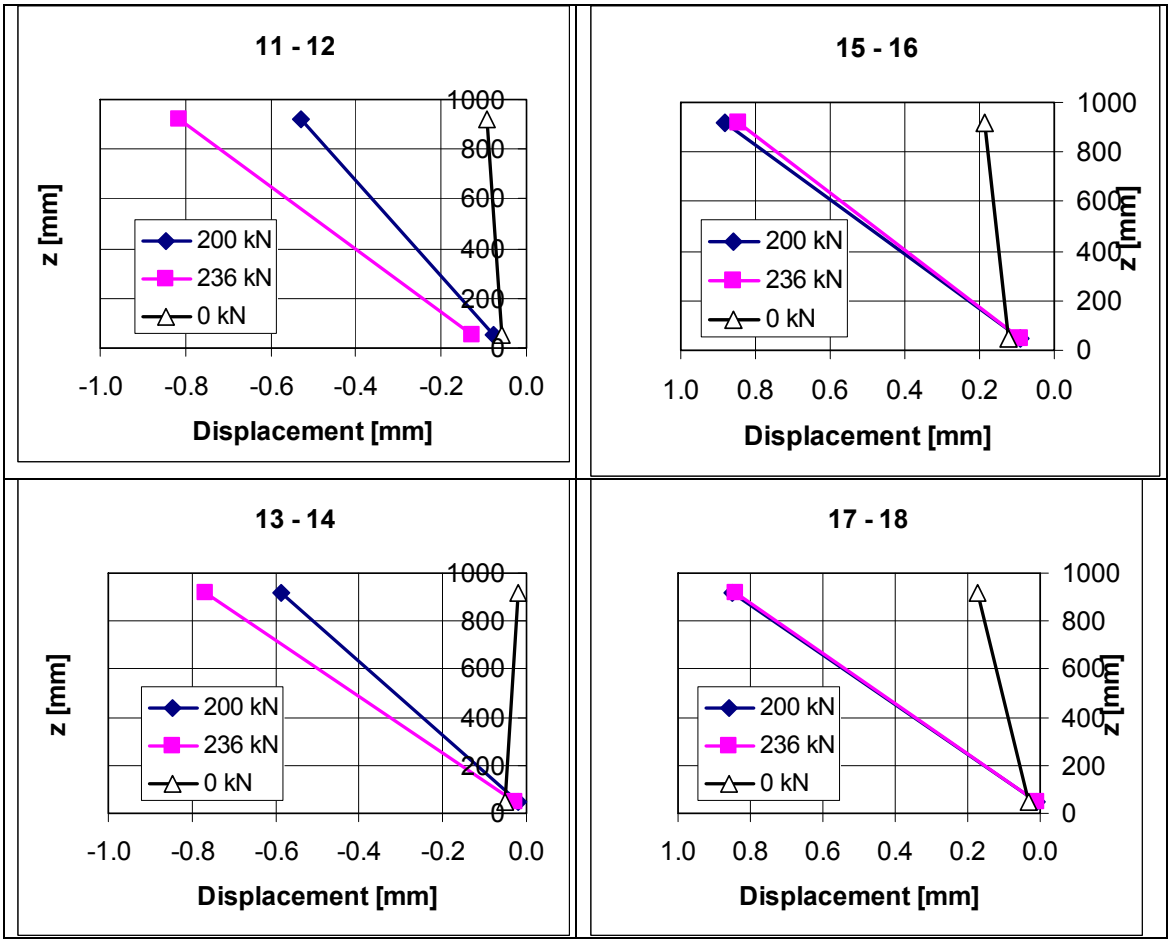

Fig. 12. FT200:12.

Published by

Series title, number and report code of publication

VTT Research Notes 2276
VTT–TIED–2276

Author(s)
Pajari, Matti

Title

Shear-torsion tests on 200 mm hollow core floor

Abstract

To clarify the interaction of shear and torsion in prestressed hollow core floors, ten service load tests and two failure tests on a 200 mm hollow core floor were carried out. The floor comprised four slab units. It was 4.8 m in width, 7.0 m in length and provided with an opening at one end. The ends of the slabs were simply supported. In each test the loading consisted of four closely spaced point loads on the same line which was perpendicular to the direction of the slab units.

The purpose of the tests was to provide experimental data for verification of computer models. For this reason, as many as 120 transducers were used to measure the loads, strains and displacements of the floor specimen.

The results were qualitatively as expected: nearly linear response not only in service load tests but also in failure tests until a high load level. The observed failure loads were considerably higher than what was observed in a similar load test on a single slab unit.

It was also observed that the trimmer beam next to the opening carried only a small share of the support reaction due to imposed load on the slab supported on the trimmer beam. The rest of the support reaction was carried by the grouted joints between slab units.

Keywords
shear tests, torsion tests, hollow core slabs, floors, testing, test specimens, load testing, failure loads, load distribution, concrete, precast, prestressed, structure

Activity unit
VTT Building and Transport, Kemistintie 3, P.O.Box 1805, FIN–02044 VTT, Finland

ISBN			Project number
951–38–6520–7 (URL: http://www.vtt.fi/inf/pdf/)			R2SU00137
Date December 2004	Language English	Pages 55 p. + app. 116 p.	Price -
Name of project Holcotors		Commissioned by EU, Concrete industry, VTT	
Series title and ISSN VTT Tiedotteita – Research Notes 1455–0865 (URL: http://www.vtt.fi/inf/pdf/)		Published by VTT Information Service P.O.Box 2000, FIN–02044 VTT, Finland Phone internat. +358 9 456 4404 Fax +358 9 456 4374	

To clarify the interaction of shear and torsion, ten service load tests and two failure tests on a full-scale 200 mm hollow core floor were carried out. In each test the loading consisted of four closely spaced point loads on the same line which was perpendicular to the direction of the slab units.

The purpose of the tests was to provide experimental data for verification of computer models. For this reason, as many as 120 transducers were used to measure the loads, strains and displacements of the floor specimen.

The results were qualitatively as expected: nearly linear response not only in service load tests but also in failure tests until a high load level. The observed failure loads were considerably higher than what was observed in a similar load test on a single slab unit.

VTT TIETOPALVELU
PL 2000
02044 VTT
Puh. 020 722 4404
Faksi 020 722 4374

VTT INFORMATIONSTJÄNST
PB 2000
02044 VTT
Tel. 020 722 4404
Fax 020 722 4374

VTT INFORMATION SERVICE
P.O.Box 2000
FIN–02044 VTT, Finland
Phone internat. + 358 20 722 4404
Fax + 358 20 722 4374

ISBN 951–38–6520–7 (URL: http://www.vtt.fi/inf/pdf/)
ISSN 1455–0865 (URL: http://www.vtt.fi/inf/pdf/)